SURFACE WAVE PROPAGATION OVER SINUSOIDALLY VARYING TOPOGRAPHY: THEORY AND OBSERVATION

BY
A.G. DAVIES AND A.D. HEATHERSHAW

REPORT NO. 159
PART I
1983

NATURAL ENVIRONMENT RESEARCH COUNCIL

INSTITUTE OF OCEANOGRAPHIC SCIENCES

INSTITUTE OF OCEANOGRAPHIC SCIENCES

Wormley, Godalming,
Surrey, GU8 5UB.
(0428 - 79 - 4141)

(Director: Dr. A.S. Laughton FRS)

Bidston Observatory,
Birkenhead,
Merseyside, L43 7RA.
(051 - 653 - 8633)

(Assistant Director: Dr. D.E. Cartwright)

Crossway,
Taunton,
Somerset, TA1 2DW.
(0823 - 86211)

(Assistant Director: M.J. Tucker)

When citing this document in a bibliography the reference should be given as follows:-

DAVIES, A.G. & HEATHERSHAW, A.D. 1983 Surface wave propagation over sinusoidally varying topography: theory and observation. *Institute of Oceanographic Sciences, Report,* No. 159, 181pp. (in 2 parts).

INSTITUTE OF OCEANOGRAPHIC SCIENCES

TAUNTON

Surface wave propagation over sinusoidally varying topography: theory and observation

by

A.G. Davies and A.D. Heathershaw

I.O.S. Report No. 159

Part I

1983

CONTENTS

		Page
Symbols		8
Summary		11
1.	INTRODUCTION	13
	1.1 Background to the present study	13
	1.2 The present study	13
2.	THEORY	14
	2.1 Introduction	14
	2.2 Formulation	17
	2.3 The function $\Lambda(\xi)$	20
	2.4 The contour integration method	24
	2.5 Solution for the general case ($1 \neq 2k$)	28
	2.6 Solution for the special case in which $1 = 2k$	35
	2.7 Discussion	44
	Appendix 2.1 Results for the functions ψ and ψ_*	51
	Appendix 2.2 The divergence of the bed velocity at the ends of the ripple patch	54
3.	EXPERIMENTAL TECHNIQUES	57
	3.1 Construction of the ripple patch	57
	3.2 The wave generator	58
	3.3 Wave measurements	59
	3.4 Wave filters	60
4.	EXPERIMENTAL RESULTS	60
	4.1 Variation of the reflection coefficient with the ratio of the water wavelength to the ripple wavelength	60
	4.2 Measurements of the variation of peak reflection coefficient as a function of the quotient of ripple amplitude (b) and water depth (h), and of the number of ripples (m) in the patch	65
	4.3 Measurements of surface elevation and reflection coefficient over, and on either side of, the ripple patch	66
	4.4 Observations of sediment movement	70

Page

5. DISCUSSION 77

5.1 The validity of the comparisons 77

5.2 The linearity of the measured wave field 79

5.3 Measurements of the reflection coefficient 80

5.4 Measurements of surface elevation and ripple reflection coefficient over, and on either side of, the ripple patch 82

5.5 Sediment transport observations 83

6. CONCLUSIONS 83

ACKNOWLEDGEMENTS 85

REFERENCES 86

FIGURES 89

TABLES 128

APPENDICES 153

LIST OF FIGURES

		Page
Figure 1	Definition sketch.	89
Figure 2	Positions of the poles in the λ-plane.	90
Figure 3	Wave modes in the perturbation solution for the general case in which $1 \neq 2k$.	91
Figure 4	Wave modes in the perturbation solution for the special case in which $1 = 2k$.	91
Figure 5	Surface wave elevations in the perturbation solution in a typical near-resonant case.	92
Figure 6	Surface wave elevations in the solution correct to second order in a typical near-resonant case.	93
Figure 7	Surface wave elevations for individual trapped wave modes.	94
Figure 8	Surface wave elevations for the complete set of trapped wave modes.	95
Figure 9	Surface wave elevations in the perturbation solution both with, and without, the trapped wave modes.	96
Figure 10	Amplitudes of horizontal velocity in the solution correct to second order, in a typical near-resonant case.	98
Figure 11	Bed velocities in the solution correct to second order, in a typical near-resonant case.	99
Figure 12	Schematic diagram of the gauges in the wave tank.	100
Figure 13	Wave generator bulkhead amplitudes.	101
Figure 14	Measured and predicted reflection coefficients.	102
Figure 15	Schematic diagram of the wave components in the tank.	105
Figure 16	Measured and predicted reflection coefficients near to resonance.	106
Figure 17	Peak (averaged) reflection coefficients near to resonance.	109
Figure 18	Measured and predicted amplitudes of surface wave elevation throughout the tank.	110
Figure 19	Measured and predicted reflection coefficients throughout the tank.	114
Figure 20	Summary of the reflection coefficients measured throughout the tank.	118
Figure 21	Schematic diagram of the formation of sand ripples of short wavelength in the tank.	121

		Page
Figure 22	Sequence of photographs showing the formation of sand ripples of short wavelength in the tank.	122
Figure 23	Predicted and observed pattern of sediment movement in the tank.	125
Figure 24	Predicted postions of the maxima and minima of the horizontal bed velocity amplitude throughout a typical ripple patch.	126
Figure 25	Variation of the measured reflection coefficient with the steepness of the incident waves.	127
Figure B.1	Schematic diagram of the filter units and their supports.	163
Figure B.2	Schematic diagram of the filter units in the wave tank.	164
Figure B.3	Measurements of wave attenuation by the filters.	165
Figure B.4	Measured reflection coefficient of the filters.	166
Figure B.5	Measured reflection coefficient of the ripple patch, with and without filters.	167
Figure B.6	Measured reflection coefficients throughout the tank, with and without filters.	168

LIST OF TABLES

Page

Table 1 Comparisons of nominal and measured wave period settings for the wave generator in the range 0.6 - 3.0 s 128

Table 2 Measurements of the ripple reflection coefficient $|K_R|$ and the beach reflection coefficient K_B, as a function of wave period, for m = 2, 4 and 10 ripples and for different water depths 129

Table 3 Measurements of the ripple reflection coefficient $|K_R|$, at or near resonance, for m = 1, 2, 4 and 10 ripples and for different water depths 138

Table 4 Measurements of the maximum and minimum surface elevation and the wave reflection coefficient K, at different positions in the wave tank, for m = 2, 4 and 10 ripples and for different water depths 140

Table 5 Estimates of phase difference between observed and predicted waves in the wave tank for m = 10, 4 and 2 ripples 150

Table 6 Variation of ripple reflection coefficient $|K_R|$ with wave steepness for m = 10 ripples 151

Table B.1 Wave filter transmission and reflection characteristics 170

Table C.1 Estimates of the proportion of the generated wave energy which is dissipated in the wave tank. 181

LIST OF APPENDICES

		Page
Appendix A	The method of Goda and Suzuki for the determination of the wave reflection coefficient	153
Appendix B	Wave filter design and characteristics	161
Appendix C	Wave energy dissipation in the tank	177

LIST OF SYMBOLS

$a = a_I$	amplitude of incident surface wave
a_B	amplitude of wave reflected by the beach
a_R	amplitude of wave reflected by the ripple patch
a_T	amplitude of wave transmitted over the ripple patch
a_{BR}	amplitude of wave from the beach, re-reflected by the ripple patch
a_{BT}	amplitude of wave from the beach, transmitted over the ripple patch
$A_b = U_b/\sigma$	semi-orbital excursion of water particles near the bed
b	amplitude of bottom ripples
$\overline{D}$	wave energy dissipation rate in the tank
D_{50}	median sand size
g	acceleration due to gravity
h	water depth
$H_I = 2a_I$	height of incident surface wave
$H_T = 2a_T$	height of transmitted surface wave
$k = 2\pi/\lambda_w$	surface wavenumber
$l = 2\pi/\lambda_R$	ripple wavenumber
L	half of the length of the ripple patch
L_1	up-wave limit of the ripple patch
L_2	down-wave limit of the ripple patch
L_*	effective down-wave limit of the ripple patch in cases of over-reflection
L_f	length of the series of wave filters
L_T	length of the wave tank
K	general wave reflection coefficient
K_R	reflection coefficient of the patch of ripples
K_B	reflection coefficient of the beach
m	number of ripples in the patch
S	stroke of the wave generator
t	time
t	modified time scale

Note: additional subscripts T and M distinguish the true (theoretical) and measured values, respectively.

$T = 2\pi/\sigma$	wave period
ΔT	increment in the wave period
u	horizontal velocity component
$U_o = gak/\sigma$	horizontal surface velocity amplitude
$U_b = U_o/\cosh(kh)$	horizontal bed velocity amplitude
$V(x,t)$	vertical velocity at the bed
$V_o(x)$	vertical velocity amplitude at the bed
x	horizontal co-ordinate
x_1, x_2	positions of the up-wave and down-wave gauges in a gauge pair, respectively
Δx	spacing between gauges in a gauge pair
y	vertical co-ordinate
$Y_b(x)$	bed profile in $L_1<x<L_2$
$\overline{W}$	rate of doing work by the wave generator
W_T	width of the tank
δ	arbitrary phase angle in the definition of $Y_b(x)$
$\delta_* = \sqrt{2\nu_w/\sigma}$	Stokes' layer thickness
δ_I, δ_R	phase angles associated with incident and reflected waves respectively, in the method of Goda and Suzuki (1976)
ε_I, ε_R	phase angles of the incident and reflected waves respectively, in the method of Goda and Suzuki
$\zeta(x)$	general bed elevation function
$\eta(x,t)$	free surface elevation in the perturbation solution
η_I, η_R	free surface elevation of the incident and reflected waves respectively, in the method of Goda and Suzuki
η_1, η_2	free surface elevation at the wave gauge positions in the method of Goda and Suzuki
θ	quotient of the wave amplitudes a_{BT} and a_R
Ⓗ	phase shift of the envelope of the partially standing waves on the up-wave side of the ripple patch
$\lambda_R = 2\pi/l$	ripple wavelength
$\lambda_W = 2\pi/k$	surface wavelength
μ	coefficient of linear friction
ν_W	kinematic viscosity of water
ρ	density of water
$\sigma = 2\pi/T$	wave frequency
Φ	unperturbed velocity potential

ϕ	perturbation potential
ϕ_* , ϕ_R	component parts of the perturbation potential ϕ

Note $\sim$ tildes are used to denote the case in which the unperturbed incident waves are linearly attenuated in amplitude as they cross the ripple patch

SUMMARY

Surface waves travelling in water of finite depth may be scattered by a region of undulating bottom topography. This is a significant phenomenon both on the continental shelf, where a wide variety of regular and irregular bed features exists, and off beaches, where rather more regular, shore-parallel, bar structures are commonly formed.

The present study is concerned with the idealized, two-dimensional, situation in which long-crested surface waves are incident upon a patch of long-crested regular bottom ripples. The principal question examined concerns the amount of incident wave energy which is reflected by the ripple patch. A secondary question concerns the nature of the wave field in the immediate vicinity of the ripple patch and, more generally, the implications of the results for the stability of ripples on the seabed.

Linear perturbation theory is used to show that the reflection coefficient of a patch of sinusoidal ripples on an otherwise flat bed is both oscillatory in the quotient of the length of the patch and the surface wavelength, and also strongly dependent upon the quotient of the surface and bed wavenumbers. In particular, it is shown that there is a resonant interaction between the surface waves and the ripples if the surface wavenumber is approximately half the ripple wavenumber. Due to the finite length of the ripple patch, there is a broad resonance in respect of the ratio of these two wavenumbers, which is associated with the reflection of incident wave energy. This phenomenon is such that surprisingly few ripples, of relatively small steepness, are required to produce a substantial reflected wave. The theory is used to predict not only the properties of the reflection coefficient of the ripple patch, but also the nature of the wave field over the ripples. In resonant cases, which are of particular interest throughout this report, it is shown how the partially standing wave on the up-wave side of the ripple patch gives way, in an almost linear manner over the ripple patch itself, to a progressive (transmitted) wave on the down-wave side.

The theoretical predictions are compared with an extensive set of laboratory observations made in a wave tank. For the experiments, a fixed patch of sinusoidal ripples was constructed on an otherwise flat bed, mid-way between a wave generator and a wave-absorbing beach. The properties of the surface wave field were determined with wave gauges, and reflection coefficients were determined with gauge pairs. In resonant cases, measurements of the reflection coefficient of the ripple patch support the theoretical predictions very well, for a wide variety of parameter settings including the length of the patch; not only are the magnitudes

of measured reflection coefficients in good agreement with the predictions, but also the width of the main resonant peak is confirmed. In general non-resonant cases, the measurements also support the theory, though the trend predicted for the reflection coefficient is concealed somewhat by a (small) amount of wave energy reflection from the beach. Comparisons between theoretical predictions and experimental observations are made also for wave elevations measured in the region of the ripple patch itself and, again, consistently good agreement is found.

Finally, the implications of the results for sediment transport on an erodible bed are examined. Calculations of the (irrotational) bed velocity field are made, and the results of one experimental run are described, in which the movement of a thin veneer of sand throughout the ripple patch, and on either side of it, was observed. It is clear, from both theory and observation, that incident wave reflection by an existing ripple patch provides a mechanism for the growth of new ripples on the up-wave side of the patch, having the same wavelength as the existing ripples. This suggests that there may be a coupling between wave reflection and ripple growth on an erodible bed, which may have important implications for coastal protection. However, it remains unclear from the results of the present study whether the existing ripple patch is likely to be a stable, or an unstable, feature on the bed, particularly in resonant cases in which there is a significant amount of wave reflection. This matter calls for further theoretical and experimental investigation.

1. INTRODUCTION

1.1 Background to the present study

The interaction of surface water waves with undulating seabed topography is a problem of fundamental importance to coastal engineers. While it has been shown that, in the nearshore zone, quite complex patterns of wave motion (eg edge waves) may lead to beach cusps, shore parallel bars and even crescentic shore welded sand bars (Holman and Bowen, 1982), the problem that concerns us in this study is how waves are likely to interact with a pre-existing pattern of regular undulations on the seabed. Such a pattern may consist of shore parallel bars formed by plane reflections of low amplitude swell waves from a beach, leading to standing waves of the type observed by Suhayda (1974). Alternatively, standing waves may occur seaward of the surf zone as a result of the time varying breakpoint forcing mechanism described by Symonds et al (1982). In this case a forced wave having incident wave group periodicity is radiated seaward from the breaker zone. Such a wave, interacting with incoming infragravity waves having periods in the range 30-300 s , might lead to standing waves and consequently bar formation. This latter mechanism seems to be the most likely candidate for generating the multiple shore parallel bars observed by Short (1975), which would require wave periods of the order 100 s.

A pre-existing pattern of bottom undulations might also consist of tidally generated features such as sand waves (eg Langhorne, 1982) or sand ridges lying transverse to the general direction of wave propagation and, as such, may occur well offshore away from the coastline. In general, surface wave/seabed interactions may occur in any depth of water where the waves are able to "feel the bottom". It follows that such interactions may occur for a wide range of surface water wavelengths and bedform length scales.

1.2 The present study

The present study arose from some theoretical predictions (Davies, 1980, 1982a) concerning the interaction of long crested incident surface waves with long crested transverse bedforms. Essentially, it was shown that significant resonant interactions, associated with wave reflection, may occur between surface waves and bottom undulations provided that their respective wavelengths are in the approximate (Bragg scattering) ratio of two to one. Furthermore, it was shown that the coefficient of wave reflection for a patch of ripples on an otherwise flat bed is oscillatory in the ratio of the length of the patch to the wavelength of the free surface wave. These results were without any detailed experimental support until, during a visit to the US Army Corps of Engineers, Coastal Engineering Research

Center, Fort Belvoir, Virginia, USA, the opportunity arose for one of the authors (A D Heathershaw) to carry out an extensive set of measurements in a wave tank to test the theory. Some preliminary aspects of this investigation have already been described by Heathershaw (1982). In the light of some of the results from these experiments, which were outside the scope of the original theoretical study, it was thought desirable to extend the theory to give a more complete description of the way in which surface waves interact with a patch of bottom undulations. Thus the original theory has been extended (see §2) to enable comparisions between measured and predicted wave properties both above the ripple patch (referred to as the 'near field'), and on either side of it (the 'far field').

In §3, the experimental set-up is described and, in §4, the results are presented. Initially in §4, results for the wave reflection coefficient are compared with the theoretical predictions. Next, measured wave elevations throughout the wave tank are examined; here a description is given of the likely effects of transmitted waves being back-reflected onto the ripple patch by some further reflector on the down-wave side (eg a beach). Finally, comparisons of observed and predicted sediment movement in a wave-reflecting ripple system are made on the basis of the near-bed velocity field both over the ripple patch, and beneath the partially standing wave pattern on its up-wave side.

2. THEORY

2.1 Introduction

When surface waves are incident on a region of undulating seabed topography, it is well known that wave energy may be scattered by the bedforms. In general, incident waves travelling onto a bed roughness patch from any one direction may be scattered into any other direction. For large roughness patches, this problem has been treated by Long (1973), who examined the case of an arbitrary spectrum of surface waves propagating over an arbitrary spectrum of bottom perturbations. A rather simpler situation, which is of particular interest to workers in the field of sediment transport and which is treated here, is that in which long-crested waves are incident upon purely transverse bed features. In this special case, there are only two types of interaction between the waves and the bed, namely back-scatter (wave reflection) and forward-scatter (wave transmission). One reason why this problem is of interest is that, on erodible beds, there is a suggestion of a coupling between wave energy reflection and bedform growth, which may have significant implications for coastal protection.

In a previous paper, Davies (1982a) considered a two-dimensional problem in which surface waves were incident upon a patch of sinusoidal transverse ripples on an otherwise flat bed. The interaction between the waves and the ripples was examined on the basis of linear perturbation theory, and results were obtained for the reflected and transmitted waves for the "far field", well away from the region of bed disturbance. Although the theory was strictly applicable only to small roughness patches, the results indicated that, in certain circumstances, very few ripples may be needed to produce a substantial back-scattered wave. Firstly, it was shown that the reflection coefficient is oscillatory in the ratio of the surface wavelength to the length of the roughness patch and, secondly, that it is resonant if the surface wavelength is twice the bed wavelength. Taken together, these two effects produce a resonant peak near this critical ratio of wavelengths, the width of which decreases, and the intensity of which increases, as the number of ripples in the patch increases. Both the oscillatory nature, and the resonance, of the reflection coefficient have been established in a number of previous related studies. The oscillatory nature has been identified by, for example, Kreisel (1949), Newman (1965), Mei and Black (1969) and Fitz-Gerald (1977) and also, for long surface waves, by Jeffries (1944); and the resonance has been at the heart of Long's (1973) study, and has been discussed by various authors in a wider context (eg Beckmann and Spizzichino (1963), Fortuin (1970)). It is believed, however, that there has been no previous attempt to combine the two effects in a single theory describing the interaction of surface water waves with a region of undulating seabed topography (see the literature review of Davies (1980)).

Results for the "near field", over the ripple patch, were presented by Davies (1982b). As expected from previous related studies, the interaction between surface waves and sinusoidal ripples was found to give rise to two new waves with wavenumbers equal to the sum and difference of those of the surface waves and the bedforms. The sum wave is always in the onward transmitted direction; the difference wave is either in the onward transmitted direction, or is back reflected, depending upon whether its wavelength is less than, or greater than, that of the ripples, respectively. Unfortunately, the theory presented in this earlier paper produced a physically unrealistic result at resonance, as a result of the physically unrealistic assumption that the ripple patch was of infinite horizontal extent; in particular, it produced an infinite reflection coefficient for bed wavelengths equal to exactly one half of the surface wavelength. The details of this infinite resonant interaction have been examined recently by

Mitra and Greenberg (1982).

The contribution of the present paper is to draw the results of the two earlier studies into a single framework. Essentially, the results of Davies (1982a) for the "far field" are extended to some considerations of the "near field", for a physically realistic ripple patch of finite extent. While the sum and difference waves are found to be present over the patch, two additional waves are found there also; these waves are such as to produce a finite reflection coefficient for all combinations of surface and bed wavelengths. Moreover, an infinite number of trapped wave modes is found at both ends of the ripple patch. Each of these modes decays exponentially with distance from the end of the patch on which it is centred. When taken together with the various progressive wave modes in the solution, the trapped modes ensure the continuity of the solution at both ends of the patch.

In §2.2, the formulation of the problem is presented. This is a steady state formulation based upon linear perturbation theory, involving the Fourier transformation of the governing equation and boundary conditions in respect of the horizontal space variable, and leading to a solution for the transform of the perturbation potential. Section 2.2 includes some comments about a linear friction term which is introduced into the analysis both to make the solution determinate, and also to ensure that the waves in the perturbation solution satisfy the radiation, or Sommerfeld, condition. In §2.3, some functions are obtained which are required in the analysis of the particular problem of progressive surface waves incident upon a patch of sinusoidal ripples. In this section, and throughout the remainder of the study, two particular cases are treated. In the first, the unperturbed incident waves in the first order solution are assumed to undergo no attenuation in amplitude as they travel across the ripple patch. This amounts to the use of the theory in a pure form; but, in cases in which there is a substantial reflected wave, it results in a physically unrealistic imbalance between the incident, reflected and transmitted wave energy fluxes. Essentially, the solution provides an upper bound on the size of the reflected wave, at least in resonant cases. The second particular case treated is that in which an energy balance is imposed on the solution by an approach suggested by Davies (1982a). This assumes, with good justification as it turns out, that the attenuation of the incident wave amplitude is a linear function of distance across the patch. On this basis, more realistic results are obtained. The solutions for both the "near" and "far fields", and for both unattenuated and attenuated incident waves, are obtained by a contour integration method which is discussed in

§2.4. Results for the general case in which $l \neq 2k$ (l = ripple wavenumber, k = surface wavenumber) are developed in §2.5, and for the special resonant case in which $l = 2k$ in §2.6. In §2.7, the wave reflection coefficient is discussed, and some computed examples are presented which demonstrate the behaviour of the solution throughout the flow field, The role of the trapped wave modes at the ends of the ripple patch is illustrated, and the implications of the results for bedform stability and sediment movement are considered.

Since we are concerned with an irrotational theory, we take no account of the presence of a (thin) wave boundary layer above the impermeable bed. More importantly, we assume that the flow above the ripples is always nonseparating. This implies that the orbital excursion of the water particles at the bed level (calculated for a notional flat bed) is less than the ripple wavelength (Sleath (1975)). This is not a severe restriction in view of the ratios of surface to bed wavelength which are of concern here, namely those ratios which give rise to substantial reflected waves. There are several further limitations on the theory, which are stated in §2.7; however these do not prevent use of the results obtained in a wide variety of physically interesting cases.

2.2 Formulation

This has been discussed previously by Davies (1980, 1982a), though in a form slightly different from that presented here. As depicted in Fig 1, the bed surface is prescribed about its mean level ($y = -h$) as

$$\zeta(x) = \begin{cases} 0 & -\infty < x \leq L_1 \\ Y_b(x) & \text{in} \quad L_1 \leq x \leq L_2 \\ 0 & L_2 \leq x < \infty \end{cases} \qquad (1)$$

and the departure of the free water surface from its mean level ($y = 0$) is given by $\eta(x,t)$. The prescribed first order velocity potential is denoted by $\Phi(x,y,t)$, and the second order perturbation potential, which expresses the interaction of $\Phi(x,y,t)$ with the bedforms, is denoted by $\phi(x,y,t)$. The governing equation and boundary conditions, correct to second order, are given by

$$\nabla^2 \phi = 0 \quad \text{in} \quad -h \leq y \leq 0 \,, \; -\infty < x < \infty \qquad (2)$$

$$\eta_t + \phi_y = 0 \quad \text{on} \quad y = 0 \quad \text{(kinematical condition)}, \qquad (3)$$

$$g\eta - \phi_t = 0 \quad \text{on} \quad y = 0 \quad \text{(pressure condition)}, \tag{4}$$

$$\phi_y - \Phi_x \zeta_x + \Phi_{yy}\zeta = 0 \quad \text{on} \quad y = -h \quad \text{(kinematical condition)}, \tag{5}$$

in which t is the time, g is gravity, and in which the subscripts indicate differentiation. A detailed derivation of these equations by standard power series expansion methods, and a discussion of their limitations, have been given by Davies (1980, Part 1, §3). In §2.7 these limitations are expressed as a series of conditions involving the length scales introduced in §2.3 to define the surface waves and the ripples. The surface boundary conditions (3) and (4) have been linearized in the usual way. The bottom boundary condition has been linearized also, and expresses the requirement that the component of fluid velocity normal to the bed must vanish. In effect, bottom topography variations are treated as small perturbations on a plane surface, such that the interaction between the (first order) flow which would be present without the perturbations, and the perturbations themselves, involves a new source of (second order) fluid motion situated on the plane surface. From Eqs (1) and (5) this new source can be seen to be a vertical velocity perturbation on y = -h which occurs in $L_1 \leqq x \leqq L_2$. It follows that we may rewrite Eq (5) as

$$\phi_y = \begin{cases} 0 & -\infty < x < L_1 \\ -V_o(x,t) & \text{in} \quad L_1 < x < L_2 \\ 0 & L_2 < x < \infty \end{cases} \tag{6}$$

where

$$V_o(x,t) = -\Phi_x(x,-h,t)\cdot\zeta_x + \Phi_{yy}(x,-h,t)\cdot\zeta \quad . \tag{7}$$

The effects of this disturbance on the fluid as a whole are described by Eqs (2)-(4).

If we prescribe Φ as a periodic function of time and seek a steady state solution of Eqs (2)-(5), we find, for reasons which are well known, that this solution is indeterminate. We therefore employ the device, described by Lamb (1932, Art 232), of introducing into the formulation a small amount of friction proportional to the relative velocity. Although the coefficient of friction is set ultimately to zero, the device ensures the convergence of the integrals arising

in the analysis, and it clarifies the way in which the radiation condition can be satisfied. It should be noted that the introduction of linear friction is essentially a mathematical device which does not accurately represent the way in which dissipation occurs in the flow in reality. It enters the formulation as an additional term in the equations of motion and, hence, appears in the surface pressure condition; in particular, following the integration of the equations of motion, the pressure condition (cf Eq (4)) becomes

$$g\eta - \phi_t - \mu\phi = 0 \qquad \text{on} \qquad y = 0 \tag{4a}$$

in which μ (>0) is the coefficient of friction. Eliminating $\eta(x,t)$ between Eqs (3) and (4a), we obtain

$$g\phi_y + \phi_{tt} + \mu\phi_t = 0 \qquad \text{on} \qquad y = 0 . \tag{8}$$

We now assume that ϕ and its first and second derivatives tend to zero as $|x| \to \infty$, in such a way that Fourier transforms[1] exist in x. Thus Eqs (2), (8) and (6) become

$$\hat{\phi}_{yy} - \xi^2\hat{\phi} = 0 \qquad \text{in} \qquad -h \leq y \leq 0 \ , \ -\infty < \xi < \infty \ , \tag{9}$$

$$g\hat{\phi}_y + \hat{\phi}_{tt} + \mu\hat{\phi}_t = 0 \qquad \text{on} \qquad y = 0 \ , \tag{10}$$

and

$$\hat{\phi}_y = \frac{1}{\sqrt{2\pi}}\int_{-\infty}^{\infty} \phi_y(x,-h,t)\, e^{i\xi x}\, dx = -\frac{1}{\sqrt{2\pi}}\int_{L_1}^{L_2} V_o(x,t)\, e^{i\xi x}\, dx$$

$$= \frac{1}{\sqrt{2\pi}}\Lambda_o(\xi,t) \ , \text{ say} . \tag{11}$$

---

1. Definition

$$\hat{\phi}(\xi,y,t) = \frac{1}{\sqrt{2\pi}}\int_{-\infty}^{\infty} \phi(x,y,t)\, e^{i\xi x}\, dx \ ;$$

$$\phi(x,y,t) = \frac{1}{\sqrt{2\pi}}\int_{-\infty}^{\infty} \hat{\phi}(\xi,y,t)\, e^{-i\xi x}\, d\xi .$$

The solution of Eq (9) is

$$\hat{\phi}(\xi, y, t) = A_0(\xi, t)\cosh(\xi y) + B_0(\xi, t)\sinh(\xi y) \quad ,$$

and we make this specific to the case of waves of frequency σ by taking

$$A_0(\xi,t) = A(\xi)e^{i\sigma t} \quad , \quad B_0(\xi,t) = B(\xi)e^{i\sigma t} \quad \text{and} \quad \Lambda_0(\xi,t) = \Lambda(\xi)e^{i\sigma t}.$$

The solution $\hat{\phi}(\xi,y,t)$ which satisfies Eqs (10) and (11) is then

$$\hat{\phi}(\xi, y, t) = \frac{g\xi\cosh(\xi y) + (\sigma^2 - i\mu\sigma)\sinh(\xi y)}{\sqrt{2\pi}\{(\sigma^2 - i\mu\sigma)\xi\cosh(\xi h) - g\xi^2\sinh(\xi h)\}} \cdot \Lambda_0(\xi, t) \quad .$$

Upon taking the inverse transform, the velocity potential $\phi(x,y,t)$ is given by

$$\phi(x, y, t) = \int_{-\infty}^{\infty} \frac{g\xi\cosh(\xi y) + (\sigma^2 - i\mu\sigma)\sinh(\xi y)}{2\pi\xi\{(\sigma^2 - i\mu\sigma)\cosh(\xi h) - g\xi\sinh(\xi h)\}} \cdot \Lambda(\xi) e^{i(\sigma t - \xi x)} d\xi \quad . \tag{12}$$

This integral determines the solution for both the "near" and "far" fields. The form of Eq (12) differs from that of the equivalent integral obtained by Davies (1982a, Eq (15)). In this earlier work, $V_0(x,t)$ was specified as a real function of space and time and this resulted, upon inversion of the transformed potential, in a purely real velocity potential. Here, for convenience, we take $V_0(x,t)$ as the real part of a complex function. Upon inversion of the transformed potential $\hat{\phi}$, this results in a complex form for ϕ, from which the required velocity potential is obtained by taking the real part. This may be demonstrated quite simply though, for brevity, the details of the argument are not included here. In §2.3 the function $\Lambda(\xi)$ is determined for both unattenuated, and attenuated, incident waves and, in §2.4, the integral in Eq (12) is evaluated by a contour integration method.

2.3 The function $\Lambda(\xi)$

The function $\Lambda(\xi)$ depends upon both the nature of the bedforms and the unperturbed first order motion. The bedforms are assumed to be sinusoidal ripples, such that $Y_b(x)$ in Eq (1) is given by

$$Y_b(x) = b \sin(\ell x + \delta) \,, \tag{13}$$

where b is the ripple amplitude, l is the ripple wavenumber and δ is an arbitrary phase angle. For continuity of bed elevation at the ends of the roughness patch, and for convenience in making comparisons with the later laboratory results, we write

$$L_2 = L = \frac{m\pi}{\ell} \,, \quad L_1 = -L = -\frac{m\pi}{\ell} \quad \text{and} \quad \delta = 0 \,, \tag{14}$$

where m is an integer. Thus there are m ripples in the patch, which is centred on x = 0 and is of length 2L.

2.3.1 Case 1. Unattenuated incident waves.

We assume initially that the incident progressive waves are not attenuated as they pass over the patch, and that the unperturbed velocity potential is given by

$$\Phi_I(x,y,t) = \frac{ga}{\sigma} \cdot \frac{\cosh\{k(y+h)\}}{\cosh(kh)} \cdot \cos(kx - \sigma t) \,, \tag{15}$$

where a, σ and k are the surface wave amplitude, frequency and wavenumber, respectively. Equation (15) corresponds to waves propagating in the +x direction, in which we note that σ, k and the depth h are related by the dispersion equation

$$\sigma^2 = gk \tanh(kh). \tag{16}$$

Using Eqs (1), (13), (14) and (15), we obtain $V_o(x,t)$ from Eq (7) as

$$V_o(x,t) = C_* \{ \ell \sin(kx - \sigma t)\cos(\ell x) + k \cos(\sigma t - kx) \sin \ell x \} \,, \tag{17}$$

where

$$C_* = \frac{gabk}{\sigma \cosh(kh)} \,.$$

It is convenient to take $V_o(x,t)$ as the real part of a complex function and, in particular, as the real part of

$$V_o(x,t) = V(x)\, e^{i\sigma t} ,$$

where, from Eq (17),

$$V(x) = C_* \left\{ \frac{i\ell}{2} \left[e^{i(-k+\ell)x} + e^{i(-k-\ell)x} \right] - \frac{ik}{2} \left[e^{i(-k+\ell)x} - e^{i(-k-\ell)x} \right] \right\} .$$

It follows from Eq (11) that

$$\Lambda(\xi) = -C_* (-1)^m \left\{ e^{i(\xi-k)L} - e^{-i(\xi-k)L} \right\} \cdot \frac{\xi\ell}{(\xi-k)^2 - \ell^2} \cdot \qquad (18)$$

Following the substitution of this expression into Eq (12), we may determine the perturbation potential ϕ for both the near and far fields, subject to the condition that solutions for the far field must only comprise waves satisfying the radiation condition as $x \to \pm \infty$. Now, as noted in §2.1, if the amplitudes of these outgoing waves (and, particularly, of the reflected wave) are not negligible compared with the amplitude a of the incident wave in the first order solution, then the combined velocity potential $(\Phi + \phi)$ will, in general, violate the overall requirements of energy conservation in the solution. This difficulty is overcome, to a great extent, by the procedure described in the following section.

2.3.2 Case 2. Attenuated incident waves

If incident waves are reflected by the bed roughness patch, then the incident wave amplitude must decrease in some way across the patch. Strictly, in the assumed absence of any mechanisms of dissipation, the incident wave energy flux must be balanced by the reflected and transmitted energy fluxes. For the reason given above, this condition is not satisfied, in general, by incident waves which are unattenuated across the patch in the first order solution. In fact, results obtained later on the basis of Eq (17) may be considered as providing upper bounds on the amplitude a_R of the reflected wave. A procedure to impose an energy balance on the solution was proposed by Davies (1982a). In this procedure, the surface wave amplitude in the first order solution was assumed to decrease linearly from its starting value a at x = -L to a new lower value $\tilde{a}_T$ at x = +L. Values of

$\tilde{a}_T$ and $\tilde{a}_R$, the modified transmitted and reflected wave amplitudes well away from the patch, respectively, were required to satisfy the equation

$$a^2 = \tilde{a}_T^2 + \tilde{a}_R^2 \ .$$

The iteration method adopted is not discussed in detail here; essentially, it involved the determination of a final value of the reflected wave amplitude $\tilde{a}_R$ from an initial estimate of a_R based upon Eq (17). There is strong justification for the assumption of linear attenuation of wave amplitude across the ripple patch, at least in resonant cases, both from the results for the wave reflection coefficient (see §2.7.1) which indicate a linear increase in a_R with the number of ripples in the patch, and also from the later experimental results (see §4)[1].

The corrected results for attenuated waves in the first order solution are obtained by replacing $V_o(x,t)$ in Eq (17) by $\tilde{V}_o(x,t)$ where

$$\tilde{V}_o(x,t) = V_o(x,t) \cdot \left\{ \frac{1}{2}\left(1 + \frac{\tilde{a}_T}{a}\right) + \frac{x}{2L}\left(\frac{\tilde{a}_T}{a} - 1\right)\right\} ,$$

such that $\tilde{V}_o(x,t) = V_o(x,t)$ at $x = -L$ and $\tilde{V}_o(x,t) = \frac{\tilde{a}_T}{a} V_o(x,t)$ at $x = L$

(Note that tildes are used hereafter to denote the case in which the incident surface waves are attenuated.) On this basis, the result equivalent to Eq (18) is

$$\tilde{\Lambda}(\xi) = -C_* (-1)^m \left[e^{i(\xi-k)L} \cdot \left\{ \frac{\tilde{a}_T}{a} \cdot \frac{\ell\xi}{(\xi-k)^2 - \ell^2} - \frac{a-\tilde{a}_T}{a} \cdot \frac{i\ell^2}{2m\pi} \cdot \frac{(\xi^2 + \ell^2 - k^2)}{\{(\xi-k)^2 - \ell^2\}^2} \right\} \right.$$

$$\left. + e^{-i(\xi-k)L} \cdot \left\{ - \frac{\ell\xi}{(\xi-k)^2 - \ell^2} + \frac{a-\tilde{a}_T}{a} \cdot \frac{i\ell^2}{2m\pi} \cdot \frac{(\xi^2 + \ell^2 - k^2)}{\{(\xi-k)^2 - \ell^2\}^2} \right\} \right] . \tag{19}$$

Clearly, Eq (18) is recovered if $\tilde{a}_T = a$

While the present approach has the obvious advantage that a proper energy balance is achieved in the solution, it has the disadvantage that the redefined first order waves ($\tilde{\Phi}(x,y,t)$) do not strictly satisfy the potential equation in $-L \leq x \leq L$. (This is an implication arising from the introduction of the linear attenuation term into the expression for the perturbing bottom velocity $\tilde{V}_o(x,t)$.)

---

1. The theory of Long (1973), when applied to the present geometry, also predicts a linear attenuation of the incident wave with penetration into the scattering patch (Long, personal communication).

However this drawback, which in practice is of minor significance, does not extend to the perturbation solution, since the disturbance wave still satisfies Eqs (2) to (5).

2.4 The contour integration method

We now consider the evaluation of the integral on the right hand side of Eq (12) by contour integration. Initially, the approach adopted is to take ξ as the real part of a complex variable $\lambda = \xi + i\chi$, and to replace the path of integration $-\infty < \xi < \infty$, by a closed contour in the λ - plane. This contour is chosen as a semi-circle of radius r, which includes the portion $-r < \xi < r$ of the real axis of λ. The semi-circle, which completes the contour, is chosen in either the upper or lower half plane such that a physically admissible solution is obtained. In this section, we identify all the singularities of the integrand in Eq (12), and we show how certain groups of these singularities contribute to the solution in different parts of the flow field. Where singularities lie on the contour of integration, in particular on the ξ - axis, the contour is indented. The indentations are made in either the upper or lower half plane, such that the contributions to the solution from the singularities in question enable the bottom boundary condition (6) to be satisfied. Ultimately, as the radii of the indentations tend to zero and as $r \to \infty$, the required path of integration, namely the ξ - axis, becomes part of the complete contour. Moreover, since the semi-circular portion of the contour makes a contribution to the solution which tends to zero as $r \to \infty$ (see Davies (1980, Part 2, §2.1.1)), the required result for the velocity potential is simply equal to the result obtained by integrating around the complete contour.

We consider, firstly, the singularities associated with the term in the brace in the denominator in (12). If we write $\lambda = \xi + i\chi$, these singularities are at positions $\lambda = \lambda_p$ which satisfy the equation

$$(\sigma^2 - i\mu\sigma)\cosh(\lambda_p h) - g\lambda_p \sinh(\lambda_p h) = 0. \qquad (20)$$

Each solution of this equation gives rise to a simple pole. Two poles lie close to the real axis of λ, at $\lambda_p = k - i\mu k_o$ and $-k + i\mu k_o (\mu > 0, k_o > 0)$, where Eq (16) has been used in the solution of (20). The first of these is displaced slightly into the fourth quadrant, and the second into the second quadrant, as a result of the presence of the linear friction term. In addition, there is an infinite number of poles (λ_p) closely adjacent to the imaginary axis of λ. For non-zero μ, these

poles are subject to small real displacements from reference positions ($\lambda_o = i\chi_o$) determined, with $\mu = 0$, from solutions of the equation

$$\sigma^2 = -g\chi_o \tan(\chi_o \ell) . \tag{21}$$

These poles are associated with trapped wave modes near both ends of the ripple patch, while the poles on, or closely adjacent to, the real axis of λ are associated with travelling waves.

We consider next the singularities associated with the functions $\Lambda(\xi)$ and $\tilde{\Lambda}(\xi)$, given by Eqs (18) and (19) respectively. We start by replacing $\Lambda(\xi)$ and $\tilde{\Lambda}(\xi)$ by $\Lambda(\lambda)$ and $\tilde{\Lambda}(\lambda)$, respectively. For convenience, we write the function $\Lambda(\lambda)$ in the form

$$\Lambda(\lambda) = f_1(\lambda)\, e^{i(\lambda-k)L} + f_2(\lambda)\, e^{-i(\lambda-k)L} , \tag{22}$$

where

$$\left.\begin{aligned} f_1(\lambda) &= -C_*(-1)^m \frac{\lambda\ell}{(\lambda-k)^2-\ell^2} , \\ \text{and} \qquad f_2(\lambda) &= C_*(-1)^m \frac{\lambda\ell}{(\lambda-k)^2-\ell^2} = -f_1(\lambda) . \end{aligned}\right\} \tag{23}$$

Note that both $f_1(\lambda)$ and $f_2(\lambda)$ are singular if $\lambda = k \pm 1$. Similarly, we write the function $\tilde{\Lambda}(\lambda)$ in the form

$$\tilde{\Lambda}(\lambda) = \tilde{f}_1(\lambda)\, e^{i(\lambda-k)L} + \tilde{f}_2(\lambda)\, e^{-i(\lambda-k)L} , \tag{24}$$

where

$$\left.\begin{aligned} \tilde{f}_1(\lambda) &= -C_*(-1)^m \left\{ \frac{\tilde{a}_r}{a} \cdot \frac{\lambda\ell}{(\lambda-k)^2-\ell^2} - \frac{a-\tilde{a}_r}{a} \cdot \frac{i\ell^2}{2m\pi} \cdot \frac{\lambda^2+\ell^2-k^2}{\{(\lambda-k)^2-\ell^2\}^2} \right\} , \\ \text{and} \qquad \tilde{f}_2(\lambda) &= -C_*(-1)^m \left\{ -\frac{\lambda\ell}{(\lambda-k)^2-\ell^2} + \frac{a-\tilde{a}_r}{a} \cdot \frac{i\ell^2}{2m\pi} \cdot \frac{\lambda^2+\ell^2-k^2}{\{(\lambda-k)^2-\ell^2\}^2} \right\} . \end{aligned}\right\} \tag{25}$$

Upon setting $\tilde{a}_T = a$ in Eqs (25), Eqs (23) are recovered, as expected. Also it may be noted that, while $f_1(\lambda)$ and $f_2(\lambda)$ have simple poles at $\lambda = k \pm 1$, the functions $\tilde{f}_1(\lambda)$ and $\tilde{f}_2(\lambda)$ have both simple and double poles at these points. A further important consideration is that, in the limits $\mu \to 0$ and $1 \to 2k$, the pole at $(k - 1)$ and the pole identified earlier at $(-k + i\mu k_o)$ approach one another; this situation constitutes a special case which is later treated separately.

To obtain a physically meaningful solution, it is necessary to ensure that the inversion integral (Eq (12)) is convergent. If we substitute Eq (22) (or Eq (24) as appropriate) into Eq (12), define the function $\psi_\mu(\lambda)$ by

$$\psi_\mu(\lambda) = \frac{g\lambda \cosh(\lambda y) + (\sigma^2 - i\mu\sigma)\sinh(\lambda y)}{2\pi\lambda\{(\sigma^2 - i\mu\sigma)\cosh(\lambda k) - g\lambda \sinh(\lambda k)\}}, \qquad (26)$$

and replace the limits of integration in (12) by integration around a closed contour C in the λ -plane, then (12) becomes

$$\phi(x,y,t) = \int_C \{\psi_\mu(\lambda) f_1(\lambda) e^{i\lambda(L-x)} e^{i(\sigma t - kL)} + \psi_\mu(\lambda) f_2(\lambda) e^{-i\lambda(L+x)} e^{i(\sigma t + kL)}\} d\lambda ,$$

$$= \qquad I_1 \qquad + \qquad I_2 \qquad , \text{ say.} \qquad (27)$$

Here we have split the integral into two parts, I_1 containing the f_1 - term and I_2 containing the f_2 - term. The convergence of these two integrals is governed by the terms $\exp(i\lambda(L - x))$ and $\exp(-i\lambda(L + x))$, and the decaying parts of these terms are

$$\left.\begin{aligned} & e^{i\lambda(L-x)} \sim e^{-\lambda(L-x)} \\ \text{and} \quad & \\ & e^{-i\lambda(L+x)} \sim e^{\lambda(L+x)} , \end{aligned}\right\} \qquad (28)$$

respectively. We are now in a position to choose contours for integration which ensure convergent solutions in the three regions $x < -L$, $|x| < L$ and $x > L$. From (12), it is required that, ultimately, each contour includes the real axis of λ. Our choice in the matter is in how to close the contours, and this is dictated by

(28) as follows:

(i) if $x < -L$, the contours for both integrals I_1 and I_2 must be closed in the upper half plane;

(ii) if $|x| < L$, the contour for integral I_1 must be closed in the upper half plane and the contour for integral I_2 must be closed in the lower half plane; and

(iii) if $x > L$, the contours for both integrals I_1 and I_2 must be closed in the lower half plane.

Evidently, the division of the integral into two parts is necessary only if $|x| < L$. If $x < -L$ or $x > +L$, the same contour is taken for I_1 and I_2 and the function $\Lambda(\lambda)$ may therefore be utilized in its original form. The significance of this is that the function $\Lambda(\lambda)$ is nonsingular at $\lambda = k \pm 1$, whereas the functions $f_1(\lambda)$ and $f_2(\lambda)$ are singular at these points, as established earlier.

At this stage, the role of the linear friction term is apparent. As a result of the displacements of the poles close to $\lambda = -k$ and $+k$ into the second and fourth quadrants respectively, the former pole is included in the contour of integration only if C is taken in the upper half plane and the latter pole is included only if C is taken in the lower half plane. Having established this, we can dispense with the friction term and, in what follows, we take $\mu = 0$ and simply refer to the positions of the poles as $\lambda = -k$ and $+k$.

In summary, the singularities to be considered are as follows:

(i) if $x < -L$, we have a simple pole at $\lambda = -k$ and an infinite number of simple poles at $\lambda = i\chi_0$ $(\chi_0 > 0)$, as given by Eq (21);

(ii) if $|x| < L$, we have simple poles at $\lambda = -k$ and $+k$, simple (or both simple and double) poles at $\lambda = k - 1$ and $k + 1$, and an infinite number of simple poles at $\lambda = i\chi_0$ $(\chi_0 \lesseqgtr 0)$; and

(iii) if $x > +L$, we have a simple pole at $\lambda = k$ and an infinite number of simple poles at $\lambda = i\chi_0$ $(\chi_0 < 0)$.

We shall find that the pole at $\lambda = -k$ is associated with the outgoing wave in $x < -L$, and that the pole at $\lambda = +k$ is associated with the outgoing wave in $x > L$. In $|x| < L$, there are contributions from these two poles, as well as from the poles at $(k \pm 1)$. These latter contributions enable the bottom boundary condition to be satisfied over the ripple patch and, in practice, this requirement dictates the sense in which indentations around the two poles are made. The poles on the imaginary axis of λ ensure the smooth continuation of the solution at the ends of the patch $(x = \pm L)$.

The required contours C_1 and C_2 are shown in Figure 2, and the interpretation to be placed on the poles shown on the contours at $\lambda = -k$ and $+k$ is as given above. For convenience, we persist with the division of the integral into two parts for the purpose of stating the results, though this is not strictly necessary if $|x| > L$. Note that as the radius of the semi-circular portion of each of the contours C_1 and C_2 tends to infinity, the contour encompasses all the poles on the χ-axis in the upper or lower half plane, respectively. The contour itself includes the entire real axis of λ as required; it may be shown that the semi-circular portion makes no contribution to the final results. It remains only to determine the residues of the various poles identified above, and to construct the solution on the basis established in Figure 2. This is done in §2.5 for the general case in which $1 \neq 2k$, and in §2.6 for the special case $1 = 2k$ in which the pole at $k - 1$ coincides with the pole at $-k$.

2.5 Solution for the general case ($1 \neq 2k$)

We consider the regions $x < -L$, $x > L$ and $|x| < L$ in turn, and state the results in a general way. We denote the residues of the poles by R, with a subscript indicating the pole position and a superscript indicating which integral (I_1 or I_2) is being considered.

2.5.1 Solution for $x < -L$

For both integrals I_1 and I_2 the contour C_1 contains the pole at $\lambda = -k$ (residue R_{-k}) and the poles on the positive imaginary axis (residues R_j, say, where $j = 1, 2, 3 \ldots$ denote the positions $\chi_0 = \chi_1, \chi_2, \chi_3 \ldots$ given by Eq (21) for $\chi_0 > 0$).

For integral I_1 we have

$$\oint_{C_1}^{(1)} = \oint_{C_1}^{(1)} \{\quad\} d\lambda = 2\pi i \left\{ R_{-k}^{(1)} + \sum_{j=1}^{\infty} R_j^{(1)} \right\} \tag{29}$$

(where the empty brace denotes the appropriate term of the integrand in Eq (27)), and for integral I_2 we have

$$\oint_{C_1}^{(2)} = \oint_{C_1}^{(2)} \{\quad\} d\lambda = 2\pi i \left\{ R_{-k}^{(2)} + \sum_{j=1}^{\infty} R_j^{(2)} \right\}. \tag{30}$$

It follows that the final result for $x < -L$ is given by

$$\phi(x,y,t) = \oint_{C_1}^{(1)} + \oint_{C_1}^{(2)} . \tag{31}$$

2.5.2 Solution for $x > +L$

For both integrals I_1 and I_2 the contour contains the pole at $\lambda = +k$ (residue R_k) and the poles on the negative imaginary axis (residues R_{-j}, say, where $j = 1, 2, 3 \ldots$ denote the positions $\chi_0 = -\chi_1, -\chi_2, -\chi_3 \ldots$ given by Eq (21) for $\chi_0 < 0$).

For integral I_1 we now have

$$\oint_{C_2}^{(1)} = -\oint_{C_2}^{(1)} \{ \quad \} d\lambda = -2\pi i \left\{ R_k^{(1)} + \sum_{j=1}^{\infty} R_{-j}^{(1)} \right\}, \tag{32}$$

and for integral I_2 we have

$$\oint_{C_2}^{(2)} = -\oint_{C_2}^{(2)} \{ \quad \} d\lambda = -2\pi i \left\{ R_k^{(2)} + \sum_{j=1}^{\infty} R_{-j}^{(2)} \right\}, \tag{33}$$

where the minus signs are included on account of the need to integrate along the ξ-axis in the ξ-positive direction. The final result for $x > +L$ is given by

$$\phi(x,y,t) = \oint_{C_2}^{(1)} + \oint_{C_2}^{(2)} . \tag{34}$$

2.5.3 Solution for $|x| < L$

Part of the solution in $|x| < L$ comprises terms identified above, namely the terms $\phi_{C_1}^{(1)}$ and $\phi_{C_2}^{(2)}$. To these terms must be added contributions from the poles at $\lambda = k \pm 1$, which we denote by ϕ_{k-1} and ϕ_{k+1}. The solution for $|x| < L$ may therefore be written

$$\phi(x,y,t) = \oint_{C_1}^{(1)} + \oint_{C_2}^{(2)} + \phi_{k-\ell} + \phi_{k+\ell} . \tag{35}$$

The essential requirement on ϕ_{k-1} and ϕ_{k+1} is that their sum satisfies the bottom

boundary condition over the ripple patch, and this is achieved by indenting the contours C_1 and C_2 as shown in Figure 2. The resulting solution (35) is then one which also provides a smooth transition in $\phi(x, y, t)$ across the ends of the ripple patch ($x = \pm L$). Since, for integral I_1, the direction of integration along the real axis is as required but, for integral I_2, this is not so, we may express the contributions to the final solution as

$$\phi_{k-\ell} = \pi i R^{(1)}_{k-\ell} - \pi i R^{(2)}_{k-\ell} \quad , \tag{36}$$

and

$$\phi_{k+\ell} = \pi i R^{(1)}_{k+\ell} - \pi i R^{(2)}_{k+\ell} \quad , \tag{37}$$

where R_{k-1} and R_{k+1} are the residues at $\lambda = (k-1)$ and $(k+1)$ respectively, and where the superscripts again denote the integral involved. The final result for $|x| < L$ may therefore be expressed by

$$\begin{aligned} \phi(x,y,t) = 2\pi i \left[R^{(1)}_{-k} + \sum_{j=1}^{\infty} R^{(1)}_{j} + R^{(2)}_{k} + \sum_{j=1}^{\infty} R^{(2)}_{-j} \right] \\ + \pi i \left[R^{(1)}_{k+\ell} - R^{(2)}_{k+\ell} + R^{(1)}_{k-\ell} - R^{(2)}_{k-\ell} \right] . \end{aligned} \tag{38}$$

2.5.4 Residues

It remains only to calculate the residues for Eqs (29), (30), (32), (33), (36) and (37). It was noted earlier that at each of the positions $\lambda = \lambda_p$ given by Eq (20), there is a simple pole provided that $1 \neq 2k$. Now since each of these positions $\lambda = \lambda_p$ is an ordinary point of the function

$$\frac{g\lambda \cosh(\lambda y) + (\sigma^2 - i\mu\sigma)\sinh(\lambda y)}{2\pi\lambda} \cdot f_1(\lambda)\, e^{i\lambda(L-x)}\, e^{i(\sigma t - kL)} \quad ,$$

and also of the function

$$\frac{g\lambda \cosh(\lambda y) + (\sigma^2 - i\mu\sigma)\sinh(\lambda y)}{2\pi\lambda} \cdot f_2(\lambda)\, e^{-i\lambda(L+x)}\, e^{i(\sigma t + kL)} \quad ,$$

which appear in the integrands of I_1 and I_2 in Eq (27) respectively, and since also

$$\lim_{\lambda \to \lambda_p} \frac{\lambda - \lambda_p}{(\sigma^2 - i\mu\sigma)\cosh(\lambda h) - g\lambda \sinh(\lambda h)} = \frac{-2\cosh(\lambda_p h)}{g\{2\lambda_p h + \sinh(2\lambda_p h)\}} ,$$

we obtain the following general results for the required residues. For integral I_1, and for the typical pole at $\lambda = \lambda_p$, we have

$$R^{(1)}_{\lambda_p} = \frac{1}{2\pi\lambda_p}\{g\lambda_p \cosh(\lambda_p y) + \sigma^2 \sinh(\lambda_p y)\} \cdot \frac{-2\cosh(\lambda_p h)}{g\{2\lambda_p h + \sinh(2\lambda_p h)\}} \cdot \cdot f_1(\lambda_p) e^{i\lambda_p(L-x)} e^{i(\sigma t - kL)} , \tag{39}$$

and, for integral I_2, we have

$$R^{(2)}_{\lambda_p} = \frac{1}{2\pi\lambda_p}\{g\lambda_p \cosh(\lambda_p y) + \sigma^2 \sinh(\lambda_p y)\} \cdot \frac{-2\cosh(\lambda_p h)}{g\{2\lambda_p h + \sinh(2\lambda_p h)\}} \cdot \cdot f_2(\lambda_p) e^{-i\lambda_p(L+x)} e^{i(\sigma t + kL)} , \tag{40}$$

in which μ has been set to zero. The particular results required are obtained by taking $\lambda_p = -k$, $+k$ or $i\chi_0$ in (39) and (40), and hence in (23) or (25), as appropriate.

Finally, we consider the residues at $\lambda = k \pm 1$. Since the functions $\tilde{f}_1(\lambda)$ and $\tilde{f}_2(\lambda)$ in Eq (25) have both simple and double poles at $\lambda = k \pm 1$, we proceed with the calculations in a rather more formal way. Initially, we define the function $F(\lambda)$ by

$$F(\lambda) = \psi(\lambda) e^{i(\sigma t - \lambda x)}$$

in which $\psi(\lambda)$ is given by Eq (26) with $\mu = 0$, and we also write

$$\Lambda(\lambda) = \Lambda_1(\lambda) + \Lambda_2(\lambda) ,$$

such that the integrand of I_1 in Eq (27) is $F(\lambda)\Lambda_1(\lambda)$ and the integrand of I_2 is $F(\lambda)\Lambda_2(\lambda)$. For convenience, we write

$$\lambda_1 = k + \ell \quad \text{and} \quad \lambda_2 = k - \ell .$$

Consider firstly, the case of incident surface waves which are unattenuated (Eqs (22) and (23)). In the neighbourhood of $\lambda = \lambda_1$, $\psi(\lambda)$ is nonsingular and may be expanded as a Taylor series, as follows:

$$\psi(\lambda) = \psi(\lambda_1) + (\lambda-\lambda_1)\psi'(\lambda_1)\cdots \quad .$$

By writing appropriate expansions for the remaining terms of both integrands in the neighbourhood of $\lambda = \lambda_1$, the required residues are given simply by the coefficients of the terms in $(\lambda - \lambda_1)^{-1}$. From the function $F(\lambda)\Lambda_1(\lambda)$, the residue $R_{\lambda_1}^{(1)} = R_{k+1}^{(1)}$ is given by

$$R_{k+\ell}^{(1)} = -\frac{C_*(-1)^m}{2} \cdot \lambda_1 \psi(\lambda_1) e^{i(L-x)\lambda_1} e^{i(\sigma t - kL)} \quad , \tag{41}$$

and, from the function $F(\lambda)\Lambda_2(\lambda)$, the residue $R_{\lambda_1}^{(2)} = R_{k+1}^{(2)}$ is given by

$$R_{k+\ell}^{(2)} = \frac{C_*(-1)^m}{2} \cdot \lambda_1 \psi(\lambda_1) e^{-i(L+x)\lambda_1} e^{i(\sigma t + kL)} \quad . \tag{42}$$

Similarly, in the neighbourhood of $\lambda = \lambda_2$, $\psi(\lambda)$ is nonsingular and may be expressed by

$$\psi(\lambda) = \psi(\lambda_2) + (\lambda-\lambda_2)\psi'(\lambda_2)\cdots \quad .$$

The results in this case are, from the function $F(\lambda)\Lambda_1(\lambda)$,

$$R_{\lambda_2}^{(1)} = R_{k-\ell}^{(1)} = \frac{C_*(-1)^m}{2} \cdot \lambda_2 \psi(\lambda_2) e^{i(L-x)\lambda_2} e^{i(\sigma t - kL)} \quad , \tag{43}$$

and, from the function $F(\lambda)\Lambda_2(\lambda)$,

$$R_{\lambda_2}^{(2)} = R_{k-\ell}^{(2)} = \frac{-C_*(-1)^m}{2} \cdot \lambda_2 \psi(\lambda_2) e^{-i(L+x)\lambda_2} e^{i(\sigma t + kL)} \quad . \tag{44}$$

The combined result for the poles at $\lambda = k \pm 1$ may therefore be written as follows:

$$\phi_{k+\ell} + \phi_{k-\ell} = 2\pi i \left\{ \psi(\lambda_1) \cdot \frac{-C_* \lambda_1}{2} \cdot e^{i(\sigma t - \lambda_1 x)} + \psi(\lambda_2) \cdot \frac{C_* \lambda_2}{2} \cdot e^{i(\sigma t - \lambda_2 x)} \right\} . \quad (45)$$

For incident waves which are attenuated, the same procedure is followed but with $f_1(\lambda)$ and $f_2(\lambda)$, given by Eq (23), replaced by $\tilde{f}_1(\lambda)$ and $\tilde{f}_2(\lambda)$, given by Eq (25). The only essential difference in the results is that the double poles at $\lambda = \lambda_1$ and λ_2 draw additional terms into the coefficients of $(\lambda - \lambda_1)^{-1}$ and $(\lambda - \lambda_2)^{-1}$. As usual, we denote all results for the case in which the incident waves are attenuated by tildes, and we write

$$\tilde{\Lambda}(\lambda) = \tilde{\Lambda}_1(\lambda) + \tilde{\Lambda}_2(\lambda)$$

where the terms on the right hand side relate to integrals I_1 and I_2, respectively. In the neighbourhood of $\lambda = \lambda_1$, the residue from the term $F(\lambda)\tilde{\Lambda}_1(\lambda)$ is given by

$$\tilde{R}^{(1)}_{\lambda_1} = \tilde{R}^{(1)}_{k+\ell} = \left[\psi(\lambda_1) \cdot \lambda_1 \frac{\tilde{a}_\tau}{a} + \psi(\lambda_1) \left(\frac{\tilde{a}_\tau - a}{a} \right) \frac{i\ell\lambda_1}{2m\pi} \cdot i(L-x) + \psi'(\lambda_1) \left(\frac{\tilde{a}_\tau - a}{a} \right) \frac{i\ell\lambda_1}{2m\pi} \right] \quad (46)$$

$$\cdot \frac{C_* (-1)^m}{2} \cdot e^{i(L-x)\lambda_1} e^{i(\sigma t - kL)} ,$$

and, from the term $F(\lambda)\tilde{\Lambda}_2(\lambda)$, by

$$\tilde{R}^{(2)}_{\lambda_1} = \tilde{R}^{(2)}_{k+\ell} = \left[-\psi(\lambda_1) \cdot \lambda_1 + \psi(\lambda_1) \left(\frac{a - \tilde{a}_\tau}{a} \right) \frac{i\ell\lambda_1}{2m\pi} \cdot -i(L+x) + \psi'(\lambda_1) \left(\frac{a - \tilde{a}_\tau}{a} \right) \frac{i\ell\lambda_1}{2m\pi} \right] \quad (47)$$

$$\cdot \frac{-C_* (-1)^m}{2} \cdot e^{-i(L+x)\lambda_1} e^{i(\sigma t + kL)} .$$

In the neighbourhood of $\lambda = \lambda_2$, the residue from the term $F(\lambda)\tilde{\Lambda}_1(\lambda)$ is given by

$$\tilde{R}^{(1)}_{\lambda_2} = \tilde{R}^{(1)}_{k-\ell} = \left[-\psi(\lambda_2) \cdot \lambda_2 \frac{\tilde{a}_\tau}{a} + \psi(\lambda_2) \left(\frac{a - \tilde{a}_\tau}{a} \right) \frac{i\ell\lambda_2}{2m\pi} \cdot i(L-x) + \psi'(\lambda_2) \left(\frac{a - \tilde{a}_\tau}{a} \right) \frac{i\ell\lambda_2}{2m\pi} \right]$$

$$\cdot \frac{-C_* (-1)^m}{2} \cdot e^{i(L-x)\lambda_2} e^{i(\sigma t - kL)} , \quad (48)$$

and, from the term $F(\lambda)\tilde{A}_2(\lambda)$, by

$$\tilde{R}^{(2)}_{\lambda_2} = \tilde{R}^{(2)}_{k-\ell} = \left[\psi(\lambda_2)\cdot\lambda_2 + \psi(\lambda_2)\left(\frac{a-\tilde{a}_T}{a}\right)\frac{i\ell\lambda_2}{2m\pi}\cdot i(L+x) + \psi'(\lambda_2)\left(\frac{a-\tilde{a}_T}{a}\right)\cdot\frac{-i\ell\lambda_2}{2m\pi}\right] \tag{49}$$

$$\cdot\frac{-C_*(-1)^m}{2}\cdot e^{-i(L+x)\lambda_2}\, e^{i(\sigma t+kL)}.$$

Note that results (41) to (44) are recovered from (46) to (49) respectively, by setting $\tilde{a}_T = a$. The combined result for the poles at $\lambda = \lambda_1$ and λ_2 in this case is

$$\tilde{\phi}_{k+\ell} + \tilde{\phi}_{k-\ell} = -\pi i C_*\left[\left\{\frac{a+\tilde{a}_T}{2a} - \frac{a-\tilde{a}_T}{a}\cdot\frac{\ell x}{2m\pi}\right\}\left\{\psi(\lambda_1)\lambda_1 e^{i(\sigma t-\lambda_1 x)} - \psi(\lambda_2)\lambda_2 e^{i(\sigma t-\lambda_2 x)}\right\}\right. \tag{50}$$

$$\left. - \frac{a-\tilde{a}_T}{a}\cdot\frac{i\ell}{2m\pi}\left\{\psi'(\lambda_1)\lambda_1 e^{i(\sigma t-\lambda_1 x)} - \psi'(\lambda_2)\lambda_2 e^{i(\sigma t-\lambda_2 x)}\right\}\right].$$

In the cases of both unattenuated and attenuated incident waves, the sum of the results for the poles at $\lambda = \lambda_1$ and λ_2 satisfies the appropriate bottom boundary condition over the ripple patch. All the other poles in the solution satisfy a flat bed boundary condition ($\phi_y = 0$ on $y = -h$). It remains only to determine the functions $\psi(\lambda_1)$, $\psi'(\lambda_1)$, $\psi(\lambda_2)$ and $\psi'(\lambda_2)$, and these results are listed in Appendix 2.1.

At this stage, let us summarize the results for the general case in which $1 \neq 2k$. In $x < -L$, the potential is given by Eq (31) and the residues in (29) and (30) are given by (39) and (40). In $x > +L$, the potential is given by Eq (34) and the residues in (32) and (33) are also given by (39) and (40). In $|x| < L$, the potential is given by Eq (35), and this involves both terms which appear in (31) and (34), and additional terms given by (45) or (50), as appropriate. In diagrammatic form, the perturbation solution comprises the various parts shown in Figure 3. Herein, each arrow represents a propagating wave mode, and against each arrow is indicated the pole position with which the wave is associated. The direction of travel of the wave is indicated by the arrow head; for example, the $(k + 1)$ -wave is in the onward transmitted $(+x)$ direction, while the $(k - 1)$ -wave may travel in either direction depending upon whether $k \gtrless 1$. Note that, from integral I_1, there is a wave associated with the pole at $(-k)$ which travels off the patch in the negative x-direction. Similarly, from integral I_2, there is a

wave associated with the pole at (+k) which travels off the patch in the positive x-direction. In the next section, we establish equivalent results for the special case in which $l = 2k$.

2.6 Solution for the special case in which $l = 2k$

As $l \to 2k$, the position of the pole at $\lambda = (k - l)$ tends towards that of the pole at $\lambda = -k$, and each of the earlier residues $R_{-k}^{(1)}$, $R_{-k}^{(2)}$, $R_{k-1}^{(1)}$ and $R_{k-1}^{(2)}$ becomes singular. For this reason, we treat $l = 2k$ as a special case. On the up-wave side of the ripple patch ($x < -L$), it is necessary to recalculate the result for the outgoing wave in the perturbation solution, since the residues $R_{-k}^{(1)}$ and $R_{-k}^{(2)}$ in Eqs (29) to (31) are separately singular. It is necessary also to recalculate the earlier results for the region of the ripple patch itself ($|x| < L$), on account of the merging of the two pole positions. In the case of unattenuated incident surface waves, this merging gives rise to a double pole at $\lambda = -k$ and, in the case of attenuated waves, to a triple pole. However, on the down-wave side of the ripple patch ($x > L$), the solution is independent of the poles at $\lambda = -k$ and $\lambda = k - 1$, and so the earlier solution remains unaltered. Let us consider the regions $x < -L$ and $|x| < L$ in turn.

2.6.1 Results for $x < -L$

In the general case in which $l \neq 2k$, the result for the outgoing wave in the perturbation solution is given, as $x \to -\infty$, by

$$\phi(x,y,t) = 2\pi i \left\{ R_{-k}^{(1)} + R_{-k}^{(2)} \right\} . \qquad (51)$$

Now, if $l = 2k$, each of the terms $f_1(-k)$ and $f_2(-k)$ for unattenuated incident waves, or $\tilde{f}_1(-k)$ and $\tilde{f}_2(-k)$ for attenuated waves, is singular, and it follows that $R_{-k}^{(1)}$ and $R_{-k}^{(2)}$ are singular also. This is not the case for the sum of these residues however, as may be demonstrated either by examining their sum in the limit $l \to 2k$, or by considering the complete functions $\Lambda(\lambda)$ or $\tilde{\Lambda}(\lambda)$, as appropriate, and calculating independently the residue of the entire integrand in (27).

For unattenuated incident waves, the function $\Lambda(\lambda)$ is given by Eq (22). If $\lambda = -k + q$ where q is small, and $\Lambda(\lambda)$ is expressed as a series in powers of q, then in the neighbourhood of $\lambda = \lambda_2 = -k$, and for $l = 2k$, we obtain

$$\Lambda(\lambda_2 + q) = -C_* \frac{im\pi}{2} + O(q) .$$

If the function $\psi(\lambda)$ is also expressed as a series in powers of q, the leading term is a term in q^{-1} and this governs the residue of the integrand in Eq (27). The final result for the potential may be expressed by

$$\phi(x,y,t) = \frac{gk\cosh(ky) + \sigma^2\sinh(ky)}{k} \cdot \frac{2\cosh(kh)}{g\{2kh + \sinh(2kh)\}} \cdot \frac{C_* m\pi}{2} \cdot e^{i(\sigma t + kx)} . \quad (52)$$

If $l = 2k$, this result replaces the contributions for the general case, which appear on the right hand side of Eq (51).

For attenuated incident waves, the function $\tilde{\Lambda}(\lambda)$ is given by Eq (24). Now, in the neighbourhood of $\lambda = \lambda_2 = -k$, we obtain

$$\tilde{\Lambda}(\lambda_2 + q) = -\frac{C_*}{2}\left[\frac{3}{4}\left(1 - \frac{\tilde{a}_T}{a}\right) + \frac{im\pi}{2}\left(1 + \frac{\tilde{a}_T}{a}\right)\right] + O(q) ,$$

and the final result for the potential is

$$\phi(x,y,t) = \frac{gk\cosh(ky) + \sigma^2\sinh(ky)}{k} \cdot \frac{2\cosh(kh)}{g\{2kh + \sinh(2kh)\}} \cdot \frac{-C_*}{2} \cdot$$
$$\cdot \left[\frac{3}{4}\left(1 - \frac{\tilde{a}_T}{a}\right) + \frac{im\pi}{2}\left(1 + \frac{\tilde{a}_T}{a}\right)\right] \cdot i\, e^{i(\sigma t + kx)} . \quad (53)$$

This reduces to Eq (52) if $\tilde{a}_T = a$, and the result replaces the contributions arising from the terms on the right hand side of (51) in the special case in which $l = 2k$.

2.6.2 Results for $|x| < L$

In the special case in which $l = 2k$, we have

$$\lambda_1 = k + l = 3k \quad \text{and} \quad \lambda_2 = k - l = -k ,$$

so that the pole at $\lambda = \lambda_2$ coincides with the existing pole at $\lambda = -k$ (see Fig 2). The way in which this merging of the poles occurs is complicated by the fact that, in the general case ($l \neq 2k$), integral I_1 involves a complete anticlockwise circuit

around the pole at $\lambda = -k$, but only half a circuit (indentation) around the pole at $(k - 1)$; by comparison, integral I_2 involves a half circuit (indentation) around the pole at $(k - 1)$, and no contribution from the pole at $(-k)$. In Eq (38), the contributions from the poles at $(-k)$ and $(k - 1)$ were expressed, for integral I_1, by

$$2\pi i R_{-k}^{(1)} + \pi i R_{k-1}^{(1)}$$

and, for integral I_2, by

$$-\pi i R_{k-1}^{(2)} .$$

If we partition the result for I_1 as follows:

$$\pi i \left(R_{-k}^{(1)} + R_{k-1}^{(1)} \right) + \pi i R_{-k}^{(1)} ,$$

we can consider the first term to consist of contributions from two indentations of the same type (ie anticlockwise half circuits) around the poles at $(-k)$ and $(k - 1)$, and the second term simply to be a residual contribution from the pole at $(-k)$. It follows that, in the limit $1 \to 2k$, only the result for the first term is directly affected by the merging of the poles, and this result must be recalculated on the basis of a single half circuit (indentation) of the combined pole at $\lambda = -k$. This new pole is a double or a triple pole for the cases of unattenuated and attenuated incident waves, respectively. We express the result for the first term by $\pi i \, R_{*\lambda_2}^{(1)}$, which is finite as required. However, as noted earlier, the residue $R_{-k}^{(1)}$ is singular if $1 = 2k$, and so the second term of the partitioned expression is singular also. We overcome this difficulty by rewriting the result for integral I_2, for the general case $(1 \neq 2k)$, as follows:

$$-\pi i \left(R_{-k}^{(2)} + R_{k-1}^{(2)} \right) + \pi i R_{-k}^{(2)} .$$

In this form, we can again consider the first term to consist of contributions from two indentations of the same type around the poles at $(-k)$ and $(k - 1)$, and the second term to be a residual contribution. As $1 \to 2k$, the result for the

first term must be recalculated and again, on account of the partitioning, the new result is obtained from a single half circuit of the combined pole at $\lambda = -k$. This result, which we express by $-\pi i R^{(2)}_{*\lambda_2}$, is finite as required, whereas the result for the second residual term involving $R^{(2)}_{-k}$ is singular. If we add the revised contributions from integrals I_1 and I_2, we obtain the combined result

$$\pi i R^{(1)}_{*\lambda_2} + \pi i R^{(1)}_{-k} - \pi i R^{(2)}_{*\lambda_2} + \pi i R^{(2)}_{-k}$$

$$= \pi i \left(R^{(1)}_{*\lambda_2} - R^{(2)}_{*\lambda_2} \right) + \pi i \left(R^{(1)}_{-k} + R^{(2)}_{-k} \right).$$

By comparison with Eq (51), the residual terms may be seen to make a contribution which is equal to exactly one half of the potential of the outgoing wave in $x < -L$ (Eq (52) or (53), as appropriate). So, although the residual terms are separately singular if $l = 2k$, their sum is finite, as required.

The result for this special case in which $l = 2k$ may be obtained alternatively by starting with the expression for the general case, namely

$$2\pi i R^{(1)}_{-k} + \pi i R^{(1)}_{k-\ell} - \pi i R^{(2)}_{k-\ell} \quad ,$$

and by formally investigating the limit $l \to 2k$. This procedure has been carried out as an independent check on the final results, for the cases of both unattenuated and attenuated incident waves. However, since lengthy calculations are involved, particularly in the latter case, the steps in this alternative argument are not presented here.

The component parts of the solution are shown in diagrammatic form in Fig 4. As compared with Fig 3, there are now two distinct contributions in $|x| < L$ arising from the pole at $-k$. The first is associated with the merging of the two poles at $(-k)$ and $(k - 1)$ as $l \to 2k$, and the second (marked with double arrowheads) is associated with the residual terms identified above. The remaining contributions in Fig 4 are either the same as, or are special cases of, those in Fig 3. The brace around each pair of $(-k)$ -terms indicates that it is the sum of these (separately singular) terms which provides the finite outgoing wave in the perturbation solution.

In summary, the action which we must take to obtain the solution for the special case in which $l = 2k$ is as follows:

1. The contribution arising in the general case ($1 \neq 2k$) from the poles at $\lambda = \lambda_2 = k - 1$ and $\lambda = -k$ must be removed.

2. A new contribution, which accounts for the merging of the poles at $\lambda = k - 1$ and $-k$ as $1 \to 2k$, must be included.

3. A further contribution, associated with the pole at $-k$ and arising from the residual terms discussed above, must be included.

We therefore replace Eq (38) by

$$\phi(x,y,t) = 2\pi i\left[\sum_{j=1}^{\infty} R_j^{(1)} + R_k^{(2)} + \sum_{j=1}^{\infty} R_{-j}^{(2)} \right] + \phi_* + \phi_R \,, \tag{54}$$

where $\phi_*(x, y, t)$ is the potential arising both from the pole at $\lambda = \lambda_1$ and also from the merging of the poles at $\lambda = \lambda_2$, and $\phi_R(x,y,t)$ is the potential associated with the residual terms.

We proceed by modifying, where necessary, the earlier analysis for the case in which $1 \neq 2k$. As far as the λ_1 -term is concerned, the analysis is unchanged, that is $R_{\lambda_1}^{(1)}$ and $R_{\lambda_1}^{(2)}$ are unchanged. But as far as the λ_2 -term is concerned, in the neighbourhood of $\lambda = \lambda_2$ it is now convenient to write

$$\psi(\lambda) = \frac{1}{\lambda - \lambda_2}\psi_*(\lambda) \,, \tag{55}$$

such that $\lambda = \lambda_2$ is an ordinary point of the function $\psi_*(\lambda)$, and $\psi(\lambda)$ itself has a simple pole at this point. This is the essential difference between the present argument and that which was adopted in obtaining the residues in Eqs (43) and (44). We now have, therefore,

$$\psi(\lambda) = \frac{1}{\lambda - \lambda_2}\left\{\psi_*(\lambda_2) + (\lambda - \lambda_2)\psi_*'(\lambda_2) + \tfrac{1}{2}(\lambda - \lambda_2)^2\psi_*''(\lambda_2) + \cdots\right\} .$$

As in the previous section, we treat separately the terms $F(\lambda)\Lambda_1(\lambda)$ and $F(\lambda)\Lambda_2(\lambda)$.

For unattenuated incident waves, and for the term $F(\lambda)\Lambda_1(\lambda)$, we have

$$F(\lambda)\Lambda_1(\lambda) = \psi(\lambda)\, e^{i(\omega t - \lambda x)} \cdot f_1(\lambda)\, e^{i(\lambda - k)L} .$$

If we write $\lambda - \lambda_2 = q$ and express the terms involving λ as power series in q then, in the neighbourhood of $\lambda = \lambda_2$, we have

$$F(\lambda)\Lambda_1(\lambda) = \left[\frac{\psi_*(\lambda_2)}{q} + \psi_*'(\lambda_2) + \cdots\right]\left[1 + iq(L-x)\cdots\right]\left[-\frac{\lambda_2}{q} + \frac{\lambda_1}{\lambda_2-\lambda_1}\left\{1 - \frac{q}{\lambda_2-\lambda_1}\right\}\right]$$

$$\cdot \frac{-C_*(-1)^m}{2} \cdot e^{i\lambda_2(L-x)}\, e^{i(\sigma t - kL)} .$$

The term in q^{-1} comprises three contributions, such that the new residue at $\lambda = \lambda_2$ is

$$R^{(1)}_{*\lambda_2} = \left[\psi_*(\lambda_2)\left\{-i(L-x)\lambda_2 + \frac{\lambda_1}{\lambda_2-\lambda_1}\right\} - \lambda_2\psi_*'(\lambda_2)\right]\left[\frac{-C_*}{2}\right] e^{i(\sigma t - \lambda_2 x)} .$$

For the term $F(\lambda)\Lambda_2(\lambda)$, the following result is obtained by a similar argument:

$$R^{(2)}_{*\lambda_2} = \left[\psi_*(\lambda_2)\left\{i(L+x)\lambda_2 + \frac{\lambda_1}{\lambda_2-\lambda_1}\right\} - \lambda_2\psi_*'(\lambda_2)\right]\left[\frac{C_*}{2}\right] e^{i(\sigma t - \lambda_2 x)} .$$

The potential $\phi_*(x,y,t)$ in Eq (54) is therefore

$$\phi_*(x,y,t) = \pi i\left(R^{(1)}_{\lambda_1} - R^{(2)}_{\lambda_1}\right) + \pi i\left(R^{(1)}_{*\lambda_2} - R^{(2)}_{*\lambda_2}\right) \tag{56}$$

$$= 2\pi i\left[\psi(\lambda_1)\cdot\frac{-C_*\lambda_1}{2}\cdot e^{i(\sigma t - \lambda_1 x)} - \frac{C_*}{2}\left[\psi_*(\lambda_2)\left\{ix\lambda_2 + \frac{\lambda_1}{\lambda_2-\lambda_1}\right\} - \lambda_2\psi_*'(\lambda_2)\right]e^{i(\sigma t - \lambda_2 x)}\right],$$

which may be compared with (45). As shown earlier, the residual term is equal to one half of the potential of the outgoing wave in $x < -L$, so that from (52)

$$\phi_R(x,y,t) = \frac{1}{2}\cdot\frac{gk\cosh(ky) + \sigma^2\sinh(ky)}{k}\cdot\frac{2\cosh(kh)}{g\{2kh + \sinh(2kh)\}}\cdot\frac{C_* m\pi}{2}\cdot e^{i(\sigma t + kx)}$$

$$= 2\pi i\cdot\frac{-C_*}{2}\cdot\psi(\lambda_2)\cdot(-iL\lambda_2)\cdot e^{i(\sigma t - \lambda_2 x)} . \tag{57}$$

If we combine (56) and (57), we obtain

$$\phi_* + \phi_R = 2\pi i \left[\psi(\lambda_1) \cdot \frac{-C_* \lambda_1}{2} \cdot e^{i(\sigma t - \lambda_1 x)} \right.$$

$$\left. - \frac{C_*}{2} \left[\psi_*(\lambda_2) \left\{ i(-L+x)\lambda_2 + \frac{\lambda_1}{\lambda_2 - \lambda_1} \right\} - \lambda_2 \psi_*'(\lambda_2) \right] e^{i(\sigma t - \lambda_2 x)} \right] \tag{58}$$

which may be substituted into Eq (54). It remains only to calculate $\psi(\lambda_1)$, $\psi_*(\lambda_2)$ and $\psi_*'(\lambda_2)$, and these results are listed in Appendix 2.1. It might be noted, finally, that the terms in (58) ensure that the bottom boundary condition is satisfied over the ripple patch.

For attenuated incident waves, the argument is as given above, but with Λ_1 and Λ_2 replaced by $\tilde{\Lambda}_1$ and $\tilde{\Lambda}_2$, respectively. The result for the λ_1-term is again unchanged, that is $\tilde{R}^{(1)}_{\lambda_1}$ and $\tilde{R}^{(2)}_{\lambda_1}$ are unchanged and, for the λ_2-term, we treat separately $F(\lambda)\tilde{\Lambda}_1(\lambda)$ and $F(\lambda)\tilde{\Lambda}_2(\lambda)$. For the term $F(\lambda)\tilde{\Lambda}_1(\lambda)$, we have

$$F(\lambda)\tilde{\Lambda}_1(\lambda) = \psi(\lambda) e^{i(\sigma t - \lambda x)} \cdot \tilde{f}_1(\lambda) e^{i(\lambda - k)L} . \tag{59}$$

If we again write $\lambda - \lambda_2 = q$, then in the neighbourhood of $\lambda = \lambda_2$ we have

$$\tilde{f}_1(\lambda) = - \frac{C_* (-1)^m}{2} \left[\frac{\tilde{A}_1}{q^2} + \frac{\tilde{B}_1}{q} + \tilde{C}_1 + \cdots \right] ,$$

where

$$\tilde{A}_1 = \frac{a - \tilde{a}_r}{a} \cdot \frac{i\ell}{2m\pi} \lambda_2 ,$$

$$\tilde{B}_1 = - \frac{\tilde{a}_r}{a} \lambda_2 ,$$

and

$$\tilde{C}_1 = \frac{\tilde{a}_r}{a} \cdot \frac{\lambda_1}{\lambda_2 - \lambda_1} - \frac{a - \tilde{a}_r}{a} \cdot \frac{i\ell}{2m\pi} \cdot \frac{\lambda_1}{(\lambda_2 - \lambda_1)^2} .$$

Expressing all the remaining terms of Eq (59) involving λ as power series in q, we

obtain

$$F(\lambda)\tilde{\Lambda}_1(\lambda) = \left[\frac{\psi_*(\lambda_2)}{q} + \psi_*'(\lambda_2) + \tfrac{1}{2}q\,\psi_*''(\lambda_2)\cdots\right]\cdot\left[1 + iq(L-x) + \tfrac{1}{2}q^2(i(L-x))^2\cdots\right]$$

$$\cdot\left[\frac{\tilde{A}_1}{q^2} + \frac{\tilde{B}_1}{q} + \tilde{C}_1 + \cdots\right]\cdot\frac{-C_*(-1)^m}{2}\cdot e^{i\lambda_2(L-x)}\, e^{i(\sigma t - kL)}.$$

The coefficient of the term in q^{-1}, that is the residue $\tilde{R}^{(1)}_{*\lambda_2}$, comprises six contributions and may be written

$$\tilde{R}^{(1)}_{*\lambda_2} = \left[\psi_*(\lambda_2)\{\tilde{C}_1 + i(L-x)\tilde{B}_1 - \tfrac{1}{2}(L-x)^2\tilde{A}_1\} + \psi_*'(\lambda_2)\{\tilde{B}_1 + i(L-x)\tilde{A}_1\} + \tfrac{1}{2}\psi_*''(\lambda_2)\cdot\tilde{A}_1\right]$$

$$\cdot\frac{-C_*}{2}\, e^{i(\sigma t - \lambda_2 x)}. \qquad (60)$$

For the term $F(\lambda)\tilde{\Lambda}_2(\lambda)$ we obtain, by a similar argument,

$$\tilde{R}^{(2)}_{*\lambda_2} = \left[\psi_*(\lambda_2)\{\tilde{C}_2 - i(L+x)\tilde{B}_2 - \tfrac{1}{2}(L+x)^2\tilde{A}_2\} + \psi_*'(\lambda_2)\{\tilde{B}_2 - i(L+x)\tilde{A}_2\} + \tfrac{1}{2}\tilde{A}_2\psi_*''(\lambda_2)\right]$$

$$\cdot\frac{-C_*}{2}\, e^{i(\sigma t - \lambda_2 x)}, \qquad (61)$$

where

$$\tilde{A}_2 = \frac{a-\tilde{a}_\tau}{a}\cdot\frac{i\ell}{2m\pi}\cdot -\lambda_2 = -\tilde{A}_1,$$

$$\tilde{B}_2 = \lambda_2,$$

and

$$\tilde{C}_2 = -\frac{\lambda_1}{\lambda_2-\lambda_1} + \frac{a-\tilde{a}_\tau}{a}\cdot\frac{i\ell}{2m\pi}\cdot\frac{\lambda_1}{(\lambda_2-\lambda_1)^2}.$$

The potential $\phi_*(x,y,t)$ is given in this case by

$$\phi_*(x,y,t) = \pi i \left(\tilde{R}^{(1)}_{\lambda_1} - \tilde{R}^{(2)}_{\lambda_1}\right) + \pi i \left(\tilde{R}^{(1)}_{*\lambda_2} - \tilde{R}^{(2)}_{*\lambda_2}\right), \tag{62}$$

in which, from (46) and (47),

$$\tilde{R}^{(1)}_{\lambda_1} - \tilde{R}^{(2)}_{\lambda_1} = -\frac{C_*}{2} e^{i(\sigma t - \lambda_1 x)} \left[\psi(\lambda_1)\cdot\lambda_1 \left(\frac{\tilde{a}_T + a}{a}\right) + \psi(\lambda_1)\left(\frac{a-\tilde{a}_T}{a}\right)\frac{i\ell}{2m\pi}\cdot\lambda_1\cdot 2ix \right.$$

$$\left. + \psi'(\lambda_1)\left(\frac{a-\tilde{a}_T}{a}\right)\frac{i\ell}{2m\pi}\cdot -2\lambda_1 \right],$$

and, from (60) and (61),

$$\tilde{R}^{(1)}_{*\lambda_2} - \tilde{R}^{(2)}_{*\lambda_2} = -\frac{C_*}{2} e^{i(\sigma t - \lambda_2 x)} \left[\psi_*(\lambda_2)\left\{\tilde{C}_3 + i(L-x)\tilde{B}_1 + i(L+x)\tilde{B}_2 - \tfrac{1}{2}(L-x)^2\tilde{A}_1 + \tfrac{1}{2}(L+x)^2\tilde{A}_2\right\} \right.$$

$$\left. + \psi_*'(\lambda_2)\left\{\tilde{B}_3 + i(L-x)\tilde{A}_1 + i(L+x)\tilde{A}_2\right\} + \tfrac{1}{2}\psi_*''(\lambda_2)\cdot\tilde{A}_3 \right],$$

where

$$\tilde{A}_3 = \tilde{A}_1 - \tilde{A}_2 \quad , \quad \tilde{B}_3 = \tilde{B}_1 - \tilde{B}_2 \quad \text{and} \quad \tilde{C}_3 = \tilde{C}_1 - \tilde{C}_2 \, .$$

It might be noted that Eq (62) reduces to Eq (56) if $\tilde{a}_T = a$. As before the residual term is equal to one half of the potential of the outgoing wave in $x < -L$ and so, from Eq (53), is given by

$$\phi_R = \frac{1}{2}\cdot\frac{gk\cosh(ky) + \sigma^2\sinh(ky)}{k}\cdot\frac{2\cosh(kh)}{g\{2kh + \sinh(2kh)\}}\cdot\frac{-C_*}{2}\left\{\frac{3}{4}\left(1-\frac{\tilde{a}_T}{a}\right) + \frac{im\pi}{2}\left(1+\frac{\tilde{a}_T}{a}\right)\right\}$$

$$\cdot i\, e^{i(\sigma t + kx)},$$

$$= 2\pi i\,\psi_*(\lambda_2)\cdot\frac{-C_*}{4}\cdot\left\{\frac{3}{4}\left(1-\frac{\tilde{a}_T}{a}\right) + \frac{im\pi}{2}\left(1+\frac{\tilde{a}_T}{a}\right)\right\} e^{i(\sigma t - \lambda_2 x)} \, . \tag{63}$$

The final solution for the case of attenuated incident waves in the special case $1 = 2k$ is obtained by substituting (62) and (63) in Eq (54), the bottom boundary condition over the ripple patch being satisfied by the terms of (62). It remains only to obtain expressions for $\psi(\lambda_1)$, $\psi'(\lambda_1)$, $\psi_*(\lambda_2)$, $\psi_*'(\lambda_2)$ and $\psi_*''(\lambda_2)$, and

these are listed in Appendix 2.1.

2.7 Discussion

2.7.1 The reflection coefficient

We state here results which are obtained from the asymptotic behaviour of the solution for the potential ϕ as $x \to -\infty$, and as $x \to +\infty$. In particular, we obtain an expression for the wave reflection coefficient, for use later in making comparisons with the experimental results. The properties of the reflection coefficient have been discussed in detail by Davies (1982a), and are not repeated here.

We define the wave reflection coefficient from the potential of the outgoing perturbation waves in $x < -L$, and from the incident waves in the first order solution. In the limit $x \to -\infty$, the former waves are given, from Eqs (29) - (31), by the real part of

$$\phi(x,y,t) = 2\pi i \left\{ R^{(1)}_{-k} + R^{(2)}_{-k} \right\} .$$

For the general case in which $l \neq 2k$, and in which the incident waves are unattenuated over the ripple patch, the required residues are obtained from Eqs (39) and (40), such that

$$\phi(x,y,t) = \frac{gk\cosh(ky) + \sigma^2 \sinh(ky)}{gk} \cdot \frac{2\cosh(kh)}{\{2kh + \sinh(2kh)\}} \cdot \frac{C_* (-1)^m (2k/l)}{(2k/l)^2 - 1} \cdot \sin(2kL)\, e^{i(\sigma t + kx)},$$

$$= \frac{2\cosh(k(y+h))}{\{2kh + \sinh(2kh)\}} \cdot \frac{C_* (-1)^m (2k/l)}{(2k/l)^2 - 1} \cdot \sin(2kL)\, e^{i(\sigma t + kx)} . \qquad (64)$$

The reflection coefficient, K_R, is defined as the quotient of the coefficient of $\cos(\sigma t + kx)$ in (64) and the equivalent coefficient for the incident surface waves in Eq (15), such that[1]

---

1. It is interesting to note that the modulus of this result for K_R is obtainable from a general result quoted by Kreisel (1949) for reflection by a "low gently sloping reef". Although, unfortunately, Kreisel simply states his result without any discussion of the approximate conformal mapping employed in his analysis, the two theories appear to yield the same result for the reflection coefficient in limiting cases in which the bottom undulations are very small.

$$K_R = \frac{a_R}{a} = \frac{2bk}{\{2kh + \sinh(2kh)\}} \cdot (-1)^m \cdot \frac{2k/\ell}{(2k/\ell)^2 - 1} \cdot \sin(2kL) \;, \quad (\ell \neq 2k). \tag{65}$$

For the special case in which $\ell = 2k$, and for which the perturbation potential is given by Eq (52), the reflection coefficient becomes

$$K_R = \frac{2bk}{\{2kh + \sinh(2kh)\}} \cdot \frac{m\pi}{2} \;, \quad (\ell = 2k) \cdot \tag{66}$$

Equivalent results for the reflection coefficient may be obtained for incident waves which are attenuated over the ripple patch. These results differ significantly from those given by Eqs (65) and (66) only if $K_R \gtrsim 0.4$ (see Davies (1982a)).

From Eq (66) it may be noted that, at resonance when $\ell = 2k$, the reflection coefficient increases linearly in the number of ripples (m) in the patch. It is for this reason that the earlier assumption of linear attenuation of incident wave amplitude across the patch is reasonable, at least near to resonance. More generally, Eq (65) reveals that, while the maximum value of K_R is found near the critical ratio of wavenumbers $2k/\ell = 1$ (in fact, at a value slightly greater than unity, but which tends to unity with increasing m), the reflection coefficient is also oscillatory in the ratio of the length of the ripple patch (2L) to the surface wavelength. It might be emphasized here that the definition adopted for K_R allows its sign to change; in particular, K_R takes a positive value at $2k/\ell = 1$ while, for general values of this quotient, its sign depends upon the value of m. The properties of K_R are discussed in more detail in the later consideration of the experimental results (§4). There it is demonstrated that surprisingly few bottom ripples, of quite modest size, are needed to produce a substantial reflected wave.

For the outgoing waves on the down-wave side of the ripple patch, the potential in the asymptotic limit $x \to +\infty$ is given, from Eqs (32) - (34), by

$$\phi(x,y,t) = -2\pi i \left\{ R_k^{(1)} + R_k^{(2)} \right\} \cdot$$

For unattenuated incident waves, this gives simply

$$\phi(x,y,t) = 0 \cdot \tag{67}$$

It is evident from Eqs (64) and (67) that the vertical velocity distribution prescribed at the bottom boundary in Eq (17) is such as to produce an outgoing

wave in the up-wave direction only. However, in the case of attenuated incident waves, there is a small outgoing wave on the down-wave side, the properties of which have been discussed by Davies (1982a).

2.7.2 Properties of the waves over the ripple patch

We turn next to some detailed considerations of the properties of the waves over the ripple patch, in which we utilize the complete solution in $-\infty < x < \infty$. The elevation in the perturbation solution $\eta(x,t)$ is given by Eq (4) (only the real part of which is of interest), and the elevation of the first order incident waves associated with Eq (15) is simply $\{a \sin(kx - \sigma t)\}$. In Figs 5 - 9, we show results for a typical case near to resonance which relates to one of the later laboratory experiments. The parameter settings are as follows: ripple amplitude b = 5 cm, ripple wavelength $(2\pi/l)$ = 100 cm, the number of ripples m = 10, the water depth h = 41.7 cm, and the wave period $(2\pi/\sigma)$ = 1.23 s, from which it follows from (16) that $2k/l = 0.985$. The incident waves are assumed to be unattenuated across the ripple patch, so that the asymptotic behaviour of the perturbation solution is given by Eq (64) as $x \to -\infty$, and by (67) as $x \to +\infty$. From Eq (65), the reflection coefficient in this case is $K_R = 0.509$. The incident wave amplitude in the laboratory experiment was a = 1.62 cm, though this is not important (beyond the fact that it well justifies the use of linear theory for comparison with the experimental results) since the results in Figs 5 - 9 are all normalised with respect to the incident wave amplitude a.

In each of Figs 5 - 9 results for the normalized elevation $\eta(x,t)/a$ have been expressed in the form

$$\frac{\eta(x,t)}{a} = E_1(x)\cos(\sigma t) + E_2(x)\sin(\sigma t), \qquad (68)$$

where $E_1(x)$ and $E_2(x)$ comprise contributions from some or all of the poles shown in Fig 2. The curves plotted in Fig 5 are for the perturbation solution only, and show the instantaneous elevations $E_1(x)$, $E_2(x)$, $-E_1(x)$, and $-E_2(x)$ at the phase angles $\sigma t = 0$, $\pi/2$, π and $3\pi/2$, respectively, together with the envelope curves for wave elevation given by $\pm\sqrt{E_1^2 + E_2^2}$. The results show that, on the down-wave side of the ripple patch ($x > L$), the water surface is motionless as required by Eq (67). Between the down-wave end of the patch ($x = L$) and the up-wave end ($x = -L$), the perturbation wave increases in size. Thereafter, in $x < -L$, the wave propagates away from the ripple patch in the negative x-direction, with amplitude $a_R = 0.509\ a$ as given by Eq (64). The result of superimposing the perturbation waves and the incident waves is shown in Fig 6, in which the elevation

curves plotted are equivalent to those in Fig 5. Now the evolution of a partially standing wave pattern is apparent in $|x| < L$, with a fully developed partially standing wave being present in $x < -L$. On the down-wave side, there is simply an outgoing transmitted wave. Since the incident waves are assumed to be unattenuated over the patch, this outgoing wave has elevation given by $a \sin(kx - \sigma t)$. In the later discussion of the experimental results, examples are included which illustrate how results of the kind shown in Fig 6 are affected by the imposition of an energy balance on the solution, in which the overall transmitted wave amplitude is constrained to satisfy the equation $\tilde{a}_T = \sqrt{a^2 - \tilde{a}_R^2}$ (see §2.3.2).

In Fig 5 the evolution of the perturbation wave in $|x| < L$ is dominated by the $(-k)$ and $(k - 1)$ -waves (see Fig 3). The $(+k)$ and $(k + 1)$ -waves have a rather small influence on the results. This is the typical situation in cases near to resonance. In general non-resonant cases, in which the perturbation waves are confined to the region of the patch, the $(k + 1)$ -wave has a greater relative influence on the results. At the ends of the patch ($x = \pm L$), a smooth transition in the solution is obtained as a result of the trapped wave modes associated with the poles on the imaginary axis of λ (see Fig 2). The properties of the two most important trapped modes are shown in Fig 7. Here we have taken the same example as in Figs 5 and 6, but have eliminated all the propagating wave modes in the solution, and all but one of the trapped wave modes. The results are plotted only for the regions near both ends of the patch, and in a manner consistent with the elevation curves plotted in Figs 5 and 6 (though with a change in the vertical scale, since the trapped waves are relatively small). In Fig 7(a), surface wave motions are shown which are associated with the pair of poles nearest to the real axis of λ in Fig 2 (at $\chi_0 = \pm 0.0662$ cm^{-1}), while, in Fig 7(b), motions are shown for the second pair of poles (at $\chi_0 = \pm 0.1464$ cm^{-1}). The magnitudes of these trapped waves at the ends of the patch ($x = \pm L$) may be seen to be of the order of 0.015 and 0.005 times the amplitude of the incident wave, respectively, or, to put it another way, about 3% and 1% of the magnitude of the reflected wave. So, while their maximum effects are small in this case, they are not entirely negligible. Away from the ends of the patch, the effects of the trapped modes decay exponentially in x, the first mode having a more extensive effect than the second, and so on. It will be noted that, while the outer envelope curves are continuous at both ends of the patch, this is not so for the instantaneous surface profiles, which are discontinuous. This emphasises the obvious fact that the trapped modes cannot exist in the absence of the propagating modes. The sum of all the trapped modes, including those in Figs 7(a) and (b), is shown in Fig 8,

and the way in which a continuous solution is brought about across the ends of the patch by the inclusion of these modes is shown in Fig 9. Continuity of both the instantaneous elevation curves, and the envelope curves, may be seen to be established by the inclusion of the trapped modes.

Finally, the horizontal velocity field ($u = -\phi_x$) associated with the waves in Fig 6 is illustrated in Fig 10. Here the amplitude of the horizontal velocity is shown as a function of horizontal distance (x) for discrete values of the normalized depth (y/h), namely y/h = 0 (free surface), -0.5, -0.75 and -1.0 (bed). Each of the curves has been normalized by $U_0 = gak/\sigma$, the horizontal velocity amplitude of the incident wave at the free surface. On the down-wave side ($x > L$), the vertical attenuation of velocity is governed by $\{\cosh k(y + h)/\cosh kh\}$ (see Eq (15)). On the up-wave side, the waves in the perturbation solution have the same dependence, as may be seen from Eq (64). The behaviour of the velocity field over the ripple patch is rather more complicated, on account of the way in which the $(k \pm 1)$ -waves are attenuated in the vertical direction. In general, the effects of these waves are most pronounced at the bed level, and they are strongly attenuated with distance above the bed. Near to resonance, however, the attenuation of the dominant $(k - 1)$ -wave is similar to that of the incident wave. In Fig 10, it may be seen that the horizontal velocity amplitudes decrease downwards from the free surface for all values of x which are off the ripple patch ($|x| > L$), but that this is not the case over the patch itself ($|x| < L$). Here, both variations in the bed velocity amplitude, and also magnitudes of the bed velocity amplitude for certain values of x, are rather larger than those at the height y/h = -0.75. In the upper layers, the velocity amplitudes increase to their peak values which are found at the surface. The vertical velocities in the flow are generally small; in the present example, the tangential velocity amplitude at the bed does not differ greatly from the horizontal velocity amplitude. This is illustrated in Fig 11 where, for the same parameter settings as in Figs 5 to 10, instantaneous horizontal bed velocities are plotted for the phase angles $\sigma t = 0$, $\pi/2$, π and $3\pi/2$, together with envelope curves which show the amplitudes of both the horizontal and tangential bed velocity. At the ends of the ripple patch ($x = \pm L$), it may be seen from Fig 10 that the trapped wave modes give a smooth transition in the horizontal velocity amplitude at all levels, other than the bed level where the velocity field is divergent. This anomaly, which is apparent also in Fig 11, is associated with the discontinuities in the prescribed bed slope at $x = \pm L$ (see Eq (13)); it has no general physical significance, and should be ignored in any considerations of sediment movement on the bed surface.

The divergence of the velocity field at $x = \pm L$, $y = -h$, is discussed in Appendix 2.2 where it is shown that, at all levels other than $y = -h$, the series expansion for the horizontal velocity associated with the trapped wave modes is convergent. The wider implications of results of the type shown in Fig 10, for sediment transport and bedform stability, are discussed briefly in §2.7.4, and also in §4 where a preliminary laboratory result is examined.

2.7.3 Limitations on the solution

There are certain physical limitations on the solution discussed earlier. These arise on account of terms dropped in linearizing the boundary conditions, and also on account of the general requirement of the method that $|\phi| \ll |\Phi|$. The limitations of the former kind have been discussed in detail by Davies (1980, 1982b), and may be stated as a set of simple conditions on the various length scales in the problem, namely

$$ak,\ a/h,\ a/k^2h^3,\ bl,\ b/h \text{ and } bk \ll 1.$$

It has been shown also that the analysis breaks down if $k \gg 1$. The requirement $|\phi| \ll |\Phi|$ imposes at the outset a condition on the size of the reflected wave. In its pure form, the theory requires both the reflected and transmitted waves in the perturbation solution to be small compared with the incident wave. However, if an energy balance is established in the solution by the ad hoc procedure described in §2.3.2, this condition may be relaxed. Unfortunately, if this procedure is adopted, the analysis becomes somewhat deficient in another respect; in particular, the first order waves do not strictly satisfy the potential equation. In view of this, it is reassuring to find quite close agreement between results for a_R calculated on the basis of both the pure perturbation theory, and the ad hoc energy balance argument, at least for cases in which K_R is not too large ($K_R \lesssim 0.4$, say). In practice, it is necessary to correct first estimates of a_R from the pure theory only in resonant cases for which the reflection coefficient is large. For example, in the limiting case in which the first estimate for a_R is such that $a_R = a$, the size of the reflected wave may be shown to be overestimated by 25%. However, this is the worst possible case and, for smaller waves in the perturbation solution, the overestimates are considerably smaller. In general, the first estimate of a_R from the pure theory should be viewed as providing an upper bound on the size of the reflected wave. It should be added here that the perturbation solution may predict over-reflection, and that particular care should

be exercised in interpreting any results which suggest that $|a_R| > a$. The perturbation solution allows this situation to arise, since it is assumed that the interaction between the incident waves and the ripples takes place over the entire ripple patch. In practice, if complete reflection occurs, the interaction region may be $-L < x < L_*$ where $L_* < L$. The present formulation does not admit this possibility, though it could be developed to do so. Finally, in the context of a total approach to the problem of wave propagation over a region of undulating seabed, the present theory is further limited by ignoring the effects of energy dissipation by bottom percolation and bottom friction. However, despite all the limitations mentioned above, the theory may be used in a variety of physically interesting cases, including the laboratory experiments described later. Ultimately, the strength of the theory lies in providing a good initial estimate for the size of the reflected wave, as well as the details of the wave motion over the ripple patch.

2.7.4 General implications of the results

The results obtained in §2 have been for sinusoidal surface waves incident upon a patch of sinusoidal ripples. Since the theory on which the results have been based is linear, it is possible to superimpose solutions and obtain results for the general case in which a spectrum of waves is incident upon a spectrum of bottom perturbations within the roughness patch. As far as the reflected wave is concerned, this general interaction amounts to a superimposition of solutions like (64) for each combination of surface and bed wavenumbers present. For the simple case of the interaction of a spectrum of incident waves with a single constituent harmonic of the bed roughness patch, the reflection coefficient given by (65) may be seen to predict reflection of wave energy in preferred groups of wavenumbers, the dominant group being that centred upon $k = 1/2$. In the general case, in which there is a spectrum of bottom perturbations as well as a spectrum of surface waves, the reflection coefficient will be a rather more complicated function than this, though, in practice, it is one which may be determined quite easily.

For the simple case of sinusoidal ripples, the reflection of incident waves at resonance ($k \approx 1/2$) gives rise to a partially standing wave pattern on the up-wave side of the ripple patch (Figs 6, 10 and 11). If the bed is erodible, this suggests the possible development of new ripples on the up-wave side of the patch. Under certain circumstances, which are discussed more fully in §4.4, the velocity field may be shown to be consistent with the continuation of an existing sinusoidal ripple patch on the up-wave side. Intuitively, it might be expected that accumu-

lation of material would occur at positions on the bed with the smallest bottom velocity amplitudes, and that erosion would occur at positions with the greatest velocity amplitudes. It is argued in §4.4, however, that the situation may be rather more complicated than this. Ultimately, for there to be a coupling between wave reflection and ripple growth, accumulation and erosion must occur on the existing ripple patch in a way which suggest ripple growth, rather than ripple destruction, by the wave action.

In general non-resonant cases, the theory predicts that the bottom velocity field over the ripple patch is such that there exist very marked variations in the amplitude of the surface velocity from ripple crest to trough positions. In many cases, these variations are confined to a near-bed layer, in that they are attenuated upwards away from the bed. Moreover, they are not associated with reflected or transmitted waves of any significance. The implications for sediment transport of the general non-resonant case have been discussed by Davies (1982b), and a set of field results has been interpreted quite successfully on the basis of the theory.

APPENDIX 2.1

Results for the functions ψ and ψ_*

The following results involving the functions ψ and ψ_* are required in Eqs (45), (50), (58), (62) and (63). From Eq (26) we have, setting $\mu = 0$,

$$\psi(\lambda) = H(\lambda)\, G(\lambda) ,$$

where

$$H(\lambda) = \frac{1}{\sigma^2 \cosh(\lambda h) - g\lambda \sinh(\lambda h)}$$

and

$$G(\lambda) = \frac{g\lambda \cosh(\lambda y) + \sigma^2 \sinh(\lambda y)}{2\pi\lambda} .$$

It follows that, for $\lambda = \lambda_1$,

$$\psi(\lambda_1) = H(\lambda_1) G(\lambda_1)$$

and

$$\psi'(\lambda_1) = H(\lambda_1) G'(\lambda_1) + H'(\lambda_1) G(\lambda_1) \ ,$$

where $H(\lambda_1)$ and $G(\lambda_1)$ are obtained by setting $\lambda = \lambda_1$ in the expressions for $H(\lambda)$ $G(\lambda)$, and in which

$$H'(\lambda_1) = \frac{-\{\sigma^2 k \sinh(\lambda_1 k) - g\lambda_1 k \cosh(\lambda_1 k) - g \sinh(\lambda_1 k)\}}{\{\sigma^2 \cosh(\lambda_1 k) - g\lambda_1 \sinh(\lambda_1 k)\}^2} \ ,$$

and

$$G'(\lambda_1) = \frac{\sigma^2 y \lambda_1 \cosh(\lambda_1 y) + (g\lambda_1^2 y - \sigma^2) \sinh(\lambda_1 y)}{2\pi \lambda_1^2} \ .$$

The results for $\psi(\lambda_2)$ and $\psi'(\lambda_2)$ are obtained by replacing λ_1 by λ_2 in each of the above expressions.

From Eq (55) we have

$$\psi_*(\lambda) = (\lambda - \lambda_2)\psi(\lambda) = (\lambda - \lambda_2) H(\lambda) G(\lambda) = H_*(\lambda) G(\lambda) \quad , \text{ say.}$$

It follows that

$$\psi_*(\lambda_2) = H_*(\lambda_2)\, G(\lambda_2) \ ,$$

$$\psi_*'(\lambda_2) = H_*(\lambda_2)\, G'(\lambda_2) + H_*'(\lambda_2)\, G(\lambda_2) \ ,$$

and

$$\psi_*''(\lambda_2) = H_*(\lambda_2)\, G''(\lambda_2) + 2H_*'(\lambda_2)\, G'(\lambda_2) + H_*''(\lambda_2)\, G(\lambda_2) \ .$$

in which

$$H_*(\lambda_2) = \frac{-2\cosh(\lambda_2 h)}{g\{2\lambda_2 h + \sinh(2\lambda_2 h)\}} \ ,$$

$$H_*'(\lambda_2) = \frac{4h\cosh^3(\lambda_2 h)}{g\{2\lambda_2 h + \sinh(2\lambda_2 h)\}^2} \ ,$$

$$H_*''(\lambda_2) = \frac{h^2\cosh(\lambda_2 h)}{g\{2\lambda_2 h + \sinh(2\lambda_2 h)\}^2} \cdot \left[\frac{2}{3}\{2\lambda_2 h + 3\sinh(2\lambda_2 h)\} - \frac{16\cosh^4(\lambda_2 h)}{\{2\lambda_2 h + \sinh(2\lambda_2 h)\}}\right]$$

and

$$G''(\lambda_2) = \frac{\cosh(\lambda_2 y)\{9\lambda_2^3 y^2 - 2\sigma^2\lambda_2 y\} + \sinh(\lambda_2 y)\{\sigma^2\lambda_2^2 y^2 + 2\sigma^2\}}{2\pi\lambda_2^3} \ .$$

The terms $G(\lambda_2)$ and $G'(\lambda_2)$ are as in the expressions for $\psi(\lambda_2)$ and $\psi'(\lambda_2)$.

APPENDIX 2.2

The divergence of the bed velocity at the ends of the ripple patch

It was pointed out in §2.7.2 that the bed velocity at both ends of the ripple patch ($x = \pm L$, $y = -h$) is divergent and that, at all other points in the flow, the velocity field is convergent. Ths is an anomalous result of no general significance, and is associated with discontinuities in the prescribed bed slope at the ends of the ripple patch (Eqs 1, 13 and 14). We show here briefly the reason for the divergences in the velocity field, by examining the properties of the trapped wave modes at the ends of the patch. We do not consider the propagating modes in the perturbation solution, all of which are well behaved.

In the region $x \lesssim -L$, which we treat as a typical region for the present discussion, the trapped wave modes are given, from Eqs (29)-(31), by

$$\phi = 2\pi i \left\{ \sum_{j=1}^{\infty} R_j^{(1)} + \sum_{j=1}^{\infty} R_j^{(2)} \right\}$$

in which, from (39) and (40),

$$R_j^{(1)} = \frac{1}{2\pi\chi_o} \left\{ g\chi_o \cos(\chi_o y) + \sigma^2 \sin(\chi_o y) \right\} \cdot \frac{-2\cos(\chi_o h)}{gi\{2\chi_o h + \sin(2\chi_o h)\}} \cdot f_1(i\chi_o)\, e^{-\chi_o(L-x)}\, e^{i(\sigma t - kL)}$$

and

$$R_j^{(2)} = \frac{1}{2\pi\chi_o} \left\{ g\chi_o \cos(\chi_o y) + \sigma^2 \sin(\chi_o y) \right\} \cdot \frac{-2\cos(\chi_o h)}{gi\{2\chi_o h + \sin(2\chi_o h)\}} \cdot f_2(i\chi_o)\, e^{\chi_o(L+x)}\, e^{i(\sigma t + kL)}$$

where each value of j is associated with a solution $\chi_o = \chi_{oj}$ of Eq (15). We may consider, without loss of generality, the case of incident first-order waves which are unattenuated over the ripple patch such that, from (23),

$$f_1(i\chi_o) = -f_2(i\chi_o) = C_* (-1)^m \frac{\ell\chi_o \{2\chi_o k - i(k^2 - \chi_o^2 - \ell^2)\}}{(k^2 - \chi_o^2 - \ell^2)^2 + 4\chi_o^2 k^2} .$$

Since $\chi_o > 0$ for $x \lesssim -L$ (see Fig 2) and since also, at the end of the ripple patch ($x = -L$), we have

$$e^{-\chi_o(L-x)} = e^{-2L\chi_o} \qquad \text{and} \qquad e^{\chi_o(L+x)} = 1 \ ,$$

it is evident that the summations involving $R_j^{(1)}$ and $R_j^{(2)}$ are associated with the trapped wave modes centred on $x = +L$ and $x = -L$, respectively. Our present concern is with the contribution from the summation $\sum_j R_j^{(2)}$ therefore; in particular, we consider whether this contribution converges or diverges at $x = -L$. It is only <u>at</u> the end of the patch that the solution may diverge since, elsewhere in $x < -L$, the exponential decay ($\sim \exp(\chi_o(L + x))$) in each term of the series ensures its convergence. At $x = -L$, the potential of the trapped wave modes may be expressed, using (21), by

$$\phi = \sum_j \cos(\chi_o(y+h)) \cdot \frac{2}{2\chi_o h + \sin(2\chi_o h)} \cdot -f_2(i\chi_o)\, e^{i(\sigma t + kL)} \ .$$

For simplicity, and bearing in mind that we are interested here in the behaviour of this series for large j, we may consider solutions of (21) to be given approximately by $\chi_o = \chi_{oj}$ where

$$\frac{\chi_{oj} h}{\pi} = j \qquad , \quad j = 1, 2, 3, 4 \cdots \ .$$

(These solutions are accurate for large j, though not for small j.) Now, for large j, and therefore large χ_o, the <u>real</u> part of $-f_2(i\chi_o)$ has the behaviour

$$\frac{C_* (-1)^m \ell \chi_o \cdot 2\chi_o k}{(k^2 - \chi_o^2 - \ell^2)^2 + 4\chi_o^2 k^2} \sim \frac{C_* (-1)^m 2k\ell}{\chi_o^2} \ ,$$

and the <u>imaginary</u> part has the behaviour

$$\frac{C_*(-1)^m \ell \chi_o \cdot -(k^2-\chi_o^2-\ell^2)}{(k^2-\chi_o^2-\ell^2)^2 + 4\chi_o^2 k^2} \sim C_*(-1)^m \frac{\ell}{\chi_o}.$$

It follows that the series may be expressed by

$$\phi \sim C_*(-1)^m e^{i(\sigma t + kL)} \sum_j \cos(\chi_o(y+h)) \cdot \frac{1}{\chi_o h} \cdot \left(\frac{2k\ell}{\chi_o^2} + i\frac{\ell}{\chi_o}\right),$$

the terms of which are accurate for large j. When horizontal velocities are considered ($u = -\phi_x$), a multiplying factor ($-\chi_o$) is introduced such that the appropriate series (again in a form which is accurate for large j) is

$$u \sim C_*(-1)^{m+1} e^{i(\sigma t + kL)} \cdot \frac{\ell}{h} \sum_j \cos(\chi_o(y+h)) \cdot \left(\frac{2k}{\chi_o^2} + \frac{i}{\chi_o}\right).$$

In the special case in which $y = -h$ ($\cos(\chi_o(y + h)) = 1$ for all j), the real part of the summation $\sum_j 2k/\chi_o^2$ clearly converges. However, the imaginary part $i\sum_j 1/\chi_o$ diverges, and it is for this reason that the horizontal velocity evaluated at $x = \pm L$, $y = -h$, diverges.

For the general case in which $0 > y > -h$, we retain the $\cos(\chi_o(y + h))$ term within the summation. As far as the real part is concerned, the fact that the reduced series $\sum_j 2k/\chi_o^2$ converges at the bed ($y = -h$) means that, by the comparison test, the new series $\sum_j 2k\cos(\chi_o(y + h))/\chi_o^2$ is absolutely convergent. For the imaginary part $i\sum_j \cos(\chi_o(y + h))/\chi_o$, the situation is not quite so straight forward, since the reduced series $i\sum_j 1/\chi_o$ diverges at the bed. In the new situation, alternating blocks of positive and negative terms occur in the series as a result of the cosine term, viz.

$$i\sum_j \frac{\cos(\chi_o(y+h))}{\chi_o} = \frac{ih}{\pi}\left\{\frac{\cos(\pi(1+y/h))}{1} + \frac{\cos(2\pi(1+y/h))}{2} + \frac{\cos(3\pi(1+y/h))}{3} + \ldots\right\}.$$

The widths of the blocks depend upon the height (y/h); in particular, the widths increase as (-y/h) tends to unity. Furthermore, the multiplying factors within

the blocks (ie the values of the cosine terms for given y/h) are not, in general, the same in adjacent blocks. In fact they are only the same if $1 + y/h = {}^1/_2, {}^1/_3, {}^1/_4 \ldots .$ (Note that these levels become increasingly bunched towards the bed.) In these special cases, the series may be shown quite simply to be conditionally convergent. More generally, however, the convergence of the series at all the intermediate levels in $0 > y > -h$ may be inferred from this, though we do not present a detailed justification for this statement here.

In conclusion, we have demonstrated that the divergences in the horizontal bed velocity field at the ends of the ripple patch ($x = \pm L$, $y = -h$) result from the discontinuities in the prescribed vertical bed velocity field at $x = \pm L$ (Eqs (6) and (17)). These discontinuities are due, in turn, to the discontinuities in the prescribed bottom slope at $x = \pm L$. Having taken the region $x \leqq -L$ as a typical region for the purpose of demonstrating the reason for one of the divergences, we infer more generally that

i) the horizontal velocity, and hence the vertical velocity, are convergent for all (x,y) except $(x = \pm L, y = -h)$; and that

ii) the horizontal bed velocity is divergent at $x = \pm L$.

It might be noted, finally, that by a simple extension of the earlier arguments, the velocity potential ϕ itself is convergent for all points (x,y) in the flow.

3. EXPERIMENTAL TECHNIQUES

3.1 Construction of the ripple patch

To test the results of the preceding section, and in particular Eqs (65) and (66), measurements were carried out by one of the authors (ADH) during a visit to the Coastal Engineering Research Center, Fort Belvoir, Virginia, USA.

The tests were carried out in a glass walled wave tank, 45.72 x .91 x .91 m (nominally 150' x 3' x 3'). Initially, calculations were made to determine the optimum ripple wavelength from the range of possible surface water wavelengths, the limiting factors being the available water depths and wave periods. A wavelength of 1 m was chosen for the ripples, and a patch of ripples was built into a false bottom in the tank. Details of the experimental set-up are shown schematically in Figure 12. The amplitude of the bedforms was chosen to be 5.0 cm (a trough to crest height of 10.0 cm), this being the steepest case examined by Davies (1982a, Figure 3), who also showed that 10 ripples of this steepness could bring about almost total reflection of wave energy for limiting values of the water depth. A 1 m wavelength for the bedforms also gave resonant wave periods approximately in the centre of the range which could reasonably be tested in the

tank (about .5 - 3.05 sec.), and thus permitted a detailed examination of the oscillatory nature of the reflection coefficient. Initially, 10 ripples were built in the tank, with later tests being carried out on 4, 2 and 1 ripples, respectively. As ripples were removed (from the down-wave end of the patch, see Figure 12) they were replaced by plywood covered, and sand filled, sections of false bottom. There was no facility for return flow through the false bottom.

The rippled test section (Figure 12) was built in-situ and consisted of a 2.5 cm thick sand cement shell overlying wet sand, which was contoured to sinusoidal plywood templates in 2 m units. Five such units were set in a 15 cm deep, plywood covered and sand-filled, false bottom. At the far end of the tank, a 1:10 slope rubberized fibre wave absorbing beach was built to prevent waves from being back-reflected onto the ripple patch. The beach was constructed so that, at the highest water level examined, the longest period waves would have to travel over about twice their own wavelength of beach material. Shorter period waves were expected to be more readily absorbed by the beach than these long period waves. The beach was anchored in the tank using stones and stainless steel clamps. Due to the buoyant nature of the rubberized fibre, and the presence of trapped air, the beach face could not be maintained entirely plane. Deviations from a plane beach face were of the order of 10 cm between supports.

3.2 The wave generator

Monochromatic sinusoidal waves were generated using an electrohydraulic piston type wave generator manufactured by Shore Western Manufacturing Inc of Monrovia, California. Design characteristics of the generator are shown in Figure 13. This shows the design operating limits for wave periods in the range .5 - 20.0 sec, with bulkhead amplitudes of up to 40 cm (a stroke of 80 cm) attainable at wave periods of about 3 sec. The generator was at all times operated within these limits, with bulkhead amplitudes being chosen to comply with the limiting criteria for the wave properties outlined in §2.7.3.

Wave period settings could be adjusted in increments of 0.01 sec. Independent checks on the accuracy of these settings were carried out in the range 0.6 to 3.0 sec by timing 30 oscillations of the wave generator bulkhead. The results, which are summarised in Table 1, indicate agreement to within ±.005s of the nominal wave period setting. Following a change in the setting, the time taken for the wave system in the tank to attain a steady state was usually of the order of 60 sec. Since the time between successive sets of measurements was in general longer than this (of the order of 3 minutes), the measurements described in §4 were

representative of equilibrium conditions.

3.3 Wave measurements

Measurements of incident, reflected and transmitted wave heights were made using CERC type parallel wire wave gauges. Details of these instruments may be found in Kellum (1956) and Stafford (1972). The CERC wave gauges were of the parallel wire resistance type and have a linear output. Similar wave gauges for use with hydraulic models have been described by Fryer and Thomas (1975). The gauges were not temperature compensated, and calibrations were carried out daily or whenever the water in the tank was changed. The tank temperature was also noted daily. Where measurements were made at different depths, this was usually done with the water level falling so as to avoid the introduction of colder water into the tank.

Two sizes of wave gauge were used for the measurements described in this report. Measurements on 10 ripples, and with water depths in the range 25.0 - 62.5 cm, were made with gold plated brass wire gauges having a nominal length of 50.0 cm and a wire spacing of approximately 3.7 cm. The wire diameter was approximately 0.25 cm. For measurements on 4, 2 and 1 ripples and with water depths in the range 12.5 - 50.0 cm, miniature stainless steel wire gauges were used. These had nominal wire lengths of 13.0 cm, with a wire separation of 1.5 cm and wire diameters of approximately 0.10 cm. Comparisons between the small and large gauges showed good agreement, with the small gauges underestimating the large ones by, on average, 4%. These comparisons are discussed later. Water depths were determined to within an estimated 0.1 cm using a pointer gauge. All gauges were mounted on stands which could be slid along the top of the tank on rails.

To determine reflection coefficients the method described by Goda and Suzuki (1977), which involves the synchronous measurement of surface elevations with a gauge pair, was employed (see Appendix A). Incident and reflected wave trains are ideally resolved by a pair of wave gauges having spacing Δx of $0.25\lambda_w$, where λ_w is the wavelength. However, Goda and Suzuki (1977) have shown that this condition may be relaxed, and that gauge spacings in the range $.05 < \Delta x/\lambda_w < .45$ are probably acceptable. In this work, gauge spacings were maintained in the range $.15 < \Delta x/\lambda_w < .35$. Two pairs of gauges and a single gauge were used to make two types of measurement:

(a) measurements of the variation in the reflection coefficient, and in the wave height, over the entire ripple patch and on either side of it; the fifth (single) gauge was positioned at the foot of the beach in these cases.

(b) measurements of the reflection coefficient at a fixed point on the up-wave side of the ripple patch, approximately mid-way between it and the wave generator, and at a fixed point on the down-wave side of the patch, approximately mid-way between it and the wave absorbing beach. The fifth gauge was positioned mid-way along the patch in these cases.

These two arrangements are illustrated schematically in Figure 12. In each case, synchronous wave records were obtained from the five gauges, by sampling each gauge 16 times per second (16 Hz) for 64 seconds, thus yielding 1024 data points for subsequent spectral analysis by the fast Fourier transform (FFT) method. Spectral coefficients were then combined to yield a reflection coefficient for each gauge pair. The wave gauges were used also to determine variations in wave height along the wave tank, and to obtain estimates of the wave steepness.

3.4 Wave filters

As a separate aspect of this study, tests were carried out on a series of wave filters. In laboratory experiments of many kinds, it is necessary to minimise re-reflection of wave energy from the blade of the wave generator. Normally this is done by inserting wave filters between the test structure and the generator. As part of the work carried out at CERC it was required to determine the wave transmission and reflection characteristics of a series of rubberized fibre, or 'hogshair', filters. These were constructed in modules, each module consisting of sheets of rubberized fibre mounted transversely, on edge, across the wave tank in wire mesh baskets. Each filter unit was approximately 0.30 m in length, and three such units were built. The filters were positioned in the tank with aluminium supports clamped to the edges. The filter length could thus be varied from 0.3 m to about 0.9 m, that is approximately half the incident water wavelength at resonance (for ripples of 1 m wavelength). Full details of the filter design and characteristics can be found in Appendix B.

4. EXPERIMENTAL RESULTS

4.1 Variation of the reflection coefficient with the ratio of the water wavelength to the ripple wavelength.

The first experimental results described here are for the wave reflection coefficient K_R, the appropriate theoretical predictions being given by Eqs (65) and (66). The variation of $|K_R|$ with the ratio of the water wavelength to the ripple wavelength is shown in Figs 14(a) - 14(c) for m = 10, 4 and 2 ripples, respectively. The results of the measurements from the up-wave pair of gauges (1 and 2) are given

in Table 2. Where practicable, the quotient (2k/1) was varied through the range $0.5 < 2k/1 < 2.5$ in steps of $\Delta(2k/1) = 0.01$ for m = 10 and 4, and in steps of $\Delta(2k/1) = 0.02$ for m = 2. However, it may be seen that, for $2k/1 \gtrsim 2$, the resolution in (2k/1) is poorer than this as a result of the limited resolution in the wave period ($\Delta T = 0.01$ sec). The results shown in Fig 14 illustrate that fine resolution in the wave period, and hence in the quotient (2k/1), is necessary to resolve the predicted oscillations in $|K_R|$, additional to the main resonance at $2k/1 \simeq 1$.

In Fig 14(a), the measured reflection coefficients for 10 ripples may be seen to follow quite closely the general trend of the theoretical predictions. The width of the main resonant peak is well established, and agreement is reasonable for values of (2k/1) up to about 2. For the cases of 4 and 2 ripples (Figs 14(b) and (c)), the theoretical predictions are again well supported by the measurements, particularly in respect of the main resonant peaks. However, there is generally more scatter in the results in these cases, probably due to the unwanted effects of wave energy reflection by the beach. This question is discussed below. In each of Figs 14(a) to (c), the experimental results are compared with theoretical predictions for incident waves which are assumed to be unattenuated (see §2.3.1), and linearly attenuated (§2.3.2), over the ripple patch. (Reflected wave amplitudes, for the case of linearly attenuated waves, have been calculated from first estimates given by Eq (65) (or(66)) by the iterative procedure proposed by Davies (1982a).) In the remaining sections, we refer to such results as being based upon uncorrected and corrected theory, respectively. In the region of the main resonant peaks in Figs 14(a) - (c), better agreement is achieved between the measurements and the corrected, rather than the uncorrected, theory, as expected.

Figures 14(a) - 14(c) also show the measured wave reflection coefficients for the wave absorbing beach (see Figure 12) for m = 10, 4 and 2 ripples, respectively. These results were obtained using the down-wave pair of gauges (gauges 3 and 4), and are also tabulated in Table 2. For the case of 10 ripples, wave reflection coefficients from the beach were of the order of $K_B \cong 0.1$, or less, corresponding to about 1% in terms of the incident wave energy. Tests on 4 and 2 ripples showed that measured reflection coefficients from the beach were in general higher, of the order of $K_B \cong 0.2$, or about 4% in terms of energy. The reasons for these differences are not clear. Comparisons between the small gauges used for the tests on 4 and 2 ripples, and the larger gauges used on 10 ripples, showed that the former underestimated K by only about 4%, which would not account for the differences in the measured values. (Further discussion on this point is included

in §4.3.)

The importance of wave energy reflection by the beach in the present context is that it introduces uncertainty into values of the reflection coefficient $|K_R|$ based upon measurements made on the up-wave side of the ripple patch. This may be demonstrated as follows:

Let K_{RT} = true reflection coefficient of the ripple patch,
K_{RM} = measured reflection coefficient of the ripple patch,
K_{BT} = true reflection coefficient of the beach,
and K_{BM} = measured reflection coefficient of the beach,

where each symbol denotes the magnitude of the reflection coefficient in question. If we start by considering an incident wave of amplitude a, which is scattered by the ripple patch (Figure 15(a)) to give a reflected wave of amplitude $\tilde{a}_R$ and a transmitted wave of amplitude $\tilde{a}_T$, energy conservation requires that

$$\tilde{a}_T^2 = a^2 - \tilde{a}_R^2 = a^2(1 - K_{RT}^2)$$

where $\tilde{a}_R = K_{RT}a$ (see §2.3.2). Re-reflection of the reflected wave $\tilde{a}_R$ by the generator is irrelevant in the present argument, provided that equilibrium conditions have been attained by the waves (see §3.2). Such re-reflected waves merely contribute to the (equilibrium) incident wave a. What is relevant is the possible reflection of the transmitted wave $\tilde{a}_T$ by the beach. Here we assume that $\tilde{a}_T$ is partially reflected by the beach, and that the reflected wave, in turn, is scattered by the ripple patch (Figure 15(b)), such that

$$a_B = \tilde{a}_T K_{BT} ,$$

and

$$a_{BR} = a_B K_{RT} ,$$

$$a_{BT} = a_B(1 - K_{RT}^2)^{1/2} = a K_{BT}(1 - K_{RT}^2) .$$

(Re-reflection of the a_{BT}-wave by the generator is irrelevant, for the reason stated above.) Further, we assume that re-reflection of the a_{BR}-wave by the beach is negligible. This is a reasonable assumption since any re-reflected wave would have amplitude $a_{BR}K_{BT} = \tilde{a}_T K_{RT} K_{BT}^2$; in practice, $K_{BT}^2 \sim 10^{-2}$, so that little error is involved if this term is ignored.

On the basis of the above assumptions, the pattern of incident, reflected and re-reflected waves is as shown in Figure 15(c). On the up-wave side of the ripple patch we have the incident wave a, the reflected wave $\tilde{a}_R = aK_{RT}$, and the transmitted wave from the beach $a_{BT} = aK_{BT}(1 - K_{RT}^2)$. The phase angle of the a_{BT}-wave in relation to the other waves is unknown, though bounds can be placed on the phase differences resulting from it, as shown later. Clearly, the measured

reflection coefficient K_{RM} has its maximum possible value when the contributions from $\tilde{a}_R$ and a_{BT} are in phase, that is when

$$K_{RM} = \frac{\tilde{a}_R + a_{BT}}{a} = K_{RT} + K_{BT}\left(1 - K_{RT}^2\right) ,$$

and it has its minimum value when the contributions are out of phase, that is when

$$K_{RM} = \frac{\left|\tilde{a}_R - a_{BT}\right|}{a} = \left|K_{RT} - K_{BT}\left(1 - K_{RT}^2\right)\right| .$$

On the down-wave side, we have the transmitted wave $\tilde{a}_T$, the reflected wave a_B and the re-reflected wave a_{BR}. By a similar argument, the minimum measured reflection coefficient for the beach will be given when the transmitted and re-reflected waves are in phase, that is when

$$K_{BM} = \frac{a_B}{\tilde{a}_T + a_{BR}} = \frac{K_{BT}}{1 + K_{BT}K_{RT}} ,$$

and the maximum value will be given when

$$K_{BM} = \frac{a_B}{\left|\tilde{a}_T - a_{BR}\right|} = \frac{K_{BT}}{\left|1 - K_{RT}K_{BT}\right|} .$$

In practice, $K_{BT}K_{RT} \ll 1$, so that $K_{BM} \approx K_{BT}$.

It follows that bounds on the true reflection coefficient K_{RT}, in terms of the measured coefficients, may be calculated from

$$K_{RM} = \left|K_{RT} \pm K_{BM}\left(1 - K_{RT}\right)^2\right| .$$

This equation may be solved for K_{RT}, subject to the further assumption $K_{RT}^2 \ll 1$, to yield, as the final result for the bounds on the true reflection coefficient:

$$K_{RT} = \frac{K_{RM} \pm K_{BM}}{1 + 2K_{BM}^2} \approx K_{RM} \pm K_{BM} ,$$

(in which the lower bound is replaced by $K_{RT} = 0$ if $K_{BM} > K_{RM}$). The true reflection coefficient is therefore subject to a maximum error of $\pm K_{BM}$, at least provided that the following assumptions are valid:

(a) $K_{BT} \sim O(0.1)$, so that $K_{BT}^2 \sim O(0.01)$ which is negligible;

(b) $K_{BT}K_{RT} \ll 1$;

and (c) $K_{RT}^4 \ll 2K_{RT}^2 \ll 1$.

The result above for the bounds on $|K_R|$ is consistent with the measurements in Figure 14. In the case of 10 ripples (Fig 14(a)), relatively low beach reflection coefficients ($K_B \approx 0.05$) have enabled reliable estimates of $|K_R|$ to be made through a number of secondary maxima on either side of the main resonant peak. However, for 4 and 2 ripples (Figs 14(b) and (c)), rather higher values of K_B have concealed the true ripple reflection coefficient $|K_R|$, at least for values of (2k/1) on either side of the main resonant peak. It may be seen that the measured values of the reflection coefficients for the ripples and the beach are of comparable size for $2k/1 < 0.75$ and $2\ k/1 > 1.25$ in the case of 4 ripples (Fig 14(b)), and for $2k/1 > 1.5$ in the case of 2 ripples (Fig 14(c)). In these cases, it would have been necessary to reduce considerably the amount of energy reflected by the beach (below the present levels of about 4%) to have enabled theoretical predictions for $|K_R|$ to be tested for values of (2k/1) outside the main resonant peak.

Figure 14(c) shows the results of wave phase angle calculations. The points plotted represent experimentally determined values of $(\varepsilon_I + \varepsilon_R)$, where ε_I and ε_R are wave phase angles defined in Goda and Suzuki's method (see Appendix A, equation (A.1)). It is argued in Appendix A that π-phase shifts in the sum $(\varepsilon_I + \varepsilon_R)$ are associated with sign changes in the elevation of the reflected wave and hence, as noted in §2.7.1, with sign changes in the reflection coefficient K_R as defined by equation (65). For the case in which m = 2, the theory in §2 suggests that the sum $(\varepsilon_I + \varepsilon_R)$ should remain constant in $0.5 < 2k/1 < 1.5$, that there should be π-phase shifts at either end of this range, constant values of the sum in $0 < 2k/1 < 0.5$ and $1.5 < 2k/1 < 2.0$ and, thereafter, for increasing (2k/1), further π-phase shifts at 2k/1 = 2.0, 2.5, 3.0, ... Although the values of $(\varepsilon_I + \varepsilon_R)$ in Figure 14(c) are plotted on a vertical scale which is arbitrary to $\pm 2\pi$, $\pm 4\pi$ ...., π-phase shifts should have the significance indicated above. It may be observed that $(\varepsilon_I + \varepsilon_R)$ remains reasonably constant in the range $0.67 < 2k/1 < 1.31$, and also in the range $1.6 \lesssim 2k/1 < 1.93$, and that phase shifts occur in the ranges $0.5 \lesssim 2k/1 \lesssim 0.6$ and $1.45 \lesssim 2k/1 \lesssim 1.55$. These phase shifts are not at discrete values of (2k/1) as predicted, probably on account of the presence of the reflected wave from the beach; this is connected, in turn, with the fact that the measured values of $|K_R|$ do not fall to zero at either 2k/1 = 0.5 or 1.5. However, the phase shift close to 2k/1 = 1.5 is approximately equal to π. For $2k/1 > 2.0$, there is a suggestion of a general increase in $(\varepsilon_I + \varepsilon_R)$, but this is probably associated with the wave reflection by the beach. Despite some uncertainty, there appears to be a strong suggestion in the measured results of the predicted behaviour of $(\varepsilon_I + \varepsilon_R)$. The detailed way in which the sum of the phase angles has

been calculated is described in Appendix A.

4.2 Measurements of the variation of peak reflection coefficient as a function of the quotient of ripple amplitude (b) and water depth (h), and of the number of ripples (m) in the patch.

Figures 16 (a) - (d) show the results of experiments carried out to measure peak reflection coefficients for different ripple amplitude to water depth quotients (b/h), and different numbers of ripples (m). The earlier measurements in Fig 14 showed considerable variations in $|K_R|$ within the central resonant peak, which may have been due either to reflection of wave energy by the wave absorbing beach or, possibly, to the effects of additional resonances not described by the perturbation theory in §2 (see Davies (1982b)). In the tests described herein, time did not permit detailed measurements of $|K_R|$ over an extensive range of values of (2k/l), for each combination of (b/h) and m values examined. It was thus necessary to make measurements of $|K_R|$ over a limited range of (2k/l) values in the vicinity of the main resonant peak, in an attempt to measure the maximum value of $|K_R|$ for given values of (b/h) and m. Unfortunately, in practice, a representative number of measurements was not always made.

The procedure adopted, for comparison of the observations with the theoretical predictions, has been to average measurements of $|K_R|$ made in the vicinity of the main resonant peak. This averaging has been carried out within a range of (2k/l) values, centred on 2k/l = 1 and representing, in each case, ±10% of the total width of the main peak. The results are shown in Table 3 and Figure 17 as means and standard deviations of the measured $|K_R|$ values lying within these ranges. In Figure 17, the averaged 'peak' $|K_R|$ values are compared with both uncorrected, and corrected, theoretical predictions for the maximum reflection coefficient. For the cases of m = 10, 4 and 2 ripples, the averaged peak values give good agreement with the corrected theory. However, for m = 1, the measured values considerably overestimate the predictions; it is thought that this is due partly to the unrepresentative nature of the measurements (see Figure 16a), and partly to the effects of wave reflection by the beach. As mentioned in §2.7.3, the theory predicts over-reflection ($|K_R| > 1$) for certain parameter settings (see, for example, the cases in Figure 16c for which b/h = 0.36 and 0.40, and in Figure 16d for which b/h = 0.18 and 0.20). Although experimental results have been obtained in such cases, no meaningful comparisons with the present theory are possible.

4.3 Measurements of surface elevation and reflection coefficient over, and on either side of, the ripple patch.

In order both to assess whether the measured values of $|K_R|$ discussed in § 4.1 and 4.2 were truly representative of the reflection coefficient, and also to obtain a general understanding of the wave field throughout the tank, a series of measurements was made with the gauge configuration shown in Figure 12, which was moved along the tank in steps of 1 m. The resulting measurements of the amplitude of the surface elevation both above the ripple patch, and on either side of it, are shown in Figures 18a - 18i, and are tabulated in Table 4. The observations were made at or near the predicted resonant peak, as were the results in Figure 16, and the measured surface elevations have been compared with predictions of elevation given by both the uncorrected and corrected theory (see §2.7.2). The incident wave amplitude used in the comparisons was obtained by averaging the first five values of $a_I(=a)$ tabulated for the up-wave side of the ripple patch in Table 4. The results for m = 2, 4 and 10 ripples show good agreement with the theory, and indicate clearly how the standing wave pattern on the up-wave side of the ripples gives way to a purely progressive wave on the down-wave side (having an envelope described by two parallel lines). On the down-wave side, agreement is better between the measurements and the corrected, rather that the uncorrected, theory. Moreover, the observations show how the incident waves are, to all intents and purposes, linearly attenuated across the ripple patch, as assumed in §2.3.2. No comparisons with theory have been possible in Figures 18h and 18i, for m = 10 ripples and water depths of h = 25.0 cm and h = 27.8 cm, respectively. For these conditions, the theory predicts over-reflection ($|K_R| > 1$, cf Figure 16d), and so the measured values have simply been joined by a cubic spline to indicate their overall trend.

In general, there is good agreement between the measured and predicted positions of the partially standing wave pattern (fixed in space) on the up-wave side of the ripple patch. This is seen in Figures 18(a) - (g) where the phase angles of the measured and predicted envelopes of wave elevation are very similar. In most cases however, there is evidence of a small progressive phase shift, indicating a slight mismatch in wave period between the nominal value adopted for the theoretical comparisons and the true experimental value. Calculations (see Table 5) have shown that this may have given rise to cumulative discrepancies in phase of 1°-3° for each wavelength of the incident wave. For the case of m = 10 ripples (Figures 18c - 18g), this implies wavelengths in the experiments which were about 0.6-1.7 cm shorter than those predicted in the theoretical comparisons

based on the nominal wave period settings. Such differences suggest true wave periods which were 0.002 - 0.006 s lower than the nominal values, for typical resonant waves with wavelength 200 cm in 50 cm depth of water. Table 1 shows that, in the range 1.2 to 1.8 s, true wave periods were between 0.001 and 0.004 s lower than the nominal settings. Since such differences are of the same order as those which may be inferred from the measurements, the observed disagreements in phase may be accounted for by a small experimental error in the wave period setting. However, calculations on the data for m = 2 and m = 4 ripples (Table 5) suggest that the mismatch may have been greater in these cases, possibly of the order of 0.02 - 0.03 s in the wave period setting. The reason for the poorer agreement in these cases is not clear.

It is possible that other factors may have contributed to the observed phase differences. For example, the cumulative phase shift described above may have been superimposed on a constant phase shift throughout the partially standing wave pattern on the up-wave side (eg Fig 18(g)). It is possible that such a phase shift may have been due, at least in part, to wave reflection by the beach. It was shown in §4.1 that this effect introduces uncertainty into the measured values of the reflection coefficient $|K_R|$. By a simple extension of the earlier argument, it may be shown that reflection by the beach may introduce also a constant phase shift in the position of the envelope of the measured partially standing wave pattern. The bounds on this phase shift may be expressed by

$$\Theta_1 = \pm \cos^{-1}\left(1 - \frac{\theta_1^2}{2}\right) \quad \text{where} \quad \theta_1^2 = \left(\frac{a_{BT}}{a_R}\right)^2 = \frac{K_{BT}^2\left(1 - K_{RT}^2\right)^2}{K_{RT}^2},$$

and where K_{RT} and K_{BT} are the true reflection coefficients for the ripples and beach, respectively. (This result has been obtained by assuming that $\theta_1 = a_{BT}/a_R \ll 1$; in particular, by neglecting terms of higher order in θ_1, than θ_1^2 in a series expansion for $\cos \Theta_1$. The assumption that θ_1 is small is clearly valid in near-resonant cases, such as those in Fig 18.) If we use the earlier results in §4.1 to relate K_{RT} and K_{BT} to their equivalent measured values K_{RM} and K_{BM}, namely

$$K_{BT} \approx K_{BM} \quad \text{and} \quad K_{RT} = K_{RM} \pm K_{BM},$$

we arrive at the final result for the bounds on the measured wave envelope:

$$\Theta_2 = \pm \cos^{-1}\left(1 - \frac{\theta_2^2}{2}\right) \quad \text{where} \quad \theta_2^2 = \frac{K_{BM}^2\left(1 - (K_{RM} - K_{BM})^2\right)^2}{(K_{RM} - K_{BM})^2}.$$

Here the worst possible case has been chosen, that is the case which maximises the

bounds on the phase shift (and which has been distinguished from the result based upon the true reflection coefficients by the change of subscript). In practice, for the results in Figs 18(a) - 18(g), the values for the bounds Θ_2 are ±5°, ±2°, ±8°, ±6°, ±5°, ±6° and ±5°, respectively. (Note here that there are two antinodes in each cycle of 360°.) The fact that these values are rather small, and that cumulative phase shifts of 1° - 3° per wavelength were consistently observed, supports the view that the disagreement in Figs 18(a) - 18(g) was most likely due to a mismatch in wave periods and not due to reflection by the beach.

It should be noted, finally, that consistent underestimates of the water depth in the wave tank might also have accounted for small progressive phase shifts. However, for this effect to have produced phase shifts of 1° - 3°, for waves of 200 cm wavelength in a nominal water depth of 50 cm, the actual water depths would have to have been 0.7 - 1.9 cm lower than indicated. Since water depths were set, using a pointer gauge, to an estimated accuracy of ±0.1 cm, this effect is unlikely to have contributed significantly to the differences in Figures 18(a) - (g).

Reflection coefficients calculated by the method of Goda and Suzuki (1977) are normally obtained from measurements made above flat beds. If the method is used with measurements made above an undulating bed of the present kind, the values obtained for the reflection coefficient need to be interpreted carefully, for the reasons given in Appendix A. In particular, the values will depend upon the gauge spacing and may contain quite marked local spatial variations. In the present context, what is obtained by the method of Goda and Suzuki is a modified reflection coefficient, K, which is such that $K \rightarrow |K_R|$ only on the up-wave side of the ripple patch. Figures 19(a) - (i) show comparisons of the measured and predicted reflection coefficients at resonance, both over the ripple patch and on either side of it, for m = 2, 4 and 10 ripples, and for different values of the ripple amplitude to water depth quotient (b/h). The results are also tabulated in Table 4. It should be noted that wave reflection measurements from gauges 1 and 2, only, have been used throughout these comparisons. Table 4 shows that for the case of m = 10 ripples, with the large gauges, gauges 1 and 2 gave measurements which were in good agreement with gauges 3 and 4. However, measurements for m = 2 and 4 ripples, with the small gauges, show that gauge pairs 1 and 2, and 3 and 4, differed consistently by as much as 0.1 in the measured reflection coefficient. Earlier tests (§3.3) had shown that the small and large gauges gave results which agreed to within 4%, and so the reasons for the differences in Tables 4(a) and 4(b) are not clear. For consistency with other measurements (eg §4.1 and §4.2), it was decided to use gauges 1 and 2 (large and small) throughout. However, gauges 3 and 4 were used

to provide some of the surface elevation data discussed earlier; this data was not found to include any spurious effects that might be attributable to the gauges (Figures 18(a) and 18(b)).

Agreement between the observations and the theory in Figure 19 is generally good, the best agreement again being achieved between the observations and the corrected, rather than the uncorrected, theory. For small amounts of reflection (eg Fig 19(c) in which $|K_R| \sim 0.15$, m = 10 and b/h = 0.08), agreement between the measured and predicted values of K is particularly good throughout the tank. However, as b/h is increased and the amount of wave reflection becomes larger, measured reflection coefficients tend to underestimate the theoretical values on the up-wave side of the patch, and to overestimate them on the down-wave side. In the case of m = 2 ripples (Figure 19(a), b/h = 0.32), the measured reflection coefficients tend to overestimate the theory on both the up-wave and down-wave sides, the best agreement being directly over the ripple patch. However, the results for m = 10 and m = 4 ripples show better agreement. A particular, though as yet unexplained (see §5.4), feature of the results is that the measured reflection coefficients tend to rise to localized maxima just before the incident waves enter the ripple patch, and fall to localized minima just as the waves leave the patch. More generally, on the down-wave side of the patch, the non-zero measured values of K indicate the effects of reflection by the beach while, on the up-wave side, the tendency for values of K to decrease steadily towards the wave generator is probably due to viscous dissipation in the tank, as discussed below. No theoretical results are shown for those cases in which over-reflection was predicted. All measurements of the present kind for m = 2, 4 and 10 ripples are summarized in Figs 20(a) - (c), in which the trends in the reflection coefficient are indicated by cubic splines fitted to the measured values.

It was suggested above that the tendency in Figs 19(c) - (i) and 20(c) for the reflection coefficient $K = |K_R|$ on the up-wave side to decrease towards the wave generator was due to viscous dissipation in the tank. Although this effect was generally a small one, it should be borne in mind in interpreting the results in Figs 13, 14, 16 and 18, for which the wave gauges were at fixed positions mid-way between the wave generator and the ripple patch. The estimates obtained for $|K_R|$ with these gauge positions may have been slightly less than estimates which could have been obtained with the gauges nearer to the ripple patch (but, necessarily, outside the region of influence of the trapped wave modes at the end of the patch). In order to obtain a rough estimate of the effects of dissipation in the tank, the simple situation of waves propagating down the tank above a purely flat bed has been examined (see Appendix C). The results obtained suggest that energy dissi-

pation rates in the approximate range 8 - 64% of the energy generated by the wavemaker may have occurred in the tank as a whole, depending upon the water depth and the surface wavelength. The low value of 8% applies to relatively long wavelengths in relatively deep water (λ_w = 400 cm, h = 62.5 cm), and the high value of 64% to short wavelengths in shallow water (λ_w = 80 cm, h = 12.5 cm). However, these rather large dissipation rates, for purely progressive waves, need to be interpreted carefully in assessing the possible effects of dissipation on estimates of the reflection coefficient in the present experiments. The particular question of dissipation in the partially standing wave structure on the up-wave side of the ripple patch is discussed in Appendix C, and it is concluded that dissipation will have tended to cause underestimates in $|K_R|$ for measurements made with gauges positioned mid-way between the wavemaker and the ripple patch (Figs 14, 16 and 17). It is concluded also that dissipation will have given rise to general decreases in measured values of $|K_R|$ with distance from the ripple patch on the up-wave side (Figs 19 and 20).

4.4 Observations of sediment movement

Davies (1980, 1982a) suggested that, in resonant cases, the near-bed velocity field associated with the partially standing wave pattern on the up-wave side of the ripple patch may give rise, on an erodible bed, to preferred regions of deposition and erosion of sediment (see also §2.7.4). It was argued that this provides a possible mechanism for the growth of the existing ripple patch in the up-wave direction and, further, that there may be a coupling between wave reflection and the growth of new bedforms.

To test this supposition, sand of mean diameter 235 μm was distributed in a thin (< 0.05 cm) uniform layer throughout the ripple patch, and for a distance of 2 m in the down-wave direction and 3.5 m in the up-wave direction. The tests were carried out with m = 2 ripples, water depth h = 15.6 cm (b/h = 0.32), and a resonant wave period of T = 1.73 s . The corresponding measured wave reflection coefficient was $|K_R| \approx 0.34$. Starting from rest the stroke of the wave generator was increased until sand motion was initiated. The subsequent development of ripples of small wavelength (O(5 cm)) was then recorded photographically at intervals over a period of approximately 130 minutes. Small sand ripples were first observed to occur both on the crests of the original long wavelength ripples, and also in the up-wave direction in patches approximately 1 m apart (ie with the same spacing as the original ripples). At the outset, these patches of small ripples formed under the nodes of the partially standing waves on the up-wave side,

where the wave-induced bed velocities were greatest. With increasing time, ripples started to form up-wave of these nodes, with the largest ripples forming about half way between the nodes and antinodes. The ripple heights increased with increasing distance from the nodes such that, at the nodes, heights were typically 0.1 to 0.2 cm while, midway between the nodes and antinodes, heights were typically about 1.5 cm and wavelengths were 5.5 cm (see Figure 21). These ripples displayed an asymmetry, having their steepest faces in the down-wave direction. Despite this, there was a net movement of sediment in the up-wave direction, associated with the action of vortex shedding from the ripple crests. In general, it might be expected that, for net sediment accumulation to occur close to an antinode of surface elevation, ripple heights would increase in this direction, even though the water particle excursions due to the waves decrease. The situation on the up-wave side of the ripple patch may be contrasted with that on the down-wave side, where small ripples, asymmetric in the down-wave direction, were observed to grow and spread over the entire bed, with uniform height and spacing. Typical ripple heights were about 0.5 to 0.8 cm, and ripple wavelengths were about 4 cm.

The development of the patch of small sand ripples on the up-wave side of the original ripples is shown schematically in Figure 21, and a sequence of photographs illustrating the evolution of the ripple patches during the 130 minute period is shown in Figures 22(a) - (f). A photograph is also included of the ripple sheet on the down-wave side (Figure 22(g)). To enable clear photographs to be taken in still water, the wave generator was stopped for each photograph, and was then restarted. The position of the ripple patches in relation to the standing wave nodes and antinodes is illustrated in Figure 21. The positions of the nodes and antinodes themselves were obtained from earlier measurements on 2 ripples with the same ripple amplitude to water depth ratio (b/h = 0.32). Details of the wave field giving rise to the observed sediment motion (Figures 22a - 22f) were also determined from these earlier measurements made without any sand in the tank. The absence of sand, and hence small ripples, in the short section of the tank near the original patch might have led to slightly different wave conditions compared with those when sand was present, due to increased wave energy dissipation. However, this effect was probably very small.

In Figure 23, theoretical results for the horizontal velocity field are shown for the parameter settings in the above sediment transport experiment (m = 2, h = 15.6 cm, T = 1.73 sec). From equation (16) the water wavelength was 206.7 cm, so that 2k/l = 0.968 which indicates that the run was close to resonance. The

predicted reflection coefficient for unattenuated incident waves is given from equation (65) by $K_R = 0.455$, and for attenuated waves by $K_R = 0.433$. These values may be compared with the measured value of $|K_R| = 0.34$. For simplicity, the horizontal velocity amplitude has been plotted, rather than the tangential; it may be recalled from Figure 11 that the two results are closely similar over the ripple patch. Also, the results plotted are for unattenuated incident waves, the results for attenuated incident waves in this case being very similar. Velocity amplitudes are plotted as functions of horizontal distance (x) for the heights (y/h) = 0 (free surface), -0.5 and -1.0 (bed). The velocities at these heights are nearly in phase in respect of variations in (x) but, as in Figure 10, are attenuated rather differently over the flat and rippled parts of the bed. (Note that the divergences in the predicted bed velocity field at the ends of the patch ($x = \pm L$, $y/h = -1.0$) have no general significance, as explained in §2.7.2) For the present purpose, we need only be concerned with the velocity amplitude at the bed, and what is of interest is the relationship between this quantity and the threshold velocity amplitude of the sand size in question (235 μm). For monochromatic waves with the experimental wave period, and for a flat bed, Komar and Miller's (1975) formula gives the threshold velocity amplitude as 11.4 cm s^{-1}, or $\hat{u}/U_o = 0.89$ in normalised form as plotted in Figure 23. It may be seen that, on the down-wave side, the threshold velocity amplitude is less than the predicted bed velocity amplitude. This is consistent with the observed formation of a sheet of ripples of short wavelength on the region of flat bed. On the up-wave side, where the reflected wave gives rise to a partially standing wave pattern, the threshold velocity amplitude is greater than the predicted velocity in certain parts of the bed (marked "D"), and less in other parts (marked "E"). In the former parts, no sediment motion should occur and deposition of sand may be expected. In the latter parts, sediment motion may occur and erosion may be expected, particularly near maxima of the bed velocity amplitude. Over the ripple patch itself predictions of this kind, based upon Komar and Miller's threshold velocity amplitude result, are complicated by the fact that the bed is not flat; in particular, on sloping parts of the bed, rather lower threshold values are expected, depending upon the local bottom slope. If we ignore this complication and treat the matter in the same way as for a flat bed, we again arrive at the prediction of regions of deposition and erosion on the bed. It may be seen from Figure 23 that, for both the flat and rippled regions of the bed, the predictions of deposition "D" and erosion "E" were reasonably well borne out by the experimental observations. On account of the grain size in use, sediment motion occurred as bed load only; if there had been a

suspended load, deposition would possibly have occurred throughout the regions marked "D".

Previous observations of patches of rippled, and of unrippled, sand on a flat erodible bed beneath partially standing waves have been made in the laboratory by Kennedy and Falcon (1965, §4.3). However, the situation described by these workers was rather different from that in the present experiment. Firstly, the partially standing wave pattern in their experiment was caused by the superimposition of incident waves and waves reflected by a beach. Secondly, their observations were made in more active conditions than those which prevailed in the present experiment, to the extent that the patches of ripples and of flat bed coincided with relatively low and high near-bottom velocity amplitudes, respectively. Furthermore, the positioning of the patches of ripples and of flat bed was complicated both by the existence of significant drift velocities in the tank, and by the asymmetrical nature of the bottom velocity field associated with the (steep) incident waves. Despite all of these differences with the present experiment, however, the observations of Kennedy and Falcon provide an interesting, and contrasting, example of the effects of a partially standing wave structure on an erodible bed.

The predicted and observed partially standing wave pattern on the up-wave side of the ripple patch in the present experiment suggests, quite unambiguously, that new ripples may develop on the region of flat bed as a result of wave reflection by the existing, longer wavelength, ripples. Indeed, this has been demonstrated clearly in the present experiment, in which it was found that deposition (D) and erosion (E) of sand occurred in regions of the bed where the predicted horizontal bed velocity amplitudes were minimum and maximum, respectively. This pattern of deposition and erosion is suggested by intuition as the most likely outcome of a standing wave structure above an erodible bed. However, as argued by Davies (1980, Part 1 §7), the situation may not be quite as clearcut as this intuitive argument suggests. The reason for this is that the residual circulation cells resulting from bottom friction under a standing wave have a rather complicated structure (Longuet-Higgins (1953), Noda (1968), Johns (1970), Liu and Davis (1977)). In particular, for a smooth flat bed and a purely standing wave, the direction of the residual velocity changes at a certain height above the bed. If the boundary layer is laminar, this height is equal to 0.93 δ_* (Longuet-Higgins, 1953) where δ_* is the Stokes' layer thickness (= $\sqrt{2\nu_w/\sigma}$ in which ν_w is the kinematic viscosity). If it is turbulent, the height is considerably larger than this (Johns 1970). In both cases, water particle residual motions immediately

above the bed, in the "inner" layer, are towards the positions of greatest horizontal motion, and away from the positions where the motion is purely vertical; that is, it is towards positions beneath nodes of elevation, and away from positions beneath antinodes. This has been demonstrated by Noda (1969), who found that vinyl pellets moving on a smooth bed accumulated beneath the nodes of a standing wave. In the upper, or "outer", layer immediately above, the residual motions are in the opposite directions. The implications of this rather complicated velocity structure for sediment movement have been discussed by Johns. For rough beds, and for laminar flow in the boundary layer, Johns has suggested that any material in motion near the bed will probably be present in the "outer layer" (by virtue of the very small "inner layer" thickness which, for the conditions shown in Figure 22, was of the order of $\delta_* = 0.07$ cm), and that the residual velocity in this layer will probably give an indication of the direction and magnitude of sediment transport. In the laminar case, therefore, the influence of the residual velocity is consistent with the earlier intuitive argument. However, in the physically more interesting case of a turbulent boundary layer, the greater thickness of the inner layer suggests that sediment motion may be confined to this layer within which the residual motion of water particles, and hence sediment, is towards positions of greatest horizontal motion. In the turbulent case, therefore, the intuitive and mass transport arguments suggest opposing tendencies. The true result will depend to a large extent on the sediment grain size involved; in particular, on whether the sediment is transported as bed load only, or as both bed load and suspended load.

The laboratory experiments of Nielsen (1979) demonstrated ripple growth beneath standing waves, with sediment accumulation occurring at the antinodes of surface elevation. For the very fine sand used ($D_{50} = 0.08$ mm), Nielsen observed an upwardly convected cloud of grains above the evolving ripple crests, and interpreted his observations on the basis of the residual transport pattern described above for a laminar boundary layer. As far as the present experiment is concerned, it should be noted, firstly, that there was a partially standing wave structure on the up-wave side of the ripple patch, rather than a purely standing wave as in Nielsen's experiments. (This does not affect any of the general implications of the qualitative argument above however.) Secondly, the boundary layer was laminar (Reynolds number, $RE = U_b^2/\sigma\nu_w \approx 3 \times 10^3$ where $U_b = U_o/\cosh kh = gak/\sigma\cosh kh$; see also Appendix C), and sediment motion occurred as bed load only. The observations of incipient ripple formation were consistent, therefore, both with the intuitive argument and with the mass transport argument for the laminar

case. The absence of a suspended load meant that ripple formation could not proceed in the manner observed by Nielsen. Instead, regions of no motion on the up-wave side of the patch marked regions of the bed which, in a more active flow, might have evolved into ripple crests. Direct evidence of the laminar nature of the flow was provided by dye tests, which showed that dye patches retained their identity for considerable periods of time and did not disperse rapidly, as would have been the case if the flow was turbulent.

It was argued in §2.7.4 that, for there to be a coupling between wave reflection and ripple growth, accumulation and erosion of sediment must occur on the existing ripple patch in a way which suggests ripple growth rather than ripple destruction by the wave action. In the earlier discussion of Figure 23, it was suggested on an intuitive argument that, if the effects of bed slope are ignored, deposition and erosion should occur at the positions marked D and E, respectively, and this theoretical prediction was quite well supported by the experimental observations. However, these observations also suggested either the destruction of the two existing ripples or, possibly, their overall movement in the up-wave direction, by erosion of sand from the regions both of their crests and their down-wave slopes, and deposition on their up-wave slopes. Unfortunately, with the fixed bed in the present experiments, it was not possible to establish which of these alternatives would have been the true outcome on a fully erodible bed of single grain size. On the one hand, it may be argued that the existing ripples were unstable, on the basis of both theory and experiment, since their crests were subjected to large bed velocities. On the other hand, the peak bed velocities, which were found down-wave of each crest position, suggest the possibility of bedform migration, and hence stability. Clearly, this matter needs further experimental investigation over a wide range of parameters settings (including grain size), not least because of the complications which may arise in cases in which the flow in the boundary layer is turbulent. There are further considerations which may be relevant to the question of the stability of the existing bedforms. For example, Sleath (1974, 1976) has shown that both a uniform oscillation, and a progressive wave motion, over a rippled bed give rise to residual circulation cells in which the fluid near the bed is transported towards the ripple crests. In the present context, the correct interpretation of this result for bedform stability and growth again depends rather critically upon the manner in which sediment is transported. As a result of all these uncertainties, and also of the possible effects of variable grain size (discussed below), it would be premature to conclude that the existing ripple patch in the present experiment was either stable or unstable.

Rather than leaving this matter entirely for further investigation, we dis-

cuss here finally some theoretical results obtained for the case of a ripple patch comprising m = 10 ripples in water of depth h = 41.7 cm, corresponding to one of the earlier experimental runs (see Figures 18e and 19e). Horizontal bed velocity amplitudes have been calculated over the entire patch, with an incremental spacing of 2.5 cm (= 1/40 x ripple wavelength), and for various values of 2k/l around the resonant peak, namely 2k/l = 0.95, 0.97, 0.99, 1.01, 1.03 and 1.05. For each of these values, the positions of each of the bed velocity maxima and minima throughout the patch have been established and, in Figure 24, these positions are compared with the fixed crest and trough positions. The results plotted are for unattenuated incident waves, almost identical results being obtained for attenuated waves. It may be seen that the maxima and minima are displaced in the down-wave direction from their respective crests and troughs. For fixed (2k/l), the displacements have a general tendency to decrease in the down-wave direction. However, they generally increase with (2k/l) itself. What the results indicate about the stability of a patch of 10 ripples is again somewhat ambiguous. For the case in which 2k/l = 0.95, velocity maxima and minima may be seen to occur close to the positions of crests and troughs, respectively. The displacements actually increase from zero at both ends of the patch, to peak values of about 5 cm in the middle. The earlier intuitive argument suggests that this is an unstable state, though, as we have suggested earlier, other considerations may need to be taken into account before the true result can be established. Through the resonant peak ($2k/l \approx 1$), the displacements from both the crest and trough positions steadily increase. For the case 2k/l = 1.05, which is still strongly resonant, the maxima and minima at the up-wave end of the patch are displaced by about 25 cm and 45 cm, respectively. The values then diminish to zero in the down-wave direction. Evidently, the displacements in this case are quite large, the extreme value of 45 cm bringing the first (significant) velocity minimum to within about 5 cm of the next crest. This suggests that the bed may be more stable for 2k/l = 1.05 than for 2k/l = 0.95, particularly at the up-wave end of the patch. For all the values of 2k/l investigated, there is the further suggestion that the ripple pattern may migrate, probably in the up-wave (-x) direction (as in the case discussed earlier in which m = 2). Finally, it might be noted that, for 2k/l = 1.05, secondary maxima and minima in bed velocity occur. These complicate the interpretation of the results somewhat, though they stand apart from the primary maxima and minima which govern the overall trends in the results.

The discussion above has been concerned with the situation in which the bed comprises a single sediment grain size only. For a bed comprising a mixture of grain sizes, the question of the stability of a patch of ripples is more involved,

as demonstrated by Scott (1954) in a laboratory study concerned mainly with onshore/offshore sediment transport on a beach. Scott commenced his experiments with an initial beach profile, and then allowed waves to "mold the beach until an approximate equilibrium profile was obtained." The beach profile changes involved the formation of a series of offshore bars, and in his description of this process Scott makes the following observations: "Reflections from the beach were visible from the start of each run, but (a pronounced) standing wave did not become visible before the offshore bars had formed. Evidently the bars caused additional reflections which built up the amplitude of the standing wave ..... The nodes of the standing waves were in all cases over the offshore bars ....." In other words, the bars (ie ripple crests in our earlier terminology) were subjected to greater horizontal velocities than were the regions between the bars (troughs), and yet the bars were stable. This was explained by Scott in terms of the observed tendency for coarser grains to be found on top of the bars, and for finer grains to be found in the troughs between the bars. Clearly, this phenomenon is highly relevant to the earlier discussion of the stability of bottom ripples, though it is not a matter which we are able to pursue further here.

In conclusion, it would appear that further theory and experiment are needed to clarify the central point of the present discussion, namely whether there is a coupling between wave reflection by an existing ripple patch and the growth of new ripples on its up-wave side. The theory required for such an investigation is beyond the scope of the irrotational model described in §2. In particular, some detailed calculations of the effects of bottom friction in the problem are needed to determine the roles of the bottom stress, and of residual velocities, in situations in which there may be suspended sediment motion, as well as bedload motion. Ideally, such work should be supported by a comprehensive experimental study with a fully erodible bed, in which both the wave parameters, and the sediment size, are varied over wide ranges.

5. DISCUSSION

5.1 The validity of the comparisons

Before the experiments described in §4 were carried out, it was thought necessary to establish that the waves generated in the tank complied with the limitations on the theory described in §2. This entailed determining optimum settings for the wave generator and, in particular, appropriate settings for the stroke (S). With this aim, tests were carried out with different water depths and different amounts of wave reflection by the ripple patch.

The limitations on the perturbation solution have been discussed in §2.7.3 where they were expressed as a set of criteria involving the various length scales in the problem, namely

$$ak,\ a/h,\ a/k^2h^3,\ bl,\ b/h \text{ and } bk \ll 1,$$

where a is the incident wave amplitude (=H/2), k is the free surface wavenumber (= $2\pi/\lambda_w$), h is the water depth, b is the ripple amplitude and l is the ripple wavenumber (= $2\pi/\lambda_R$). Of these criteria, the one most easily violated, in practice, was that which concerns the wave steepness ak (= $\pi H/\lambda_w$). Tables 2 and 3 show that typical wave steepnesses for the test described in this report were usually at the low end of the range $0 < ak \lesssim 0.16$ (or $0 < H/\lambda_w \lesssim 0.05$), well within the limitation above. However, in order to investigate the effects of different settings of the wave generator for the present experimental set up, a series of tests was carried out with m = 10 ripples. The purpose of these tests was to establish whether variations occurred in the measured wave reflection coefficient on the up-wave side of the ripple patch, as the wave steepness was increased. The results in Figure 25 and Table 6 show that, for values of the reflection coefficient $|K_R|$ in the range 0 - 0.65, the amount of wave reflection remained relatively constant with increasing wave steepness, and therefore stroke (S), up to values of ak of about 0.16 ($H/\lambda_w \approx 0.05$). The numbers above the data points in Figure 25 indicate the stroke (S) of the wave generator in centimeters. Since the majority of the tests described in this report (see Tables 2 and 3) were carried with values of S of 2 cm, they were well within the required limits.

As far as the two remaining criteria involving the wave amplitude (a) are concerned, the criterion involving (a/h) was well satisfied, since a was always less than 2 cm and the depth (h) was always greater that 12.5 cm. Thus $a/h \lesssim 0.16$, though in general the quotient was much smaller than this limiting value. As far as the limitation involving the Ursell parameter (a/k^2h^3) is concerned, the criterion is actually less severe than indicated above, and may be expressed by $a/k^2h^3 \ll 8/3$ (Davies 1982b). The worst case in the present experiments (see Table 2b), was that in which $\lambda_w \approx 400$ cm, h = 15.6 cm and a = 0.41 cm, so that $a/k^2h^3 \approx 0.44$. A contrasting value for short wavelength conditions (Table 2b) was that in which λ_w = 79.9 cm, h = 15.6 cm and a = 0.76 cm so that $a/k^2h^3 = 0.032$. In general, all the criteria involving the wave amplitude appear to have been satisfied in the experiments. As a further check on this, the results of spectral analysis of the measured data have been examined, in order to investigate the linearity of the measured wave field. The results are described in the next section.

The three remaining criteria involve the ripple amplitude (b). Clearly, the ripple steepness (bl) was fixed by the chosen ripple geometry (b = 5 cm, λ_R = 100 cm), so that bl = $\pi/10$. (This value was chosen because of its similarity to actual ripple and sandwave steepnesses.) The largest experimental value of the quotient b/h was 0.4, and the largest value of bk was about 0.39. While these values are perhaps larger than might have been desirable, the majority of the experiments were carried out with significantly smaller values. Moreover, as argued in the next section, spectral analysis has revealed that the wave field was almost always linear; this would not have been so if, for example, b/h had been too large. So we may conclude that the comparisons between the experiments described in §4 and the theory in §2 were carried out with parameter settings which generally satisfied the criteria in §2.7.3.

A final limitation on the theory was that the flow above the rippled bed was always nonseparating. This requirement was satisfied in all of the experimental runs described in §4. The criterion for nonseparating oscillatory flow above a rippled bed is that the ripple wavelength (λ_R) is greater that the orbital excursion ($2A_b$) of the water particles close to an equivalent flat bed ($A_b = U_b/\sigma$ and $U_b = gak/\sigma\cosh kh$) (Sleath, 1975). In the present experiments, values of $2A_b/\lambda_R$ were generally $O(10^{-1})$, and typically in the range 0.05 - 0.15. Although the dimensionless parameter ($2A_b/\lambda_R$) takes no account of the presence of the reflected wave over the patch, it is clear that there was no possibility of separation in any of the experimental runs; this was confirmed by introducing dye into the flow in some selected cases.

5.2 The linearity of the measured wave field

Calculations of the reflection coefficient were generally made in such a way that the final results were relatively insensitive to any redistribution of wave energy from the fundamental frequency, into the first and higher harmonics (see Appendix A). However, since the theory in §2 assumes a monochromatic wave field, it was thought desirable to re-examine the data in a sufficiently detailed way that the presence of harmonics could be identified, and their causes could be examined. Thus, all the wave gauge data was Fourier analyzed once again, both over the standard measurement period of 64 sec, and also over reduced periods which were chosen such that the truncated records contained an integral number of wave cycles (see Appendix A). The results of this investigation revealed that, in the overwhelming majority of experimental runs, more than 95% of the total wave energy was at the fundamental frequency, most of the remainder being in the first harmonic. In fact, in most cases, the fundamental accounted for 98%, or more, of the total

energy. This provides a clear demonstration of the linearity of the wave field.

However, in certain cases, rather less energy was found in the fundamental frequency; in particular, levels of 85 - 90% were measured in several runs. The reason for the presence of a significant first harmonic in these runs has been analyzed in relation to various of the non-dimensional parameters discussed in §5.1, namely the wave steepness (ak), the wave amplitude to depth quotient (a/h), the ripple amplitude to depth quotient (b/h) and the ripple amplitude to wavelength quotient (bk). (It might be noted that $bk = \frac{\pi}{20} \cdot \frac{2k}{1}$ for the fixed bed geometry in the experiments.) Each of these parameters was required by the theory in §2 to remain small, a violation of this requirement being expected to give rise, in each case, to nonlinearities in the wave field, that is to the presence of harmonics of the fundamental. However, detailed analysis of all the available data revealed no discernable reduction in the proportion of energy in the fundamental with increases in any of the four parameters investigated. Moreover, a similar investigation carried out in respect of the reflection coefficient of the beach K_B also indicated no correlation of the kind sought. The only reasonably distinct correlation was between low proportions of energy in the fundamental and low values of the wave steepness (ak). This rather unlikely result is probably explained by the inability of the wave gauges to resolve very low waves adequately. However, since there were many more runs at low values of wave steepness for which the wave field was essentially linear, rather than partly nonlinear, this conclusion is, at best, tentative. The important point is that, for high values of (ak), (a/h), (b/h) and (bk), the wave field was linear, as required for meaningful comparisons with the theory.

5.3 Measurements of the reflection coefficient

The results shown in Figure 14 provide substantial experimental confirmation of the two main features of the theoretical predictions in §2. Firstly, they demonstrate the resonant interaction between the surface waves and the bottom undulations for wavenumbers such that $2k/l \approx 1$ and, secondly, they confirm the oscillatory nature of the wave reflection coefficient as 2k/l is varied. Figure 14 shows that the measured values follow closely the trend of the predicted central resonant peak, and even reproduce the trend in the adjacent secondary peaks (Fig 14a). As shown in §4.1, some loss of resolution is to be expected for values of (2k/l) outside the central resonant peak, due to the effects of wave reflection by the beach. In particular, it has been shown that the true ripple reflection coefficient has probably been estimated in the experiments only to within a range of uncertainty around the measured value K_{RM} given by $K_{RM} \pm K_{BM}$, where K_{BM} is the

measured reflection coefficient of the beach. Since, in general, K_{RM} was less than 0.2 for values of (2k/1) outside the main resonant peak, a meaningful comparison with the theory in §2 may be expected only if $K_{BM} << 0.2$. Only in the case of m = 10 ripples was $K_{BM} << 0.2$, and this was particularly so for $2k/1 > 1.3$. As expected therefore, Figure 14a shows the measurements following the general trend of the theory down to quite low values of K_{RM} (of the order of 0.05 and less). However, in the cases of m = 4 and 2 ripples, values of K_{BM} were in the approximate range 0.10 - 0.15, so that the theoretical predictions for K_{RM}, which were lower than this, could not have been expected to be clearly resolved.

Phase angle comparisons were possible only in the cases of m = 4 and 2 ripples and, of these, the measurements with 4 ripples were complicated by the presence of large amounts of wave energy reflected by the beach. However, the tests with 2 ripples have provided some quantitative evidence to support the predicted π-phase shifts in the wave reflection coefficient. (It will be recalled that K_R changes sign in the original formulation as 2k/1 is varied (Eq (65))). The solid line step function in Figure 14(c) shows the predicted phase shifts.

The variation of the maximum possible wave reflection coefficient for a given number of ripples in the patch, and a given quotient for the ripple amplitude to water depth, is shown in Figure 17. The variation of the measured $|K_R|$ values within the chosen ±10% width limits around the main resonant peak has been discussed in §4.2 (see Figs 16(a)-(d)). In Figure 17 this variation is indicated by the standard deviation bars. Figure 17 shows that in the case of m = 10 ripples, for which the representative measurements of peak reflection coefficient are shown in Figure 16(d), the averaged peak reflection coefficient underestimates the predictions of the corrected theory by about 15% at b/h = 0.18. Measurements for m = 4 ripples follow the predicted peak values quite closely up to b/h = 0.2 but, above this, underestimate the corrected theory by about 10%. However, of these comparisons, it may be seen from Figure 16(c) that only for b/h settings of 0.10, 0.12, 0.16 and 0.40 were representative values of $|K_R|$ obtained. In the case of m = 2 ripples, measured peak reflection coefficients are in good agreement with the theory, despite the lack of representative measurements within the ±10% width limits (Fig 16(b)). By comparison, the measurements on m = 1 ripple were not representative of the true variation around the peak (Fig 16(a)), and the averaged $|K_R|$ values consistently overestimate the predicted values by about 30%. (Additional uncertainty may have been introduced into these (relatively low) values of $|K_R|$ by the effects of wave reflection from the beach.) Despite the lack of representative sampling, the results are generally supportive of the two main theoretical

predictions evident in Figure 17, namely

(a) that the peak reflection coefficient increases linearly with the number of ripples; and

(b) that for a given number of ripples, and a given ripple steepness, the peak reflection coefficient increases both with increasing ripple amplitude and decreasing depth.

5.4 Measurements of surface elevation and ripple reflection coefficient over, and on either side of, the ripple patch

Further evidence of the way in which significant amounts of wave energy may be reflected by a patch of bottom undulations has been provided by measurements of surface elevation made throughout the tank in resonant cases. Figures 18(a)-(i) show the envelopes of partially standing waves on the up-wave side of the ripple patch; these give way to the (parallel line) envelopes of progressive waves on the down-wave side, which leave the region of the ripple patch and travel towards the beach. The results show also that the transition from partially standing to progressive wave motions is gradual, and is accomplished in an approximately linear manner over the full extent of the ripple patch.

This linear transition is confirmed in Figures 19(a)-(i), which show the measured reflection coefficient falling steadily across the patch. For m = 10 ripples (Figs 19(c)-(i)), agreement between measured and predicted values of K is generally good, at least over the ripple patch itself. However, only for small amounts of reflection (eg b/h = 0.08, Fig 19(c)) is there also good agreement on both the up-wave and down-wave sides of the patch. As the reflection coefficient increases (Figs 19(d)-(i)), the measured values consistently underestimate the theory on the up-wave side, and overestimate it on the down-wave side. The reason for the discrepancies is not entirely clear. It is possible that reflection of wave energy by the wave absorbing beach, which manifests itself in the non-zero values of K on the down-wave side (but which, as we have seen, was only of the order of 1 - 4%), may have provided an unwanted contribution to the wave field on the up-wave side. In particular, waves reflected by the beach may have interfered destructively with waves directly reflected by the ripples, and this may have led to the observed reduction in the ripple reflection coefficient for values of (b/h) greater than 0.08 (Figs 19(d)-(i)). By comparison, Figure 19(a), for m = 2 ripples and b/h = 0.32, shows the measured reflection coefficients overestimating the theoretical values by significant amounts on the up-wave side of the ripple patch. This suggests that the phase angle of the wave reflected by the beach, which propagates across the ripple patch towards the wave generator, may

lead to constructive, as well as destructive, interference effects. An alternative explanation for the more generally occurring underestimates in the measured values of $|K_R|$ on the up-wave side (Figs 19(d)-(i)) is that a non-negligible amount of available wave energy may have been dissipated in the tank. As argued in §4.3, the general tendency for values of $|K_R|$ to decrease towards the wave generator is consistent with this explanation. It should be appreciated also that the linear perturbation theory itself is probably somewhat over-simplified, in that it does not take into account any higher order resonant interactions between the surface waves and the ripples (Davies, 1980, 1982b).

Finally, Figures 19(c)-(i) show that, in general, the measured reflection coefficient increases to a localized peak value in front of the ripple patch and then, having fallen linearly over the patch, passes through a localized minimum at the end of the patch. The reasons for this behaviour are not clear. It was thought initially that the localized maximum and minimum were associated with the trapped modes in the vicinity of the ends of the patch. However, attempts to reproduce the effect on the basis of the theory have been unsuccessful, essentially on account of the fact that the trapped waves are of insufficient horizontal extent.

5.5 Sediment transport observations

Detailed comparisons of observed and predicted sediment motion have been discussed in §4.4. These results support the general theoretical expectation that wave reflection from seabed undulations may, potentially, provide a mechanism for the growth of an existing ripple patch in the up-wave direction. This conclusion is based upon observations of areas of erosion and deposition on the up-wave side of the ripple patch, which exhibited the same spacing as the original ripples within the patch. However, the results are somewhat ambiguous, since they do not represent a true equilibrium between the incident waves and the bed-forms, such as would have existed if the bed had been fully erodible. For example, both the observations (Figs 22(a)-(f)) and the theory (Fig 23) suggest that the crests of the ripples may have been unstable, that is that the crests may have been subject to erosion. However, as argued in §4.4, further tests on the stability of fully erodible ripple patches are needed before any firm conclusions can be reached.

6 CONCLUSIONS

Measurements of the wave reflection coefficient for a patch of sinusoidal ripples have confirmed the principal conclusions of the earlier studies of Davies

(1980, 1982a), namely

(a) that, for a given number of ripples in the patch, the wave reflection coefficient is oscillatory in the quotient of the surface (k) and ripple (l) wavenumbers;

(b) that a resonant interaction occurs at $2k/l \approx 1$, associated with which there may be a significant amount of reflected wave energy;

(c) that, at resonance, the amount of wave reflection increases linearly with the number of ripples in the patch.

Unfortunately, the measurements were hampered to some extent by the presence of a small amount of wave energy which was back-reflected from the beach at the down-wave end of the tank. This unwanted effect in the results tended to mask the aniticipated theoretical trends for low values of the wave reflection coefficient.

A further prediction of Davies (1980, 1982a) was that the partially standing wave formed in resonant cases on the up-wave side of the ripple patch might provide a mechanism for the growth of the ripple patch in the up-wave direction. An experiment carried out with medium quartz sand in the tank has shown that areas of preferential erosion and deposition do indeed occur on the up-wave side of the ripple patch, and that the distance between areas of erosion is equal to the original ripple spacing. Potentially, at least, resonant interaction between surface waves and bottom undulations provides a mechanism for the growth of a ripple patch in the up-wave direction. The observations have confirmed that no such mechanism exists down-wave of the ripple patch.

More recent theoretical results (see §2) than those presented by Davies (1980, 1982a) have enabled detailed comparisons to be made between the predicted and measured wave fields over the ripple patch itself. In general, the agreement between the observations and the theory has been convincing; in particular, predictions concerning the development of the wave field over the ripple patch have been well supported by observations both of the surface elevation and of the wave reflection coefficient.

ACKNOWLEDGEMENTS

We are grateful to the Commander and Director of the US Army Corps of Engineers, Coastal Engineering Research Center, Fort Belvoir, Virginia, USA, for providing experimental facilities. We are grateful also to Professor T V Davies for his valuable comments on aspects of the theory in §2.

Computer programming and analyses were carried out by Mrs D J Corns, illustrations were prepared by Mrs C D Kemp and the report was typed by Mrs J Reeves and Mrs M Ridge.

REFERENCES

BECKMANN, P and SPIZZICHINO, A, 1963. The scattering of electromagnetic waves from rough surfaces. Pergamon Press, Oxford, 503 pp.

DAVIES, A G, 1980. Some interactions between surface water waves and ripples and dunes on the seabed. Institute of Oceanographic Sciences Report, No 108, 134 pp.

DAVIES, A G, 1982a. The reflection of wave energy by undulations on the seabed. Dynamics of Atmospheres and Oceans, 6, 207-232.

DAVIES, A G, 1982b. On the interaction between surface waves and undulations on the seabed. Journal of Marine Research, 40 (2), 331-368.

FITZ-GERALD, G F, 1976. The reflexion of plane gravity waves travelling in water of variable depth. Philosophical Transactions of the Royal Society of London Series A, 284 (1317), 49-89.

FORTUIN, L, 1970. Survey of literature on reflection and scattering of sound waves at the sea surface. Journal of the Acoustical Society of America, 47: 5(2), 1209-1228.

FRYER, D K and THOMAS, M W S, 1975. A linear twin wire probe for measuring water waves. Journal of Physics E: Scientific Instruments, 8, 405-408.

GODA, Y and SUZUKI, Y, 1977. Estimation of incident and reflected waves in random wave experiments. Proceedings of the 15th International Conference on Coastal Engineering, 1976. American Society of Civil Engineers, 828-845.

HEATHERSHAW, A D, 1982. Seabed-wave resonance and sand bar growth. Nature, 296, 343-345.

HOLMAN, R A and BOWEN, A J, 1982. Bars, bumps and holes: Models for the generation of complex beach topography. Journal of Geophysical Research, 87, 457-468.

JEFFREYS, H, 1944. Motion of waves in shallow water. Note on the offshore bar problem and reflexion from a bar. London: Ministry of Supply Wave Report, No 3.

JOHNS, B, 1970. On the mass transport induced by oscillatory flow in a turbulent boundary layer. Journal of Fluid Mechanics, 43 (1), 177-185.

JONSSON, I G, 1967. Wave boundary layers and friction factors. Proceedings of the 10th International Conference on Coastal Engineering, 1966. American Society of Civil Engineers, 127-148.

KELLUM, F W, 1956. An electronic gage for measurement of small waves and ripples. Bulletin of the Beach Erosion Board, US Army, Corps of Engineers, 10 (1), 32-40.

KENNEDY, J F, and FALCON M, 1965. Wave-generated sediment ripples. Massachusetts Institute of Technology, Hydrodynamics Laboratory Report 86, 55 pp.

KOMAR, P D, and MILLER, M C, 1975. Sediment threshold under oscillatory waves. Proceedings of the 14th International Conference on Coastal Engineering, 1974. American Society of Civil Engineers, 756-775.

KREISEL, G, 1949. Surface waves. Quarterly Journal of Applied Mathematics, 7 (1), 21-44.

LAMB, H, 1932. Hydrodynamics. (6th Edition) Cambridge University Press, 738 pp.

LIU, A-K, and DAVIS, S H, 1977. Viscous attenuation of mean drift in water waves. Journal of Fluid Mechanics, 81(1), 63-84.

LONG, R B, 1973. Scattering of surface waves by an irregular bottom. Journal of Geophysical Research, 78, 7861-7870.

LONGUET-HIGGINS, M S, 1953. Mass transport in water waves. Philosophical transactions of the Royal Society of London Series A, 245, 535-581.

MEI, C C, and BLACK, J L, 1969. Scattering of surface waves by rectangular obstacles in waters of finite depth. Journal of Fluid Mechanics, 38(3), 499-511.

MITRA, A, and GREENBERG, M D, 1982. Slow interactions of gravity waves and a corrugated seabed. Journal of Applied Mechanics, submitted.

NEWMAN, J N, 1965. Propagation of water waves past long two-dimensional obstacles. Journal of Fluid Mechanics, 23, 1, 23-29.

NIELSEN, P, 1979. Some basic concepts of wave sediment transport. Technical University of Denmark. Institute of Hydrodynamics and Hydraulic Engineering. Series Paper No 20, 160 pp.

NODA, H, 1969. A study of mass transport in boundary layers in standing waves. Proceedings of the 11th International Conference on Coastal Engineering, 1968. American Society of Civil Engineers, 227-247.

SCOTT, T, 1954. Sand movement by waves. US Army Corps of Engineers, Beach Erosion Board, Technical Memorandum Number 48, 37 pp.

SHORT, A D, 1975. Multiple offshore bars and standing waves. Journal of Geophysical Research, 80, 3838-3840.

SLEATH, J F A, 1974. Mass transport over a rough bed. Journal of Marine Research, 32, 1, 13-24.

SLEATH, J F A, 1975. Transition in oscillatory flow over rippled beds. Proceedings of the Institution of Civil Engineers, 59, 2, 309-322.

SLEATH, J F A, 1976. On rolling-grain ripples. Journal of Hydraulic Research, 14, 1, 69-81.

STAFFORD, R B, 1972. Investigation and procedure for calibration of CERC laboratory wave gage FWK Model - 1. Washington, DC, Coastal Engineering Research Center, 25 pp (unpublished document).

SUHAYDA, J N, 1974. Standing waves on beaches. Journal of Geophysical Research, 79, 3065-3071.

SYMONDS, G, HUNTLEY, D A, and BOWEN, A J, 1982. Two dimensional surf beat : Long wave generation by a time varying breakpoint. Journal of Geophysical Research, 87, 492-498.

SURFACE WAVE PROPAGATION OVER SINUSOIDALLY VARYING TOPOGRAPHY: THEORY AND OBSERVATION

BY
A.G. DAVIES AND A.D. HEATHERSHAW

REPORT NO. 159
PART II
1983

NATURAL ENVIRONMENT RESEARCH COUNCIL

INSTITUTE OF OCEANOGRAPHIC SCIENCES

INSTITUTE OF OCEANOGRAPHIC SCIENCES

Wormley, Godalming,
Surrey, GU8 5UB.
(0428 - 79 - 4141)

(Director: Dr. A.S. Laughton FRS)

Bidston Observatory,
Birkenhead,
Merseyside, L43 7RA.
(051 - 653 - 8633)

(Assistant Director: Dr. D.E. Cartwright)

Crossway,
Taunton,
Somerset, TA1 2DW.
(0823 - 86211)

(Assistant Director: M.J. Tucker)

When citing this document in a bibliography the reference should be given as follows:-

DAVIES, A.G. & HEATHERSHAW, A.D. 1983 Surface wave propagation over sinusoidally varying topography: theory and observation.
Institute of Oceanographic Sciences, Report, No. 159, 181pp. (in 2 parts).

INSTITUTE OF OCEANOGRAPHIC SCIENCES

TAUNTON

Surface wave propagation over sinusoidally varying topography: theory and observation

by

A.G. Davies and A.D. Heathershaw

I.O.S. Report No. 159

Part II

(Figures, tables & appendices)

1983

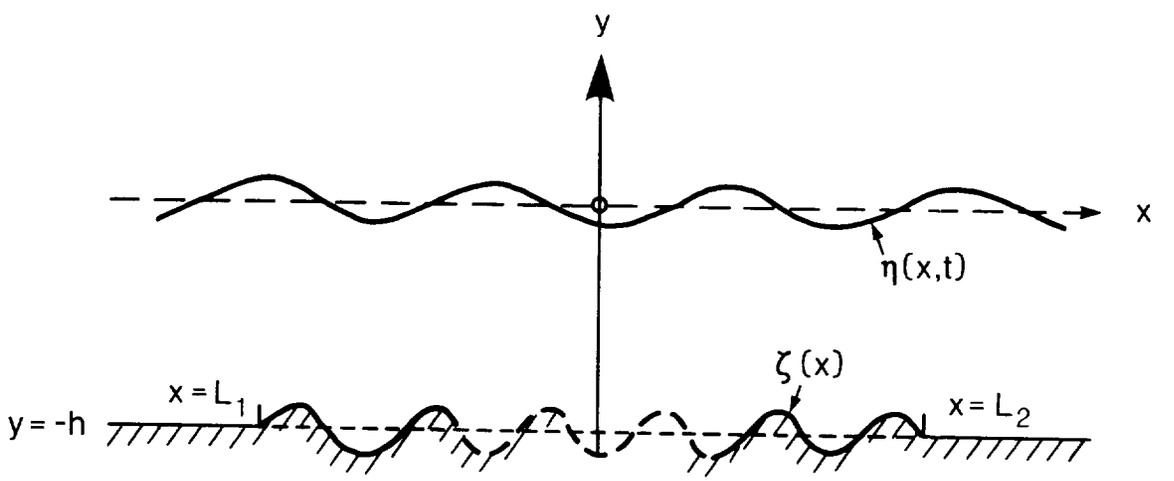

Figure 1 Definition sketch

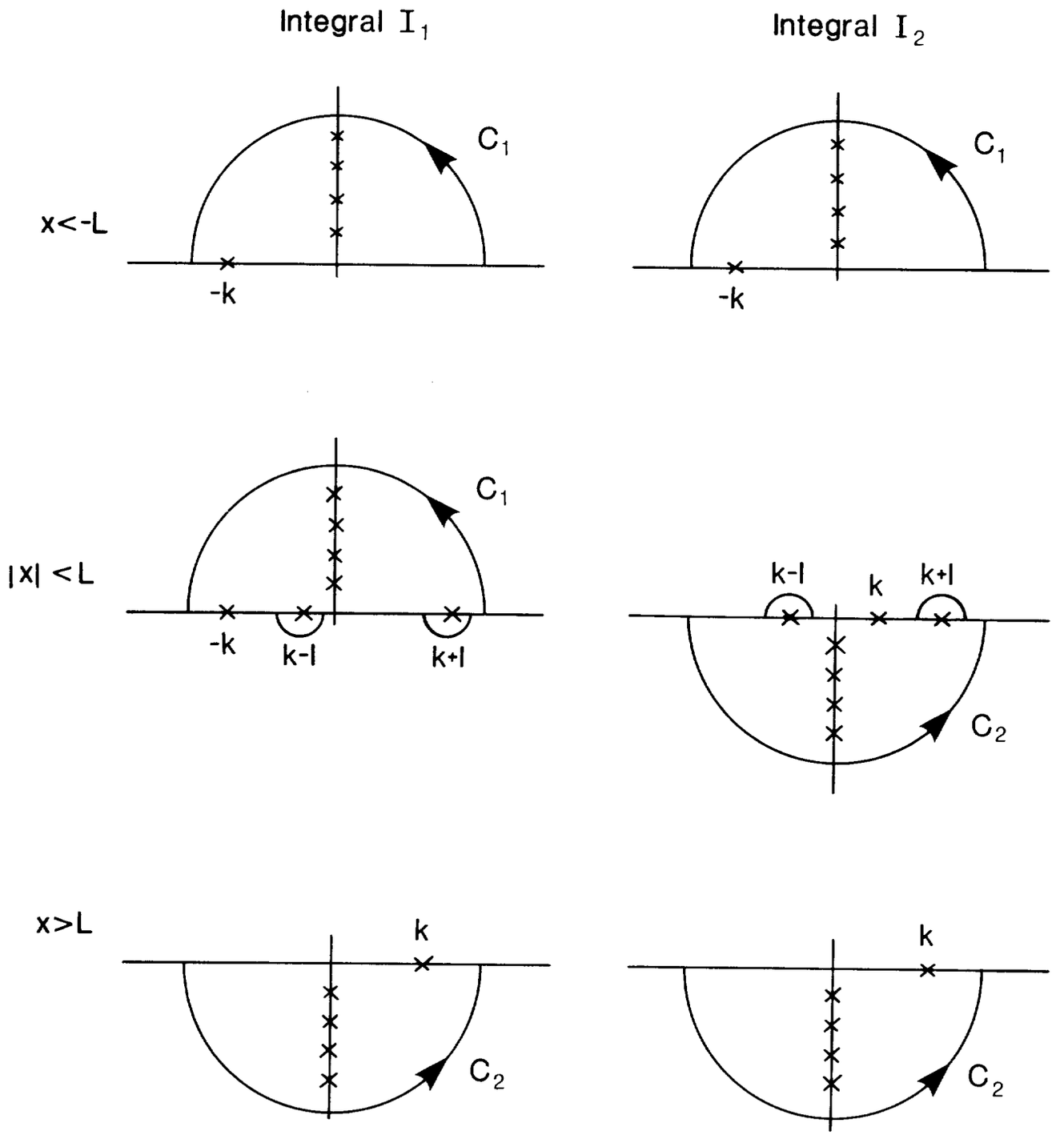

Figure 2 The positions of those poles in the λ-plane which contribute to the final result, for each region of the flow. The pole positions are shown for the general case in which $l \neq 2k$, and for $\mu = 0$.

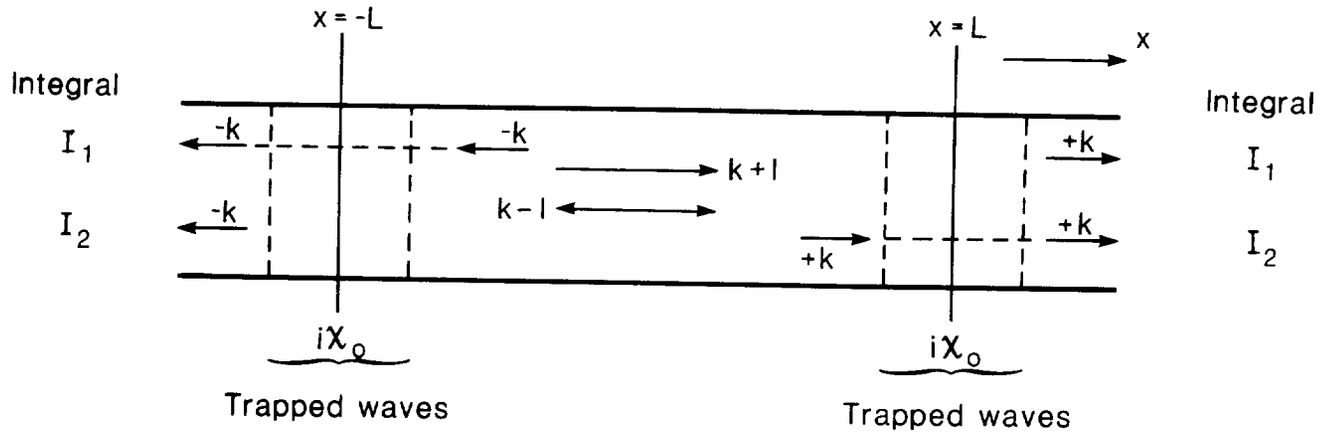

Figure 3 Wave modes in the perturbation solution for the general case in which $l \neq 2k$. Each arrow represents a propagating wave mode, and against each arrow is indicated the pole position with which it is associated. The direction of travel is indicated by the arrow head. The trapped wave modes are confined to the regions near the ends of the ripple patch.

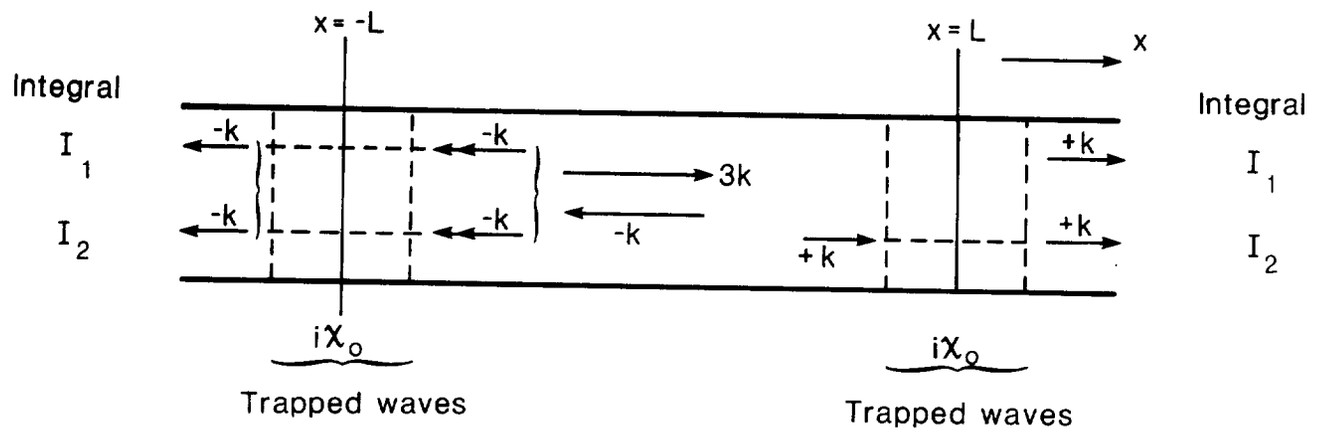

Figure 4 Wave modes in the perturbation solution for the special case in which $l = 2k$ (cf Fig 3).

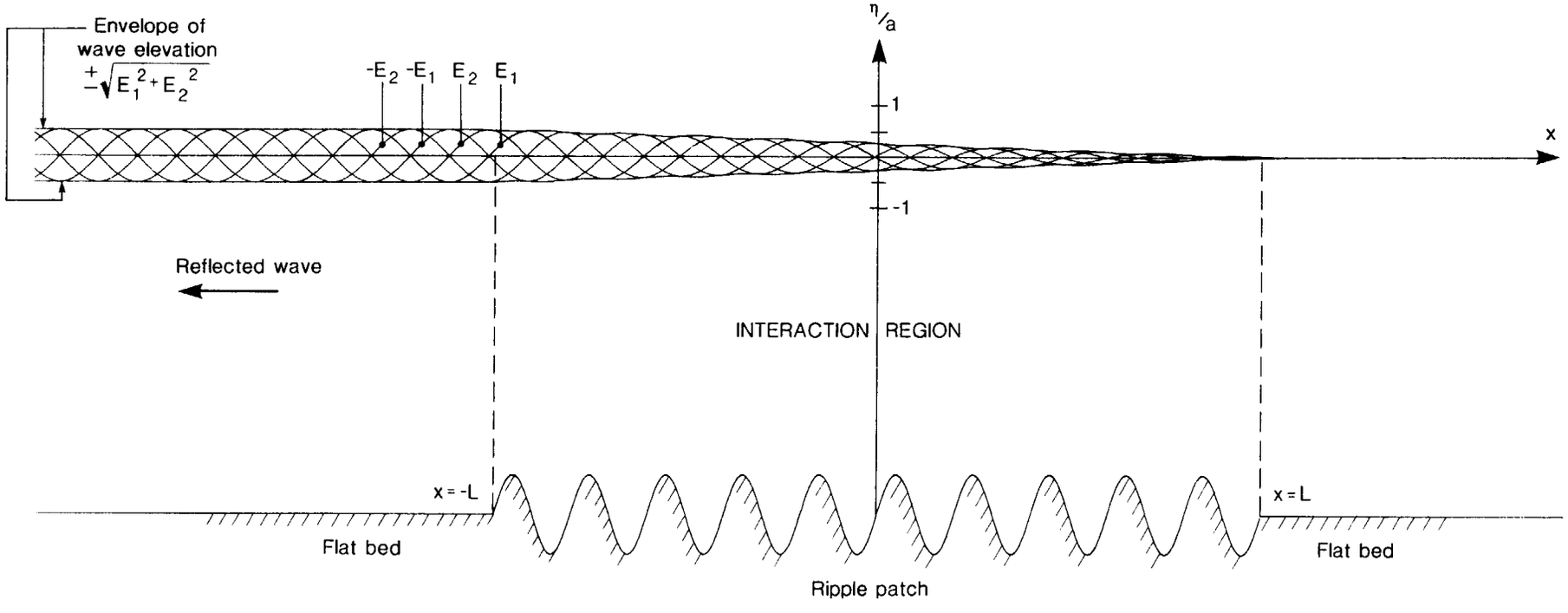

Figure 5 Perturbation solution for the near-resonant case in which m = 10, L = 500 cm, b = 5 cm, λ_R = 100 cm, h = 41.7 cm and T = 1.23 s, (2k/1 = 0.985). The development of the reflected wave in the interaction region is illustrated by the instantaneous surface wave profiles $\pm E_1$, $\pm E_2$ (see Eq (68)), and by the envelope of wave elevation $\pm\sqrt{E_1^2 + E_2^2}$. There is an almost linear increase in the reflected wave amplitude between x = +L and x = -L. Thereafter, in x < -L, the reflected wave is an outgoing wave, with amplitude a_R = 0.509 a.

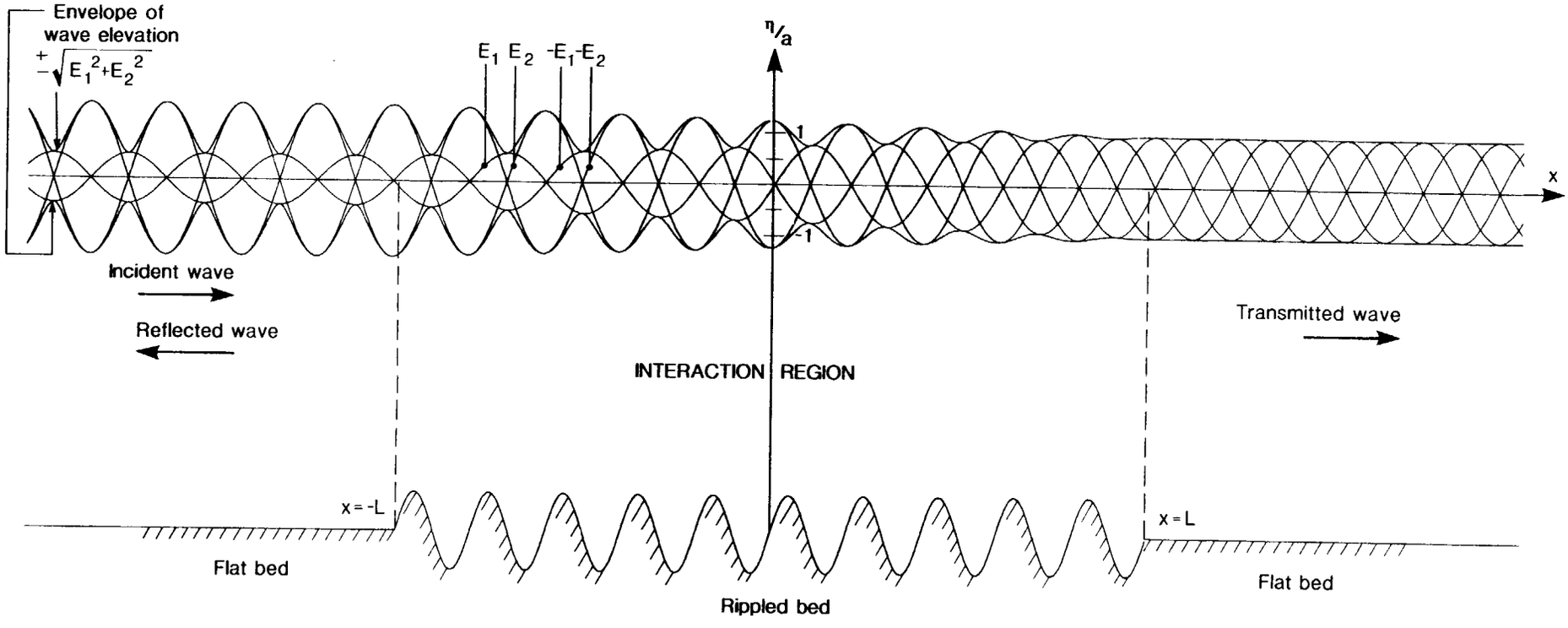

Figure 6 Superimposition of the first order and perturbation solutions (see Fig 5 for the perturbation solution) for the near-resonant case in which m = 10, L = 500 cm, b = 5 cm, λ_R = 100 cm, h = 41.7 cm and T = 1.23s (2k/1 = 0.985). The instantaneous profiles of wave elevation $\pm E_1$, $\pm E_2$ (see Eq (68)) are plotted, together with the envelope of wave elevation $\pm\sqrt{E_1^2 + E_2^2}$. The development of a partially standing wave structure between x = +L and x = -L is evident.

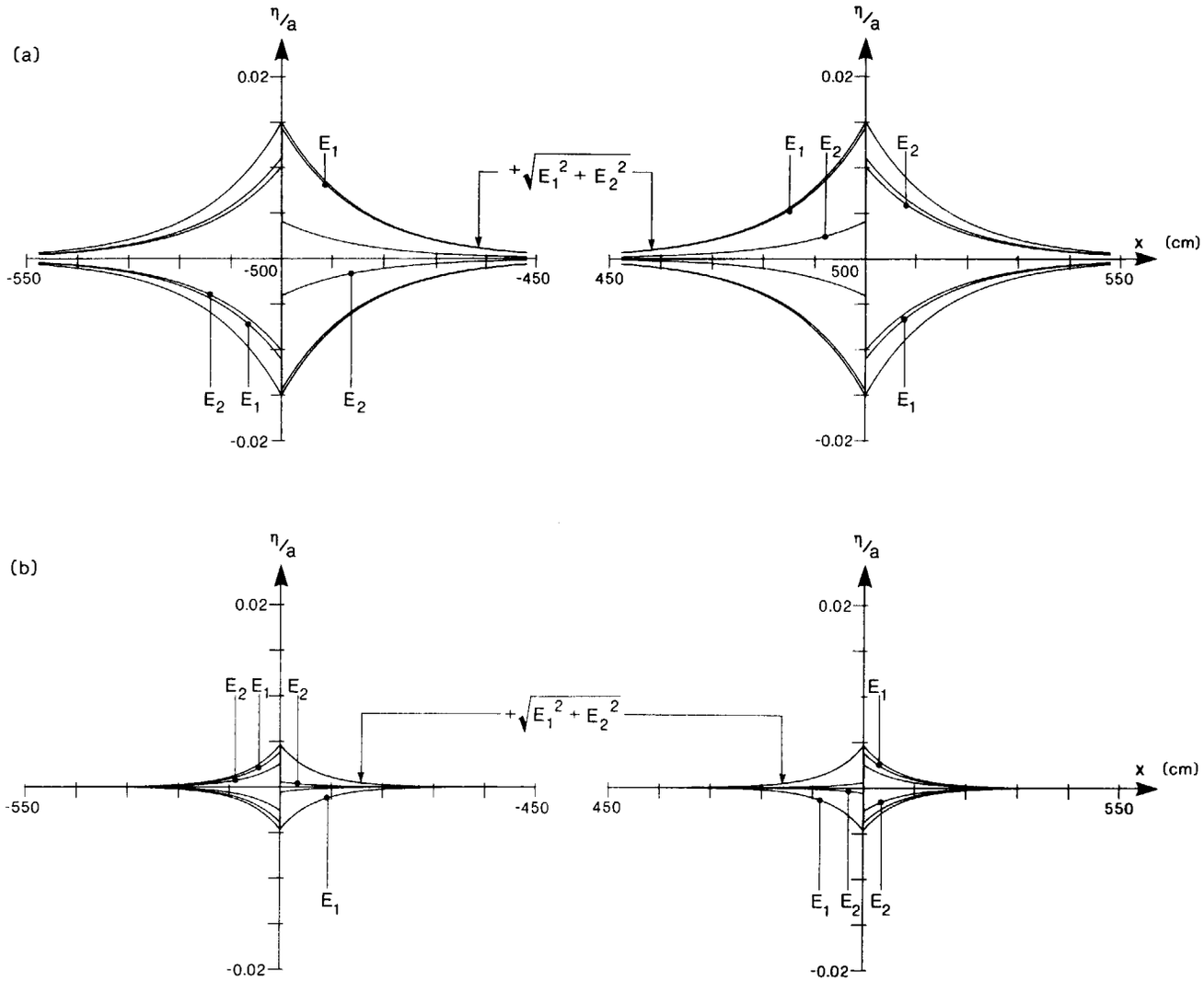

Figure 7 Individual trapped wave modes for the near-resonant case in which m = 10, L = 500 cm, b = 5 cm, λ_R = 100 cm, h = 41.7 cm and T = 1.23 s (2k/l = 0.985). In Fig 7(a) the trapped wave elevations associated with the poles at $\chi_0 = \pm 0.0662$ cm^{-1} are shown. In Fig 7(b) the elevations associated with the poles at $\chi_0 = \pm 0.1464$ cm^{-1} are shown. In each case, instantaneous profiles of elevation $\pm E_1$, $\pm E_2$ (see Eq (68)) are plotted, together with the envelope of wave elevation $\pm \sqrt{E_1^2 + E_2^2}$.

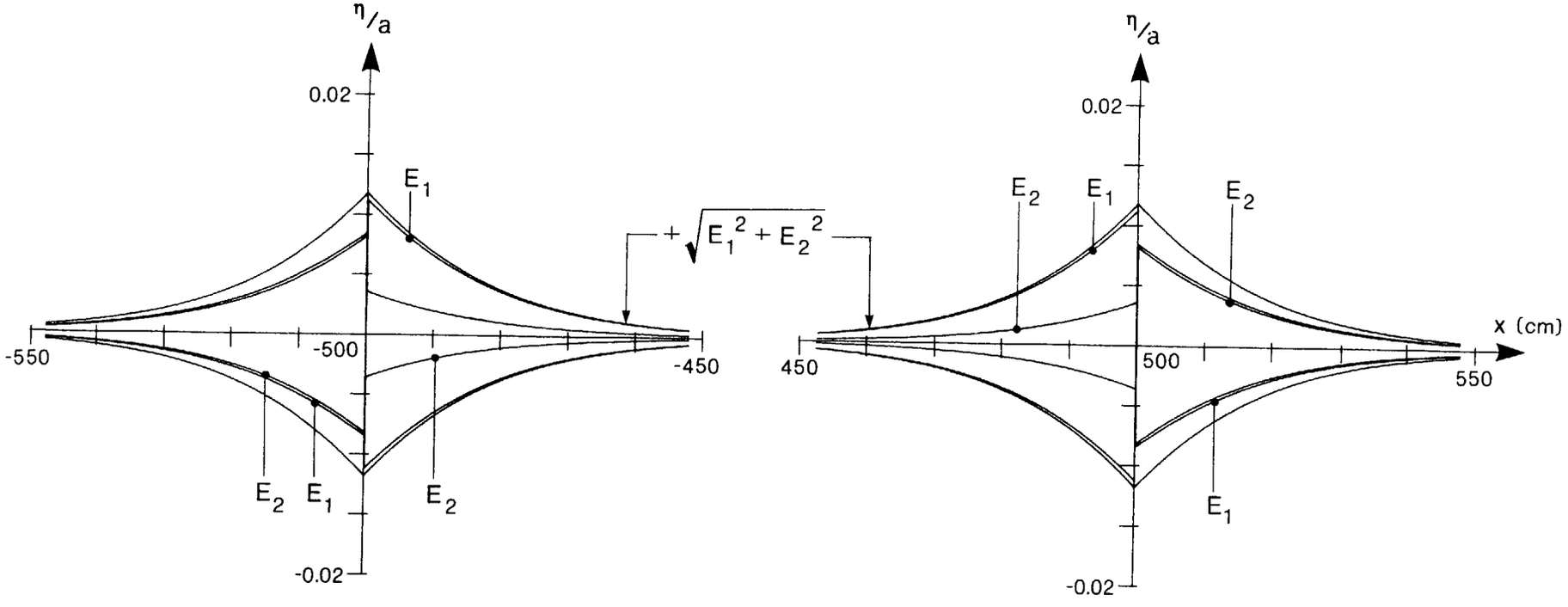

Figure 8 Superimposition of the complete set of trapped wave modes for the near-resonant case in which m = 10, L = 500 cm, b = 5 cm, λ_R = 100 cm, h = 41.7 cm and T = 1.23 s (2k/1 = 0.985). Instantaneous profiles of wave elevation $\pm E_1$, $\pm E_2$ (see Eq (68)) are plotted, together with the envelope of wave elevation $\pm \sqrt{E_1^2 + E_2^2}$.

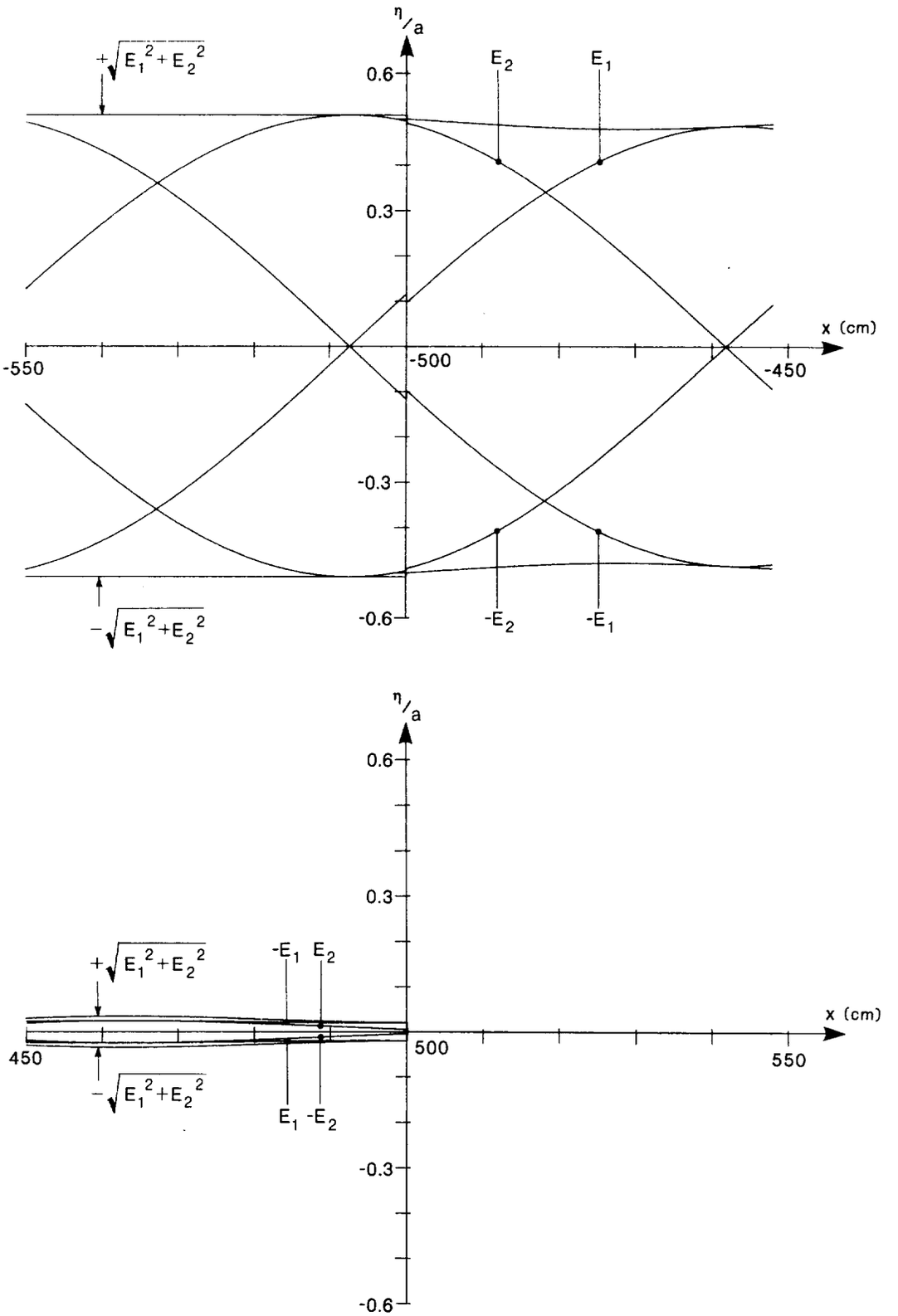

Figure 9(a) Perturbation solution in the region of both ends of the ripple patch for the same near-resonant case as in Fig 5. All the trapped wave modes have been removed, causing discontinuities in each of the instantaneous elevation curves $\pm E_1$ and $\pm E_2$, and in the wave envelope curves $\pm \sqrt{E_1^2 + E_2^2}$, at x = ±L (L = 500 cm).

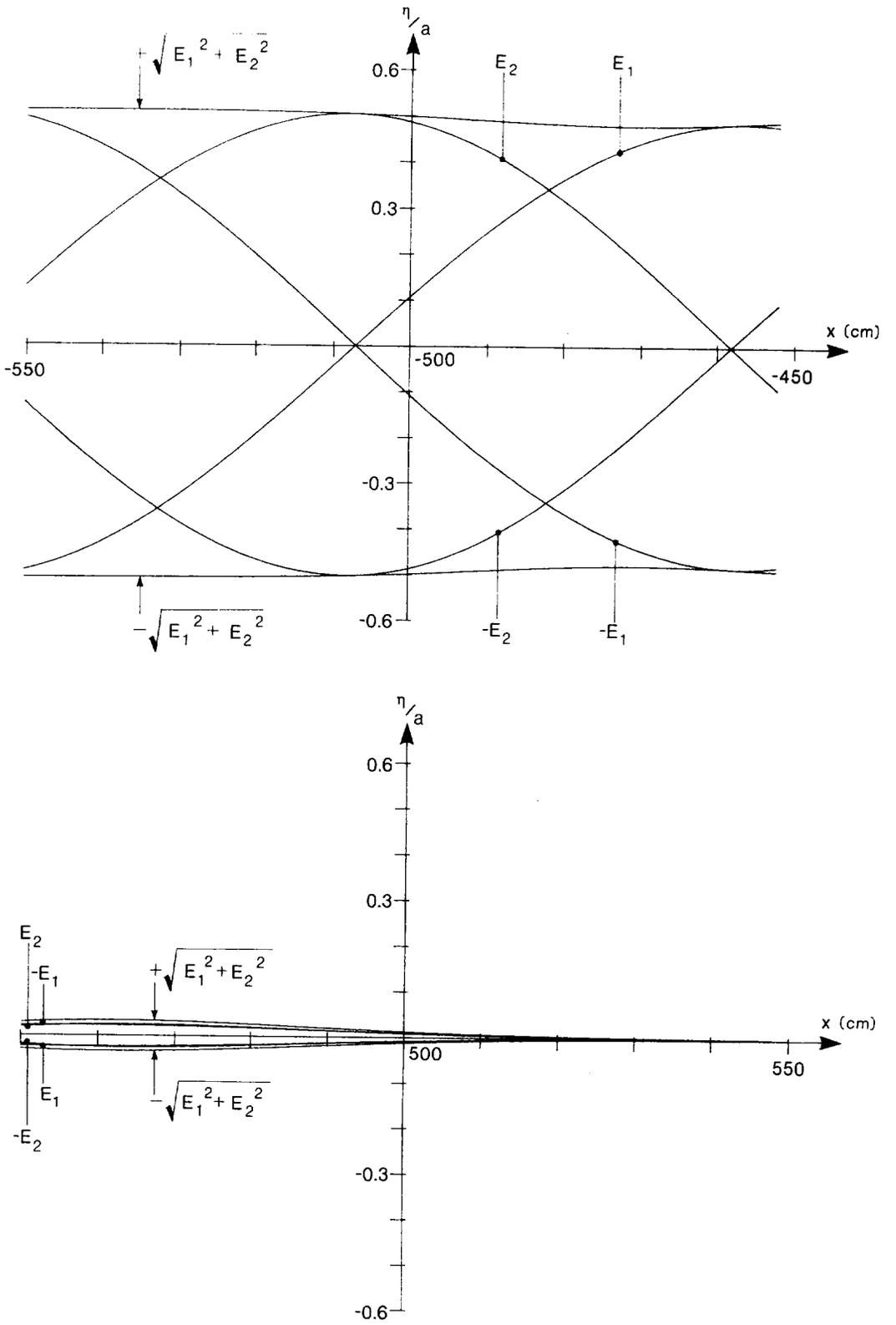

Figure 9(b) Perturbation solution, as in Figure 9(a), for the region of both ends of the ripple patch. The addition of the trapped wave modes removes the discontinuities in each of the instantaneous elevation curves $\pm E_1$ and $\pm E_2$, and in the wave envelope curves $\pm\sqrt{E_1^2 + E_2^2}$, at $x = \pm L$ ($L = 500$ cm).

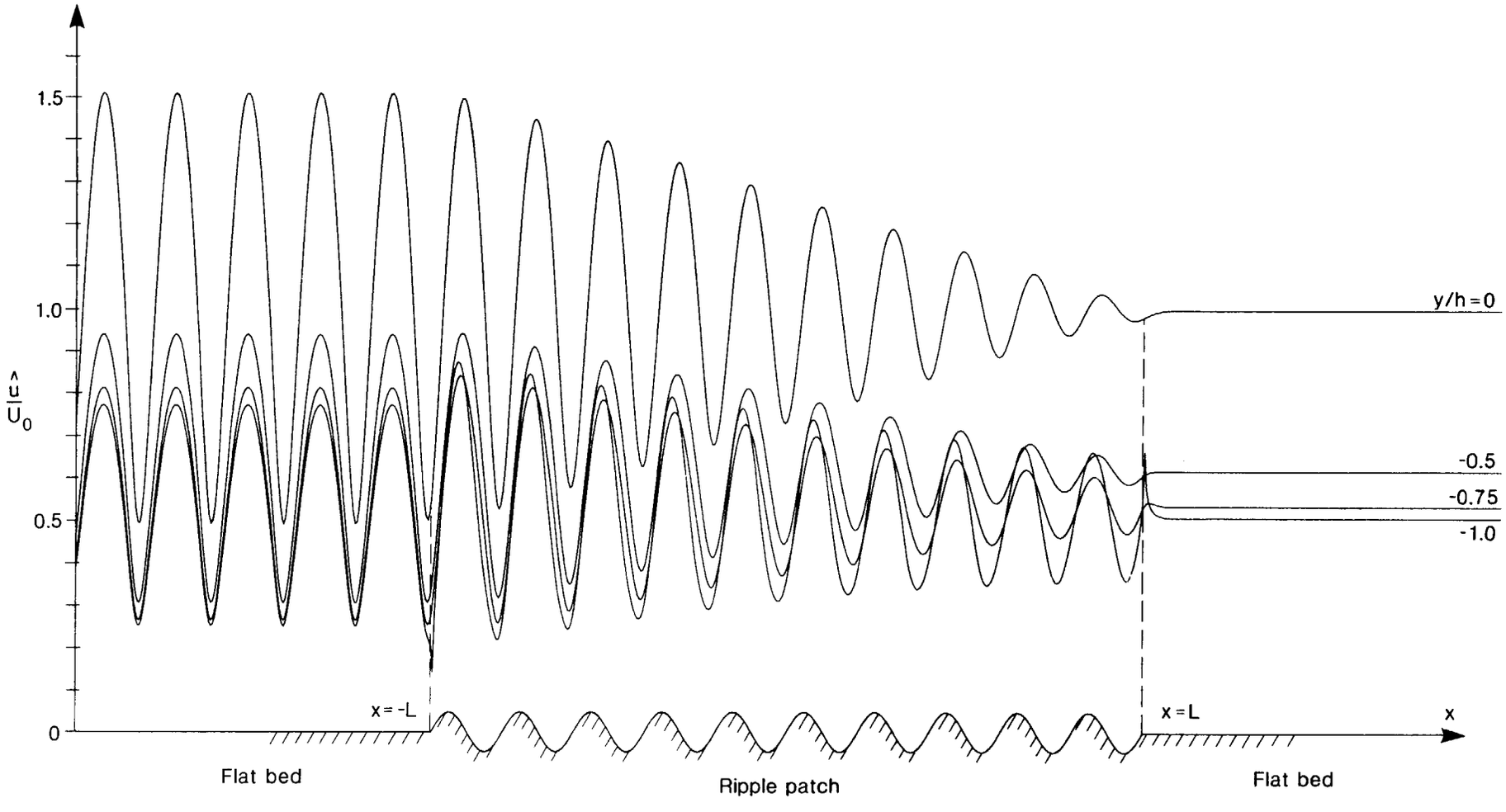

Figure 10 Amplitude of horizontal velocity $\hat{u}$, normalized by $U_0 = gak/\sigma$, for the near-resonant case in Fig 6, and for the levels y/h = 0, -0.5, -0.75 and -1.0.

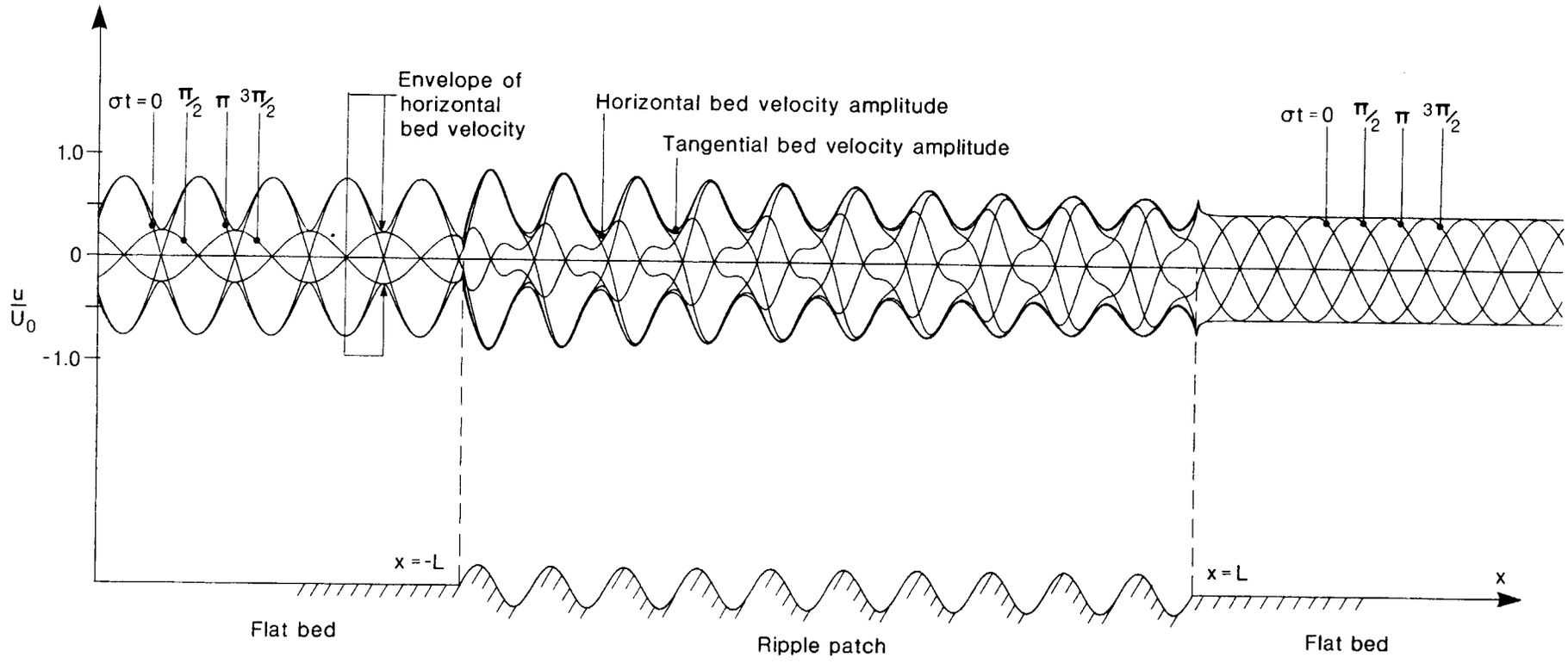

Figure 11 Bed velocities for the near-resonant case in Fig 6 (including the curve for level y/h = -1.0 in Fig 10). The envelope of the horizontal bed velocity field is shown, together with instantaneous horizontal bed velocity distributions for the phase angles $\sigma t = 0$, $\pi/2$, π and $3\pi/2$. In addition, the tangential bed velocity amplitude is shown for the region of rippled bed. This is closely similar to the envelope curves for the horizontal bed velocity amplitude.

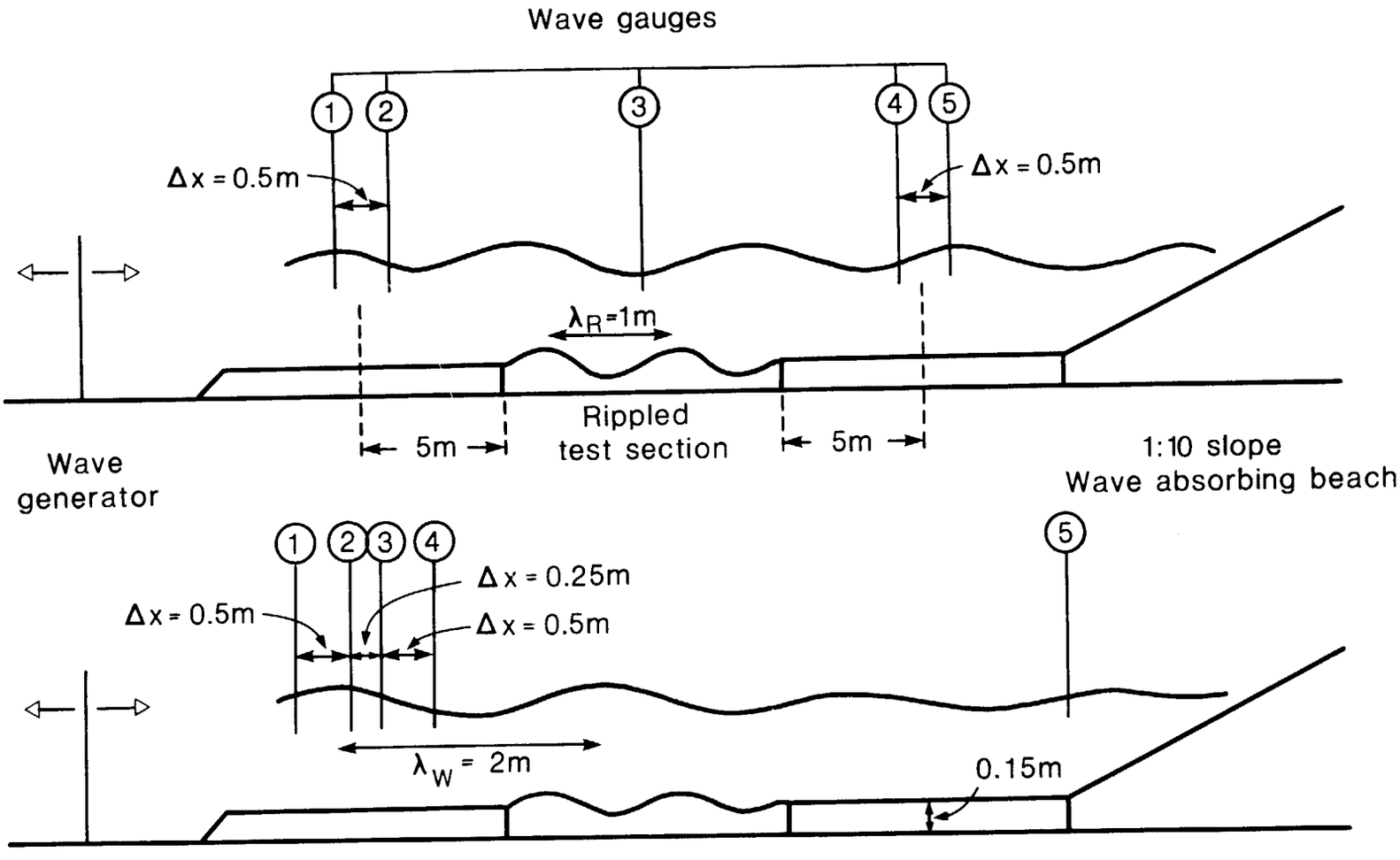

Figure 12 Schematic diagram showing the positions of the gauges in relation to the ripple patch and the wave absorbing beach, for the two main types of measurement in the experiments.

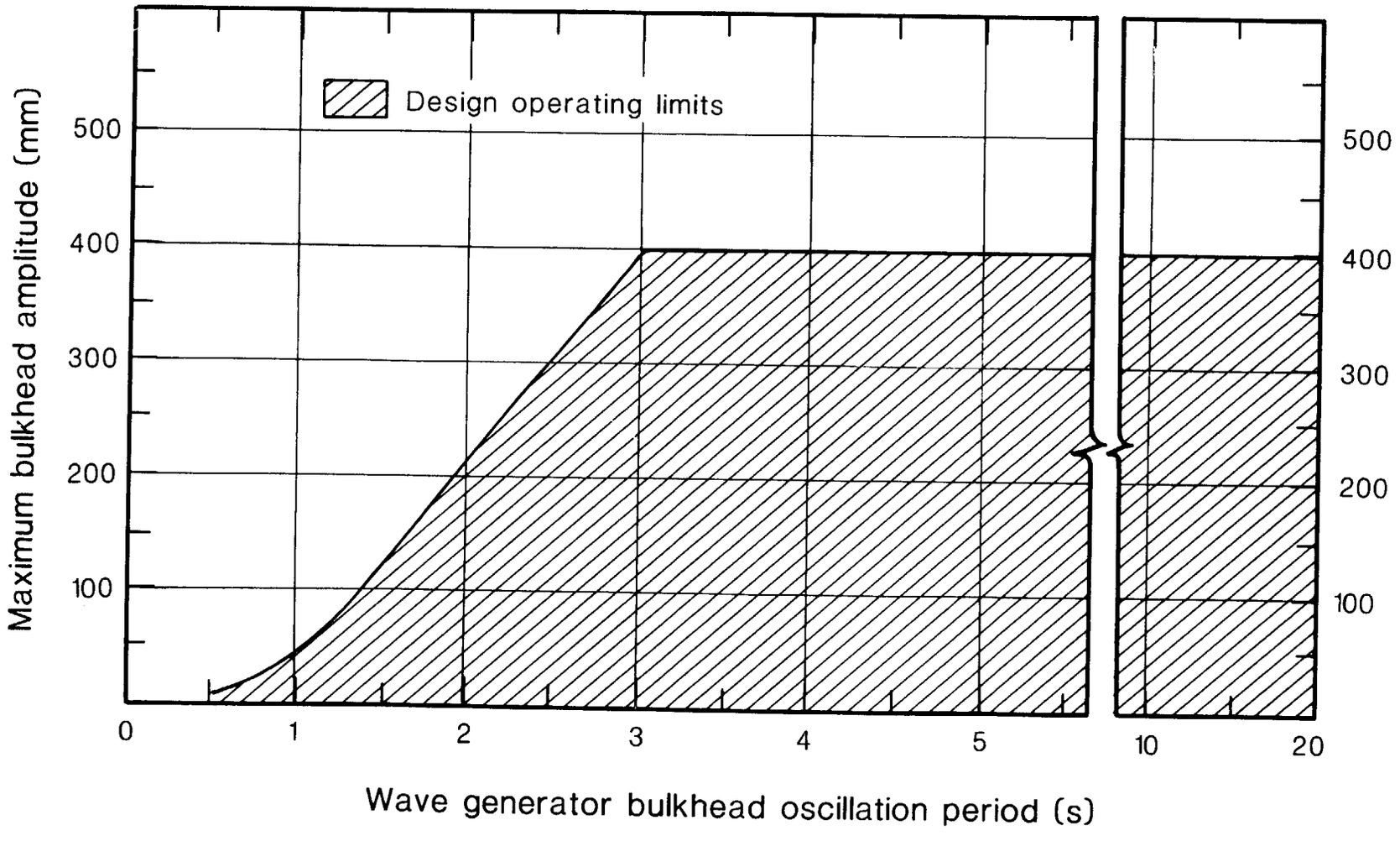

Figure 13 Maximum wave generator bulkhead amplitudes for various wave periods.

Figure 14 Results of measurements of the reflection coefficient of both the ripple patch ($|K_R|$) and the beach (K_B), as functions of 2k/l, for m = 10, 4 and 2 ripples. Phase measurements are shown for the case of m = 2 ripples only. The solid and broken curves represent the predictions of the uncorrected and corrected theory, respectively. Further details of these measurements may be found in Table 2.

Figure 14(a) Variation of $|K_R|$ and K_B with 2k/l, for m = 10 ripples and b/h = 0.16

Figure 14(b) Variation of $|K_R|$ and K_B with 2k/l, for m = 4 ripples and b/h = 0.32

Figure 14(c) Variation of $|K_R|$, K_B and the phase ($\varepsilon_I + \varepsilon_R$) with 2k/l, for m = 2 ripples and b/h = 0.32

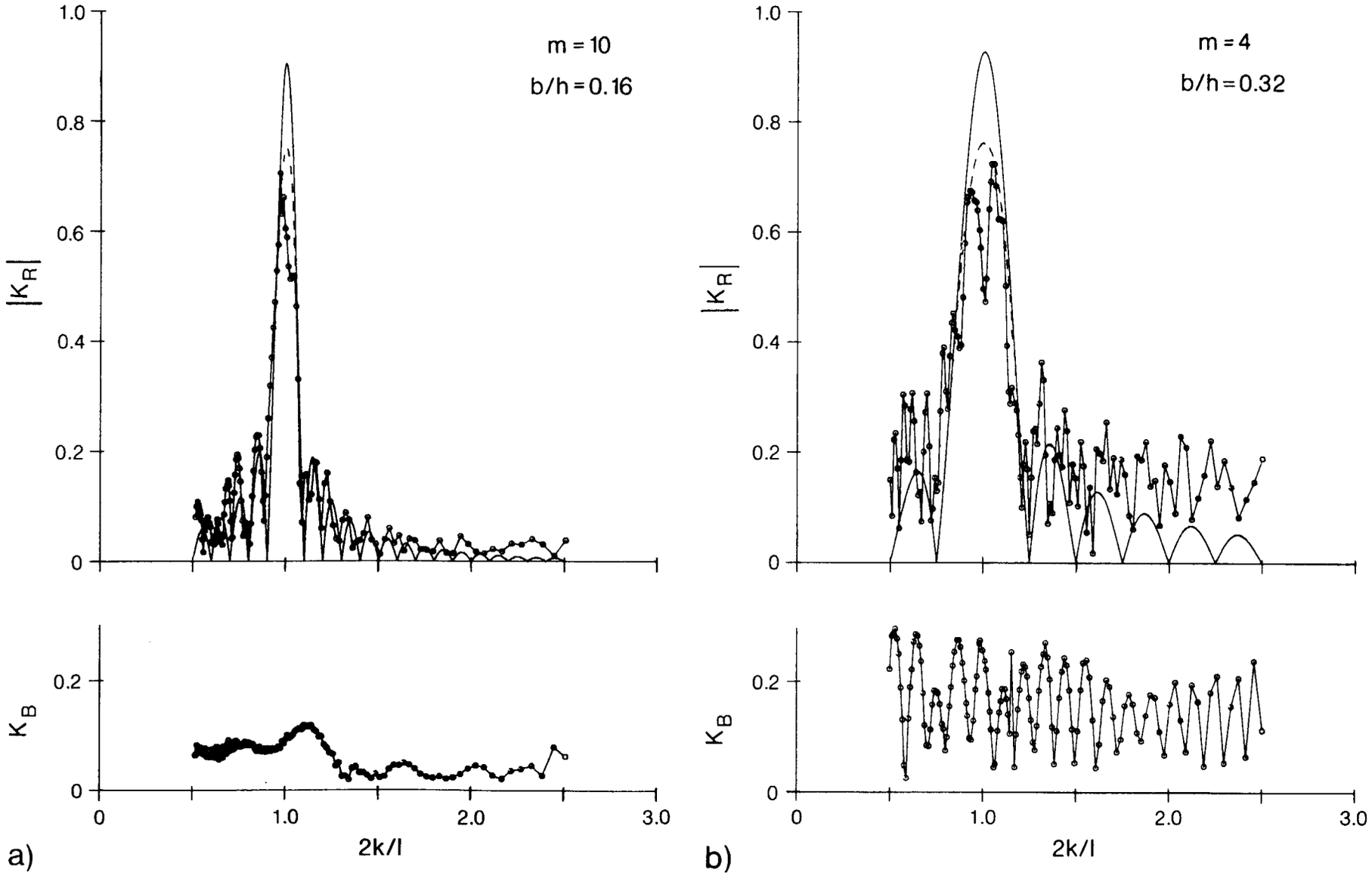
m = 10
b/h = 0.16
m = 4
b/h = 0.32
$|K_R|$
K_B
2k/l
a)
b)

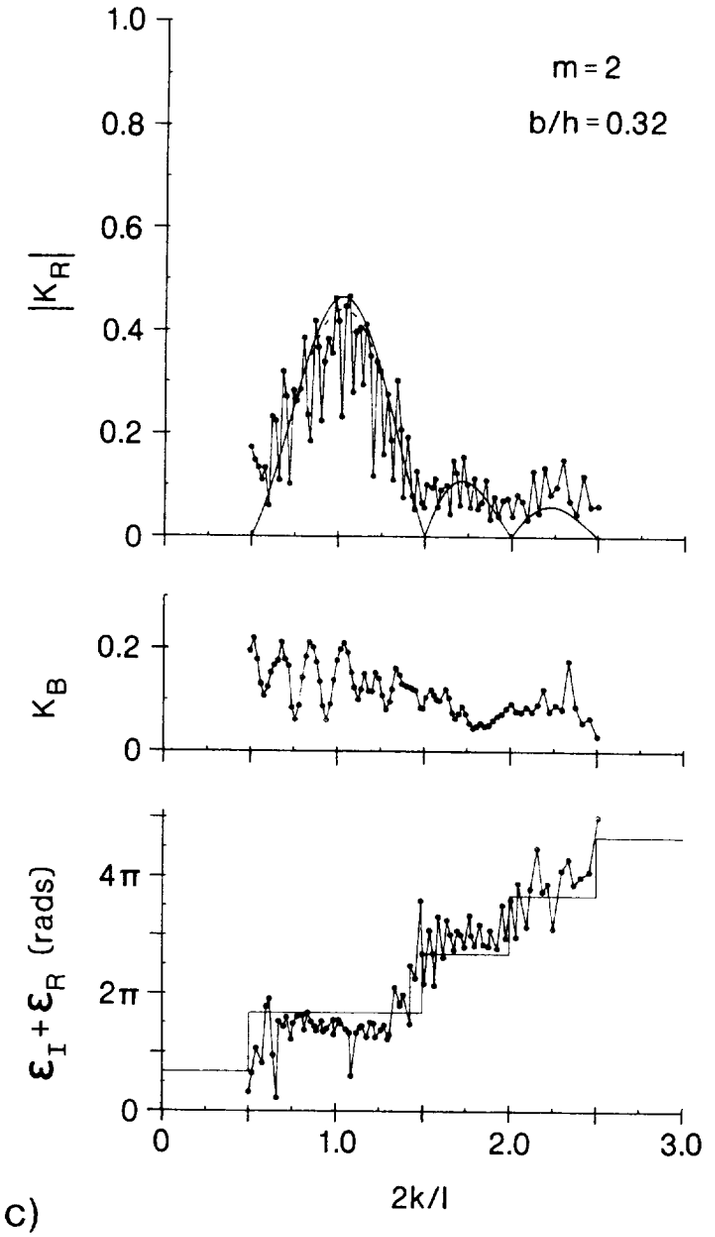
m = 2
b/h = 0.32
$|K_R|$
K_B
$\varepsilon_I + \varepsilon_R$ (rads)
1.0
0.8
0.6
0.4
0.2
0
0.2
0
4π
2π
0
0
1.0
2.0
3.0
2k/l

c)

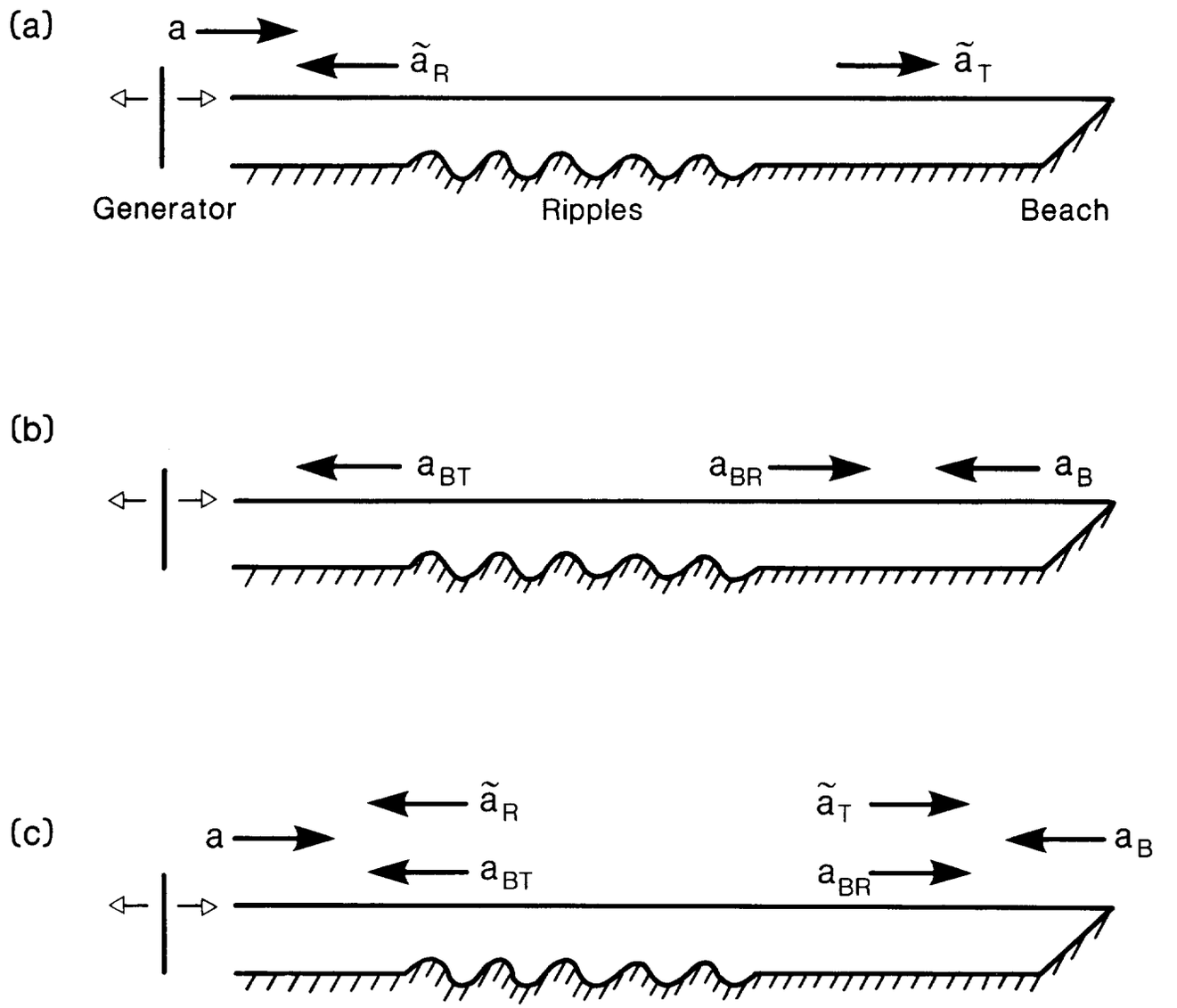

Figure 15 The effects of wave reflection by the beach. The symbol a denotes the wave amplitude of each constituent, and the arrow head indicates the direction of wave propagation.

Figure 16 Measurements of the reflection coefficient $|K_R|$ of the ripple patch, at or near resonance, for different numbers of ripples (m) and for different values of the quotient (b/h) of the ripple amplitude (b) and the water depth (h). The vertical bars denote limits which correspond to ±10% of the total width of the main resonant peak.

Figure 16(a) The variation of $|K_R|$ with 2k/l for m = 1

Figure 16(b) The variation of $|K_R|$ with 2k/l for m = 2

Figure 16(c) The variation of $|K_R|$ with 2k/l for m = 4

Figure 16(d) The variation of $|K_R|$ with 2k/l for m = 10

Note : The origin of each plot is displaced vertically by an amount equal to 0.4 in $|K_R|$.

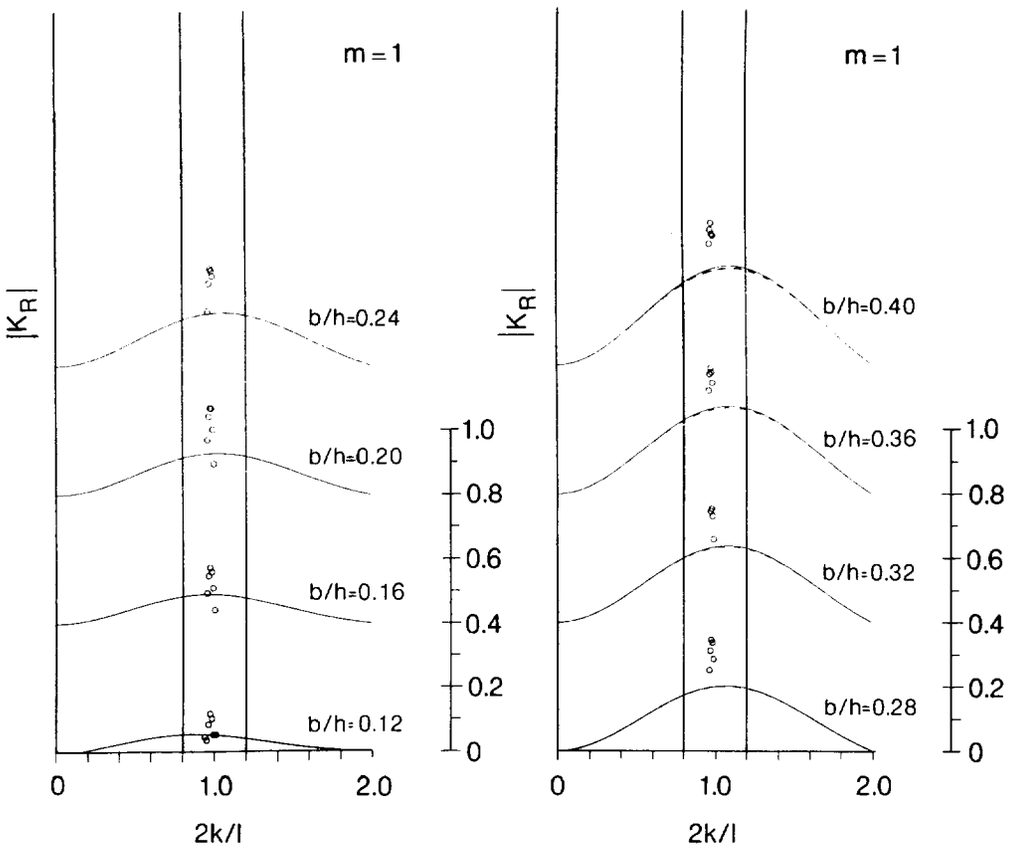
m = 1
m = 1
|K_R|
|K_R|
b/h=0.24
b/h=0.20
b/h=0.16
b/h=0.12
b/h=0.40
b/h=0.36
b/h=0.32
b/h=0.28
1.0
0.8
0.6
0.4
0.2
0
0
1.0
2.0
2k/l
2k/l

a)

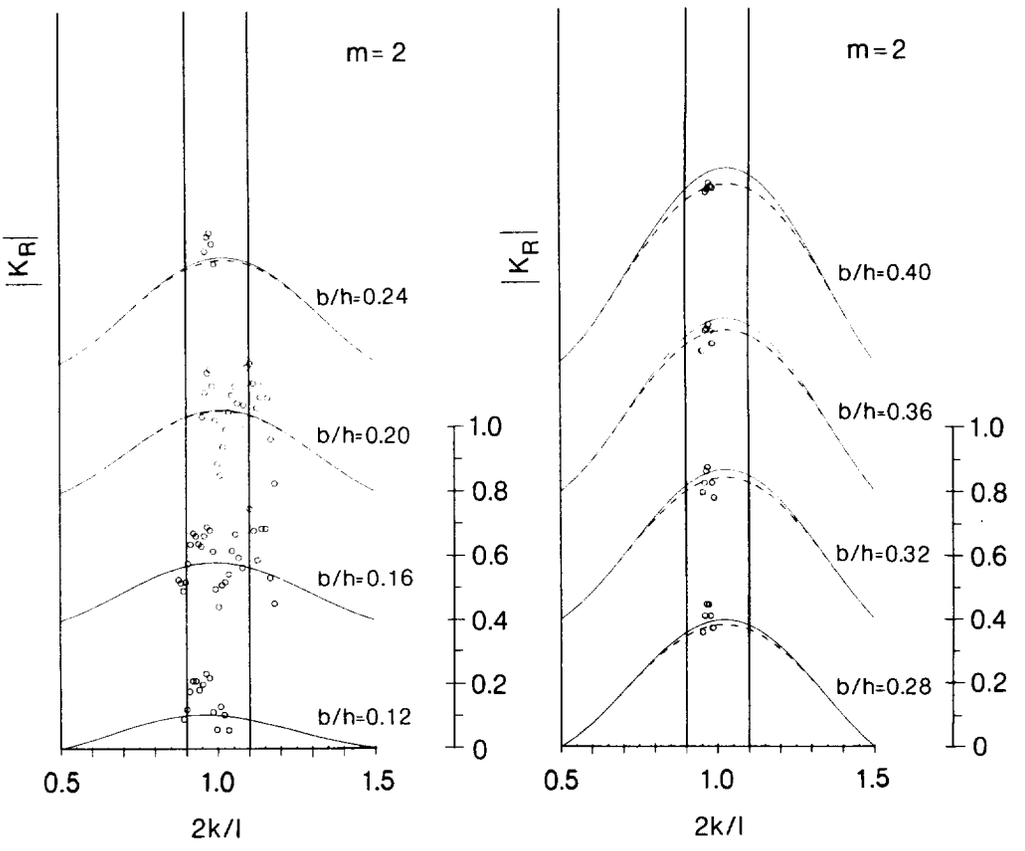
m = 2
m = 2
|K_R|
|K_R|
b/h=0.24
b/h=0.20
b/h=0.16
b/h=0.12
b/h=0.40
b/h=0.36
b/h=0.32
b/h=0.28
1.0
0.8
0.6
0.4
0.2
0
0.5
1.0
1.5
2k/l
2k/l

b)

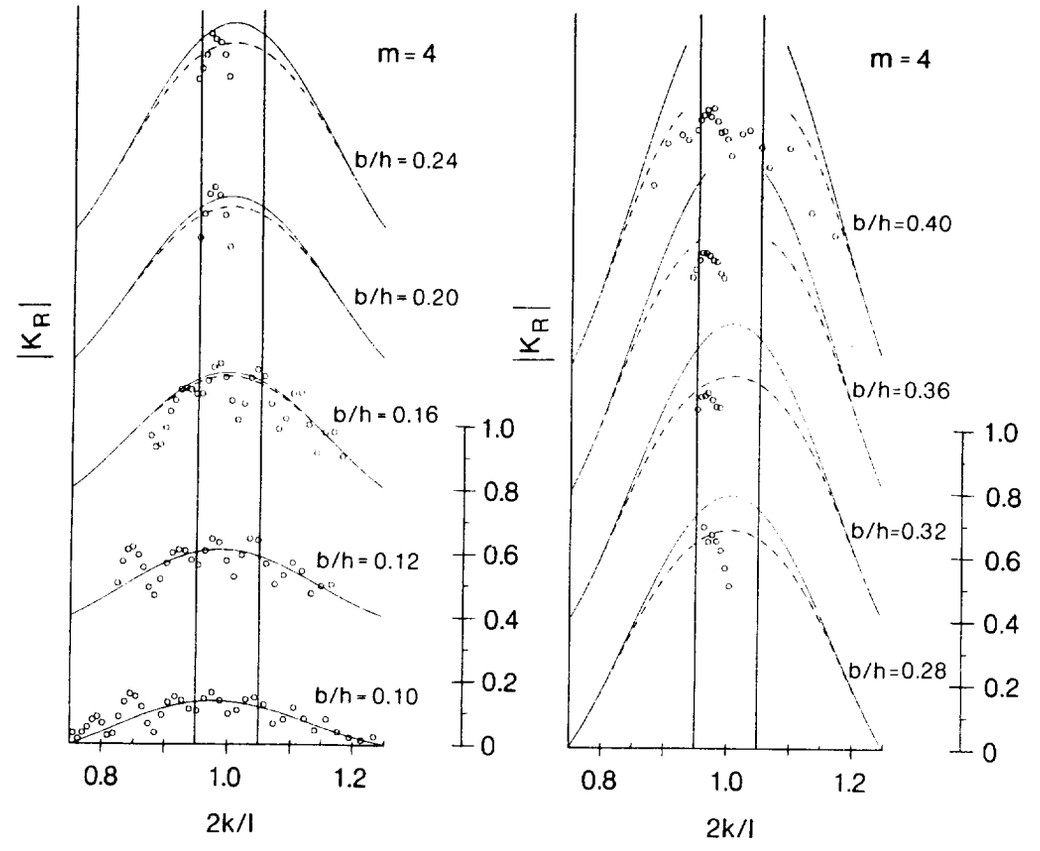
m = 4
b/h = 0.24
b/h = 0.20
b/h = 0.16
b/h = 0.12
b/h = 0.10
|K_R|
0.8
1.0
1.2
2k/l
0
0.2
0.4
0.6
0.8
1.0
m = 4
b/h=0.40
b/h=0.36
b/h=0.32
b/h=0.28
|K_R|
0.8
1.0
1.2
2k/l
0
0.2
0.4
0.6
0.8
1.0

c)

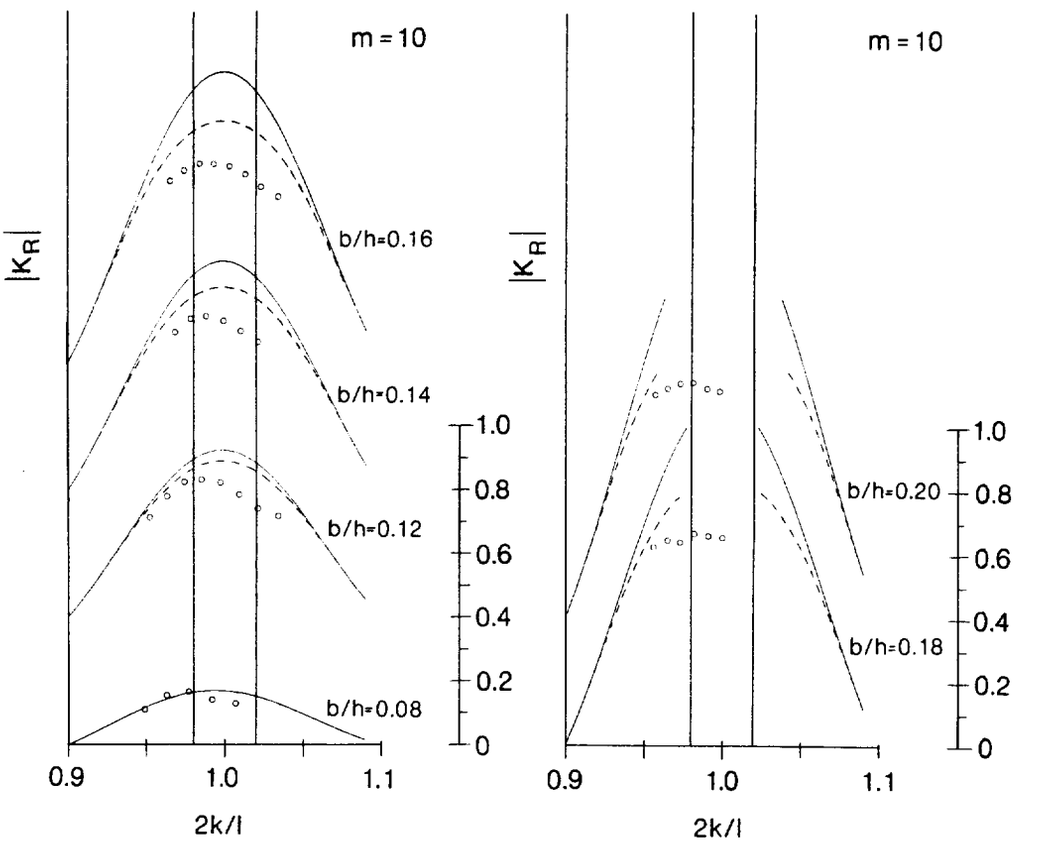
m = 10
b/h=0.16
b/h=0.14
b/h=0.12
b/h=0.08
|K_R|
0.9
1.0
1.1
2k/l
0
0.2
0.4
0.6
0.8
1.0
m = 10
b/h=0.20
b/h=0.18
|K_R|
0.9
1.0
1.1
2k/l
0
0.2
0.4
0.6
0.8
1.0

d)

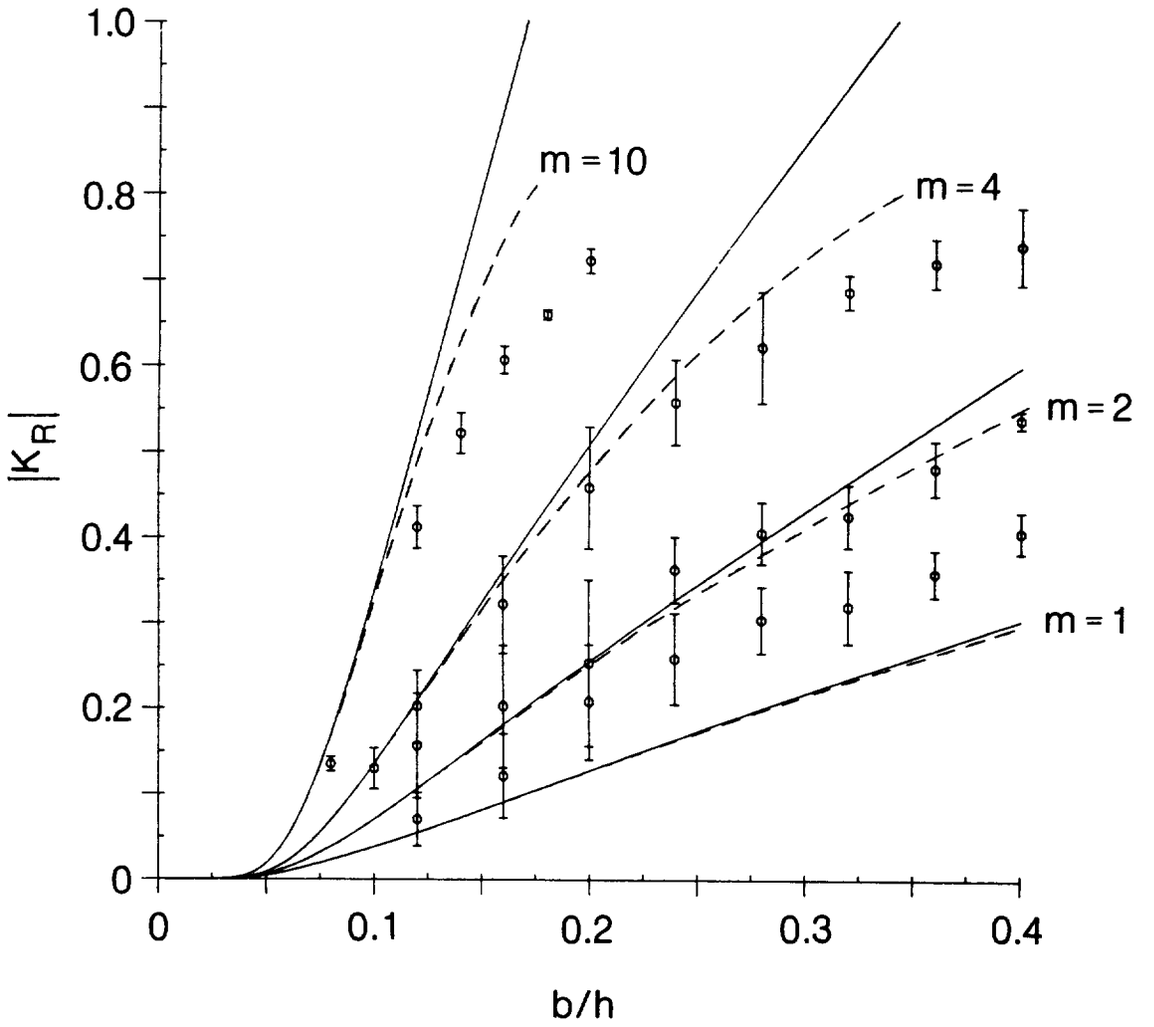

Figure 17 Variation of the measured mean value of $|K_R|$, at or near resonance ($2k/l \cong 1$), as a function of the quotient (b/h) of the ripple amplitude (b) and the water depth (h), and for different numbers of ripples m. Error bars denote plus or minus one standard deviation from the mean. Further details of these measurements may be found in Table 3.

Figure 18 Variation of the amplitude of surface elevation throughout the wave tank at or near resonance ($2k/l \cong 1$), for different numbers of ripples (m) and different values of the quotient (b/h) of the ripple amplitude (b) and the water depth (h). Curves (a) and (b) represent the wave envelopes given by the uncorrected and corrected theoretical results, respectively (see §2.7.2 and §4.3). In Figures 18(h) and 18(i) trend curves (cubic splines) have been fitted to the data since, in these cases, the theory predicts over-reflection. T denotes the wave period, and S the stroke of the wave generator. Further details of these measurements are given in Table 4.

Figure 18(a) m = 2, b/h = 0.32, T = 1.73 s

Figure 18(b) m = 4, b/h = 0.32, T = 1.73 s

Figure 18(c) m = 10, b/h = 0.08, T = 1.17 s

Figure 18(d) m = 10, b/h = 0.10, T = 1.20 s

Figure 18(e) m = 10, b/h = 0.12, T = 1.23 s

Figure 18(f) m = 10, b/h = 0.14, T = 1.28 s

Figure 18(g) m = 10, b/h = 0.16, T = 1.31 s

Figure 18(h) m = 10, b/h = 0.18, T = 1.37 s

Figure 18(i) m = 10, b/h = 0.20, T = 1.42 s

Note : In these diagrams, the origin of the x-axis has been taken (largely for experimental reasons) at the up-wave end of the ripple patch. Elsewhere (eg §2) the origin is taken at the centre of the patch.

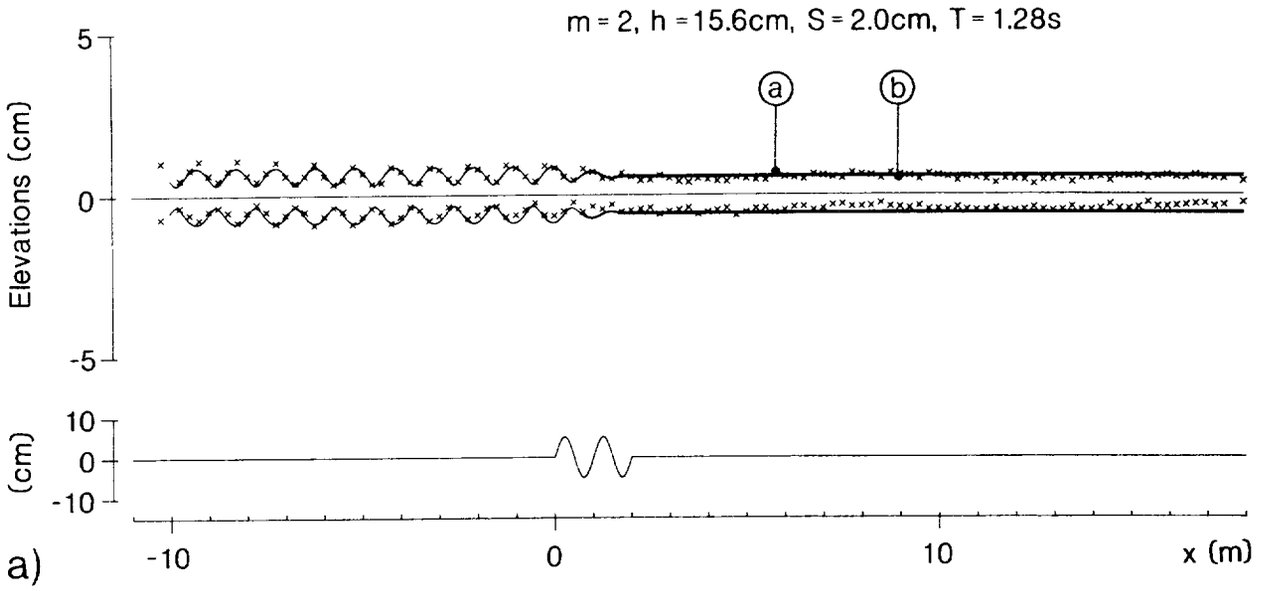
m = 2, h = 15.6cm, S = 2.0cm, T = 1.28s
a
b
Elevations (cm)
5
0
-5
(cm)
10
0
-10
-10
0
10
x (m)

a)

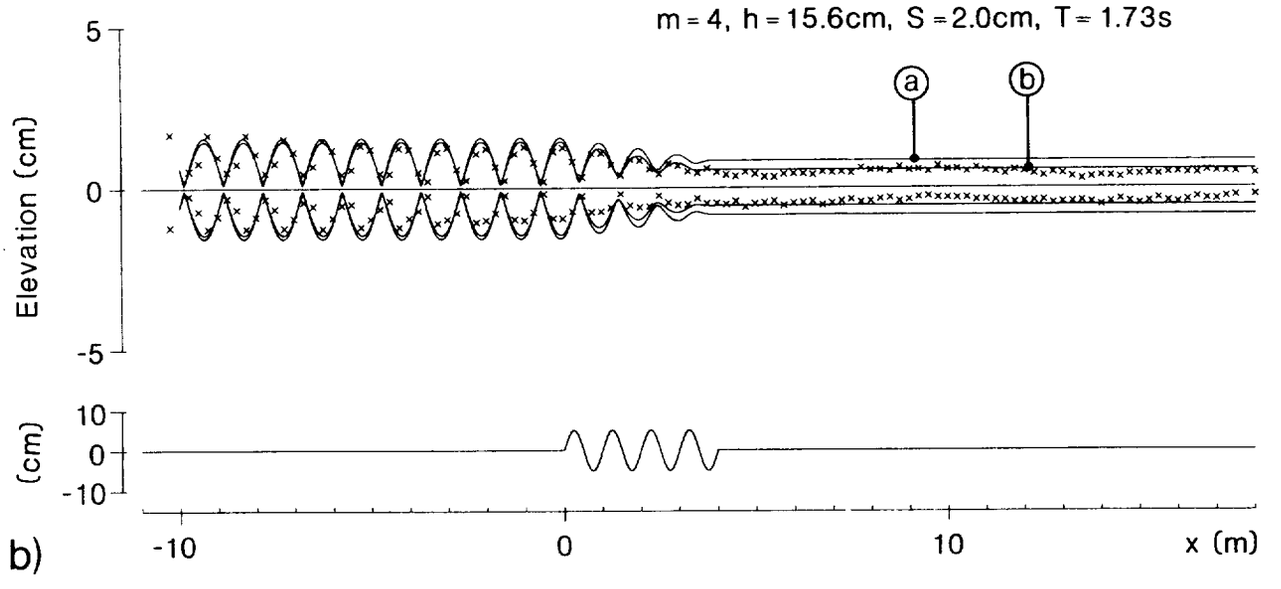
m = 4, h = 15.6cm, S = 2.0cm, T = 1.73s
a
b
Elevation (cm)
5
0
-5
(cm)
10
0
-10
-10
0
10
x (m)

b)

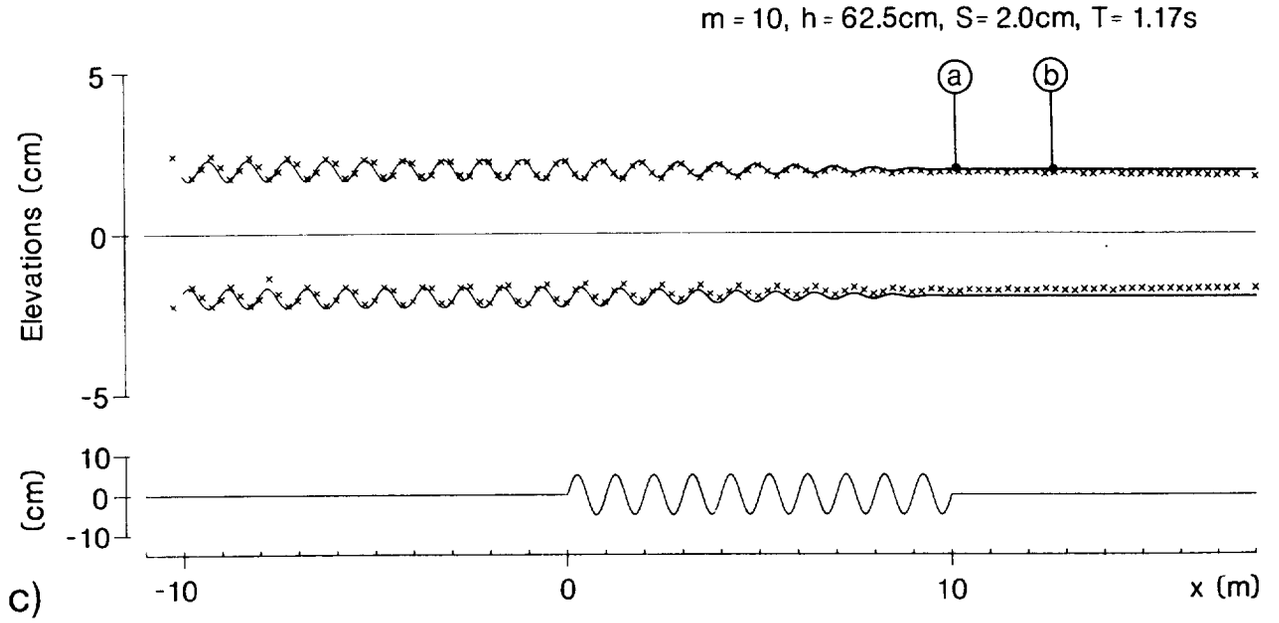
m = 10, h = 62.5cm, S = 2.0cm, T = 1.17s
a
b
Elevations (cm)
5
0
-5
(cm)
10
0
-10
-10
0
10
x (m)

c)

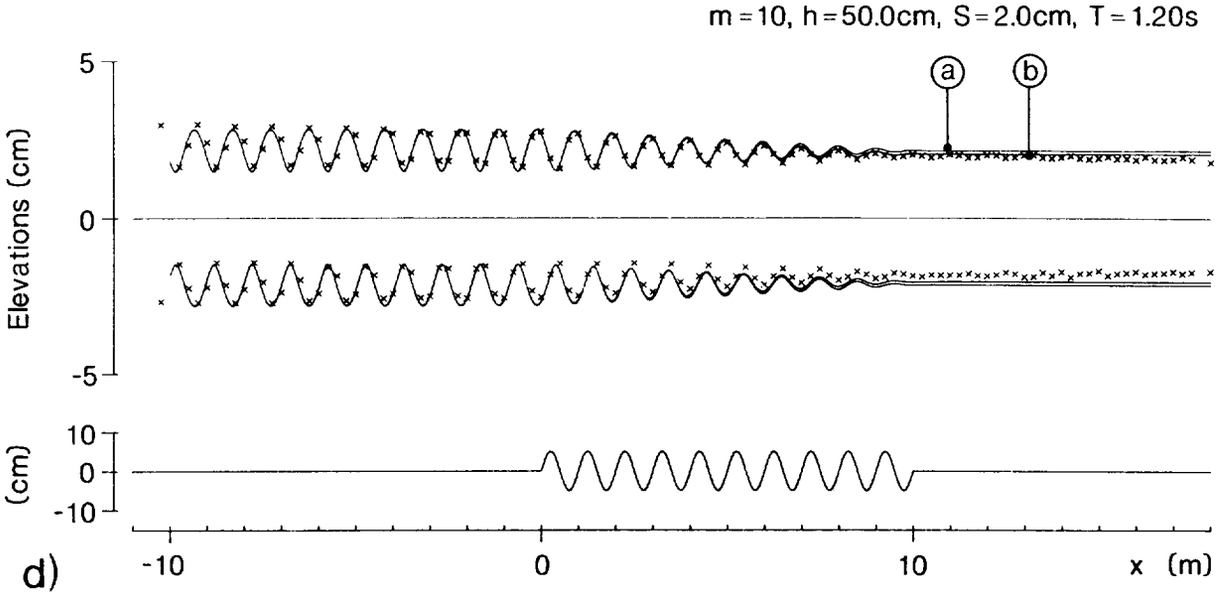
m = 10, h = 50.0cm, S = 2.0cm, T = 1.20s
Elevations (cm)
5
0
-5
a
b
(cm)
10
0
-10
-10
0
10
x (m)
d)

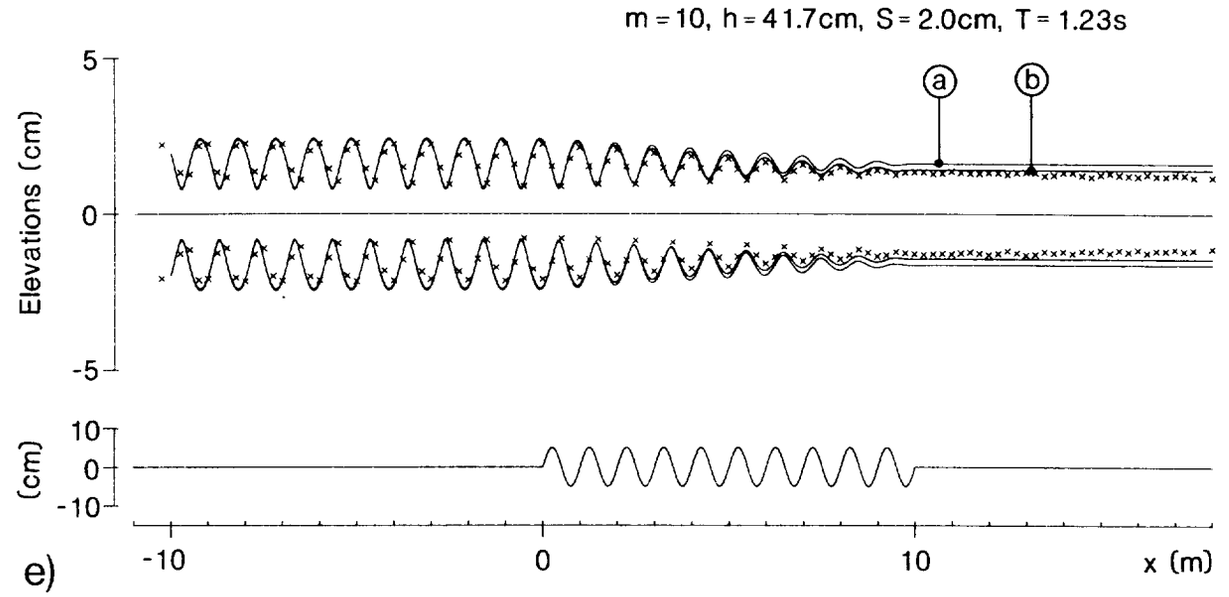
m = 10, h = 41.7cm, S = 2.0cm, T = 1.23s
Elevations (cm)
5
0
-5
a
b
(cm)
10
0
-10
-10
0
10
x (m)
e)

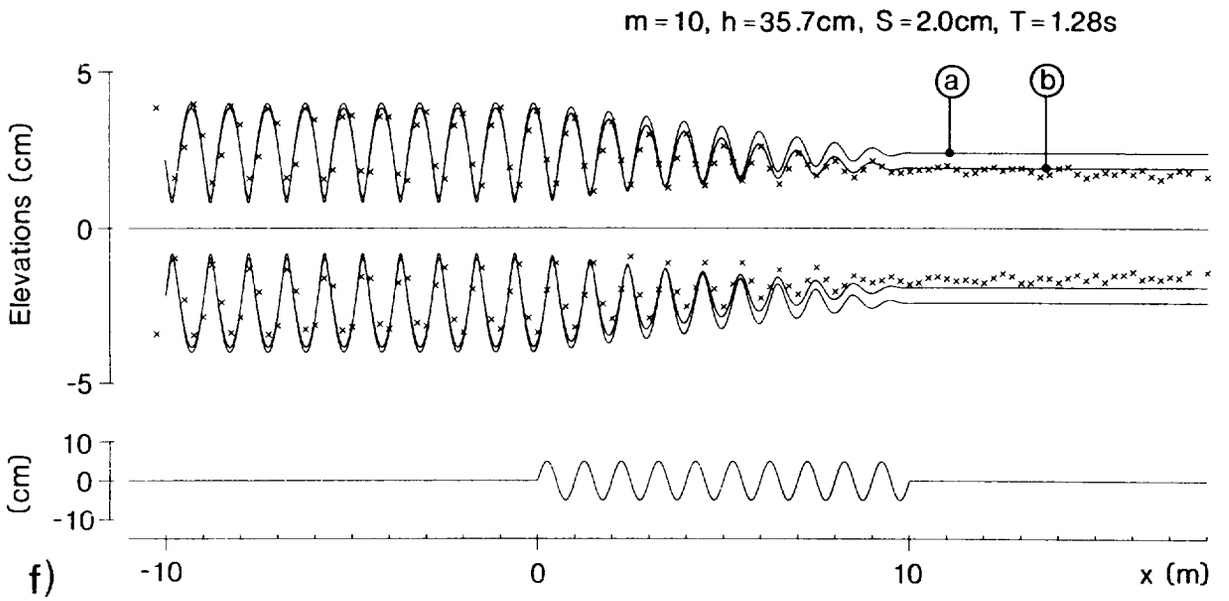
m = 10, h = 35.7cm, S = 2.0cm, T = 1.28s
Elevations (cm)
5
0
-5
a
b
(cm)
10
0
-10
-10
0
10
x (m)
f)

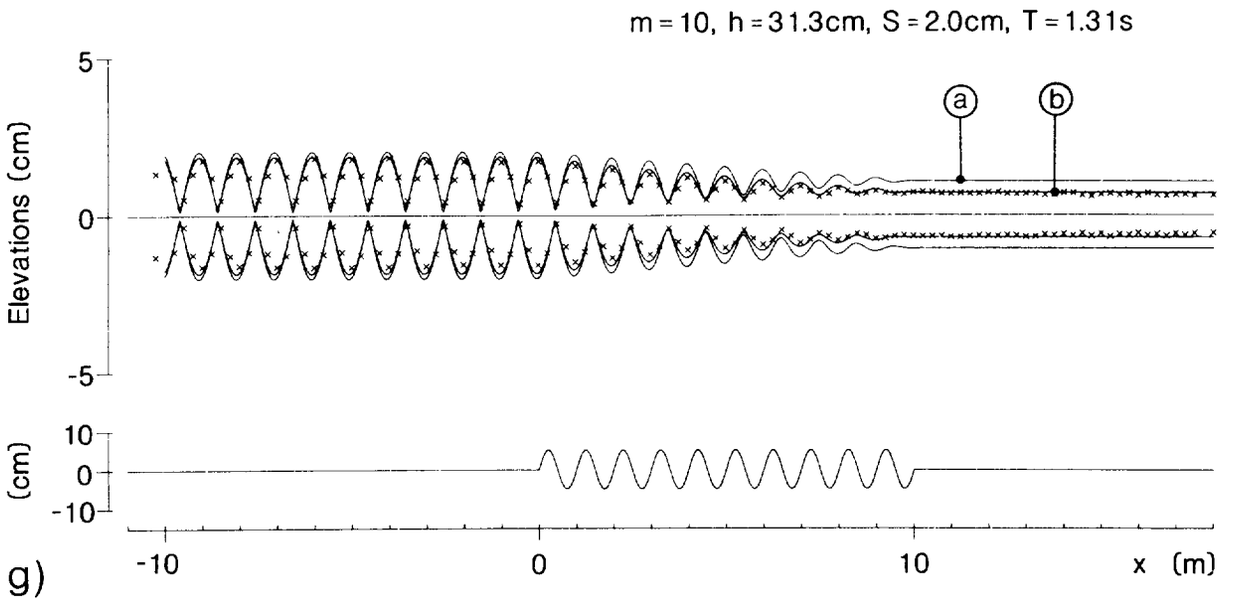
m = 10, h = 31.3cm, S = 2.0cm, T = 1.31s
Elevations (cm)
5
0
-5
a
b
(cm)
10
0
-10
-10
0
10
x (m)

g)

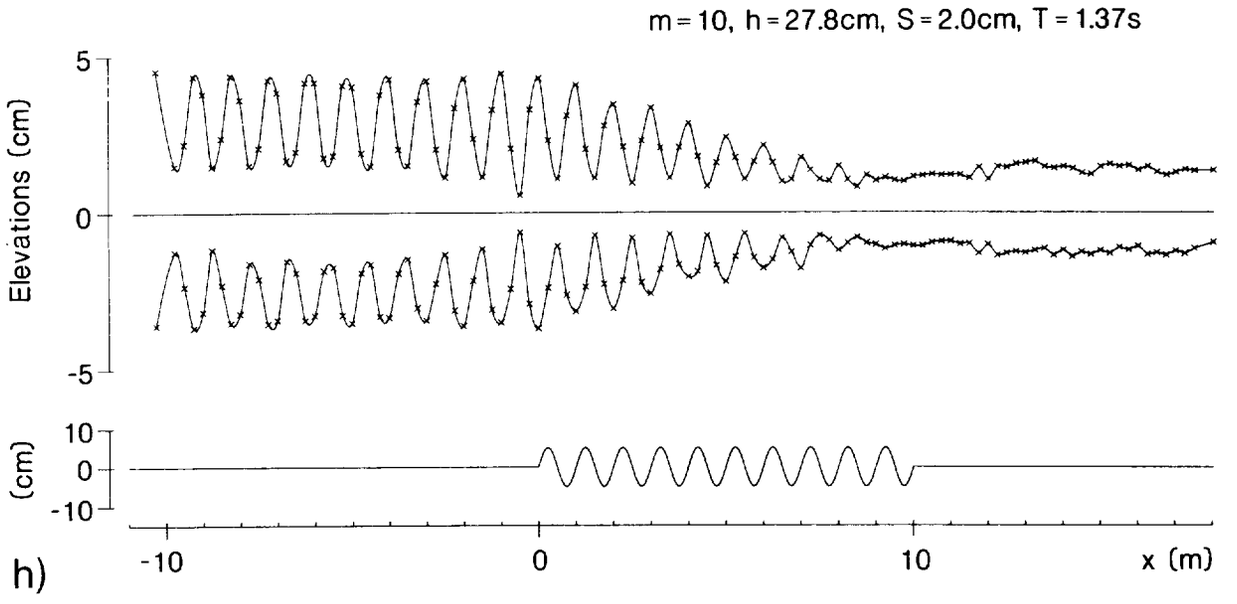
m = 10, h = 27.8cm, S = 2.0cm, T = 1.37s
Elevations (cm)
5
0
-5
(cm)
10
0
-10
-10
0
10
x (m)

h)

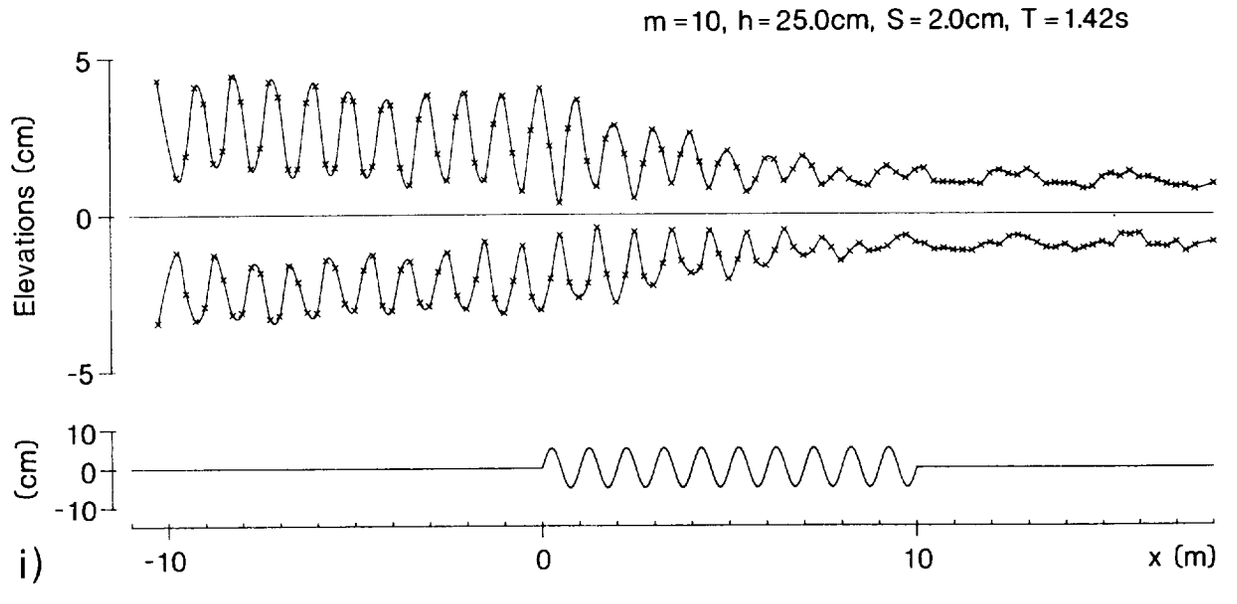
m = 10, h = 25.0cm, S = 2.0cm, T = 1.42s
Elevations (cm)
5
0
-5
(cm)
10
0
-10
-10
0
10
x (m)

i)

Figure 19 Variation of the wave reflection coefficient, K, throughout the wave tank at or near resonance ($2k/l \cong 1$), for different numbers of ripples (m) and different values of the quotient (b/h) of the ripple amplitude (b) and the water depth (h). Solid and broken curves represent the uncorrected and corrected theoretical results, respectively (see §2.7.2 and §4.3). T denotes the wave period. Further details of these measurements are given in Table 4. On the up-wave side of the ripple patch, $K \to |K_R|$ the ripple reflection coefficient, while, on the down-wave side, $K \to K_B$ the beach reflection coefficient.

Figure 19(a) m = 2, b/h = 0.32, T = 1.73 s

Figure 19(b) m = 4, b/h = 0.32, T = 1.73 s

Figure 19(c) m = 10, b/h = 0.08, T = 1.17 s

Figure 19(d) m = 10, b/h = 0.10, T = 1.20 s

Figure 19(e) m = 10, b/h = 0.12, T = 1.23 s

Figure 19(f) m = 10, b/h = 0.14, T = 1.28 s

Figure 19(g) m = 10, b/h = 0.16, T = 1.31 s

Figure 19(h) m = 10, b/h = 0.18, T = 1.37 s (no theory shown)

Figure 19(i) m = 10, b/h = 0.20, T = 1.42 s (no theory shown)

Note : In these diagrams, the origin of the x-axis has been taken (largely for experimental reasons) at the up-wave end of the ripple patch. Elsewhere (eg §2) the origin is taken at the centre of the patch.

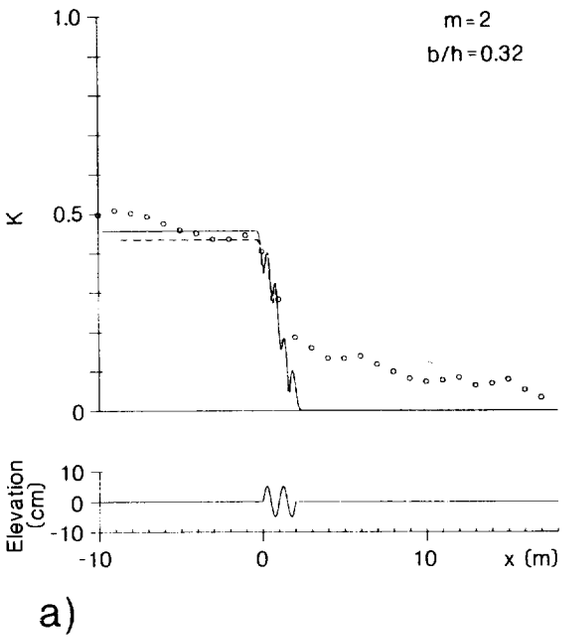
m = 2
b/h = 0.32
1.0
0.5
0
K
Elevation (cm)
10
0
-10
-10
0
10
x (m)

a)

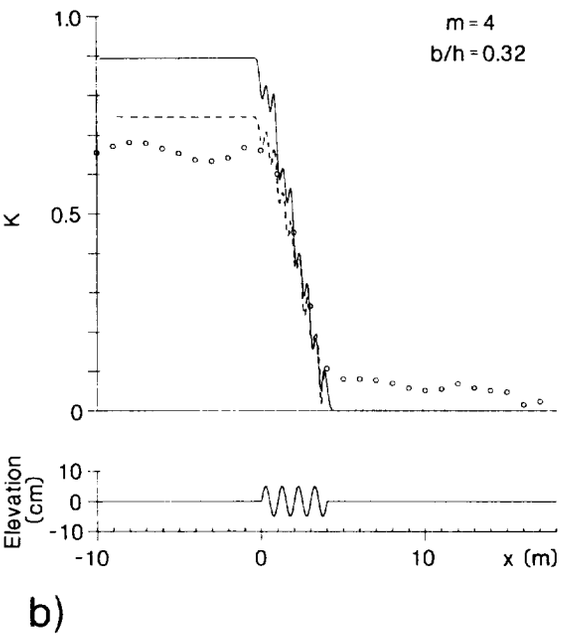
m = 4
b/h = 0.32
1.0
0.5
0
K
Elevation (cm)
10
0
-10
-10
0
10
x (m)

b)

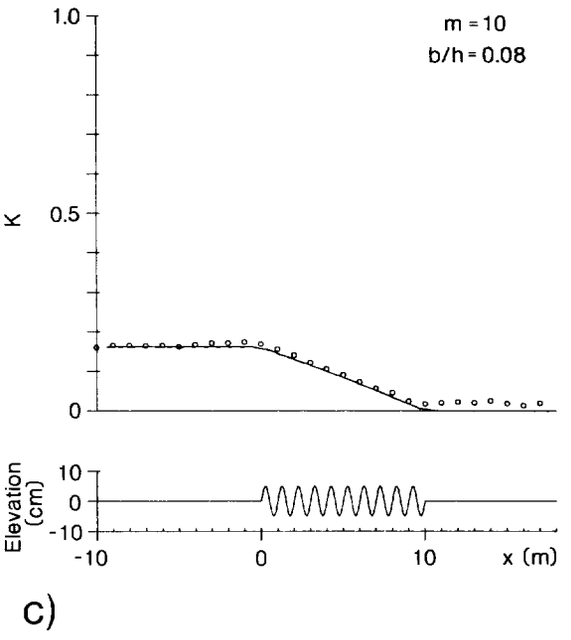
m = 10
b/h = 0.08
1.0
0.5
0
K
Elevation (cm)
10
0
-10
-10
0
10
x (m)

c)

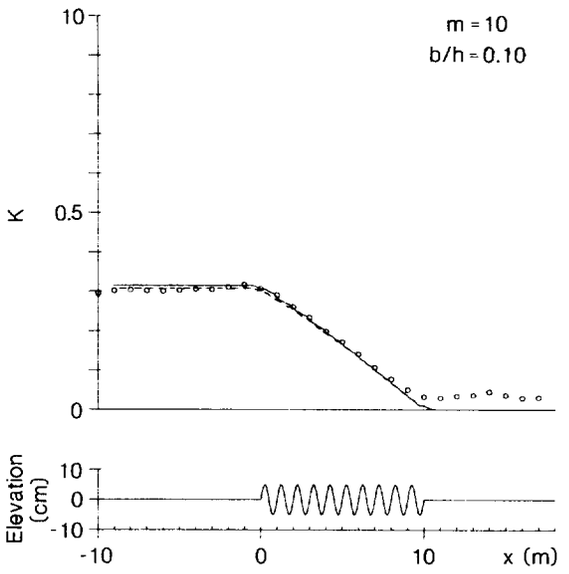
m = 10
b/h = 0.10
K
10
0.5
0
Elevation (cm)
10
0
-10
-10
0
10
x (m)

d)

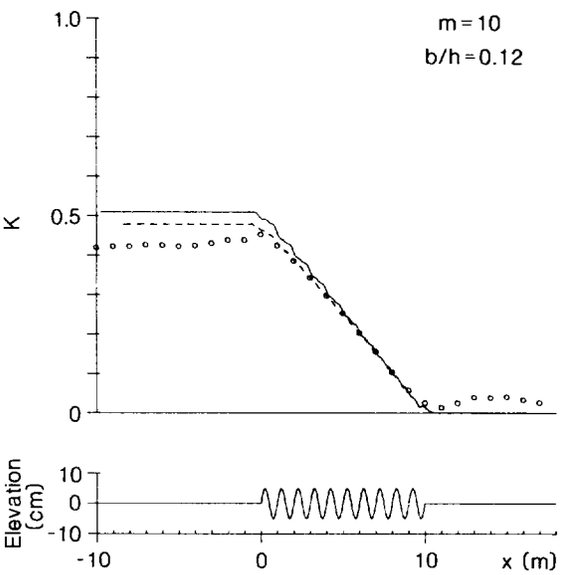
m = 10
b/h = 0.12
K
1.0
0.5
0
Elevation (cm)
10
0
-10
-10
0
10
x (m)

e)

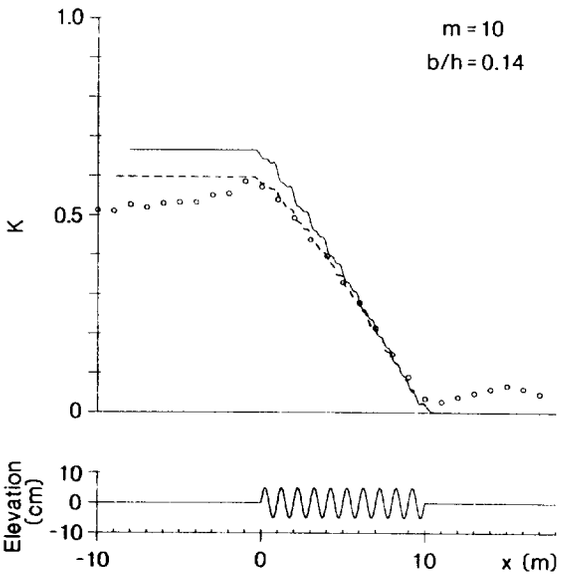
m = 10
b/h = 0.14
K
1.0
0.5
0
Elevation (cm)
10
0
-10
-10
0
10
x (m)

f)

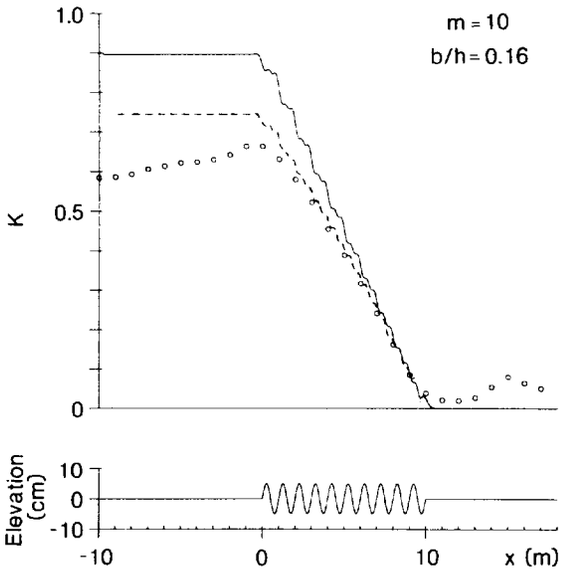
m = 10
b/h = 0.16
K
1.0
0.5
0
Elevation (cm)
10
0
-10
-10
0
10
x (m)

g)

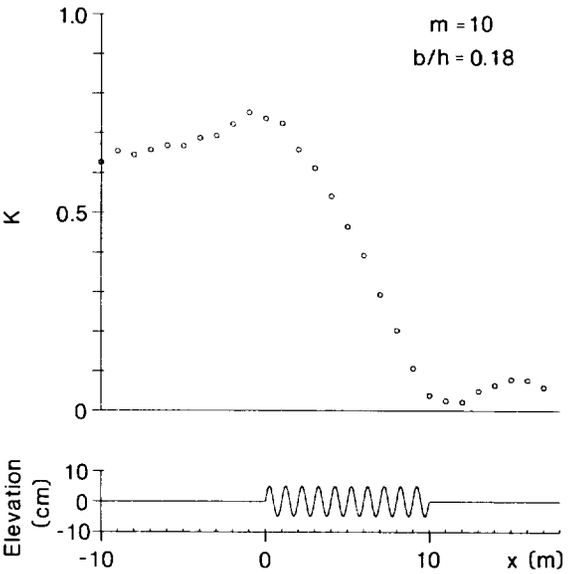
m = 10
b/h = 0.18
K
1.0
0.5
0
Elevation (cm)
10
0
-10
-10
0
10
x (m)

h)

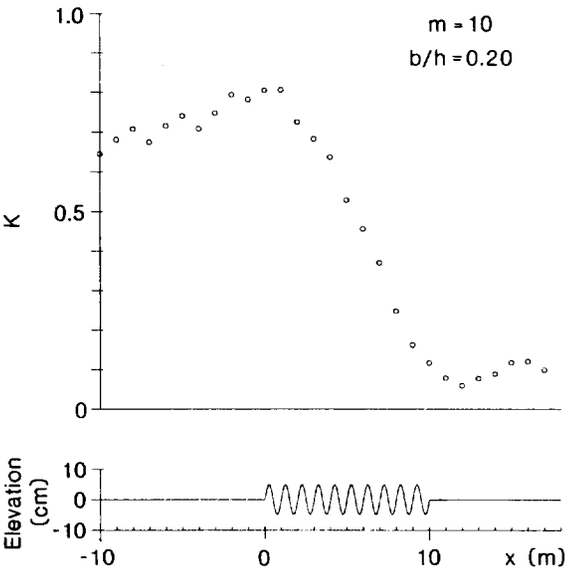
m = 10
b/h = 0.20
K
1.0
0.5
0
Elevation (cm)
10
0
-10
-10
0
10
x (m)

i)

Figure 20 Summary of measurements of the wave reflection coefficient (K) throughout the tank, at or near resonance. Smooth trend curves (cubic splines) have been fitted to the data. m denotes the number of ripples, and (b/h) the quotient of the ripple amplitude (b) and the water depth (h). Further details of these measurements are given in Table 4. On the up-wave side of the ripple patch, $K \to |K_R|$ the ripple reflection coefficient while, on the down-wave side, $K \to K_B$ the beach reflection coefficient.

Figure 20(a) m = 2 ripples

Figure 20(b) m = 4 ripples

Figure 20(c) m = 10 ripples

Note : In these diagrams, the origin of the x-axis has been taken (largely for experimental reasons) at the up-wave end of the ripple patch. Elsewhere (eg §2) the origin is taken at the centre of the patch.

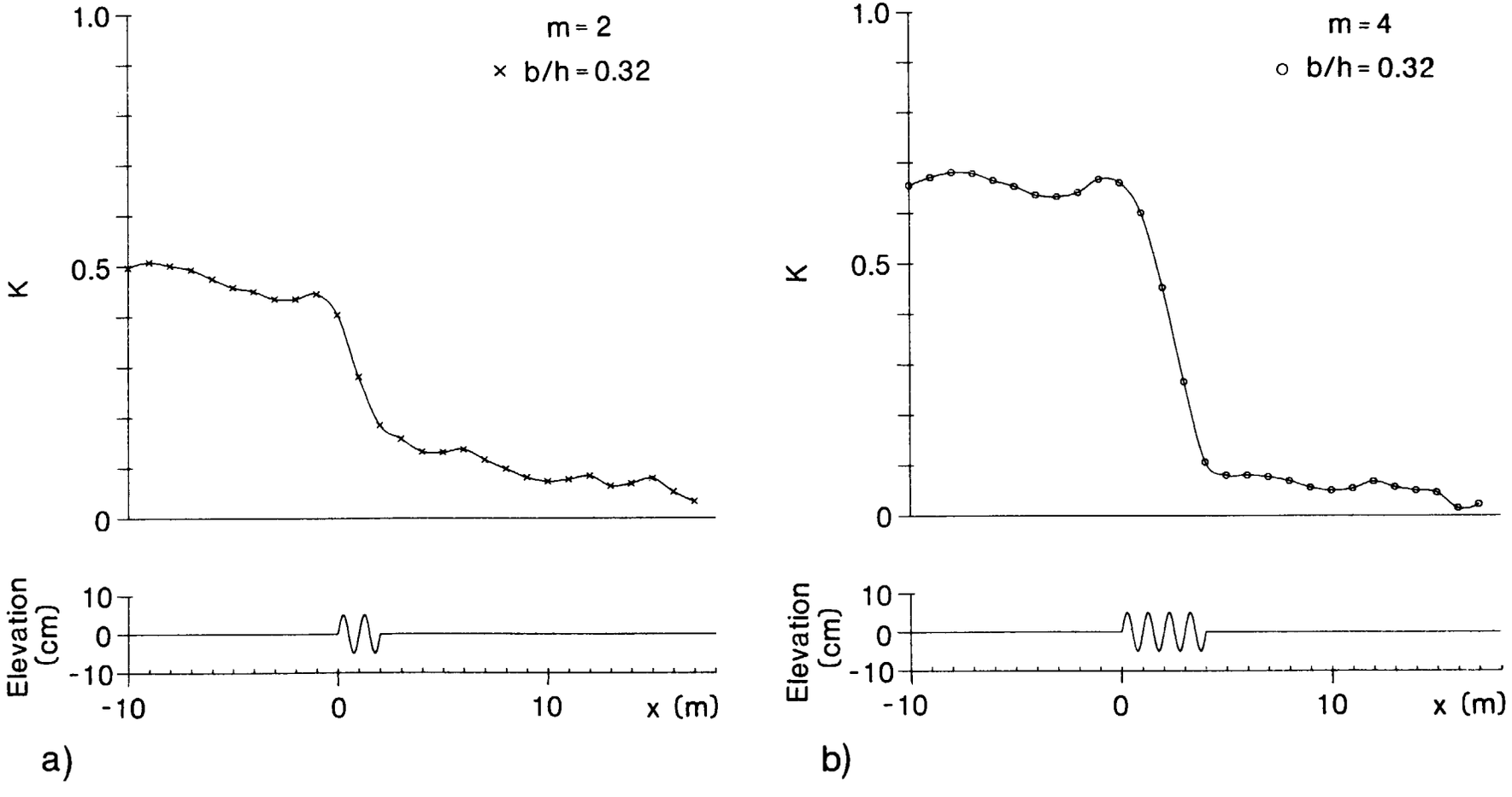
m = 2
× b/h = 0.32
1.0
0.5
0
K
Elevation (cm)
10
0
-10
-10
0
10
x (m)
a)
m = 4
○ b/h = 0.32
1.0
0.5
0
K
Elevation (cm)
10
0
-10
-10
0
10
x (m)
b)

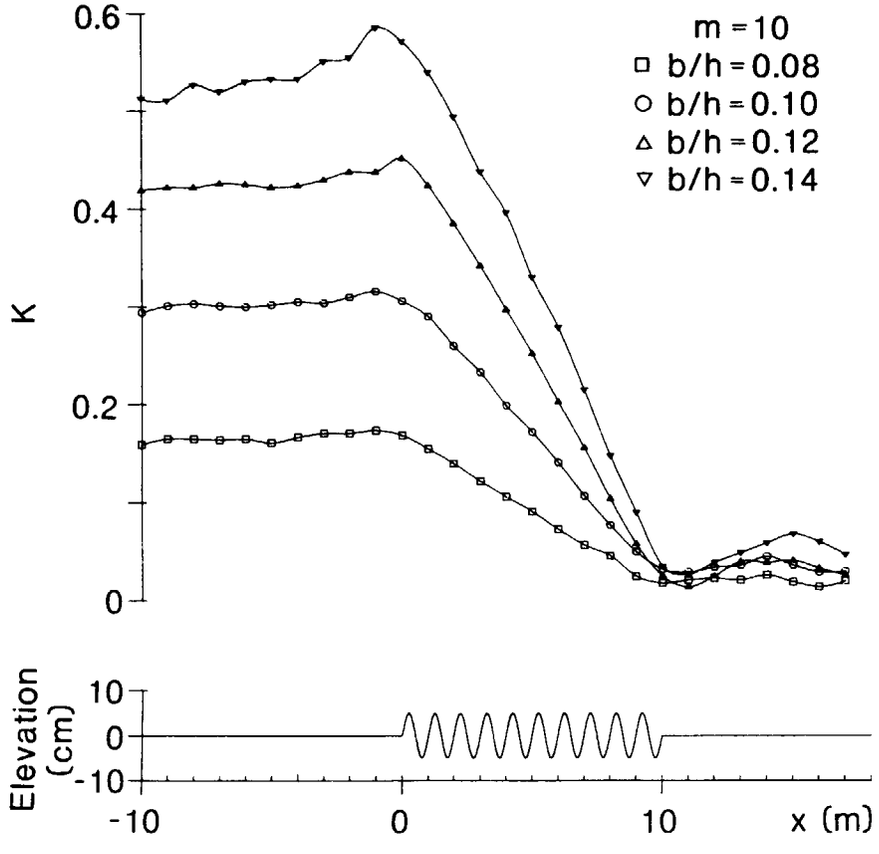
0.6
0.4
0.2
0
K
m = 10
b/h = 0.08
b/h = 0.10
b/h = 0.12
b/h = 0.14
Elevation (cm)
10
0
-10
-10
0
10
x (m)

c)

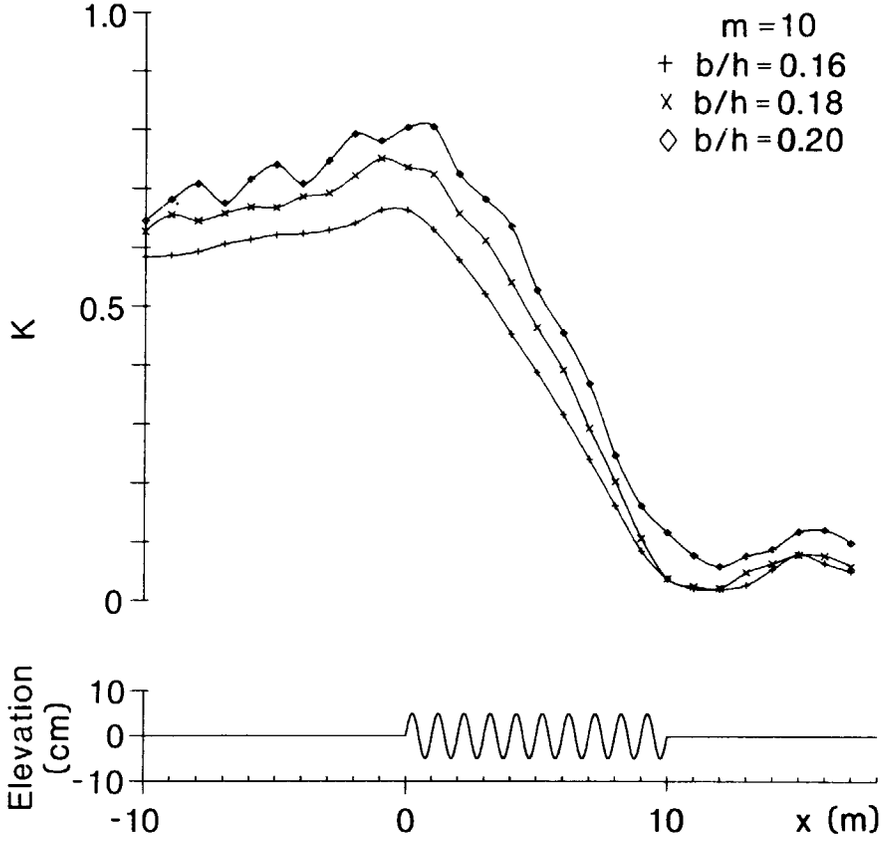
1.0
0.5
0
K
m = 10
b/h = 0.16
b/h = 0.18
b/h = 0.20
Elevation (cm)
10
0
-10
-10
0
10
x (m)

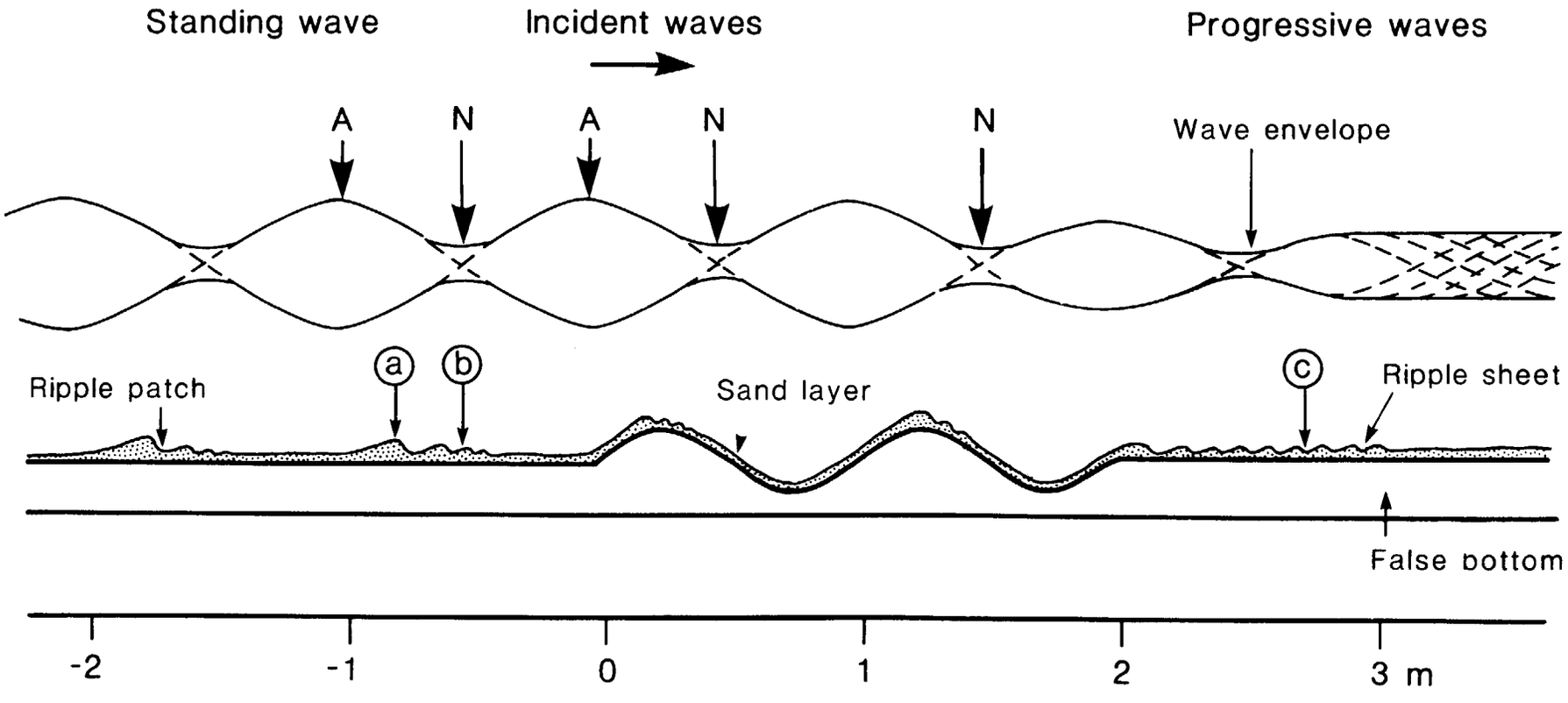

Figure 21 Schematic diagram showing the formation of short wavelength ripple patches beneath the partially standing wave pattern resulting from reflection by the long wavelength (1 m) ripples. Ripples appear first in small patches beneath the nodes (N), and these patches then grow in extent towards the anti-nodes (A). Within a ripple patch the wavelength decreases from about 5 cm near the anti-node (a) to about 2 cm near the node (b). There is a corresponding decrease in ripple height from about 1.5 cm to 0.2 cm within a patch. Ripple asymmetry throughout the test section, and on either side of it,was found to be in the down-wave direction.

Figure 22 Sequence of photographs showing the formation of patches of ripples of short wavelength in 235 μm sand, beneath the partially standing wave pattern up-wave of two (5 cm amplitude by 1 m wavelength) sinusoidal ripples. The water depth was h = 15.6 cm and the wave period was T = 1.73 s, such that the free surface wavelength was λ_w = 206.5 cm. The measured reflection coefficient of the ripple patch was $|K_R| \cong 0.34$. The following sequence shows how the ripple patches evolved with increasing time t.

Figure 22(a) t = 0. Sand lying in a thin layer (< 0.05 cm) throughout the ripple patch, and on either side of it.

Figure 22(b) t = 10 min. Small patches on the crest of the first ripple, and at a distance of 1 m up-wave of this crest.

Figure 22(c) t = 30 min. Formation of three ripple patches with 1 m spacing, beneath the nodes of surface elevation.

Figure 22(d) t = 50 min. Ripple patches increasing in extent.

Figure 22(e) t = 90 min. Ripple patches increasing in extent.

Figure 22(f) t = 130 min. Ripple patches increasing in extent.

Finally, in Figure 22(g), a photograph shows the continuous sheet of ripples of short wavelength, at least 1 m in extent, formed on the down-wave side of the ripple patch.

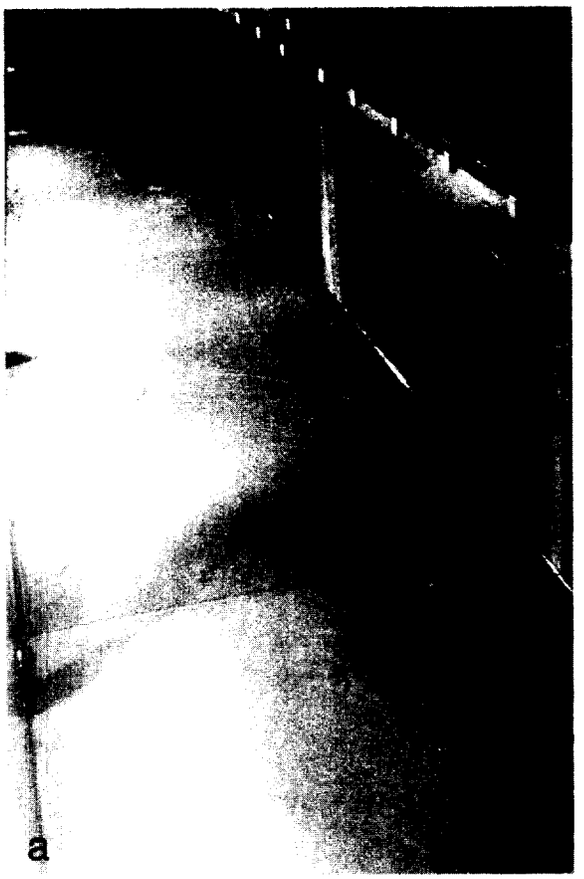
a


b

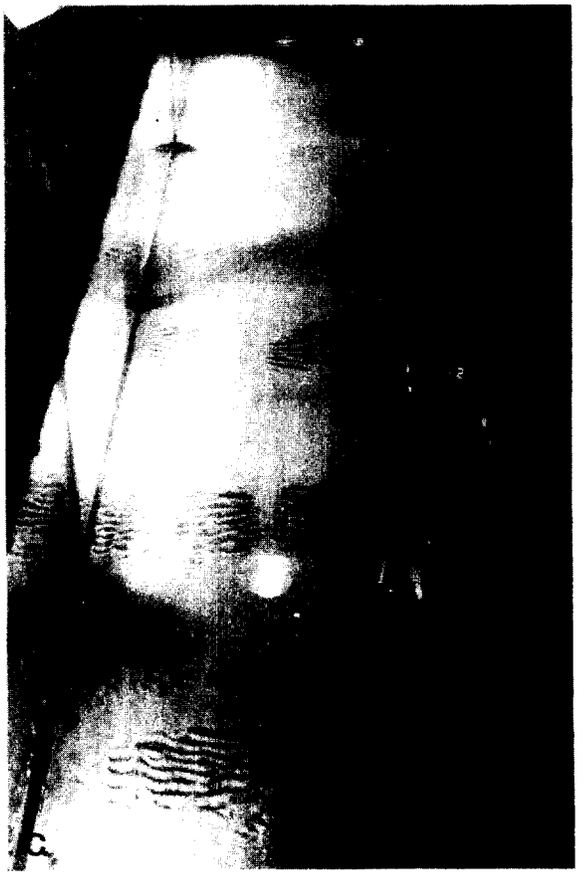
c

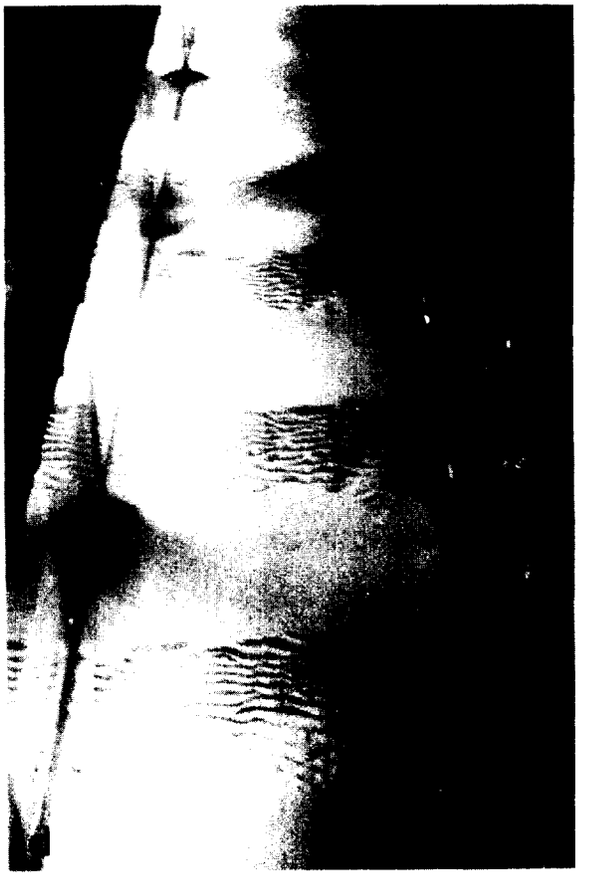

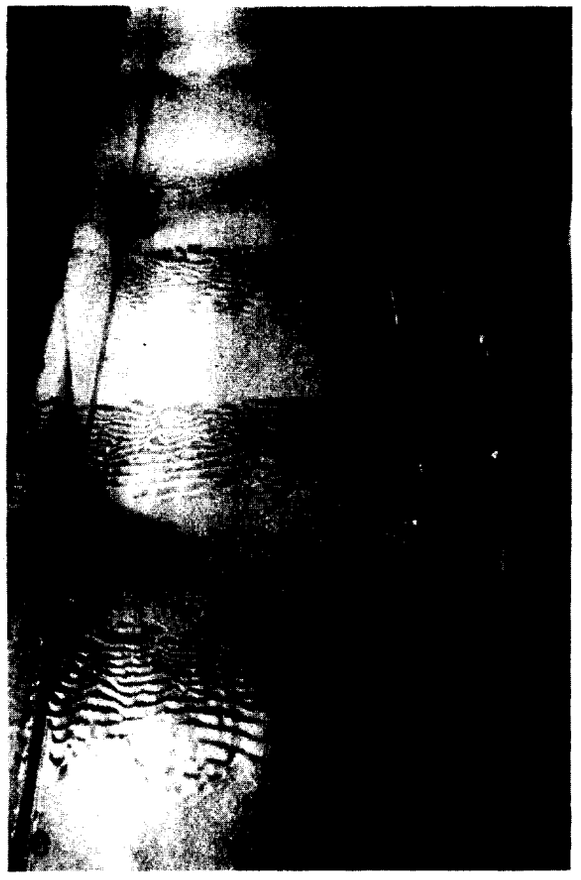

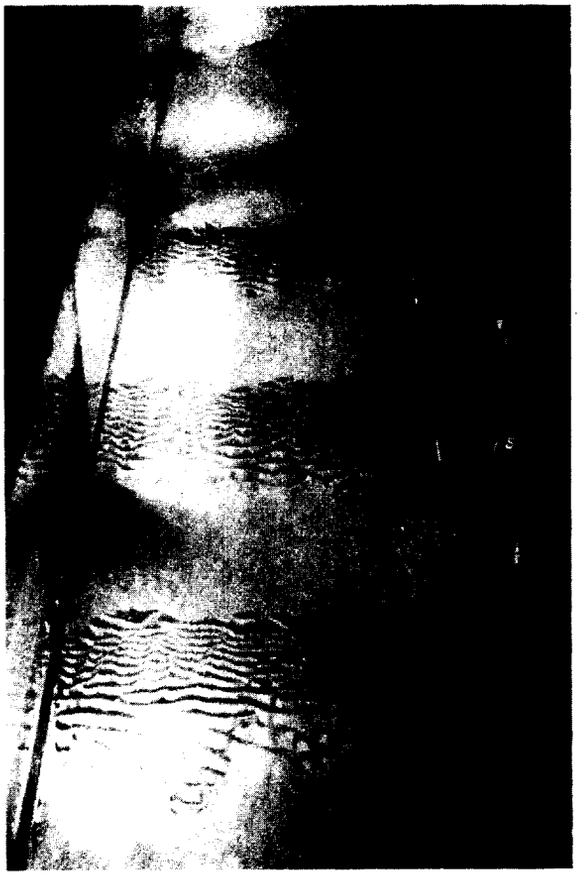

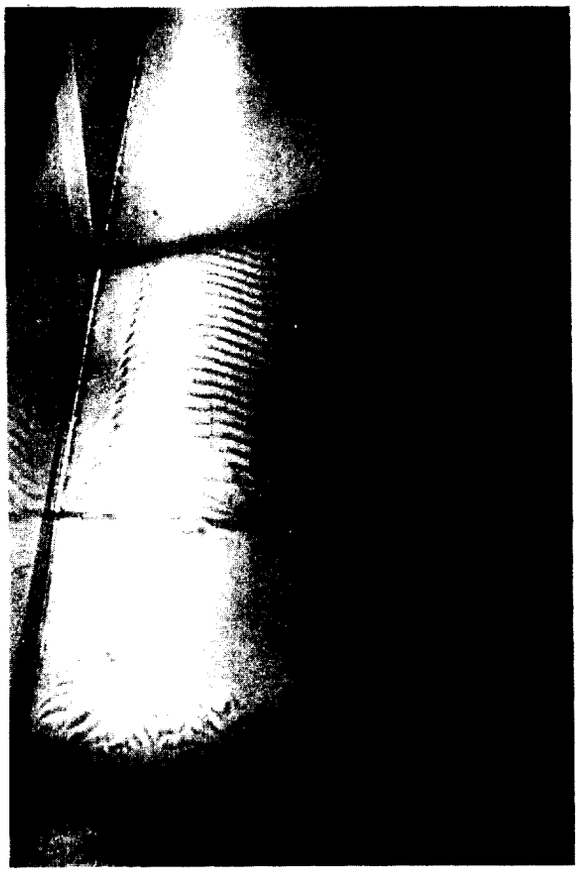

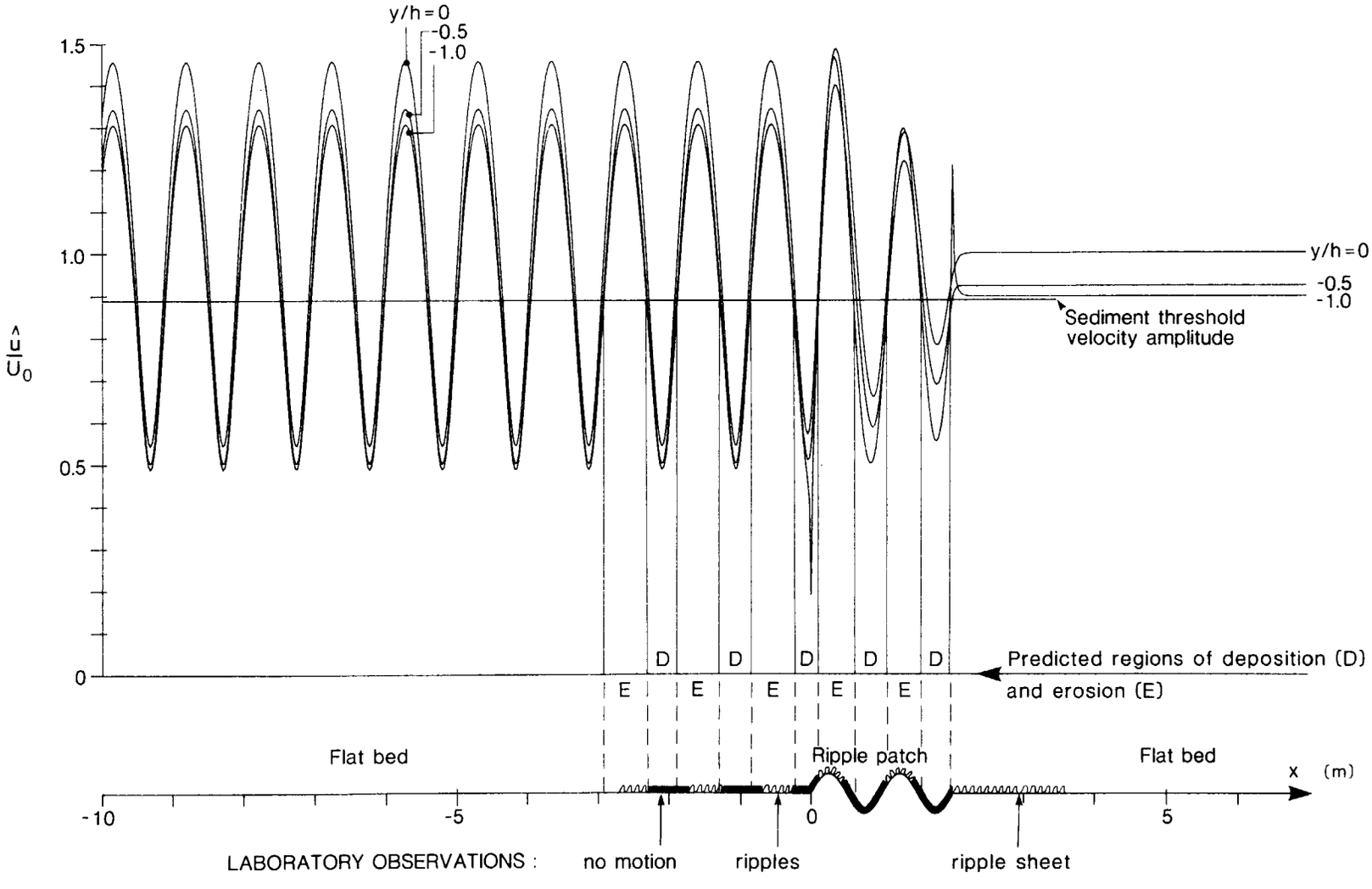

Figure 23 Predicted horizontal velocity amplitudes are compared with observations of sediment movement in the wave tank, for the case in which m = 2, b = 5 cm, λ_R = 100 cm, h = 15.6 cm and T = 1.73 s (2k/l = 0.968). The predicted reflection coefficient of the ripple patch was K_R = 0.455, which may be compared with the measured value of $|K_R| \cong 0.34$. Horizontal velocity amplitudes (cf Fig 10) are plotted for the levels y/h = 0, -0.5 and -1.0, and the predicted bed velocity amplitude (y/h = -1.0) is compared with the sediment threshold velocity amplitude for the grain size (235 μm) in question. Thus regions on the bed of deposition (D) and erosion (E) are predicted, and these are compared with the laboratory observations. [Note that, for consistency with Figs 18 - 20, the origin of the x-axis has been taken up-wave of the ripple patch.]

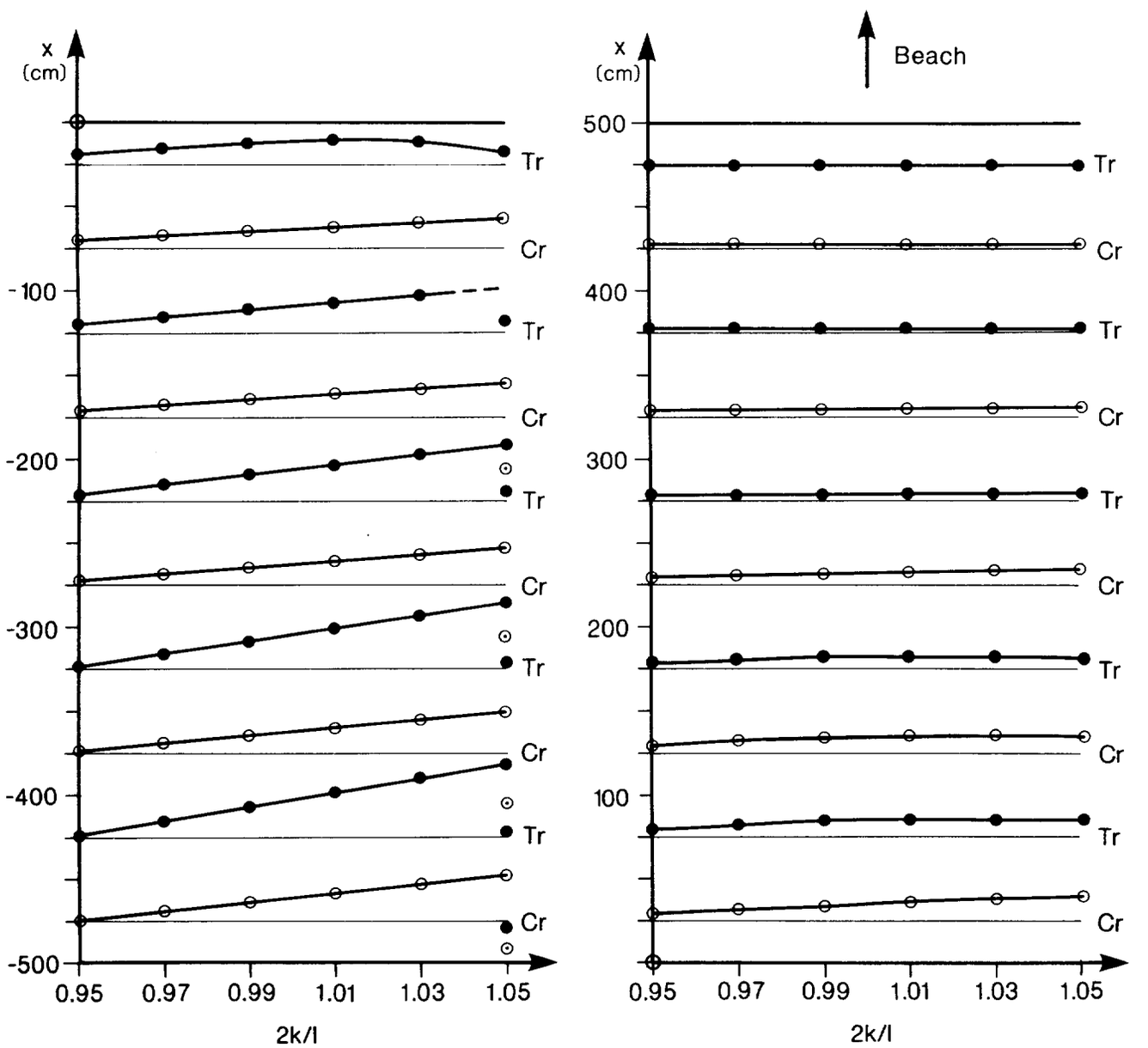

Figure 24 Positions of horizontal bed velocity maxima (○) and minima (●) throughout the ripple patch for the case in which m = 10, b = 5 cm, λ_R = 100 cm and h = 41.7 cm, and for 2k/l = 0.95 to 1.05.

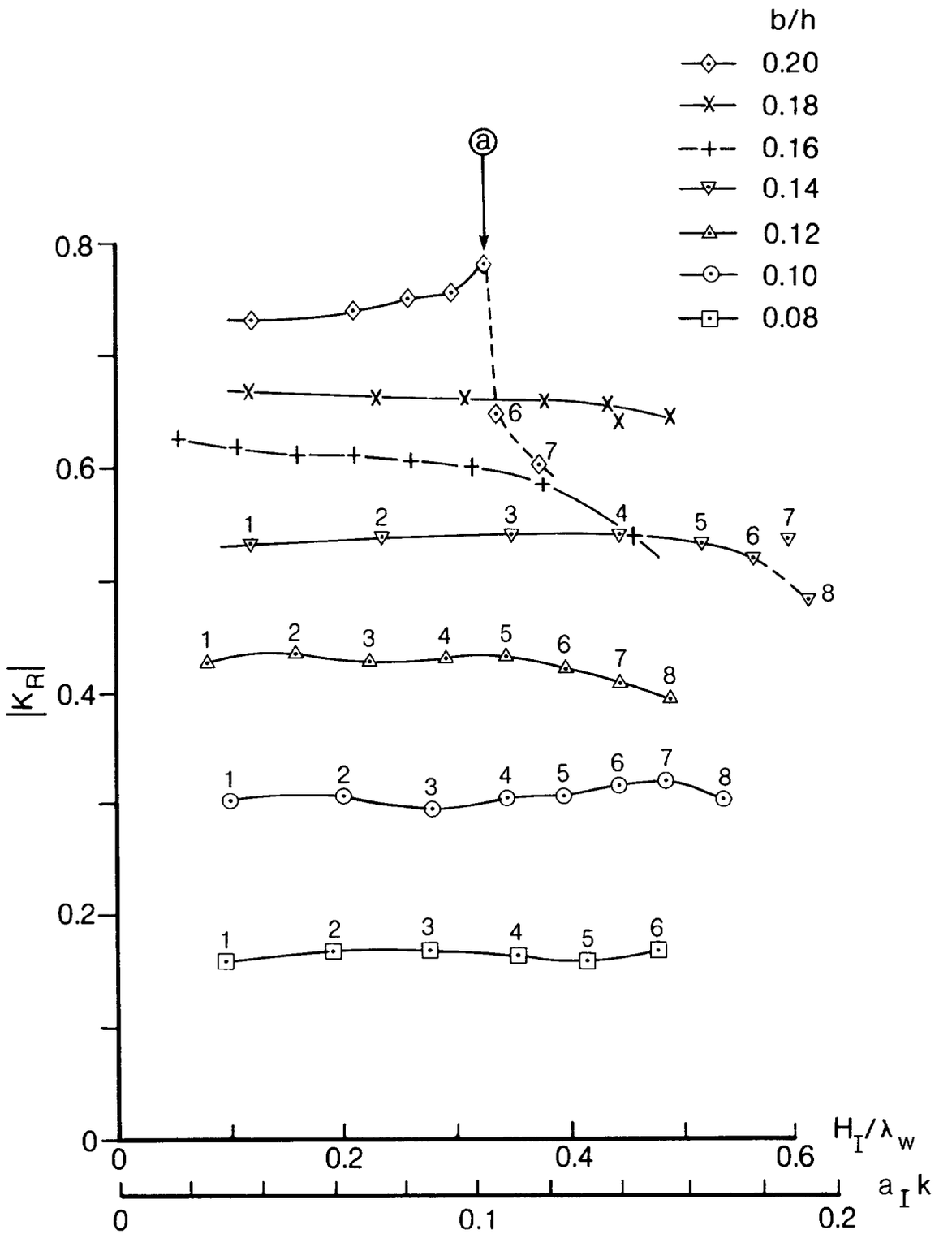

Figure 25 Variation of the reflection coefficient $|K_R|$ of the ripple patch, at or near resonance, as a function of the wave steepness. Note that the wave steepness is given in terms both of H_I/λ_W and $a_I k$ ($a_I k = \pi H_I/\lambda_W$). $|K_R|$ is shown for different values of b/h, and the number against each point refers to the stroke of the wave generator in cms. All measurements were made with m = 10 ripples.
Note : (a) indicates unstable wave conditions in the tank.

TABLE 1

Comparison of the nominal and measured wave period settings for the wave generator, in the range 0.6-3.0s

Nominal T(s)	Actual T(s)
.6	.600
.8	.799
1.0	1.002
1.2	1.197
1.4	1.396
1.6	1.597
1.8	1.799
2.0	2.005
2.2	2.201
2.4	2.397
2.6	2.602
2.8	2.799
3.0	2.998

Wave periods were determined by timing the passage of thirty waves past a fixed point in the tank.

TABLE 2

Measurements of the ripple reflection coefficient $|K_R|$ and the beach reflection coefficient K_B, as functions of the wave period, for m = 2, 4 and 10 ripples in the patch and for different water depths. Gauges 1 and 2 give the measurements relating to reflection by the ripples, and gauges 3 and 4 the measurements relating to reflection by the beach. Values of the incident and reflected wave amplitudes a_I and a_R, and of the wave steepness H_I/λ_w, are also included. (For convenience, the wave steepness has been defined in these tables as H_I/λ_w. Elsewhere the definition $a_I k = \pi H_I/\lambda_w$ has been adopted.)

Table 2a	m = 2,	h = 15.6 cm
Table 2b	m = 4,	h = 15.6 cm
Table 2c	m = 10,	h = 31.3 cm

Note: In these tables, the origin of the x-axis has been taken (largely for experimental reasons) at the up-wave end of the ripple patch. Elsewhere (eg §2) the origin is taken at the centre of the patch.

TABLE 2a

Monochromatic wave reflection results CERC 150x3x3 ft wave tank.

Date(s)	Depth (cm)	No.of ripples	Ripple Amplitude (cm)	Amplitude / filter / Depth ratio	No Filter	Beach slope	Water temperature (deg C)
25/8/81	h=15.6	m= 2	b=5	b/h=0.32	NF	1:10	22.5

Gauge positions(x) (m)				Wave period	Stroke	Wave reflection results from Gauges 1 & 2						Wave reflection results from Gauges 3 & 4					
1	2	3	4	T (s)	S (cm)	a_I (cm)	a_R (cm)	H_I (cm)	λ_w (cm)	H_I/λ_w	$\lvert K_R \rvert$	a_I (cm)	a_R (cm)	H_I (cm)	λ_w (cm)	H_I/λ_w	K_B
-5.125	-4.875	6.875	7.125	0.78	1.0	0.66	0.041	1.33	79.9	0.01670	0.061	0.63	0.018	1.27	79.9	0.01592	0.029
-5.125	-4.875	6.875	7.125	0.79	1.0	0.72	0.042	1.44	81.4	0.01769	0.059	0.63	0.041	1.25	81.4	0.01536	0.065
-5.125	-4.875	6.875	7.125	0.80	1.0	0.61	0.073	1.22	82.8	0.01471	0.119	0.59	0.033	1.19	82.8	0.01439	0.056
-5.125	-4.875	6.875	7.125	0.81	1.0	0.73	0.033	1.47	84.2	0.01743	0.045	0.61	0.053	1.22	84.2	0.01449	0.087
-5.125	-4.875	6.875	7.125	0.82	1.0	0.73	0.051	1.47	85.7	0.01718	0.070	0.59	0.105	1.19	85.7	0.01389	0.176
-5.125	-4.875	6.875	7.125	0.83	1.0	0.63	0.095	1.26	87.1	0.01450	0.151	0.62	0.050	1.23	87.1	0.01412	0.082
-5.125	-4.875	6.875	7.125	0.84	1.0	0.66	0.064	1.31	88.5	0.01476	0.097	0.58	0.052	1.16	88.5	0.01315	0.090
-5.125	-4.875	6.875	7.125	0.85	1.0	0.58	0.048	1.15	89.9	0.01278	0.083	0.55	0.043	1.11	89.9	0.01239	0.078
-5.125	-4.875	6.875	7.125	0.86	1.0	0.63	0.086	1.27	91.3	0.01390	0.135	0.58	0.070	1.16	91.3	0.01267	0.121
-5.125	-4.875	6.875	7.125	0.87	1.0	0.65	0.030	1.29	92.7	0.01393	0.046	0.58	0.052	1.15	92.7	0.01246	0.091
-5.125	-4.875	6.875	7.125	0.88	1.0	0.63	0.081	1.27	94.1	0.01347	0.128	0.56	0.044	1.13	94.1	0.01196	0.077
-5.125	-4.875	6.875	7.125	0.89	1.0	0.63	0.022	1.27	95.5	0.01332	0.034	0.57	0.049	1.14	95.5	0.01199	0.086
-5.125	-4.875	6.875	7.125	0.90	1.0	0.59	0.040	1.17	96.9	0.01205	0.069	0.52	0.040	1.04	96.9	0.01075	0.076
-5.125	-4.875	6.875	7.125	0.91	1.0	0.56	0.046	1.12	98.3	0.01142	0.082	0.50	0.039	0.99	98.3	0.01012	0.078
-5.125	-4.875	6.875	7.125	0.92	1.0	0.59	0.024	1.18	99.7	0.01184	0.040	0.53	0.049	1.06	99.7	0.01061	0.093
-5.125	-4.875	6.875	7.125	0.93	1.0	0.59	0.044	1.18	101.1	0.01171	0.075	0.53	0.044	1.06	101.1	0.01047	0.083
-5.125	-4.875	6.875	7.125	0.94	1.0	0.63	0.045	1.26	102.5	0.01233	0.071	0.56	0.041	1.12	102.5	0.01095	0.073
-5.125	-4.875	6.875	7.125	0.95	1.0	0.60	0.024	1.20	103.8	0.01157	0.040	0.53	0.036	1.06	103.8	0.01024	0.068
-5.125	-4.875	6.875	7.125	0.96	1.0	0.55	0.043	1.11	105.2	0.01052	0.078	0.49	0.029	0.98	105.2	0.00927	0.059
-5.125	-4.875	6.875	7.125	0.97	1.0	0.58	0.020	1.15	106.6	0.01083	0.034	0.52	0.026	1.04	106.6	0.00975	0.050
-5.125	-4.875	6.875	7.125	0.98	1.0	0.59	0.065	1.18	108.0	0.01089	0.110	0.52	0.025	1.04	108.0	0.00968	0.048
-5.125	-4.875	6.875	7.125	0.99	1.0	0.55	0.037	1.10	109.3	0.01007	0.067	0.49	0.026	0.98	109.3	0.00895	0.054
-5.125	-4.875	6.875	7.125	1.00	1.0	0.58	0.031	1.16	110.7	0.01045	0.054	0.52	0.025	1.03	110.7	0.00933	0.048
-5.125	-4.875	6.875	7.125	1.01	1.0	0.56	0.064	1.13	112.1	0.01004	0.113	0.50	0.022	1.00	112.1	0.00888	0.044
-5.125	-4.875	6.875	7.125	1.02	1.0	0.48	0.028	0.97	113.4	0.00857	0.057	0.44	0.024	0.88	113.4	0.00772	0.054
-5.125	-4.875	6.875	7.125	1.03	1.0	0.51	0.052	1.01	114.8	0.00878	0.102	0.45	0.033	0.90	114.8	0.00783	0.073
-5.125	-4.875	6.875	7.125	1.04	1.0	0.59	0.091	1.18	116.2	0.01013	0.155	0.52	0.045	1.04	116.2	0.00898	0.087
-5.125	-4.875	6.875	7.125	1.05	1.0	0.52	0.032	1.04	117.5	0.00882	0.061	0.46	0.034	0.93	117.5	0.00793	0.073
-5.125	-4.875	6.875	7.125	1.06	1.0	0.48	0.060	0.96	118.9	0.00805	0.124	0.43	0.027	0.85	118.9	0.00716	0.063
-5.125	-4.875	6.875	7.125	1.07	1.0	0.61	0.090	1.22	120.2	0.01013	0.148	0.55	0.041	1.09	120.2	0.00905	0.075
-5.125	-4.875	6.875	7.125	1.08	1.0	0.53	0.024	1.07	121.6	0.00880	0.044	0.48	0.050	0.97	121.6	0.00798	0.104
-5.125	-4.875	6.875	7.125	1.09	1.0	0.55	0.055	1.10	122.9	0.00893	0.100	0.49	0.059	0.98	122.9	0.00799	0.120
-5.125	-4.875	6.875	7.125	1.11	1.0	0.57	0.052	1.14	125.6	0.00908	0.091	0.51	0.049	1.01	125.6	0.00807	0.098
-5.125	-4.875	6.875	7.125	1.12	1.0	0.55	0.032	1.09	126.9	0.00855	0.058	0.48	0.048	0.97	126.9	0.00761	0.100
-5.125	-4.875	6.875	7.125	1.13	1.0	0.55	0.062	1.10	128.3	0.00858	0.112	0.49	0.053	0.98	128.3	0.00766	0.109
-5.125	-4.875	6.875	7.125	1.14	1.0	0.53	0.051	1.07	129.6	0.00823	0.095	0.48	0.057	0.96	129.6	0.00740	0.119
-5.125	-4.875	6.875	7.125	1.16	1.0	0.50	0.050	1.00	132.3	0.00756	0.101	0.45	0.047	0.90	132.3	0.00681	0.104
-5.125	-4.875	6.875	7.125	1.17	1.0	0.53	0.030	1.07	133.6	0.00804	0.057	0.48	0.040	0.97	133.6	0.00726	0.083
-5.125	-4.875	6.875	7.125	1.18	1.0	0.51	0.034	1.02	135.0	0.00760	0.066	0.46	0.039	0.92	135.0	0.00683	0.084
-5.125	-4.875	6.875	7.125	1.20	1.0	0.48	0.061	0.96	137.6	0.00701	0.127	0.43	0.051	0.86	137.6	0.00628	0.118
-5.125	-4.875	6.875	7.125	1.21	1.0	0.55	0.029	1.11	138.9	0.00796	0.053	0.50	0.059	1.00	138.9	0.00718	0.119
-5.125	-4.875	6.875	7.125	1.22	1.0	0.50	0.039	0.99	140.3	0.00707	0.079	0.45	0.055	0.89	140.3	0.00363	0.123
-5.125	-4.875	6.875	7.125	1.24	1.0	0.53	0.102	1.06	142.9	0.00739	0.193	0.47	0.059	0.94	142.9	0.00656	0.126
-5.125	-4.875	6.875	7.125	1.26	1.0	0.48	0.037	0.97	145.6	0.00664	0.076	0.44	0.057	0.88	145.6	0.00602	0.130
-5.125	-4.875	6.875	7.125	1.27	1.0	0.44	0.092	0.88	146.9	0.00601	0.208	0.39	0.058	0.78	146.9	0.00534	0.148
-5.125	-4.875	6.875	7.125	1.29	1.0	0.59	0.180	1.19	149.5	0.00799	0.303	0.52	0.083	1.03	149.5	0.00692	0.161
-5.250	-4.750	6.750	7.250	1.31	1.0	0.48	0.053	0.97	152.1	0.00636	0.110	0.43	0.051	0.85	152.1	0.00562	0.120
-5.250	-4.750	6.750	7.250	1.32	1.0	0.44	0.082	0.88	153.4	0.00574	0.187	0.39	0.037	0.77	153.4	0.00499	0.096
-5.250	-4.750	6.750	7.250	1.34	1.0	0.62	0.171	1.24	156.1	0.00796	0.276	0.52	0.042	1.03	156.1	0.00662	0.081
-5.250	-4.750	6.750	7.250	1.36	1.0	0.51	0.081	1.02	158.7	0.00641	0.159	0.45	0.048	0.89	158.7	0.00559	0.108

TABLE 2a

Monochromatic wave reflection results CERC 150x3x3 ft wave tank.

Date(s)	Depth (cm)	No.of ripples	Ripple Amplitude (cm)	Amplitude / filter / Depth ratio	No Filter	Beach slope	Water temperature (deg C)
25/8/81	h=15.6	m= 2	b=5	b/h=0.32	NF	1:10	22.5

Gauge positions(x) (m)				Wave period	Stroke	Wave reflection results from Gauges 1 & 2						Wave reflection results from Gauges 3 & 4					
1	2	3	4	T (s)	S (cm)	a_I (cm)	a_R (cm)	H_I (cm)	λ_w (cm)	H_I/λ_w	$\|K_R\|$	a_I (cm)	a_R (cm)	H_I (cm)	λ_w (cm)	H_I/λ_w	K_B
-5.250	-4.750	6.750	7.250	1.38	1.0	0.39	0.124	0.77	161.3	0.00475	0.321	0.32	0.045	0.64	161.3	0.00397	0.141
-5.250	-4.750	6.750	7.250	1.40	1.0	0.52	0.176	1.04	163.9	0.00634	0.339	0.43	0.066	0.87	163.9	0.00529	0.152
-5.250	-4.750	6.750	7.250	1.42	1.0	0.51	0.060	1.02	166.5	0.00615	0.117	0.45	0.053	0.91	166.5	0.00545	0.116
-5.250	-4.750	6.750	7.250	1.44	1.0	0.41	0.144	0.82	169.1	0.00483	0.350	0.34	0.040	0.69	169.1	0.00406	0.116
-5.250	-4.750	6.750	7.250	1.47	1.0	0.39	0.159	0.77	173.0	0.00444	0.413	0.32	0.047	0.63	173.0	0.00363	0.150
-5.250	-4.750	6.750	7.250	1.49	1.0	0.52	0.154	1.05	175.6	0.00597	0.294	0.45	0.054	0.91	175.6	0.00521	0.119
-5.250	-4.750	6.750	7.250	1.51	1.0	0.48	0.195	0.96	178.2	0.00537	0.406	0.39	0.039	0.78	178.2	0.00439	0.100
-5.250	-4.750	6.750	7.250	1.54	1.0	0.30	0.121	0.61	182.1	0.00333	0.398	0.24	0.030	0.49	182.1	0.00272	0.123
-5.250	-4.750	6.750	7.250	1.56	1.0	0.36	0.099	0.71	184.7	0.00382	0.279	0.31	0.047	0.62	184.7	0.00334	0.152
-5.250	-4.750	6.750	7.250	1.59	1.0	0.55	0.257	1.10	188.5	0.00584	0.467	0.43	0.082	0.86	188.5	0.00456	0.191
-5.250	-4.750	6.750	7.250	1.62	1.0	0.28	0.125	0.56	192.4	0.00289	0.447	0.22	0.046	0.44	192.4	0.00228	0.209
-5.250	-4.750	6.750	7.250	1.65	1.0	0.30	0.071	0.61	196.2	0.00313	0.232	0.27	0.053	0.54	196.2	0.00276	0.197
-5.250	-4.750	6.750	7.250	1.68	1.0	0.39	0.163	0.78	200.1	0.00388	0.419	0.31	0.055	0.62	200.1	0.00311	0.176
-5.250	-4.750	6.750	7.250	1.71	1.0	0.38	0.174	0.75	203.9	0.00370	0.463	0.29	0.040	0.58	203.9	0.00283	0.137
-5.250	-4.750	6.750	7.250	1.74	1.0	0.26	0.092	0.52	207.8	0.00248	0.355	0.21	0.019	0.42	207.8	0.00204	0.091
-5.250	-4.750	6.750	7.250	1.78	1.0	0.28	0.108	0.56	212.9	0.00261	0.384	0.22	0.014	0.45	212.9	0.00214	0.060
-5.250	-4.750	6.750	7.250	1.82	1.0	0.39	0.132	0.78	218.0	0.00358	0.338	0.33	0.029	0.66	218.0	0.00305	0.087
-5.250	-4.750	6.750	7.250	1.85	1.0	0.29	0.065	0.58	221.8	0.00259	0.224	0.25	0.034	0.51	221.8	0.00232	0.134
-5.250	-4.750	6.750	7.250	1.89	1.0	0.22	0.083	0.45	226.9	0.00198	0.367	0.19	0.033	0.38	226.9	0.00168	0.173
-5.250	-4.750	6.750	7.250	1.93	1.0	0.33	0.138	0.66	232.0	0.00283	0.419	0.27	0.055	0.55	232.0	0.00236	0.201
-5.250	-4.750	6.750	7.250	1.98	1.0	0.27	0.049	0.53	238.4	0.00222	0.185	0.24	0.051	0.48	238.4	0.00200	0.211
-5.250	-4.750	6.750	7.250	2.02	1.0	0.24	0.057	0.48	243.5	0.00197	0.236	0.21	0.039	0.43	243.5	0.00175	0.183
-5.250	-4.750	6.750	7.250	2.07	1.0	0.21	0.083	0.43	249.8	0.00174	0.386	0.18	0.026	0.36	249.8	0.00143	0.142
-5.250	-4.750	6.750	7.250	2.12	1.0	0.32	0.093	0.65	256.1	0.00253	0.285	0.28	0.025	0.56	256.1	0.00219	0.088
-5.250	-4.750	6.750	7.250	2.18	1.0	0.24	0.064	0.49	263.7	0.00185	0.263	0.21	0.013	0.42	263.7	0.00161	0.061
-5.250	-4.750	6.750	7.250	2.23	1.0	0.20	0.055	0.39	270.1	0.00145	0.283	0.17	0.014	0.34	270.1	0.00126	0.084
-5.250	-4.750	6.750	7.250	2.29	1.0	0.24	0.025	0.49	277.6	0.00176	0.102	0.22	0.037	0.45	277.6	0.00162	0.166
-5.250	-4.750	6.750	7.250	2.36	1.0	0.28	0.076	0.56	286.5	0.00196	0.271	0.24	0.044	0.49	286.5	0.00172	0.178
-5.250	-4.750	6.750	7.250	2.42	1.0	0.16	0.053	0.33	294.0	0.00111	0.319	0.14	0.031	0.29	294.0	0.00097	0.211
-5.500	-4.500	6.500	7.500	2.49	1.0	0.41	0.045	0.83	302.8	0.00274	0.109	0.38	0.066	0.75	302.8	0.00249	0.176
-5.500	-4.500	6.500	7.500	2.57	1.0	0.39	0.088	0.79	312.9	0.00253	0.224	0.36	0.060	0.72	312.9	0.00229	0.167
-5.500	-4.500	6.500	7.500	2.65	1.0	0.39	0.092	0.79	322.9	0.00244	0.232	0.36	0.054	0.71	322.9	0.00220	0.152
-5.500	-4.500	6.500	7.500	2.73	1.0	0.38	0.023	0.76	333.0	0.00228	0.060	0.32	0.040	0.64	333.0	0.00193	0.124
-5.500	-4.500	6.500	7.500	2.83	1.0	0.35	0.047	0.70	345.5	0.00202	0.133	0.30	0.032	0.60	345.5	0.00174	0.107
-5.500	-4.500	6.500	7.500	2.92	1.0	0.39	0.043	0.78	356.8	0.00218	0.110	0.34	0.044	0.68	356.8	0.00192	0.130
-5.500	-4.500	6.500	7.500	3.03	1.0	0.39	0.053	0.79	370.6	0.00214	0.134	0.32	0.058	0.65	370.6	0.00176	0.178
-5.500	-4.500	6.500	7.500	3.14	1.0	0.31	0.046	0.62	384.3	0.00161	0.148	0.28	0.061	0.56	384.3	0.00145	0.219
-5.500	-4.500	6.500	7.500	3.27	1.0	0.38	0.066	0.76	400.6	0.00190	0.173	0.32	0.062	0.64	400.6	0.00161	0.194

TABLE 2b

Monochromatic wave reflection results CERC 150x3x3 ft wave tank.

Date(s)	Depth (cm)	No.of ripples	Ripple Amplitude (cm)	Amplitude / filter / Depth ratio	No Filter	Beach slope	Water temperature (deg C)
12/8/81	h=15.6	m= 4	b=5	b/h=0.32	NF	1:10	23.0

Gauge positions(x) (m)				Wave period	Stroke	Wave reflection results from Gauges 1 & 2						Wave reflection results from Gauges 3 & 4					
1	2	3	4	T (s)	S (cm)	a_I (cm)	a_R (cm)	H_I (cm)	λ_w (cm)	H_I/λ_w	K_R	a_I (cm)	a_R (cm)	H_I (cm)	λ_w (cm)	H_I/λ_w	K_B
-5.125	-4.875	8.875	9.125	0.78	1.0	0.76	0.144	1.52	79.9	0.01901	0.190	0.64	0.072	1.28	79.9	0.01608	0.112
-5.125	-4.875	8.875	9.125	0.79	1.0	0.72	0.106	1.44	81.4	0.01767	0.147	0.63	0.149	1.25	81.4	0.01534	0.238
-5.125	-4.875	8.875	9.125	0.80	1.0	0.73	0.085	1.47	82.8	0.01772	0.116	0.66	0.043	1.33	82.8	0.01611	0.064
-5.125	-4.875	8.875	9.125	0.81	1.0	0.77	0.063	1.53	84.2	0.01819	0.082	0.69	0.142	1.37	84.2	0.01623	0.207
-5.125	-4.875	8.875	9.125	0.82	1.0	0.72	0.099	1.43	85.7	0.01675	0.138	0.59	0.092	1.18	85.7	0.01381	0.156
-5.125	-4.875	8.875	9.125	0.83	1.0	0.79	0.147	1.58	87.1	0.01811	0.186	0.64	0.034	1.28	87.1	0.01473	0.053
-5.125	-4.875	8.875	9.125	0.84	1.0	0.76	0.106	1.52	88.5	0.01714	0.139	0.69	0.146	1.38	88.5	0.01560	0.211
-5.125	-4.875	8.875	9.125	0.85	1.0	0.73	0.163	1.47	89.9	0.01637	0.222	0.64	0.116	1.28	89.9	0.01425	0.181
-5.125	-4.875	8.875	9.125	0.86	1.0	0.73	0.115	1.45	91.3	0.01585	0.159	0.62	0.029	1.24	91.3	0.01354	0.047
-5.125	-4.875	8.875	9.125	0.87	1.0	0.76	0.089	1.51	92.7	0.01626	0.118	0.65	0.106	1.29	92.7	0.01396	0.164
-5.125	-4.875	8.875	9.125	0.88	1.0	0.70	0.055	1.40	94.1	0.01491	0.079	0.60	0.118	1.21	94.1	0.01286	0.195
-5.125	-4.875	8.875	9.125	0.89	1.0	0.76	0.160	1.52	95.5	0.01587	0.210	0.64	0.047	1.28	95.5	0.01339	0.073
-5.125	-4.875	8.875	9.125	0.90	1.0	0.68	0.156	1.36	96.9	0.01405	0.230	0.58	0.075	1.15	96.9	0.01188	0.131
-5.125	-4.875	8.875	9.125	0.91	1.0	0.68	0.061	1.36	98.3	0.01385	0.090	0.58	0.116	1.16	98.3	0.01181	0.200
-5.125	-4.875	8.875	9.125	0.92	1.0	0.69	0.101	1.37	99.7	0.01373	0.148	0.58	0.092	1.15	99.7	0.01152	0.160
-5.125	-4.875	8.875	9.125	0.93	1.0	0.70	0.124	1.39	101.1	0.01377	0.178	0.59	0.039	1.17	101.1	0.01155	0.067
-5.125	-4.875	8.875	9.125	0.94	1.0	0.63	0.042	1.25	102.5	0.01217	0.068	0.53	0.058	1.06	102.5	0.01035	0.110
-5.125	-4.875	8.875	9.125	0.95	1.0	0.66	0.099	1.32	103.8	0.01272	0.150	0.55	0.095	1.11	103.8	0.01073	0.172
-5.125	-4.875	8.875	9.125	0.96	1.0	0.63	0.088	1.27	105.2	0.01212	0.139	0.54	0.096	1.08	105.2	0.01027	0.177
-5.125	-4.875	8.875	9.125	0.97	1.0	0.66	0.144	1.31	106.6	0.01232	0.220	0.55	0.077	1.11	106.6	0.01046	0.139
-5.125	-4.875	8.875	9.125	0.98	1.0	0.66	0.122	1.31	108.0	0.01212	0.187	0.55	0.052	1.11	108.0	0.01032	0.093
-5.125	-4.875	8.875	9.125	0.99	1.0	0.59	0.114	1.18	109.3	0.01081	0.194	0.51	0.055	1.01	109.3	0.00928	0.108
-5.125	-4.875	8.875	9.125	1.00	1.0	0.66	0.041	1.33	110.7	0.01199	0.061	0.58	0.093	1.16	110.7	0.01046	0.160
-5.125	-4.875	8.875	9.125	1.01	1.0	0.64	0.055	1.28	112.1	0.01143	0.086	0.56	0.100	1.12	112.1	0.01001	0.178
-5.125	-4.875	8.875	9.125	1.02	1.0	0.59	0.094	1.17	113.4	0.01032	0.161	0.50	0.078	1.00	113.4	0.00881	0.157
-5.125	-4.875	8.875	9.125	1.03	1.0	0.64	0.120	1.28	114.8	0.01115	0.188	0.55	0.052	1.09	114.8	0.00952	0.096
-5.125	-4.875	8.875	9.125	1.04	1.0	0.62	0.077	1.24	116.2	0.01064	0.125	0.53	0.039	1.06	116.2	0.00910	0.073
-5.125	-4.875	8.875	9.125	1.05	1.0	0.63	0.121	1.27	117.5	0.01079	0.191	0.55	0.075	1.09	117.5	0.00930	0.137
-5.125	-4.875	8.875	9.125	1.06	1.0	0.63	0.085	1.27	118.9	0.01072	0.134	0.55	0.107	1.11	118.9	0.00933	0.192
-5.125	-4.875	8.875	9.125	1.07	1.0	0.59	0.151	1.18	120.2	0.00984	0.256	0.51	0.103	1.01	120.2	0.00838	0.204
-5.125	-4.875	8.875	9.125	1.08	1.0	0.66	0.121	1.31	121.6	0.01081	0.185	0.57	0.095	1.14	121.6	0.00395	0.166
-5.125	-4.875	8.875	9.125	1.09	1.0	0.66	0.131	1.32	122.9	0.01077	0.199	0.56	0.049	1.12	122.9	0.00910	0.087
-5.125	-4.875	8.875	9.125	1.10	1.0	0.57	0.118	1.14	124.3	0.00921	0.207	0.49	0.022	0.98	124.3	0.00789	0.044
-5.125	-4.875	8.875	9.125	1.11	1.0	0.58	0.010	1.15	125.6	0.00919	0.017	0.50	0.065	1.00	125.6	0.00795	0.131
-5.125	-4.875	8.875	9.125	1.12	1.0	0.65	0.088	1.29	126.9	0.01019	0.137	0.56	0.117	1.12	126.9	0.00880	0.209
-5.125	-4.875	8.875	9.125	1.13	1.0	0.67	0.037	1.34	128.3	0.01049	0.055	0.59	0.143	1.19	128.3	0.00925	0.240
-5.125	-4.875	8.875	9.125	1.14	1.0	0.60	0.106	1.21	129.6	0.00936	0.176	0.52	0.121	1.03	129.6	0.00794	0.235
-5.125	-4.875	8.875	9.125	1.15	1.0	0.63	0.139	1.26	131.0	0.00960	0.220	0.53	0.099	1.06	131.0	0.00808	0.186
-5.125	-4.875	8.875	9.125	1.16	1.0	0.60	0.062	1.20	132.3	0.00909	0.103	0.52	0.058	1.04	132.3	0.00785	0.111
-5.125	-4.875	8.875	9.125	1.17	1.0	0.60	0.093	1.21	133.6	0.00908	0.154	0.52	0.027	1.03	133.6	0.00771	0.053
-5.125	-4.875	8.875	9.125	1.18	1.0	0.60	0.107	1.20	135.0	0.00888	0.179	0.51	0.058	1.02	135.0	0.00758	0.114
-5.125	-4.875	8.875	9.125	1.19	1.0	0.63	0.069	1.26	136.3	0.00928	0.109	0.55	0.101	1.09	136.3	0.00804	0.185
-5.125	-4.875	8.875	9.125	1.20	1.0	0.62	0.148	1.23	137.6	0.00896	0.240	0.52	0.120	1.04	137.6	0.00758	0.231
-5.125	-4.875	8.875	9.125	1.21	1.0	0.55	0.154	1.11	138.9	0.00800	0.278	0.47	0.115	0.94	138.9	0.00674	0.244
-5.125	-4.875	8.875	9.125	1.22	1.0	0.62	0.107	1.23	140.3	0.00877	0.174	0.52	0.115	1.05	140.3	0.00745	0.219
-5.125	-4.875	8.875	9.125	1.23	1.0	0.62	0.122	1.24	141.6	0.00875	0.196	0.52	0.089	1.04	141.6	0.00738	0.171
-5.125	-4.875	8.875	9.125	1.24	1.0	0.66	0.162	1.32	142.9	0.00925	0.245	0.55	0.062	1.11	142.9	0.00774	0.111
-5.125	-4.875	8.875	9.125	1.25	1.0	0.52	0.096	1.03	144.2	0.00716	0.187	0.43	0.022	0.86	144.2	0.00598	0.051
-5.125	-4.875	8.875	9.125	1.26	1.0	0.48	0.044	0.97	145.6	0.00670	0.090	0.41	0.048	0.82	145.6	0.00561	0.118
-5.125	-4.875	8.875	9.125	1.27	1.0	0.55	0.059	1.11	146.9	0.00754	0.107	0.47	0.096	0.94	146.9	0.00643	0.205

TABLE 2b

Monochromatic wave reflection results CERC 150x3x3 ft wave tank.

Date(s)	Depth (cm)	No.of ripples	Ripple Amplitude (cm)	Amplitude / filter / Depth ratio	No Filter	Beach slope	Water temperature (deg C)
12/8/81	h=15.6	m= 4	b=5	b/h=0.32	NF	1:10	23.0

Gauge positions(x) (m)				Wave period	Stroke	Wave reflection results from Gauges 1 & 2						Wave reflection results from Gauges 3 & 4					
1	2	3	4	T (s)	S (cm)	a_I (cm)	a_R (cm)	H_I (cm)	λ_w (cm)	H_I/λ_w	$\lvert K_R \rvert$	a_I (cm)	a_R (cm)	H_I (cm)	λ_w (cm)	H_I/λ_w	K_B
-5.125	-4.875	8.875	9.125	1.28	1.0	0.58	0.041	1.16	148.2	0.00785	0.071	0.50	0.122	1.00	148.2	0.00675	0.245
-5.125	-4.875	8.875	9.125	1.29	1.0	0.71	0.139	1.42	149.5	0.00952	0.196	0.59	0.159	1.17	149.5	0.00784	0.271
-5.250	-4.750	8.750	9.250	1.30	1.0	0.58	0.191	1.15	150.8	0.00761	0.332	0.50	0.124	0.99	150.8	0.00656	0.251
-5.250	-4.750	8.750	9.250	1.31	1.0	0.49	0.178	0.98	152.1	0.00647	0.364	0.43	0.097	0.85	152.1	0.00560	0.228
-5.250	-4.750	8.750	9.250	1.32	1.0	0.52	0.150	1.04	153.4	0.00676	0.289	0.46	0.086	0.93	153.4	0.00608	0.184
-5.250	-4.750	8.750	9.250	1.33	1.0	0.55	0.119	1.10	154.8	0.00713	0.216	0.50	0.060	1.00	154.8	0.00647	0.120
-5.250	-4.750	8.750	9.250	1.34	1.0	0.59	0.143	1.17	156.1	0.00747	0.244	0.53	0.040	1.06	156.1	0.00678	0.076
-5.250	-4.750	8.750	9.250	1.35	1.0	0.58	0.139	1.16	157.4	0.00735	0.239	0.53	0.048	1.06	157.4	0.00677	0.090
-5.250	-4.750	8.750	9.250	1.36	1.0	0.50	0.077	1.00	158.7	0.00633	0.155	0.47	0.062	0.94	158.7	0.00591	0.131
-5.250	-4.750	8.750	9.250	1.37	1.0	0.50	0.025	0.99	160.0	0.00622	0.051	0.46	0.080	0.93	160.0	0.00584	0.171
-5.250	-4.750	8.750	9.250	1.38	1.0	0.54	0.092	1.08	161.3	0.00670	0.170	0.50	0.104	0.99	161.3	0.00613	0.210
-5.250	-4.750	8.750	9.250	1.39	1.0	0.50	0.108	0.99	162.6	0.00609	0.219	0.45	0.103	0.91	162.6	0.00558	0.227
-5.250	-4.750	8.750	9.250	1.40	1.0	0.47	0.084	0.94	163.9	0.00575	0.178	0.43	0.101	0.87	163.9	0.00533	0.232
-5.250	-4.750	8.750	9.250	1.41	1.0	0.50	0.049	0.99	165.2	0.00600	0.100	0.46	0.101	0.92	165.2	0.00556	0.219
-5.250	-4.750	8.750	9.250	1.42	1.0	0.48	0.075	0.97	166.5	0.00586	0.155	0.45	0.084	0.90	166.5	0.00538	0.186
-5.250	-4.750	8.750	9.250	1.43	1.0	0.50	0.115	0.99	167.8	0.00591	0.232	0.45	0.067	0.90	167.8	0.00534	0.150
-5.250	-4.750	8.750	9.250	1.44	1.0	0.58	0.161	1.16	169.1	0.00686	0.277	0.52	0.054	1.04	169.1	0.00613	0.104
-5.250	-4.750	8.750	9.250	1.45	1.0	0.52	0.149	1.03	170.4	0.00608	0.290	0.45	0.020	0.90	170.4	0.00528	0.045
-5.250	-4.750	8.750	9.250	1.47	1.0	0.36	0.116	0.73	173.0	0.00419	0.318	0.28	0.071	0.56	173.0	0.00324	0.254
-5.250	-4.750	8.750	9.250	1.48	1.0	0.37	0.107	0.74	174.3	0.00422	0.289	0.30	0.032	0.61	174.3	0.00353	0.106
-5.250	-4.750	8.750	9.250	1.49	1.0	0.41	0.129	0.83	175.6	0.00471	0.311	0.34	0.049	0.69	175.6	0.00393	0.141
-5.250	-4.750	8.750	9.250	1.50	1.0	0.49	0.193	0.98	176.9	0.00556	0.394	0.39	0.065	0.77	176.9	0.00438	0.169
-5.250	-4.750	8.750	9.250	1.51	1.0	0.68	0.342	1.36	178.2	0.00764	0.503	0.50	0.094	1.00	178.2	0.00559	0.187
-5.250	-4.750	8.750	9.250	1.53	1.0	0.50	0.307	0.99	180.8	0.00547	0.621	0.33	0.062	0.66	180.8	0.00366	0.187
-5.250	-4.750	8.750	9.250	1.54	1.0	0.35	0.218	0.70	182.1	0.00384	0.622	0.23	0.039	0.47	182.1	0.00258	0.165
-5.250	-4.750	8.750	9.250	1.55	1.0	0.32	0.203	0.65	183.4	0.00352	0.624	0.22	0.032	0.45	183.4	0.00246	0.144
-5.250	-4.750	8.750	9.250	1.56	1.0	0.32	0.197	0.63	184.7	0.00340	0.624	0.22	0.025	0.45	184.7	0.00243	0.111
-5.250	-4.750	8.750	9.250	1.58	1.0	0.36	0.246	0.72	187.2	0.00382	0.684	0.24	0.012	0.49	187.2	0.00355	0.051
-5.250	-4.750	8.750	9.250	1.59	1.0	0.48	0.348	0.96	188.5	0.00508	0.724	0.31	0.014	0.62	188.5	0.00331	0.044
-5.250	-4.750	8.750	9.250	1.61	1.0	0.59	0.427	1.18	191.1	0.00618	0.724	0.38	0.043	0.76	191.1	0.00399	0.113
-5.250	-4.750	8.750	9.250	1.62	1.0	0.38	0.260	0.75	192.4	0.00391	0.692	0.24	0.036	0.49	192.4	0.00256	0.146
-5.250	-4.750	8.750	9.250	1.63	1.0	0.29	0.183	0.57	193.7	0.00294	0.642	0.20	0.035	0.39	193.7	0.00200	0.180
-5.250	-4.750	8.750	9.250	1.65	1.0	0.25	0.129	0.50	196.2	0.00256	0.516	0.19	0.041	0.37	196.2	0.00188	0.222
-5.250	-4.750	8.750	9.250	1.66	1.0	0.26	0.123	0.52	197.5	0.00264	0.474	0.19	0.045	0.38	197.5	0.00194	0.238
-5.250	-4.750	8.750	9.250	1.68	1.0	0.34	0.171	0.69	200.1	0.00343	0.497	0.22	0.058	0.45	200.1	0.00227	0.257
-5.250	-4.750	8.750	9.250	1.70	1.0	0.73	0.418	1.46	202.7	0.00720	0.572	0.40	0.110	0.80	202.7	0.00395	0.275
-5.250	-4.750	8.750	9.250	1.71	1.0	0.70	0.426	1.41	203.9	0.00690	0.604	0.36	0.097	0.72	203.9	0.00355	0.270
-5.250	-4.750	8.750	9.250	1.73	1.0	0.38	0.243	0.76	206.5	0.00368	0.640	0.20	0.042	0.40	206.5	0.00192	0.210
-5.250	-4.750	8.750	9.250	1.74	1.0	0.30	0.197	0.60	207.8	0.00290	0.655	0.16	0.030	0.32	207.8	0.00155	0.186
-5.250	-4.750	8.750	9.250	1.76	1.0	0.24	0.158	0.48	210.4	0.00228	0.658	0.14	0.018	0.28	210.4	0.00133	0.129
-5.250	-4.750	8.750	9.250	1.78	1.0	0.26	0.175	0.52	212.9	0.00243	0.673	0.15	0.015	0.31	212.9	0.00148	0.094
-5.250	-4.750	8.750	9.250	1.80	1.0	0.34	0.233	0.69	215.5	0.00318	0.676	0.21	0.021	0.43	215.5	0.00198	0.097
-5.250	-4.750	8.750	9.250	1.82	1.0	0.55	0.362	1.09	218.0	0.00500	0.664	0.38	0.052	0.75	218.0	0.00344	0.138
-5.250	-4.750	8.750	9.250	1.83	1.0	0.52	0.337	1.03	219.3	0.00468	0.655	0.36	0.058	0.72	219.3	0.00330	0.161
-5.250	-4.750	8.750	9.250	1.85	1.0	0.29	0.168	0.58	221.8	0.00260	0.580	0.21	0.043	0.43	221.8	0.00195	0.202
-5.250	-4.750	8.750	9.250	1.87	1.0	0.23	0.111	0.46	224.4	0.00205	0.482	0.19	0.043	0.37	224.4	0.00164	0.234
-5.250	-4.750	8.750	9.250	1.89	1.0	0.22	0.089	0.45	226.9	0.00198	0.395	0.19	0.049	0.37	226.9	0.00164	0.263
-5.250	-4.750	8.750	9.250	1.91	1.0	0.23	0.090	0.46	229.5	0.00202	0.390	0.19	0.051	0.37	229.5	0.00162	0.276
-5.250	-4.750	8.750	9.250	1.93	1.0	0.30	0.125	0.61	232.0	0.00261	0.411	0.22	0.062	0.45	232.0	0.00195	0.276
-5.250	-4.750	8.750	9.250	1.96	1.0	0.49	0.207	0.98	235.8	0.00415	0.423	0.34	0.085	0.67	235.8	0.00283	0.254

TABLE 2b

Monochromatic wave reflection results CERC 150x3x3 ft wave tank.

Date(s)	Depth (cm)	No.of ripples	Ripple Amplitude (cm)	Amplitude / filter / Depth ratio	No Filter	Beach slope	Water temperature (deg C)
12/8/81	h=15.6	m= 4	b=5	b/h=0.32	NF	1:10	23.0

Gauge positions(x) (m)				Wave period	Stroke	Wave reflection results from Gauges 1 & 2						Wave reflection results from Gauges 3 & 4					
1	2	3	4	T (s)	S (cm)	a_I (cm)	a_R (cm)	H_I (cm)	λ_w (cm)	H_I/λ_w	K_R	a_I (cm)	a_R (cm)	H_I (cm)	λ_w (cm)	H_I/λ_w	K_B
-5.250	-4.750	8.750	9.250	1.98	1.0	0.30	0.138	0.61	238.4	0.00258	0.453	0.21	0.047	0.41	238.4	0.00173	0.229
-5.250	-4.750	8.750	9.250	2.00	1.0	0.24	0.107	0.49	240.9	0.00205	0.436	0.18	0.033	0.35	240.9	0.00145	0.190
-5.250	-4.750	8.750	9.250	2.02	1.0	0.23	0.086	0.46	243.5	0.00189	0.375	0.18	0.028	0.36	243.5	0.00146	0.155
-5.250	-4.750	8.750	9.250	2.05	1.0	0.25	0.070	0.50	247.3	0.00202	0.279	0.21	0.021	0.42	247.3	0.00168	0.099
-5.250	-4.750	8.750	9.250	2.07	1.0	0.26	0.081	0.52	249.8	0.00210	0.311	0.21	0.016	0.43	249.8	0.00173	0.075
-5.250	-4.750	8.750	9.250	2.10	1.0	0.32	0.127	0.65	253.6	0.00255	0.391	0.27	0.031	0.54	253.6	0.00212	0.114
-5.250	-4.750	8.750	9.250	2.12	1.0	0.35	0.133	0.70	256.1	0.00275	0.380	0.30	0.036	0.59	256.1	0.00230	0.123
-5.250	-4.750	8.750	9.250	2.15	1.0	0.27	0.074	0.54	259.9	0.00206	0.275	0.23	0.037	0.47	259.9	0.00180	0.159
-5.250	-4.750	8.750	9.250	2.18	1.0	0.24	0.035	0.48	263.7	0.00184	0.145	0.21	0.038	0.43	263.7	0.00163	0.179
-5.250	-4.750	8.750	9.250	2.20	1.0	0.25	0.033	0.51	266.3	0.00190	0.130	0.22	0.041	0.45	266.3	0.00167	0.182
-5.250	-4.750	8.750	9.250	2.23	1.0	0.24	0.037	0.48	270.1	0.00179	0.154	0.21	0.039	0.42	270.1	0.00156	0.184
-5.250	-4.750	8.750	9.250	2.26	1.0	0.25	0.024	0.50	273.8	0.00183	0.097	0.21	0.034	0.43	273.8	0.00158	0.158
-5.250	-4.750	8.750	9.250	2.29	1.0	0.27	0.021	0.55	277.6	0.00199	0.076	0.23	0.027	0.47	277.6	0.00170	0.113
-5.250	-4.750	8.750	9.250	2.32	1.0	0.23	0.049	0.46	281.4	0.00163	0.211	0.20	0.016	0.39	281.4	0.00137	0.083
-5.250	-4.750	8.750	9.250	2.36	1.0	0.23	0.072	0.47	286.5	0.00163	0.307	0.20	0.017	0.40	286.5	0.00139	0.084
-5.250	-4.750	8.750	9.250	2.39	1.0	0.29	0.079	0.58	290.2	0.00201	0.273	0.25	0.031	0.51	290.2	0.00176	0.121
-5.250	-4.750	8.750	9.250	2.42	1.0	0.24	0.048	0.48	294.0	0.00165	0.201	0.21	0.038	0.43	294.0	0.00145	0.179
-5.250	-4.750	8.750	9.250	2.46	1.0	0.20	0.015	0.40	299.1	0.00133	0.074	0.18	0.041	0.35	299.1	0.00117	0.237
-5.500	-4.500	8.500	9.500	2.49	1.0	0.41	0.052	0.82	302.8	0.00272	0.128	0.41	0.110	0.83	302.8	0.00275	0.265
-5.500	-4.500	8.500	9.500	2.53	1.0	0.37	0.045	0.74	307.9	0.00241	0.122	0.38	0.106	0.75	307.9	0.00245	0.283
-5.500	-4.500	8.500	9.500	2.57	1.0	0.34	0.056	0.68	312.9	0.00217	0.164	0.33	0.094	0.66	312.9	0.00212	0.286
-5.500	-4.500	8.500	9.500	2.61	1.0	0.44	0.113	0.88	317.9	0.00277	0.257	0.38	0.103	0.76	317.9	0.00238	0.272
-5.500	-4.500	8.500	9.500	2.65	1.0	0.50	0.154	1.00	322.9	0.00308	0.308	0.44	0.098	0.88	322.9	0.00273	0.222
-5.500	-4.500	8.500	9.500	2.69	1.0	0.41	0.114	0.82	328.0	0.00251	0.278	0.36	0.067	0.71	328.0	0.00216	0.190
-5.500	-4.500	8.500	9.500	2.73	1.0	0.38	0.070	0.76	333.0	0.00229	0.183	0.34	0.045	0.68	333.0	0.00204	0.133
-5.500	-4.500	8.500	9.500	2.78	1.0	0.39	0.073	0.79	339.2	0.00232	0.186	0.34	0.008	0.68	339.2	0.00200	0.025
-5.500	-4.500	8.500	9.500	2.83	1.0	0.35	0.100	0.70	345.5	0.00201	0.285	0.30	0.014	0.60	345.5	0.00174	0.048
-5.500	-4.500	8.500	9.500	2.87	1.0	0.36	0.110	0.72	350.5	0.00206	0.305	0.31	0.041	0.62	350.5	0.00178	0.131
-5.500	-4.500	8.500	9.500	2.92	1.0	0.45	0.083	0.89	356.8	0.00249	0.186	0.37	0.070	0.74	356.8	0.00206	0.189
-5.500	-4.500	8.500	9.500	2.98	1.0	0.37	0.023	0.74	364.3	0.00202	0.062	0.34	0.084	0.67	364.3	0.00183	0.251
-5.500	-4.500	8.500	9.500	3.03	1.0	0.36	0.061	0.71	370.6	0.00193	0.171	0.29	0.079	0.57	370.6	0.00153	0.278
-5.500	-4.500	8.500	9.500	3.09	1.0	0.43	0.101	0.86	378.1	0.00228	0.235	0.36	0.105	0.71	378.1	0.00188	0.296
-5.500	-4.500	8.500	9.500	3.14	1.0	0.36	0.079	0.71	384.3	0.00184	0.223	0.31	0.089	0.62	384.3	0.00161	0.287
-5.500	-4.500	8.500	9.500	3.20	1.0	0.30	0.026	0.61	391.8	0.00157	0.084	0.25	0.071	0.50	391.8	0.00128	0.283
-5.500	-4.500	8.500	9.500	3.27	1.0	0.41	0.062	0.83	400.6	0.00207	0.150	0.34	0.075	0.67	400.6	0.00167	0.223

TABLE 2c

Monochromatic wave reflection results CERC 150x3x3 ft wave tank.

Date(s)	Depth (cm)	No.of ripples	Ripple Amplitude (cm)	Amplitude / Depth ratio	filter / No Filter	Beach slope	Water temperature (deg C)
21/7/81-23/7/81	h=31.3	m=10	b=5	b/h=0.16	NF	1:10	23.2

Gauge positions(x) (m)				Wave period	Stroke	Wave reflection results from Gauges 1 & 2						Wave reflection results from Gauges 3 & 4					
1	2	3	4	T (s)	S (cm)	a_I (cm)	a_R (cm)	H_I (cm)	λ_w (cm)	H_I/λ_w	$\|K_R\|$	a_I (cm)	a_R (cm)	H_I (cm)	λ_w (cm)	H_I/λ_w	K_B
-5.125	-4.875	14.875	15.125	0.72	1.0	1.57	0.060	3.14	79.8	0.03938	0.038	1.53	0.095	3.05	79.8	0.03825	0.062
-5.125	-4.875	14.875	15.125	0.73	1.0	1.61	0.016	3.21	81.9	0.03921	0.010	1.53	0.120	3.05	81.9	0.03733	0.079
-5.125	-4.875	14.875	15.125	0.74	1.0	1.64	0.051	3.28	83.9	0.03911	0.031	1.41	0.038	2.81	83.9	0.03348	0.027
-5.125	-4.875	14.875	15.125	0.75	1.0	1.66	0.066	3.31	86.0	0.03852	0.040	1.44	0.065	2.89	86.0	0.03363	0.045
-5.125	-4.875	14.875	15.125	0.76	1.0	1.46	0.044	2.92	88.1	0.03319	0.030	1.28	0.050	2.57	88.1	0.02922	0.039
-5.125	-4.875	14.875	15.125	0.77	1.0	1.50	0.048	2.99	90.2	0.03313	0.032	1.33	0.048	2.67	90.2	0.02965	0.036
-5.125	-4.875	14.875	15.125	0.78	1.0	1.65	0.030	3.30	92.3	0.03575	0.018	1.44	0.030	2.87	92.3	0.03110	0.021
-5.125	-4.875	14.875	15.125	0.79	1.0	1.64	0.036	3.28	94.5	0.03475	0.022	1.47	0.040	2.93	94.5	0.03100	0.027
-5.125	-4.875	14.875	15.125	0.80	1.0	1.64	0.023	3.28	96.6	0.03402	0.014	1.47	0.062	2.93	96.6	0.03037	0.042
-5.125	-4.875	14.875	15.125	0.81	1.0	1.61	0.027	3.21	98.7	0.03258	0.017	1.45	0.065	2.91	98.7	0.02951	0.045
-5.125	-4.875	14.875	15.125	0.82	1.0	1.64	0.051	3.27	100.8	0.03242	0.031	1.47	0.057	2.93	100.8	0.02905	0.039
-5.125	-4.875	14.875	15.125	0.83	1.0	1.53	0.069	3.06	102.9	0.02971	0.045	1.89	0.055	3.78	102.9	0.02705	0.029
-5.125	-4.875	14.875	15.125	0.84	1.0	1.58	0.022	3.17	105.1	0.03018	0.014	1.43	0.033	2.86	105.1	0.02720	0.023
-5.125	-4.875	14.875	15.125	0.85	1.0	1.58	0.024	3.15	107.2	0.02939	0.015	1.42	0.030	2.84	107.2	0.02649	0.021
-5.125	-4.875	14.875	15.125	0.86	1.0	1.61	0.060	3.22	109.3	0.02950	0.037	1.45	0.036	2.91	109.3	0.02661	0.025
-5.125	-4.875	14.875	15.125	0.87	1.0	1.58	0.027	3.15	111.4	0.02825	0.017	1.42	0.031	2.84	111.4	0.02551	0.022
-5.125	-4.875	14.875	15.125	0.88	1.0	1.60	0.032	3.20	113.6	0.02842	0.020	1.45	0.035	2.91	113.6	0.02561	0.024
-5.125	-4.875	14.875	15.125	0.89	1.0	1.56	0.033	3.12	115.7	0.02702	0.021	1.41	0.041	2.82	115.7	0.02442	0.029
-5.125	-4.875	14.875	15.125	0.90	1.0	1.58	0.058	3.15	117.8	0.02679	0.037	1.42	0.056	2.85	117.8	0.02425	0.039
-5.125	-4.875	14.875	15.125	0.91	1.0	1.55	0.062	3.10	119.9	0.02590	0.040	1.41	0.065	2.81	119.9	0.02344	0.046
-5.125	-4.875	14.875	15.125	0.92	1.0	1.55	0.028	3.09	122.0	0.02533	0.018	1.40	0.069	2.80	122.0	0.02297	0.049
-5.125	-4.875	14.875	15.125	0.93	1.0	1.61	0.074	3.21	124.1	0.02584	0.046	1.45	0.065	2.91	124.1	0.02342	0.045
-5.125	-4.875	14.875	15.125	0.94	1.0	1.50	0.048	3.01	126.2	0.02382	0.032	1.36	0.061	2.73	126.2	0.02165	0.045
-5.125	-4.875	14.875	15.125	0.95	1.0	1.42	0.084	2.84	128.3	0.02218	0.059	1.30	0.049	2.59	128.3	0.02021	0.038
-5.125	-4.875	14.875	15.125	0.96	1.0	1.51	0.059	3.02	130.4	0.02314	0.039	1.37	0.034	2.74	130.4	0.02105	0.025
-5.125	-4.875	14.875	15.125	0.97	1.0	1.50	0.018	3.00	132.5	0.02267	0.012	1.37	0.032	2.74	132.5	0.02069	0.023
-5.125	-4.875	14.875	15.125	0.98	1.0	1.52	0.047	3.03	134.6	0.02249	0.031	1.39	0.040	2.78	134.6	0.02066	0.029
-5.125	-4.875	14.875	15.125	0.99	1.0	1.54	0.059	3.08	136.7	0.02252	0.038	1.42	0.030	2.83	136.7	0.02071	0.021
-5.125	-4.875	14.875	15.125	1.00	1.0	1.44	0.114	2.88	138.8	0.02076	0.079	1.33	0.036	2.65	138.8	0.01911	0.027
-5.125	-4.875	14.875	15.125	1.01	1.0	1.47	0.074	2.95	140.9	0.02098	0.050	1.36	0.043	2.71	140.9	0.01928	0.032
-5.125	-4.875	14.875	15.125	1.02	1.0	1.53	0.057	3.07	142.9	0.02152	0.037	1.41	0.045	2.82	142.9	0.01976	0.032
-5.125	-4.875	14.875	15.125	1.03	1.0	1.44	0.047	2.87	145.0	0.01978	0.033	1.30	0.056	2.59	145.0	0.01784	0.043
-5.125	-4.875	14.875	15.125	1.04	1.0	1.43	0.033	2.86	147.1	0.01946	0.023	1.31	0.052	2.61	147.1	0.01773	0.040
-5.125	-4.875	14.875	15.125	1.05	1.0	1.39	0.104	2.78	149.1	0.01868	0.075	1.28	0.024	2.57	149.1	0.01721	0.019
-5.250	-4.750	14.750	15.250	1.06	1.0	2.03	0.179	4.06	151.2	0.02684	0.088	1.84	0.048	3.68	151.2	0.02436	0.026
-5.250	-4.750	14.750	15.250	1.07	1.0	1.81	0.134	3.63	153.3	0.02369	0.074	1.65	0.041	3.30	153.3	0.02156	0.025
-5.250	-4.750	14.750	15.250	1.08	1.0	1.86	0.067	3.71	155.3	0.02387	0.036	1.69	0.084	3.37	155.3	0.02172	0.050
-5.250	-4.750	14.750	15.250	1.09	1.0	1.84	0.074	3.69	157.3	0.02349	0.040	1.68	0.074	3.36	157.3	0.02136	0.044
-5.250	-4.750	14.750	15.250	1.10	1.0	1.90	0.122	3.80	159.4	0.02388	0.064	1.73	0.114	3.46	159.4	0.02174	0.066
-5.250	-4.750	14.750	15.250	1.11	1.0	1.97	0.213	3.95	161.4	0.02451	0.108	1.80	0.122	3.59	161.4	0.02227	0.068
-5.250	-4.750	14.750	15.250	1.12	1.0	1.67	0.268	3.35	163.5	0.02053	0.160	1.52	0.117	3.04	163.5	0.01861	0.077
-5.250	-4.750	14.750	15.250	1.13	1.0	1.82	0.257	3.64	165.5	0.02201	0.141	1.66	0.137	3.31	165.5	0.02002	0.083
-5.250	-4.750	14.750	15.250	1.14	1.0	1.91	0.112	3.81	167.5	0.02274	0.059	1.74	0.171	3.48	167.5	0.02076	0.098
-5.250	-4.750	14.750	15.250	1.15	1.0	1.79	0.200	3.58	169.5	0.02116	0.112	1.63	0.158	3.25	169.5	0.01917	0.097
-5.250	-4.750	14.750	15.250	1.16	1.0	2.07	0.371	4.15	171.6	0.02420	0.179	1.86	0.200	3.73	171.6	0.02173	0.107
-5.250	-4.750	14.750	15.250	1.17	1.0	1.62	0.292	3.24	173.6	0.01870	0.180	1.45	0.160	2.90	173.6	0.01674	0.110
-5.250	-4.750	14.750	15.250	1.18	1.0	1.59	0.193	3.19	175.6	0.01819	0.121	1.45	0.172	2.91	175.6	0.01661	0.118
-5.250	-4.750	14.750	15.250	1.19	1.0	1.75	0.194	3.50	177.6	0.01970	0.111	1.58	0.184	3.17	177.6	0.01784	0.116
-5.250	-4.750	14.750	15.250	1.20	1.0	1.98	0.313	3.96	179.6	0.02208	0.158	1.79	0.206	3.58	179.6	0.01994	0.115
-5.250	-4.750	14.750	15.250	1.21	1.0	1.89	0.296	3.79	181.6	0.02089	0.156	1.71	0.202	3.42	181.6	0.01884	0.118

TABLE 2c

Monochromatic wave reflection results CERC 150x3x3 ft wave tank.

Date(s)	Depth (cm)	No.of ripples	Ripple Amplitude (cm)	Amplitude / filter / Depth ratio	No Filter	Beach slope	Water temperature (deg C)
21/7/81-23/7/81	h=31.3	m=10	b=5	b/h=0.16	NF	1:10	23.2

Gauge positions(x) (m)				Wave period	Stroke	Wave reflection results from Gauges 1 & 2						Wave reflection results from Gauges 3 & 4					
1	2	3	4	T (s)	S (cm)	a_I (cm)	a_R (cm)	H_I (cm)	λ_w (cm)	H_I/λ_w	$\lvert K_R \rvert$	a_I (cm)	a_R (cm)	H_I (cm)	λ_w (cm)	H_I/λ_w	K_B
-5.250	-4.750	14.750	15.250	1.22	1.0	1.66	0.116	3.31	183.6	0.01802	0.070	1.51	0.168	3.02	183.6	0.01645	0.111
-5.250	-4.750	14.750	15.250	1.23	1.0	1.88	0.265	3.76	185.6	0.02030	0.141	1.69	0.189	3.38	185.6	0.01825	0.112
-5.250	-4.750	14.750	15.250	1.24	1.0	1.37	0.453	2.74	187.6	0.01460	0.331	1.16	0.128	2.32	187.6	0.01235	0.110
-5.250	-4.750	14.750	15.250	1.25	1.0	1.28	0.593	2.56	189.5	0.01352	0.463	1.02	0.109	2.04	189.5	0.01075	0.107
-5.250	-4.750	14.750	15.250	1.26	1.0	1.97	1.020	3.94	191.5	0.02060	0.518	1.53	0.155	3.06	191.5	0.01597	0.101
-5.250	-4.750	14.750	15.250	1.27	1.0	2.78	1.437	5.55	193.5	0.02871	0.518	2.07	0.203	4.15	193.5	0.02148	0.098
-5.250	-4.750	14.750	15.250	1.28	1.0	1.70	0.870	3.40	195.5	0.01741	0.512	1.28	0.122	2.56	195.5	0.01311	0.095
-5.250	-4.750	14.750	15.250	1.29	1.0	1.18	0.631	2.36	197.4	0.01198	0.535	0.85	0.085	1.71	197.4	0.00867	0.100
-5.250	-4.750	14.750	15.250	1.30	1.0	1.06	0.623	2.12	199.4	0.01064	0.588	0.72	0.066	1.44	199.4	0.00723	0.092
-5.250	-4.750	14.750	15.250	1.31	1.0	1.28	0.776	2.57	201.4	0.01275	0.604	0.80	0.068	1.61	201.4	0.00798	0.085
-5.250	-4.750	14.750	15.250	1.32	1.0	2.51	1.662	5.03	203.3	0.02477	0.661	1.63	0.145	3.26	203.3	0.01603	0.089
-5.250	-4.750	14.750	15.250	1.33	1.0	2.76	1.745	5.53	205.3	0.02693	0.631	1.72	0.131	3.45	205.3	0.01680	0.076
-5.250	-4.750	14.750	15.250	1.34	1.0	1.48	1.045	2.97	207.3	0.01436	0.704	1.08	0.085	2.15	207.3	0.01036	0.079
-5.250	-4.750	14.750	15.250	1.35	1.0	1.05	0.603	2.10	209.2	0.01003	0.574	0.71	0.055	1.42	209.2	0.00679	0.077
-5.250	-4.750	14.750	15.250	1.36	1.0	1.06	0.559	2.12	211.2	0.01006	0.527	0.76	0.055	1.52	211.2	0.00720	0.073
-5.250	-4.750	14.750	15.250	1.37	1.0	1.28	0.605	2.57	213.1	0.01207	0.471	0.97	0.072	1.94	213.1	0.00913	0.074
-5.250	-4.750	14.750	15.250	1.38	1.0	1.75	0.744	3.51	215.1	0.01634	0.424	1.42	0.108	2.83	215.1	0.01316	0.076
-5.250	-4.750	14.750	15.250	1.39	1.0	2.06	0.764	4.13	217.0	0.01904	0.370	1.68	0.119	3.36	217.0	0.01550	0.071
-5.250	-4.750	14.750	15.250	1.40	1.0	1.66	0.528	3.31	218.9	0.01513	0.319	1.39	0.100	2.78	218.9	0.01271	0.072
-5.250	-4.750	14.750	15.250	1.41	1.0	1.28	0.334	2.57	220.9	0.01166	0.260	1.10	0.084	2.20	220.9	0.00997	0.076
-5.250	-4.750	14.750	15.250	1.42	1.0	1.22	0.231	2.44	222.8	0.01097	0.189	1.06	0.075	2.13	222.8	0.00957	0.070
-5.250	-4.750	14.750	15.250	1.43	1.0	1.35	0.161	2.70	224.7	0.01202	0.119	1.19	0.088	2.39	224.7	0.01063	0.074
-5.250	-4.750	14.750	15.250	1.44	1.0	1.47	0.108	2.95	226.7	0.01304	0.073	1.31	0.100	2.62	226.7	0.01157	0.076
-5.250	-4.750	14.750	15.250	1.45	1.0	1.39	0.152	2.79	228.6	0.01221	0.109	1.23	0.086	2.46	228.6	0.01077	0.070
-5.250	-4.750	14.750	15.250	1.46	1.0	1.26	0.204	2.52	230.5	0.01094	0.162	1.11	0.078	2.21	230.5	0.00959	0.071
-5.250	-4.750	14.750	15.250	1.47	1.0	1.25	0.256	2.49	232.5	0.01074	0.206	1.08	0.085	2.15	232.5	0.00924	0.079
-5.250	-4.750	14.750	15.250	1.48	1.0	1.46	0.334	2.92	234.4	0.01248	0.229	1.27	0.092	2.53	234.4	0.01080	0.073
-5.250	-4.750	14.750	15.250	1.49	1.0	1.72	0.394	3.44	236.3	0.01456	0.229	1.48	0.105	2.97	236.3	0.01260	0.071
-5.250	-4.750	14.750	15.250	1.50	1.0	1.56	0.353	3.12	238.2	0.01310	0.226	1.36	0.101	2.73	238.2	0.01147	0.074
-5.250	-4.750	14.750	15.250	1.51	1.0	1.27	0.257	2.54	240.1	0.01059	0.202	1.11	0.088	2.22	240.1	0.00927	0.079
-5.250	-4.750	14.750	15.250	1.52	1.0	1.17	0.191	2.33	242.0	0.00961	0.164	1.03	0.087	2.06	242.0	0.00851	0.084
-5.250	-4.750	14.750	15.250	1.53	1.0	1.19	0.140	2.38	244.0	0.00975	0.118	1.06	0.089	2.11	244.0	0.00864	0.084
-5.250	-4.750	14.750	15.250	1.54	1.0	1.22	0.083	2.45	245.9	0.00998	0.068	1.09	0.090	2.18	245.9	0.00886	0.083
-5.250	-4.750	14.750	15.250	1.55	1.0	1.23	0.038	2.46	247.8	0.00993	0.031	1.09	0.094	2.19	247.8	0.00884	0.086
-5.250	-4.750	14.750	15.250	1.56	1.0	1.22	0.039	2.43	249.7	0.00975	0.032	1.08	0.094	2.16	249.7	0.00867	0.087
-5.250	-4.750	14.750	15.250	1.57	1.0	1.20	0.066	2.41	251.6	0.00957	0.055	1.06	0.088	2.13	251.6	0.00847	0.083
-5.250	-4.750	14.750	15.250	1.58	1.0	1.21	0.080	2.42	253.5	0.00953	0.066	1.06	0.087	2.13	253.5	0.00839	0.082
-5.250	-4.750	14.750	15.250	1.59	1.0	1.24	0.087	2.48	255.4	0.00970	0.070	1.09	0.096	2.18	255.4	0.00853	0.088
-5.250	-4.750	14.750	15.250	1.60	1.0	1.26	0.064	2.52	257.3	0.00981	0.051	1.11	0.095	2.22	257.3	0.00862	0.086
-5.250	-4.750	14.750	15.250	1.61	1.0	1.25	0.056	2.51	259.2	0.00967	0.045	1.10	0.089	2.20	259.2	0.00850	0.081
-5.250	-4.750	14.750	15.250	1.62	1.0	1.26	0.092	2.52	261.1	0.00964	0.073	1.11	0.091	2.21	261.1	0.00846	0.082
-5.250	-4.750	14.750	15.250	1.63	1.0	1.31	0.145	2.63	263.0	0.01000	0.110	1.14	0.092	2.29	263.0	0.00871	0.080
-5.250	-4.750	14.750	15.250	1.64	1.0	1.33	0.194	2.67	264.8	0.01010	0.145	1.16	0.092	2.32	264.8	0.00877	0.079
-5.250	-4.750	14.750	15.250	1.65	1.0	1.25	0.211	2.50	266.7	0.00938	0.169	1.08	0.085	2.15	266.7	0.00807	0.079
-5.250	-4.750	14.750	15.250	1.66	1.0	1.11	0.208	2.22	268.6	0.00826	0.187	0.95	0.082	1.91	268.6	0.00710	0.086
-5.250	-4.750	14.750	15.250	1.67	1.0	1.03	0.200	2.06	270.5	0.00762	0.194	0.88	0.078	1.76	270.5	0.00650	0.089
-5.250	-4.750	14.750	15.250	1.68	1.0	1.03	0.191	2.07	272.4	0.00761	0.185	0.88	0.080	1.77	272.4	0.00650	0.090
-5.250	-4.750	14.750	15.250	1.69	1.0	1.11	0.173	2.21	274.3	0.00805	0.157	0.95	0.077	1.90	274.3	0.00692	0.081
-5.250	-4.750	14.750	15.250	1.70	1.0	1.19	0.148	2.38	276.2	0.00861	0.124	1.03	0.076	2.05	276.2	0.00744	0.074
-5.250	-4.750	14.750	15.250	1.71	1.0	1.22	0.100	2.44	278.0	0.00878	0.082	1.06	0.088	2.12	278.0	0.00762	0.083

TABLE 2c

Monochromatic wave reflection results CERC 150x3x3 ft wave tank.

Date(s)	Depth (cm)	No.of ripples	Ripple Amplitude (cm)	Amplitude / filter / Depth ratio	No Filter	Beach slope	Water temperature (deg C)
21/7/81-23/7/81	h=31.3	m=10	b=5	b/h=0.16	NF	1:10	23.2

Gauge positions(x) (m)				Wave period	Stroke	Wave reflection results from Gauges 1 & 2						Wave reflection results from Gauges 3 & 4					
1	2	3	4	T (s)	S (cm)	a_I (cm)	a_R (cm)	H_I (cm)	λ_w (cm)	H_I/λ_w	$\|K_R\|$	a_I (cm)	a_R (cm)	H_I (cm)	λ_w (cm)	H_I/λ_w	K_B
-5.250	-4.750	14.750	15.250	1.72	1.0	1.19	0.051	2.37	279.9	0.00848	0.043	1.03	0.084	2.07	279.9	0.00738	0.081
-5.250	-4.750	14.750	15.250	1.73	1.0	1.13	0.046	2.26	281.8	0.00803	0.041	0.98	0.072	1.96	281.8	0.00697	0.073
-5.250	-4.750	14.750	15.250	1.74	1.0	1.08	0.078	2.16	283.7	0.00763	0.072	0.94	0.068	1.88	283.7	0.00664	0.072
-5.250	-4.750	14.750	15.250	1.75	1.0	1.08	0.119	2.16	285.5	0.00759	0.110	0.94	0.072	1.88	285.5	0.00658	0.077
-5.250	-4.750	14.750	15.250	1.76	1.0	1.14	0.157	2.28	287.4	0.00794	0.138	0.98	0.090	1.97	287.4	0.00687	0.091
-5.250	-4.750	14.750	15.250	1.77	1.0	1.22	0.180	2.45	289.3	0.00848	0.147	1.06	0.091	2.12	289.3	0.00733	0.086
-5.250	-4.750	14.750	15.250	1.78	1.0	1.26	0.176	2.52	291.2	0.00867	0.140	1.08	0.074	2.17	291.2	0.00747	0.068
-5.250	-4.750	14.750	15.250	1.79	1.0	1.21	0.161	2.42	293.0	0.00826	0.133	1.05	0.069	2.09	293.0	0.00714	0.066
-5.250	-4.750	14.750	15.250	1.80	1.0	1.11	0.147	2.23	294.9	0.00756	0.132	0.96	0.075	1.92	294.9	0.00650	0.078
-5.250	-4.750	14.750	15.250	1.81	1.0	1.03	0.111	2.07	296.8	0.00698	0.107	0.89	0.064	1.78	296.8	0.00600	0.072
-5.250	-4.750	14.750	15.250	1.82	1.0	1.01	0.086	2.02	298.6	0.00676	0.085	0.87	0.070	1.74	298.6	0.00584	0.080
-5.500	-4.500	14.500	15.500	1.83	1.0	0.73	0.034	1.45	300.5	0.00481	0.047	0.63	0.037	1.26	300.5	0.00419	0.059
-5.500	-4.500	14.500	15.500	1.84	1.0	0.73	0.021	1.47	302.3	0.00487	0.029	0.64	0.040	1.28	302.3	0.00424	0.063
-5.500	-4.500	14.500	15.500	1.85	1.0	0.73	0.031	1.46	304.2	0.00482	0.043	0.63	0.048	1.27	304.2	0.00417	0.076
-5.500	-4.500	14.500	15.500	1.86	1.0	0.72	0.035	1.44	306.1	0.00470	0.048	0.63	0.048	1.25	306.1	0.00407	0.076
-5.500	-4.500	14.500	15.500	1.87	1.0	0.70	0.025	1.41	307.9	0.00459	0.036	0.61	0.040	1.22	307.9	0.00397	0.066
-5.500	-4.500	14.500	15.500	1.88	1.0	0.70	0.030	1.41	309.8	0.00454	0.042	0.60	0.034	1.21	309.8	0.00392	0.056
-5.500	-4.500	14.500	15.500	1.89	1.0	0.70	0.035	1.41	311.6	0.00451	0.049	0.60	0.036	1.21	311.6	0.00389	0.059
-5.500	-4.500	14.500	15.500	1.90	1.0	0.70	0.048	1.40	313.5	0.00446	0.068	0.60	0.041	1.20	313.5	0.00384	0.069
-5.500	-4.500	14.500	15.500	1.91	1.0	0.66	0.050	1.31	315.4	0.00416	0.076	0.56	0.045	1.13	315.4	0.00357	0.079
-5.500	-4.500	14.500	15.500	1.92	1.0	0.67	0.038	1.34	317.2	0.00423	0.057	0.58	0.037	1.15	317.2	0.00363	0.065
-5.500	-4.500	14.500	15.500	1.93	1.0	0.68	0.032	1.36	319.1	0.00427	0.047	0.59	0.037	1.17	319.1	0.00368	0.063
-5.500	-4.500	14.500	15.500	1.94	1.0	0.69	0.027	1.38	320.9	0.00430	0.039	0.59	0.035	1.18	320.9	0.00369	0.059
-5.500	-4.500	14.500	15.500	1.95	1.0	0.70	0.022	1.39	322.8	0.00431	0.032	0.59	0.037	1.19	322.8	0.00370	0.063
-5.500	-4.500	14.500	15.500	1.96	1.0	0.67	0.020	1.35	324.6	0.00417	0.030	0.59	0.043	1.17	324.6	0.00360	0.073
-5.500	-4.500	14.500	15.500	1.97	1.0	0.66	0.030	1.32	326.5	0.00406	0.045	0.57	0.039	1.14	326.5	0.00350	0.069
-5.500	-4.500	14.500	15.500	1.98	1.0	0.66	0.022	1.32	328.3	0.00402	0.033	0.57	0.043	1.14	328.3	0.00348	0.075
-5.500	-4.500	14.500	15.500	1.99	1.0	0.70	0.023	1.40	330.1	0.00425	0.033	0.61	0.040	1.22	330.1	0.00369	0.066
-5.500	-4.500	14.500	15.500	2.00	1.0	0.72	0.025	1.43	332.0	0.00423	0.035	0.62	0.037	1.24	332.0	0.00375	0.060
-5.500	-4.500	14.500	15.500	2.02	1.0	0.72	0.044	1.43	335.7	0.00425	0.062	0.60	0.039	1.20	335.7	0.00356	0.065
-5.500	-4.500	14.500	15.500	2.04	1.0	0.66	0.046	1.31	339.4	0.00386	0.070	0.55	0.034	1.10	339.4	0.00325	0.061
-5.500	-4.500	14.500	15.500	2.06	1.0	0.63	0.050	1.25	343.0	0.00365	0.080	0.53	0.032	1.06	343.0	0.00308	0.060
-5.500	-4.500	14.500	15.500	2.08	1.0	0.62	0.046	1.24	346.7	0.00359	0.075	0.53	0.035	1.06	346.7	0.00305	0.066
-5.500	-4.500	14.500	15.500	2.10	1.0	0.64	0.042	1.28	350.4	0.00364	0.066	0.55	0.041	1.09	350.4	0.00310	0.076
-5.500	-4.500	14.500	15.500	2.12	1.0	0.66	0.037	1.33	354.1	0.00375	0.055	0.56	0.037	1.13	354.1	0.00320	0.065
-5.500	-4.500	14.500	15.500	2.14	1.0	0.66	0.010	1.31	357.7	0.00366	0.016	0.56	0.037	1.12	357.7	0.00314	0.066
-5.500	-4.500	14.500	15.500	2.16	1.0	0.62	0.024	1.23	361.4	0.00340	0.039	0.53	0.038	1.06	361.4	0.00293	0.071
-5.500	-4.500	14.500	15.500	2.18	1.0	0.60	0.044	1.20	365.1	0.00329	0.074	0.52	0.041	1.04	365.1	0.00284	0.078
-5.500	-4.500	14.500	15.500	2.20	1.0	0.63	0.054	1.26	368.7	0.00343	0.086	0.55	0.039	1.09	368.7	0.00296	0.071
-5.500	-4.500	14.500	15.500	2.22	1.0	0.67	0.063	1.34	372.4	0.00361	0.094	0.58	0.039	1.16	372.4	0.00312	0.068
-5.500	-4.500	14.500	15.500	2.24	1.0	0.66	0.068	1.33	376.0	0.00354	0.102	0.58	0.043	1.15	376.0	0.00307	0.074
-5.500	-4.500	14.500	15.500	2.26	1.0	0.63	0.068	1.26	379.7	0.00332	0.108	0.55	0.045	1.10	379.7	0.00290	0.082
-5.500	-4.500	14.500	15.500	2.28	1.0	0.59	0.059	1.19	383.3	0.00312	0.099	0.52	0.035	1.05	383.3	0.00273	0.066
-5.500	-4.500	14.500	15.500	2.30	1.0	0.58	0.046	1.16	387.0	0.00300	0.080	0.51	0.032	1.02	387.0	0.00264	0.063

TABLE 3

Means and standard deviations (s.d) of the measured ripple reflection coefficient $|K_R|$, at or near resonance, for different numbers (m) of ripples in the patch. b/h denotes the quotient of the ripple amplitude (b) and the water depth (h), and N is the number of measurements entering into each mean. The details of the measurements are illustrated in Figures 16 and 17.

Number of ripples m = 1

b/h	$\|K_R\|$		2k/1		N
	mean	s.d	mean	s.d	
.12	.0703	.0312	.9744	.0244	7
.16	.1212	.0491	.9792	.0176	6
.20	.2078	.0671	.9773	.0154	6
.24	.2586	.0537	.9734	.0115	5
.28	.3044	.0388	.9764	.0106	5
.32	.3197	.0429	.9840	.0077	4
.36	.3588	.0276	.9742	.0092	5
.40	.4068	.0240	.9788	.0087	5

Number of ripples m = 2

b/h	$\|K_R\|$		2k/1		N
	mean	s.d	mean	s.d	
.12	.1562	.0609	.9647	.0429	13
.16	.2022	.0716	.9865	.0538	19
.20	.2535	.0974	1.0171	.0446	17
.24	.3630	.0386	.9734	.0115	5
.28	.4062	.0363	.9667	.0120	6
.32	.4260	.0365	.9678	.0139	6
.36	.4818	.0318	.9705	.0122	6
.40	.5388	.0104	.9734	.0084	5

Number of ripples m = 4

b/h	$\|K_R\|$		2k/1		N
	mean	s.d	mean	s.d	
.10	.1299	.0240	.9966	.0323	8
.12	.2021	.0423	.9980	.0325	9
.16	.3218	.0569	.9989	.0297	10
.20	.4586	.0711	.9734	.0174	7
.24	.5584	.0493	.9734	.0156	7
.28	.6223	.0645	.9833	.0147	7
.32	.6869	.0201	.9689	.0130	7
.36	.7205	.0286	.9714	.0139	8
.40	.7407	.0448	.9892	.0291	13

Number of ripples m = 10

b/h	$\|K_R\|$		2k/1		N
	mean	s.d	mean	s.d	
.08	.1350	.0085	.9995	.0106	2
.12	.4123	.0249	.9970	.0120	3
.14	.5220	.0236	.9990	.0110	3
.16	.6070	.0159	.9983	.0125	4
.18	.6597	.0060	.9910	.0090	3
.20	.7227	.0139	.9897	.0085	3

TABLE 4

Measurements of the maximum and minimum surface elevation, and of the wave reflection coefficient K, at different positions in the wave tank, for m = 2, 4 and 10 ripples and for different water depths. Gauges 1, 2, 3 and 4, were moved as a set (see §3.3 and Figure 12) from the wave generator towards the beach; with the gauges on the up-wave side of the ripple patch $K \to |K_R|$, and with the gauges on the down-wave side $K \to K_B$. Values of the incident and reflected wave amplitudes a_I and a_R, and of the wave steepness H_I/λ_w, are also included. (For convenience, the wave steepness has been defined in these tables as H_I/λ_w. Elsewhere the definition $a_I k = \pi H_I/\lambda_w$ has been adopted.)

Table 4a	m = 2,	h = 15.6 cm,	T = 1.73s
Table 4b	m = 4,	h = 15.6 cm,	T = 1.73s
Table 4c	m = 10,	h = 62.5 cm,	T = 1.17s
Table 4d	m = 10,	h = 50.0 cm,	T = 1.20s
Table 4e	m = 10,	h = 41.7 cm,	T = 1.23s
Table 4f	m = 10,	h = 35.7 cm,	T = 1.28s
Table 4g	m = 10,	h = 31.3 cm,	T = 1.31s
Table 4h	m = 10,	h = 27.8 cm,	T = 1.37s
Table 4i	m = 10,	h = 25.0 cm,	T = 1.42s

Note: In these tables, the origin of the x-axis has been taken (largely for experimental reasons) at the up-wave end of the ripple patch. Elsewhere (eg §2) the origin is taken at the centre of the patch.

TABLE 4a

Monochromatic wave reflection results. CERC 150x3x3 ft Wave Tank.

Date(s)	Depth (cm)	No.of ripples	Ripple amplitude (cm)	Amplitude / Depth ratio	Stroke (cm)	Wave period (s)	Wave length (cm)	Filter / No filter	Beach slope	Water temperature (deg C)
20/8/81	h=15.6	m= 2	b=5	b/h=0.32	S=2.0	T=1.73	λ_w=206.51	NF	1:10	21.8

Gauge positions(x)				Max/min surface elevation						Wave reflection results from Gauges 1 & 2					Wave reflection results from Gauges 3 & 4				
1	2	3	4	1		2		3		4		a_I	a_R	H_I	H_I/λ_w	K	a_I	a_R	H_I	H_I/λ_w	K
(m)				(cm)								(cm)	(cm)	(cm)			(cm)	(cm)	(cm)		
-10.25	-9.75	-9.50	-9.00	1.02	-0.707	0.495	-0.350	0.811	-0.566	0.644	-0.469	0.59	0.29	1.17	0.00569	0.497	0.52	0.21	1.05	0.00508	0.401
-9.25	-8.75	-8.50	-8.00	1.08	-0.727	0.470	-0.365	0.775	-0.504	0.639	-0.512	0.59	0.30	1.19	0.00578	0.508	0.52	0.21	1.05	0.00507	0.403
-8.25	-7.75	-7.50	-7.00	1.08	-0.811	0.448	-0.260	0.728	-0.495	0.607	-0.585	0.60	0.30	1.20	0.00580	0.501	0.52	0.22	1.05	0.00511	0.412
-7.25	-6.75	-6.50	-6.00	1.03	-0.854	0.386	-0.335	0.601	-0.500	0.601	-0.636	0.60	0.30	1.21	0.00588	0.493	0.53	0.22	1.06	0.00514	0.410
-6.25	-5.75	-5.50	-5.00	0.97	-0.914	0.349	-0.371	0.483	-0.496	0.667	-0.659	0.62	0.29	1.23	0.00595	0.475	0.53	0.22	1.06	0.00512	0.407
-5.25	-4.75	-4.50	-4.00	0.88	-0.890	0.355	-0.400	0.389	-0.485	0.723	-0.661	0.62	0.28	1.23	0.00595	0.458	0.52	0.21	1.04	0.00505	0.405
-4.25	-3.75	-3.50	-3.00	0.88	-0.867	0.419	-0.352	0.380	-0.464	0.778	-0.639	0.60	0.27	1.21	0.00587	0.450	0.51	0.22	1.02	0.00495	0.422
-3.25	-2.75	-2.50	-2.00	0.84	-0.782	0.516	-0.365	0.424	-0.398	0.793	-0.613	0.59	0.25	1.17	0.00569	0.435	0.50	0.21	0.99	0.00481	0.427
-2.25	-1.75	-1.50	-1.00	0.90	-0.725	0.548	-0.399	0.417	-0.344	0.834	-0.613	0.57	0.25	1.14	0.00551	0.435	0.50	0.23	0.99	0.00478	0.461
-1.25	-0.75	-0.50	0.	0.92	-0.668	0.579	-0.453	0.423	-0.236	0.822	-0.636	0.56	0.25	1.13	0.00546	0.445	0.48	0.23	0.97	0.00471	0.481
-0.25	0.25	0.50	1.00	0.90	-0.621	0.556	-0.501	0.459	-0.231	0.705	-0.356	0.55	0.22	1.10	0.00535	0.404	0.44	0.16	0.88	0.00424	0.371
0.75	1.25	1.50	2.00	0.80	-0.528	0.507	-0.435	0.488	-0.299	0.553	-0.484	0.52	0.14	1.03	0.00500	0.281	0.43	0.09	0.85	0.00411	0.206
1.75	2.25	2.50	3.00	0.67	-0.525	0.437	-0.438	0.454	-0.395	0.507	-0.515	0.49	0.09	0.98	0.00475	0.185	0.45	0.14	0.89	0.00432	0.315
2.75	3.25	3.50	4.00	0.59	-0.606	0.407	-0.462	0.384	-0.395	0.465	-0.537	0.50	0.08	0.99	0.00482	0.158	0.45	0.06	0.90	0.00435	0.130
3.75	4.25	4.50	5.00	0.49	-0.608	0.421	-0.472	0.408	-0.411	0.492	-0.535	0.50	0.07	1.00	0.00484	0.132	0.45	0.06	0.90	0.00437	0.124
4.75	5.25	5.50	6.00	0.52	-0.643	0.455	-0.420	0.443	-0.401	0.550	-0.478	0.50	0.07	1.00	0.00482	0.131	0.44	0.05	0.88	0.00424	0.121
5.75	6.25	6.50	7.00	0.59	-0.560	0.517	-0.383	0.478	-0.367	0.586	-0.428	0.48	0.07	0.96	0.00466	0.137	0.43	0.05	0.85	0.00412	0.129
6.75	7.25	7.50	8.00	0.63	-0.478	0.533	-0.324	0.495	-0.297	0.626	-0.368	0.47	0.05	0.94	0.00455	0.116	0.42	0.06	0.84	0.00408	0.137
7.75	8.25	8.50	9.00	0.67	-0.367	0.593	-0.348	0.498	-0.269	0.606	-0.389	0.46	0.05	0.93	0.00450	0.098	0.42	0.06	0.84	0.00409	0.151
8.75	9.25	9.50	10.00	0.67	-0.369	0.573	-0.418	0.460	-0.352	0.579	-0.452	0.46	0.04	0.93	0.00452	0.081	0.43	0.06	0.85	0.00412	0.147
9.75	10.25	10.50	11.00	0.64	-0.455	0.532	-0.488	0.419	-0.394	0.491	-0.485	0.47	0.03	0.94	0.00457	0.073	0.43	0.06	0.86	0.00415	0.134
10.75	11.25	11.50	12.00	0.55	-0.472	0.448	-0.485	0.343	-0.426	0.447	-0.518	0.47	0.04	0.94	0.00454	0.077	0.43	0.06	0.85	0.00413	0.144
11.75	12.25	12.50	13.00	0.48	-0.504	0.429	-0.482	0.311	-0.402	0.456	-0.505	0.47	0.04	0.94	0.00453	0.084	0.42	0.07	0.84	0.00405	0.175
12.75	13.25	13.50	14.00	0.43	-0.483	0.494	-0.483	0.369	-0.387	0.482	-0.486	0.46	0.03	0.92	0.00444	0.064	0.41	0.07	0.82	0.00395	0.167
13.75	14.25	14.50	15.00	0.49	-0.489	0.522	-0.451	0.415	-0.312	0.539	-0.443	0.45	0.03	0.89	0.00433	0.069	0.40	0.07	0.80	0.00390	0.178
14.75	15.25	15.50	16.00	0.56	-0.452	0.559	-0.404	0.485	-0.259	0.536	-0.379	0.44	0.03	0.88	0.00428	0.079	0.39	0.06	0.78	0.00379	0.162
15.75	16.25	16.50	17.00	0.59	-0.384	0.534	-0.357	0.504	-0.330	0.537	-0.299	0.43	0.02	0.85	0.00411	0.052	0.38	0.06	0.76	0.00366	0.148
16.75	17.25	17.50	18.00	0.59	-0.283	0.504	-0.375	0.487	-0.332	0.406	-0.259	0.41	0.01	0.81	0.00392	0.033	0.33	0.02	0.66	0.00318	0.061

TABLE 4b

Monochromatic wave reflection results. CERC 150x3x3 ft Wave Tank.

Date(s)	Depth (cm)	No.of ripples	Ripple amplitude (cm)	Amplitude / Depth ratio	Stroke (cm)	Wave period (s)	Wave length (cm)	Filter / No filter	Beach slope	Water temperature (deg C)
13/8/81	h=15.6	m= 4	b=5	b/h=0.32	S=2.0	T=1.73	λ_w=206.51	NF	1:10	22.5

Gauge positions(x)				Max/min surface elevation				Wave reflection results from Gauges 1 & 2					Wave reflection results from Gauges 3 & 4				
1	2	3	4	1	2	3	4	a_I	a_R	H_I	H_I/λ_w	K	a_I	a_R	H_I	H_I/λ_w	K
(m)				(cm)				(cm)	(cm)	(cm)			(cm)	(cm)	(cm)		
-10.25	-9.75	-9.50	-9.00	1.68 -1.212	0.526 -0.252	0.778 -0.711	0.967 -0.871	0.84	0.55	1.69	0.00820	0.655	0.69	0.41	1.38	0.00670	0.596
-9.25	-8.75	-8.50	-8.00	1.66 -1.255	0.496 -0.320	0.744 -0.658	1.060 -0.891	0.84	0.56	1.68	0.00815	0.671	0.69	0.42	1.37	0.00661	0.612
-8.25	-7.75	-7.50	-7.00	1.66 -1.250	0.465 -0.344	0.765 -0.638	1.121 -0.930	0.83	0.57	1.66	0.00806	0.681	0.68	0.43	1.36	0.00659	0.633
-7.25	-6.75	-6.50	-6.00	1.55 -1.230	0.437 -0.439	0.676 -0.556	1.181 -0.915	0.83	0.56	1.66	0.00803	0.679	0.67	0.43	1.35	0.00653	0.638
-6.25	-5.75	-5.50	-5.00	1.48 -1.243	0.417 -0.533	0.566 -0.498	1.209 -0.950	0.82	0.55	1.64	0.00793	0.665	0.66	0.43	1.33	0.00646	0.641
-5.25	-4.75	-4.50	-4.00	1.33 -1.192	0.453 -0.640	0.440 -0.397	1.193 -0.922	0.80	0.53	1.61	0.00781	0.653	0.66	0.42	1.32	0.00640	0.641
-4.25	-3.75	-3.50	-3.00	1.24 -1.198	0.489 -0.692	0.218 -0.251	1.248 -0.958	0.78	0.50	1.57	0.00763	0.636	0.66	0.43	1.31	0.08033	0.656
-3.25	-2.75	-2.50	-2.00	1.12 -1.079	0.584 -0.756	0.246 -0.237	1.211 -0.986	0.77	0.48	1.53	0.00742	0.633	0.64	0.44	1.28	0.00619	0.682
-2.25	-1.75	-1.50	-1.00	1.06 -1.053	0.655 -0.778	0.230 -0.230	1.266 -0.993	0.74	0.47	1.48	0.00717	0.641	0.63	0.45	1.26	0.00609	0.717
-1.25	-0.75	-0.50	0.	1.05 -0.960	0.766 -0.743	0.192 -0.190	1.243 -0.944	0.73	0.49	1.46	0.00706	0.667	0.62	0.46	1.23	0.00598	0.754
-0.25	0.25	0.50	1.00	1.12 -0.940	0.802 -0.719	0.322 -0.258	1.068 -0.725	0.70	0.46	1.39	0.00675	0.660	0.51	0.35	1.01	0.00490	0.701
0.75	1.25	1.50	2.00	1.05 -0.745	0.700 -0.605	0.384 -0.194	0.834 -0.597	0.60	0.36	1.21	0.00587	0.600	0.43	0.25	0.87	0.00423	0.567
1.75	2.25	2.50	3.00	0.86 -0.544	0.564 -0.577	0.414 -0.252	0.666 -0.535	0.52	0.24	1.04	0.00506	0.452	0.39	0.15	0.79	0.00385	0.385
2.75	3.25	3.50	4.00	0.74 -0.468	0.491 -0.527	0.438 -0.337	0.461 -0.479	0.48	0.13	0.95	0.00460	0.265	0.38	0.06	0.76	0.00370	0.155
3.75	4.25	4.50	5.00	0.58 -0.496	0.390 -0.514	0.346 -0.428	0.404 -0.503	0.45	0.05	0.90	0.00434	0.106	0.41	0.05	0.82	0.00395	0.119
4.75	5.25	5.50	6.00	0.47 -0.598	0.328 -0.469	0.316 -0.416	0.419 -0.484	0.45	0.04	0.91	0.00441	0.080	0.40	0.04	0.80	0.00390	0.109
5.75	6.25	6.50	7.00	0.41 -0.549	0.421 -0.469	0.389 -0.433	0.452 -0.490	0.45	0.04	0.89	0.00432	0.080	0.39	0.04	0.78	0.00380	0.099
6.75	7.25	7.50	8.00	0.48 -0.536	0.467 -0.416	0.438 -0.371	0.531 -0.419	0.43	0.03	0.87	0.00421	0.077	0.39	0.04	0.77	0.00372	0.106
7.75	8.25	8.50	9.00	0.60 -0.451	0.537 -0.347	0.482 -0.320	0.529 -0.372	0.43	0.03	0.85	0.00410	0.069	0.38	0.04	0.75	0.00365	0.118
8.75	9.25	9.50	10.00	0.64 -0.423	0.552 -0.292	0.488 -0.261	0.559 -0.312	0.42	0.02	0.84	0.00405	0.056	0.38	0.04	0.75	0.00362	0.120
9.75	10.25	10.50	11.00	0.66 -0.310	0.568 -0.327	0.487 -0.314	0.513 -0.369	0.41	0.02	0.83	0.00401	0.050	0.37	0.04	0.74	0.00357	0.098
10.75	11.25	11.50	12.00	0.62 -0.384	0.474 -0.392	0.414 -0.396	0.485 -0.432	0.41	0.02	0.81	0.00392	0.054	0.36	0.04	0.73	0.00356	0.104
11.75	12.25	12.50	13.00	0.54 -0.464	0.411 -0.406	0.358 -0.388	0.418 -0.454	0.41	0.03	0.81	0.00391	0.068	0.36	0.05	0.73	0.00355	0.133
12.75	13.25	13.50	14.00	0.46 -0.490	0.320 -0.444	0.258 -0.412	0.348 -0.457	0.41	0.02	0.81	0.00393	0.057	0.36	0.05	0.72	0.00351	0.131
13.75	14.25	14.50	15.00	0.31 -0.536	0.339 -0.448	0.302 -0.361	0.381 -0.436	0.40	0.02	0.80	0.00387	0.050	0.36	0.05	0.72	0.00347	0.138
14.75	15.25	15.50	16.00	0.39 -0.502	0.413 -0.433	0.386 -0.333	0.436 -0.431	0.39	0.02	0.79	0.00381	0.046	0.35	0.05	0.70	0.00337	0.150
15.75	16.25	16.50	17.00	0.45 -0.467	0.425 -0.394	0.427 -0.304	0.483 -0.361	0.38	0.01	0.76	0.00367	0.015	0.34	0.05	0.67	0.00324	0.135
16.75	17.25	17.50	18.00	0.51 -0.373	0.478 -0.296	0.465 -0.259	0.405 -0.236	0.36	0.01	0.72	0.00351	0.023	0.30	0.02	0.59	0.00283	0.052

TABLE 4c

Monochromatic wave reflection results. CERC 150x3x3 ft Wave Tank.

Date(s)	Depth (cm)	No.of ripples	Ripple amplitude (cm)	Amplitude / Depth ratio	Stroke (cm)	Wave period (s)	Wave length (cm)	Filter / No filter	Beach slope	Water temperature (deg C)
16/6/81	h=62.5	m=10	b=5	b/h=0.08	S=2.0	T=1.17	λ_w=204.70	NF	1:10	23.7

Gauge positions(x)				Max/min surface elevation				Wave reflection results from Gauges 1 & 2					Wave reflection results from Gauges 3 & 4				
1	2	3	4	1	2	3	4	a_I	a_R	H_I	H_I/λ_w	K	a_I	a_R	H_I	H_I/λ_w	K
(m)				(cm)				(cm)	(cm)	(cm)			(cm)	(cm)	(cm)		
-10.25	-9.75	-9.50	-9.00	2.40 -2.246	1.749 -1.622	2.036 -1.918	2.095 -2.008	1.99	0.32	3.98	0.01946	0.159	1.97	0.31	3.94	0.01926	0.158
-9.25	-8.75	-8.50	-8.00	2.42 -2.231	1.728 -1.615	1.995 -1.888	2.112 -2.015	1.98	0.33	3.96	0.01937	0.165	1.96	0.31	3.92	0.01915	0.158
-8.25	-7.75	-7.50	-7.00	2.38 -2.207	1.729 -1.364	1.939 -1.850	2.187 -2.049	1.97	0.33	3.94	0.01928	0.165	1.97	0.32	3.93	0.01920	0.162
-7.25	-6.75	-6.50	-6.00	2.37 -2.223	1.739 -1.628	1.927 -1.826	2.200 -2.033	1.97	0.32	3.94	0.01928	0.164	1.95	0.31	3.90	0.01909	0.159
-6.25	-5,75	-5.50	-5.00	2.34 -2.214	1.740 -1.630	1.890 -1.771	2.224 -2.049	1.96	0.32	3.92	0.01915	0.165	1.94	0.31	3.88	0.01899	0.158
-5.25	-4.75	-4.50	-4.00	2.30 -2.160	1.769 -1.640	1.818 -1.746	2.202 -2.080	1.94	0.31	3.89	0.01900	0.161	1.93	0.30	3.86	0.01885	0.158
-4.25	-3.75	-3.50	-3.00	2.26 -2.172	1.794 -1.646	1.821 -1.674	2.239 -2.095	1.94	0.32	3.88	0.01895	0.167	1.92	0.31	3.85	0.01881	0.159
-3.25	-2.75	-2.50	-2.00	2.24 -2.135	1.816 -1.662	1.783 -1.630	2.233 -2.136	1.93	0.33	3.86	0.01885	0.171	1.92	0.32	3.83	0.01874	0.167
-2.25	-1.75	-1.50	-1.00	2.23 -2.108	1.823 -1.675	1.758 -1.603	2.227 -2.149	1.92	0.33	3.84	0.01878	0.171	1.91	0.32	3.81	0.01864	0.168
-1.25	-0.75	-0.50	0.	2.20 -2.082	1.826 -1.706	1.719 -1.566	2.251 -2.140	1.92	0.33	3.83	0.01872	0.174	1.89	0.32	3.79	0.01853	0.169
-0.25	0.25	0.50	1.00	2.16 -2.025	1.852 -1.736	1.705 -1.550	2.226 -2.122	1.91	0.32	3.81	0.01861	0.169	1.88	0.30	3.76	0.01839	0.161
0.75	1.25	1.50	2.00	2.13 -1.971	1.867 -1.768	1.695 -1.570	2.190 -2.078	1.89	0.29	3.79	0.01852	0.155	1.86	0.26	3.73	0.01825	0.140
1.75	2.25	2.50	3.00	2.07 -1.915	1.872 -1.785	1.691 -1.591	2.146 -2.038	1.88	0.26	3.75	0.01835	0.140	1.86	0.24	3.71	0.01814	0.128
2.75	3.25	3.50	4.00	2.01 -1.882	1.887 -1.777	1.713 -1.603	2.120 -1.997	1.86	0.23	3.72	0.01818	0.122	1.84	0.21	3.69	0.01804	0.112
3.75	4.25	4.50	5.00	1.97 -1.867	1.893 -1.793	1.725 -1.626	2.098 -1.959	1.86	0.20	3.71	0.01814	0.106	1.84	0.18	3.68	0.01798	0.097
4.75	5.25	5.50	6.00	1.93 -1.846	1.909 -1.790	1.751 -1.642	2.057 -1.924	1.84	0.17	3.69	0.01805	0.091	1.83	0.15	3.66	0.01791	0.082
5.75	6.25	6.50	7.00	1.93 -1.812	1.918 -1.784	1.783 -1.655	1.993 -1.909	1.84	0.13	3.68	0.01799	0.073	1.83	0.12	3.65	0.01783	0.065
6.75	7.25	7.50	8.00	1.90 -1.785	1.921 -1.794	1.806 -1.677	1.952 -1.874	1.83	0.10	3.66	0.01791	0.057	1.81	0.09	3.63	0.01775	0.049
7.75	8.25	8.50	9.00	1.89 -1.760	1.904 -1.816	1.825 -1.707	1.921 -1.830	1.83	0.08	3.66	0.01788	0.046	1.81	0.07	3.62	0.01770	0.037
8.75	9.25	9.50	10.00	1.88 -1.741	1.907 -1.803	1.852 -1.728	1.888 -1.798	1.82	0.05	3.64	0.01779	0.025	1.81	0.04	3.61	0.01765	0.021
9.75	10.25	10.50	11.00	1.88 -1.753	1.882 -1.808	1.863 -1.748	1.902 -1.767	1.82	0.03	3.64	0.01779	0.018	1.81	0.03	3.62	0.01769	0.016
10.75	11.25	11.50	12.00	1.89 -1.762	1.882 -1.775	1.842 -1.734	1.892 -1.768	1.81	0.04	3.63	0.01775	0.021	1.80	0.04	3.60	0.01758	0.021
11.75	12.25	12.50	13.00	1.88 -1.760	1.866 -1.766	1.821 -1.717	1.908 -1.768	1.81	0.04	3.61	0.01766	0.023	1.80	0.04	3.59	0.01753	0.025
12.75	13.25	13.50	14.00	1.86 -1.746	1.889 -1.783	1.813 -1.731	1.877 -1.741	1.81	0.04	3.61	0.01767	0.021	1.78	0.05	3.56	0.01741	0.027
13.75	14.25	14.50	15.00	1.83 -1.715	1.887 -1.773	1.816 -1.726	1.818 -1.711	1.79	0.05	3.58	0.01750	0.026	1.76	0.05	3.52	0.01720	0.027
14.75	15.25	15.50	16.00	1.81 -1.700	1.877 -1.739	1.816 -1.714	1.800 -1.708	1.77	0.03	3.54	0.01731	0.019	1.75	0.03	3.50	0.01711	0.019
15.75	16.25	16.50	17.00	1.79 -1.716	1.836 -1.732	1.816 -1.691	1.788 -1.694	1.76	0.02	3.52	0.01720	0.014	1.74	0.03	3.48	0.01699	0.020
16.75	17.25	17.50	18.00	1.79 -1.694	1.831 -1.710	1.809 -1.677	1.759 -1.682	1.75	0.03	3.49	0.01706	0.020	1.72	0.03	3.44	0.01682	0.018

TABLE 4d

Monochromatic wave reflection results. CERC 150x3x3 ft Wave Tank.

Date(s)	Depth (cm)	No.of ripples	Ripple amplitude (cm)	Amplitude / Depth ratio	Stroke (cm)	Wave period (s)	Wave length (cm)	Filter / No filter	Beach slope	Water temperature (deg C)
15/6/81-16/6/81	h=50.0	m=10	b=5	b/h=0.10	S=2.0	T=1.20	λ_w=204.83	NF	1:10	23.4

Gauge positions(x)				Max/min surface elevation															
1	2	3	4	1		2		3		4		Wave reflection results from Gauges 1 & 2					Wave reflection results from Gauges 3 & 4				
												a_I	a_R	H_I	H_I/λ_w	K	a_I	a_R	H_I	H_I/λ_w	K
(m)				(cm)								(cm)	(cm)	(cm)			(cm)	(cm)	(cm)		
-10.25	-9.75	-9.50	-9.00	2.96	-2.679	1.636	-1.468	2.324	-2.241	2.407	-2.221	2.16	0.64	4.32	0.02111	0.294	2.15	0.62	4.29	0.02095	0.291
-9.25	-8.75	-8.50	-8.00	2.98	-2.704	1.653	-1.427	2.249	-2.152	2.450	-2.286	2.15	0.65	4.30	0.02100	0.301	2.13	0.61	4.27	0.02088	0.286
-8.25	-7.75	-7.50	-7.00	2.92	-2.713	1.675	-1.421	2.214	-2.058	2.510	-2.390	2.15	0.65	4.29	0.02093	0.303	2.14	0.63	4.28	0.02092	0.296
-7.25	-6.75	-6.50	-6.00	2.92	-2.724	1.685	-1.445	2.155	-1.985	2.500	-2.426	2.15	0.65	4.29	0.02096	0.301	2.13	0.63	4.25	0.02074	0.296
-6.25	-5.75	-5.50	-5.00	2.88	-2.657	1.692	-1.566	1.972	-1.858	2.639	-2.449	2.13	0.64	4.26	0.02081	0.300	2.10	0.63	4.21	0.02055	0.297
-5.25	-4.75	-4.50	-4.00	2.86	-2.648	1.675	-1.559	1.921	-1.832	2.676	-2.431	2.12	0.64	4.23	0.02065	0.302	2.09	0.62	4.18	0.02044	0.297
-4.25	-3.75	-3.50	-3.00	2.82	-2.590	1.753	-1.570	1.865	-1.753	2.673	-2.509	2.09	0.64	4.19	0.02049	0.305	2.09	0.63	4.17	0.02036	0.302
-3.25	-2.75	-2.50	-2.00	2.73	-2.564	1.818	-1.608	1.807	-1.625	2.699	-2.576	2.08	0.63	4.16	0.02034	0.304	2.07	0.64	4.15	0.02029	0.309
-2.25	-1.75	-1.50	-1.00	2.66	-2.501	1.825	-1.632	1.723	-1.543	2.677	-2.565	2.04	0.63	4.09	0.02000	0.310	2.03	0.64	4.07	0.01986	0.316
-1.25	-0.75	-0.50	0.	2.63	-2.440	1.848	-1.747	1.619	-1.469	2.750	-2.537	2.04	0.64	4.08	0.01993	0.316	2.01	0.64	4.03	0.01970	0.316
-0.25	0.25	0.50	1.00	2.56	-2.339	1.902	-1.821	1.565	-1.458	2.687	-2.498	2.03	0.62	4.05	0.01978	0.306	1.99	0.59	3.98	0.01945	0.298
0.75	1.25	1.50	2.00	2.47	-2.333	1.918	-1.807	1.619	-1.468	2.600	-2.406	2.01	0.58	4.02	0.01962	0.290	1.97	0.53	3.94	0.01923	0.269
1.75	2.25	2.50	3.00	2.37	-2.228	1.984	-1.803	1.643	-1.446	2.501	-2.383	1.98	0.52	3.97	0.01938	0.260	1.94	0.48	3.89	0.01903	0.245
2.75	3.25	3.50	4.00	2.28	-2.148	1.985	-1.857	1.668	-1.474	2.455	-2.281	1.97	0.46	3.93	0.01920	0.233	1.92	0.42	3.85	0.01882	0.217
3.75	4.25	4.50	5.00	2.24	-2.054	1.975	-1.867	1.688	-1.519	2.393	-2.201	1.95	0.39	3.90	0.01903	0.199	1.91	0.35	3.82	0.01867	0.183
4.75	5.25	5.50	6.00	2.17	-1.970	1.997	-1.872	1.706	-1.573	2.299	-2.143	1.93	0.33	3.86	0.01884	0.172	1.89	0.29	3.79	0.01853	0.153
5.75	6.25	6.50	7.00	2.09	-1.925	2.023	-1.867	1.750	-1.617	2.209	-2.078	1.91	0.27	3.82	0.01869	0.141	1.88	0.23	3.76	0.01837	0.121
6.75	7.25	7.50	8.00	2.02	-1.906	2.033	-1.870	1.818	-1.640	2.145	-1.991	1.91	0.20	3.81	0.01860	0.107	1.87	0.17	3.74	0.01826	0.092
7.75	8.25	8.50	9.00	2.01	-1.841	2.008	-1.885	1.863	-1.710	2.062	-1.935	1.89	0.15	3.78	0.01849	0.077	1.86	0.11	3.72	0.01816	0.061
8.75	9.25	9.50	10.00	1.98	-1.808	1.999	-1.887	1.923	-1.761	2.028	-1.848	1.88	0.09	3.76	0.01838	0.050	1.86	0.06	3.71	0.01813	0.031
9.75	10.25	10.50	11.00	1.98	-1.792	1.985	-1.882	1.932	-1.823	2.030	-1.835	1.88	0.06	3.75	0.01830	0.032	1.87	0.06	3.74	0.01828	0.034
10.75	11.25	11.50	12.00	1.96	-1.830	2.005	-1.830	1.924	-1.789	2.011	-1.859	1.87	0.05	3.74	0.01828	0.029	1.86	0.05	3.73	0.01820	0.027
11.75	12.25	12.50	13.00	1.94	-1.843	2.009	-1.818	1.928	-1.743	2.006	-1.882	1.86	0.06	3.73	0.01823	0.034	1.86	0.07	3.71	0.01814	0.039
12.75	13.25	13.50	14.00	1.94	-1.790	2.017	-1.875	1.932	-1.752	1.944	-1.851	1.87	0.07	3.74	0.01827	0.036	1.83	0.08	3.67	0.01794	0.041
13.75	14.25	14.50	15.00	1.91	-1.720	1.993	-1.895	1.910	-1.782	1.921	-1.761	1.84	0.08	3.69	0.01804	0.045	1.81	0.08	3.62	0.01768	0.045
14.75	15.25	15.50	16.00	1.89	-1.690	1.969	-1.845	1.901	-1.783	1.901	-1.747	1.81	0.07	3.63	0.01773	0.036	1.80	0.07	3.60	0.01760	0.041
15.75	16.25	16.50	17.00	1.87	-1.712	1.963	-1.802	1.866	-1.770	1.876	-1.758	1.80	0.05	3.60	0.01761	0.029	1.78	0.07	3.57	0.01745	0.038
16.75	17.25	17.50	18.00	1.86	-1.711	1.950	-1.775	1.873	-1.731	1.787	-1.705	1.79	0.05	3.58	0.01750	0.030	1.74	0.04	3.48	0.01702	0.023

TABLE 4e

Monochromatic wave reflection results. CERC 150x3x3 ft Wave Tank.

Date(s)	Depth (cm)	No.of ripples	Ripple amplitude (cm)	Amplitude / Depth ratio	Stroke (cm)	Wave period (s)	Wave length (cm)	Filter / No filter	Beach slope	Water temperature (deg C)
17/6/81	h=41.7	m=10	b=5	b/h=0.12	S=2.0	T=1.23	λ_w=202.98	NF	1:10	23.8

Gauge positions(x) (m)				Max/min surface elevation (cm)						Wave reflection results from Gauges 1 & 2					Wave reflection results from Gauges 3 & 4				
1	2	3	4	1		2		3		a_I (cm)	a_R (cm)	H_I (cm)	H_I/λ_w	K	a_I (cm)	a_R (cm)	H_I (cm)	H_I/λ_w	K
-10.25	-9.75	-9.50	-9.00	2.22	-2.064	1.335	-1.266	1.283	-1.145	2.247	-2.075	1.63	0.68	3.26	0.01606	0.419	1.61	0.66	3.22	0.01588	0.413
-9.25	-8.75	-8.50	-8.00	2.19	-2.113	1.351	-1.251	1.189	-1.086	2.265	-2.152	1.63	0.69	3.25	0.01601	0.422	1.61	0.67	3.21	0.01584	0.417
-8.25	-7.75	-7.50	-7.00	2.19	-2.032	1.373	-1.286	1.183	-1.101	2.251	-2.130	1.61	0.68	3.23	0.01592	0.422	1.61	0.68	3.21	0.01580	0.423
-7.25	-6.75	-6.50	-6.00	2.16	-1.984	1.417	-1.379	1.121	-1.042	2.276	-2.111	1.62	0.69	3.24	0.01596	0.426	1.60	0.67	3.20	0.01575	0.421
-6.25	-5.75	-5.50	-5.00	2.04	-1.994	1.464	-1.394	1.056	-0.931	2.288	-2.152	1.60	0.68	3.20	0.01576	0.425	1.58	0.67	3.15	0.01555	0.425
-5.25	-4.75	-4.50	-4.00	2.06	-1.966	1.463	-1.376	1.087	-0.952	2.249	-2.126	1.58	0.67	3.17	0.01562	0.422	1.56	0.66	3.12	0.01536	0.422
-4.25	-3.75	-3.50	-3.00	1.99	-1.809	1.514	-1.464	1.006	-0.907	2.241	-2.079	1.56	0.66	3.12	0.01540	0.424	1.54	0.66	3.08	0.01520	0.426
-3.25	-2.75	-2.50	-2.00	1.91	-1.841	1.502	-1.445	0.954	-0.839	2.262	-2.115	1.54	0.66	3.08	0.01520	0.430	1.53	0.67	3.06	0.01510	0.437
-2.25	-1.75	-1.50	-1.00	1.89	-1.839	1.540	-1.438	0.985	-0.822	2.248	-2.140	1.53	0.67	3.06	0.01508	0.438	1.52	0.68	3.03	0.01496	0.450
-1.25	-0.75	-0.50	0.	1.85	-1.705	1.599	-1.545	0.898	-0.776	2.243	-2.088	1.53	0.67	3.06	0.01508	0.438	1.52	0.68	3.03	0.01496	0.450
-0.25	0.25	0.50	1.00	1.86	-1.765	1.542	-1.505	0.896	-0.783	2.141	-2.033	1.52	0.68	3.03	0.01496	0.452	1.47	0.64	2.93	0.01447	0.434
0.75	1.25	1.50	2.00	1.77	-1.732	1.538	-1.459	0.968	-0.809	2.063	-1.950	1.49	0.63	2.98	0.01467	0.424	1.44	0.57	2.87	0.01413	0.399
1.75	2.25	2.50	3.00	1.69	-1.577	1.526	-1.477	0.968	-0.851	1.956	-1.831	1.45	0.56	2.91	0.01434	0.385	1.40	0.51	2.80	0.01383	0.361
2.75	3.25	3.50	4.00	1.62	-1.505	1.486	-1.440	0.968	-0.898	1.850	-1.746	1.42	0.49	2.85	0.01404	0.342	1.38	0.43	2.76	0.01359	0.314
3.75	4.25	4.50	5.00	1.52	-1.483	1.468	-1.387	1.056	-0.948	1.775	-1.681	1.39	0.41	2.79	0.01377	0.297	1.36	0.37	2.71	0.01336	0.272
4.75	5.25	5.50	6.00	1.47	-1.393	1.442	-1.371	1.099	-0.977	1.665	-1.572	1.38	0.35	2.75	0.01355	0.252	1.33	0.30	2.67	0.01316	0.226
5.75	6.25	6.50	7.00	1.45	-1.317	1.418	-1.367	1.097	-1.044	1.589	-1.493	1.36	0.28	2.71	0.01336	0.203	1.32	0.23	2.64	0.01300	0.178
6.75	7.25	7.50	8.00	1.39	-1.322	1.399	-1.317	1.176	-1.114	1.510	-1.430	1.34	0.21	2.68	0.01320	0.156	1.31	0.17	2.61	0.01287	0.128
7.75	8.25	8.50	9.00	1.33	-1.283	1.381	-1.307	1.253	-1.131	1.419	-1.349	1.33	0.14	2.65	0.01306	0.104	1.30	0.11	2.59	0.01276	0.084
8.75	9.25	9.50	10.00	1.35	-1.238	1.369	-1.315	1.276	-1.205	1.359	-1.276	1.31	0.08	2.63	0.01297	0.058	1.29	0.05	2.58	0.01272	0.036
9.75	10.25	10.50	11.00	1.35	-1.243	1.355	-1.292	1.302	-1.278	1.382	-1.274	1.31	0.03	2.62	0.01292	0.025	1.31	0.03	2.62	0.01290	0.026
10.75	11.25	11.50	12.00	1.32	-1.264	1.349	-1.248	1.318	-1.220	1.346	-1.298	1.31	0.02	2.61	0.01288	0.014	1.30	0.04	2.60	0.01281	0.030
11.75	12.25	12.50	13.00	1.32	-1.257	1.335	-1.261	1.288	-1.177	1.359	-1.304	1.30	0.03	2.60	0.01281	0.025	1.29	0.06	2.58	0.01274	0.047
12.75	13.25	13.50	14.00	1.34	-1.238	1.344	-1.288	1.241	-1.198	1.349	-1.245	1.30	0.05	2.60	0.01282	0.040	1.27	0.07	2.53	0.01245	0.053
13.75	14.25	14.50	15.00	1.27	-1.197	1.345	-1.259	1.248	-1.184	1.281	-1.206	1.27	0.05	2.54	0.01253	0.039	1.23	0.08	2.46	0.01210	0.067
14.75	15.25	15.50	16.00	1.21	-1.147	1.325	-1.242	1.270	-1.155	1.242	-1.205	1.23	0.05	2.47	0.01217	0.041	1.22	0.07	2.45	0.01208	0.054
15.75	16.25	16.50	17.00	1.22	-1.146	1.286	-1.237	1.225	-1.167	1.266	-1.174	1.22	0.04	2.45	0.01205	0.033	1.21	0.06	2.42	0.01192	0.048
16.75	17.25	17.50	18.00	1.22	-1.123	1.260	-1.189	1.194	-1.149	1.195	-1.098	1.20	0.03	2.41	0.01187	0.026	1.16	0.03	2.32	0.01142	0.023

TABLE 4f

Monochromatic wave reflection results. CERC 150x3x3 ft Wave Tank.

Date(s)	Depth (cm)	No.of ripples	Ripple amplitude (cm)	Amplitude / Depth ratio	Stroke (cm)	Wave period (s)	Wave length (cm)	Filter / No filter	Beach slope	Water temperature (deg C)
22/6/81	h=35.7	m=10	b=5	b/h=0.14	S=2.0	T=1.28	λ_w=204.49	NF	1:10	23.4

Gauge positions(x) (m)				Max/min surface elevation (cm)																
1	2	3	4	1		2		3		4		Wave reflection results from Gauges 1 & 2					Wave reflection results from Gauges 3 & 4				
												a_I (cm)	a_R (cm)	H_I (cm)	H_I/λ_w	K	a_I (cm)	a_R (cm)	H_I (cm)	H_I/λ_w	K
-10.25	-9.75	-9.50	-9.00	3.85	-3.405	1.597	-0.969	2.591	-2.297	2.973	-2.868	2.39	1.23	4.78	0.02340	0.513	2.38	1.20	4.77	0.02335	0.502
-9.25	-8.75	-8.50	-8.00	3.96	-3.435	1.463	-1.171	2.342	-2.385	3.308	-2.881	2.44	1.25	4.88	0.02387	0.511	2.41	1.24	4.83	0.02365	0.514
-8.25	-7.75	-7.50	-7.00	3.90	-3.367	1.586	-1.299	2.300	-2.062	3.359	-3.146	2.40	1.26	4.80	0.02346	0.527	2.44	1.26	4.87	0.02383	0.517
-7.25	-6.75	-6.50	-6.00	3.81	-3.427	1.613	-1.333	2.044	-2.031	3.458	-3.134	2.42	1.26	4.84	0.02366	0.520	2.40	1.26	4.79	0.02342	0.528
-6.25	-5.75	-5.50	-5.00	3.82	-3.264	1.569	-1.621	1.856	-1.876	3.596	-3.193	2.38	1.26	4.76	0.02331	0.530	2.39	1.26	4.78	0.02338	0.527
-5.25	-4.75	-4.50	-4.00	3.55	-3.296	1.828	-1.566	1.792	-1.625	3.551	-3.252	2.35	1.25	4.70	0.02298	0.533	2.34	1.26	4.67	0.02285	0.541
-4.25	-3.75	-3.50	-3.00	3.56	-3.102	1.729	-1.767	1.515	-1.628	3.698	-3.149	2.31	1.23	4.62	0.02259	0.533	2.31	1.26	4.62	0.02259	0.544
-3.25	-2.75	-2.50	-2.00	3.28	-3.059	1.985	-1.850	1.561	-1.278	3.650	-3.341	2.26	1.25	4.52	0.02211	0.551	2.30	1.29	4.60	0.02252	0.563
-2.25	-1.75	-1.50	-1.00	3.27	-2.955	2.030	-1.967	1.348	-1.283	3.843	-3.259	2.25	1.25	4.51	0.02205	0.555	2.27	1.33	4.54	0.02223	0.585
-1.25	-0.75	-0.50	0.	3.28	-2.953	1.936	-2.050	1.373	-1.173	3.752	-3.363	2.22	1.30	4.45	0.02176	0.586	2.26	1.33	4.53	0.02218	0.589
-0.25	0.25	0.50	1.00	3.11	-2.901	2.186	-2.006	1.410	-1.132	3.503	-3.197	2.22	1.27	4.43	0.02167	0.572	2.15	1.23	4.30	0.02103	0.573
0.75	1.25	1.50	2.00	3.02	-2.533	1.982	-2.160	1.174	-1.137	3.402	-2.927	2.13	1.15	4.26	0.02083	0.540	2.09	1.08	4.19	0.02049	0.516
1.75	2.25	2.50	3.00	2.47	-2.439	2.160	-1.966	1.383	-0.926	2.996	-2.897	2.00	0.99	4.01	0.01960	0.494	2.00	0.96	4.00	0.01959	0.478
2.75	3.25	3.50	4.00	2.50	-2.155	2.040	-1.989	1.289	-1.130	3.017	-2.522	1.97	0.86	3.93	0.01924	0.438	1.94	0.81	3.87	0.01894	0.419
3.75	4.25	4.50	5.00	2.23	-2.065	2.031	-1.921	1.358	-1.118	2.624	-2.530	1.89	0.75	3.78	0.01849	0.396	1.89	0.69	3.78	0.01850	0.364
4.75	5.25	5.50	6.00	2.07	-1.960	2.097	-1.805	1.513	-1.119	2.606	-2.247	1.86	0.61	3.72	0.01821	0.330	1.83	0.57	3.66	0.01792	0.310
5.75	6.25	6.50	7.00	2.08	-1.705	1.897	-1.894	1.405	-1.344	2.381	-2.122	1.81	0.50	3.61	0.01769	0.279	1.81	0.43	3.61	0.01767	0.238
6.75	7.25	7.50	8.00	1.89	-1.868	2.033	-1.684	1.684	-1.263	2.149	-2.039	1.81	0.39	3.63	0.01778	0.215	1.77	0.32	3.53	0.01728	0.182
7.75	8.25	8.50	9.00	1.96	-1.663	1.812	-1.851	1.617	-1.527	2.144	-1.755	1.80	0.27	3.59	0.01756	0.148	1.75	0.19	3.50	0.01710	0.108
8.75	9.25	9.50	10.00	1.86	-1.648	1.976	-1.680	1.781	-1.560	1.811	-1.812	1.76	0.16	3.52	0.01723	0.090	1.74	0.09	3.48	0.01704	0.053
9.75	10.25	10.50	11.00	1.76	-1.698	1.857	-1.750	1.874	-1.603	1.999	-1.630	1.77	0.06	3.53	0.01725	0.035	1.76	0.04	3.52	0.01723	0.025
10.75	11.25	11.50	12.00	1.94	-1.563	1.880	-1.698	1.716	-1.664	1.885	-1.758	1.75	0.05	3.50	0.01712	0.027	1.76	0.07	3.52	0.01722	0.038
11.75	12.25	12.50	13.00	1.77	-1.710	1.947	-1.599	1.840	-1.459	1.916	-1.762	1.75	0.07	3.49	0.01707	0.039	1.73	0.11	3.47	0.01698	0.061
12.75	13.25	13.50	14.00	1.90	-1.551	1.792	-1.762	1.635	-1.595	1.912	-1.616	1.73	0.09	3.47	0.01699	0.049	1.69	0.11	3.38	0.01656	0.066
13.75	14.25	14.50	15.00	1.72	-1.747	1.959	-1.605	1.732	-1.502	1.698	-1.673	1.69	0.10	3.38	0.01655	0.059	1.65	0.14	3.30	0.01613	0.082
14.75	15.25	15.50	16.00	1.61	-1.492	1.776	-1.738	1.724	-1.517	1.850	-1.503	1.65	0.11	3.30	0.01615	0.068	1.64	0.11	3.28	0.01606	0.065
15.75	16.25	16.50	17.00	1.72	-1.409	1.864	-1.650	1.657	-1.585	1.705	-1.647	1.64	0.10	3.29	0.01609	0.060	1.65	0.11	3.30	0.01614	0.068
16.75	17.25	17.50	18.00	1.55	-1.560	1.842	-1.604	1.773	-1.398	1.638	-1.421	1.64	0.08	3.27	0.01602	0.047	1.55	0.05	3.09	0.01511	0.035

TABLE 4g

Monochromatic wave reflection results. CERC 150x3x3 ft Wave Tank.

Date(s)	Depth (cm)	No.of ripples	Ripple amplitude (cm)	Amplitude / Depth ratio	Stroke (cm)	Wave period (s)	Wave length (cm)	Filter / No filter	Beach slope	Water temperature (deg C)
23/6/81	h=31.3	m=10	b=5	b/h=0.16	S=2.0	T=1.31	λ_w=201.38	NF	1:10	23.5

Gauge positions(x) (m)				Max/min surface elevation (cm)																
1	2	3	4	1		2		3		4		Wave reflection results from Gauges 1 & 2					Wave reflection results from Gauges 3 & 4				
												a_I (cm)	a_R (cm)	H_I (cm)	H_I/λ_w	K	a_I (cm)	a_R (cm)	H_I (cm)	H_I/λ_w	K
-10.25	-9.75	-9.50	-9.00	1.33	-1.320	1.198	-1.142	0.513	-0.358	1.731	-1.623	1.08	0.63	2.15	0.01071	0.584	1.07	0.64	2.14	0.01061	0.594
-9.25	-8.75	-8.50	-8.00	1.31	-1.249	1.200	-1.194	0.472	-0.355	1.738	-1.595	1.06	0.62	2.13	0.01060	0.586	1.06	0.63	2.13	0.01061	0.596
-8.25	-7.75	-7.50	-7.00	1.28	-1.284	1.207	-1.168	0.503	-0.372	1.755	-1.623	1.06	0.63	2.12	0.01052	0.593	1.06	0.64	2.12	0.01055	0.607
-7.25	-6.75	-6.50	-6.00	1.27	-1.206	1.241	-1.283	0.481	-0.371	1.792	-1.638	1.06	0.64	2.12	0.01055	0.606	1.06	0.65	2.11	0.01049	0.614
-6.25	-5.75	-5.50	-5.00	1.20	-1.193	1.280	-1.229	0.485	-0.322	1.765	-1.640	1.05	0.64	2.09	0.01039	0.614	1.04	0.66	2.08	0.01031	0.630
-5.25	-4.75	-4.50	-4.00	1.24	-1.163	1.269	-1.275	0.474	-0.374	1.811	-1.628	1.06	0.66	2.11	0.01046	0.622	1.05	0.66	2.10	0.01041	0.625
-4.25	-3.75	-3.50	-3.00	1.18	-1.173	1.228	-1.200	0.466	-0.324	1.697	-1.604	1.02	0.63	2.03	0.01010	0.624	1.01	0.64	2.02	0.01004	0.637
-3.25	-2.75	-2.50	-2.00	1.17	-1.109	1.234	-1.217	0.424	-0.332	1.691	-1.558	1.00	0.63	2.01	0.00997	0.630	1.00	0.65	2.01	0.00998	0.643
-2.25	-1.75	-1.50	-1.00	1.12	-1.141	1.228	-1.200	0.397	-0.285	1.676	-1.570	0.98	0.63	1.97	0.00981	0.642	0.99	0.66	1.98	0.00984	0.664
-1.25	-0.75	-0.50	0.	1.14	-1.096	1.228	-1.224	0.366	-0.256	1.704	-1.570	0.98	0.65	1.96	0.00973	0.664	0.98	0.67	1.96	0.00975	0.681
-0.25	0.25	0.50	1.00	1.09	-1.096	1.239	-1.195	0.415	-0.248	1.568	-1.473	0.97	0.64	1.93	0.00958	0.664	0.91	0.60	1.83	0.00911	0.651
0.75	1.25	1.50	2.00	1.09	-0.989	1.121	-1.151	0.390	-0.341	1.448	-1.342	0.92	0.58	1.85	0.00917	0.631	0.87	0.52	1.74	0.00864	0.596
1.75	2.25	2.50	3.00	0.97	-0.971	1.064	-1.022	0.458	-0.340	1.308	-1.244	0.88	0.51	1.75	0.00867	0.580	0.83	0.45	1.65	0.00818	0.547
2.75	3.25	3.50	4.00	0.95	-0.857	0.946	-0.981	0.430	-0.408	1.196	-1.108	0.83	0.43	1.66	0.00824	0.522	0.78	0.38	1.57	0.00781	0.479
3.75	4.25	4.50	5.00	0.84	-0.841	0.931	-0.881	0.488	-0.397	1.075	-1.039	0.79	0.36	1.58	0.00786	0.454	0.76	0.31	1.51	0.00749	0.416
4.75	5.25	5.50	6.00	0.82	-0.724	0.855	-0.881	0.479	-0.470	1.001	-0.935	0.76	0.30	1.52	0.00755	0.389	0.73	0.25	1.46	0.00724	0.342
5.75	6.25	6.50	7.00	0.74	-0.735	0.836	-0.787	0.555	-0.477	0.902	-0.882	0.73	0.23	1.47	0.00730	0.317	0.70	0.19	1.41	0.00701	0.268
6.75	7.25	7.50	8.00	0.74	-0.659	0.752	-0.776	0.568	-0.579	0.846	-0.800	0.72	0.17	1.43	0.00712	0.241	0.69	0.13	1.38	0.00688	0.182
7.75	8.25	8.50	9.00	0.67	-0.668	0.759	-0.707	0.650	-0.585	0.759	-0.753	0.70	0.11	1.40	0.00695	0.162	0.68	0.07	1.36	0.00676	0.108
8.75	9.25	9.50	10.00	0.69	-0.635	0.702	-0.725	0.660	-0.674	0.715	-0.663	0.69	0.06	1.38	0.00687	0.085	0.67	0.02	1.35	0.00673	0.029
9.75	10.25	10.50	11.00	0.66	-0.643	0.730	-0.677	0.718	-0.676	0.678	-0.692	0.68	0.03	1.36	0.00678	0.038	0.69	0.01	1.38	0.00685	0.021
10.75	11.25	11.50	12.00	0.68	-0.662	0.691	-0.701	0.677	-0.678	0.712	-0.659	0.69	0.01	1.37	0.00679	0.021	0.69	0.01	1.37	0.00680	0.014
11.75	12.25	12.50	13.00	0.68	-0.650	0.717	-0.665	0.678	-0.641	0.675	-0.690	0.67	0.01	1.35	0.00671	0.020	0.67	0.02	1.35	0.00671	0.026
12.75	13.25	13.50	14.00	0.66	-0.651	0.678	-0.680	0.632	-0.619	0.703	-0.639	0.66	0.02	1.33	0.00662	0.027	0.65	0.04	1.30	0.00645	0.057
13.75	14.25	14.50	15.00	0.64	-0.603	0.702	-0.653	0.628	-0.583	0.658	-0.662	0.65	0.03	1.29	0.00641	0.054	0.63	0.06	1.26	0.00628	0.088
14.75	15.25	15.50	16.00	0.59	-0.580	0.683	-0.682	0.633	-0.608	0.690	-0.623	0.63	0.05	1.27	0.00631	0.080	0.63	0.05	1.27	0.00632	0.075
15.75	16.25	16.50	17.00	0.61	-0.570	0.693	-0.642	0.633	-0.597	0.653	-0.655	0.63	0.04	1.26	0.00626	0.064	0.63	0.04	1.26	0.00628	0.064
16.75	17.25	17.50	18.00	0.60	-0.584	0.655	-0.637	0.613	-0.576	0.631	-0.561	0.63	0.03	1.25	0.00619	0.050	0.59	0.00	1.19	0.00590	0.005

TABLE 4h

Monochromatic wave reflection results. CERC 150x3x3 ft Wave Tank.

Date(s)	Depth (cm)	No.of ripples	Ripple amplitude (cm)	Amplitude / Depth ratio	Stroke (cm)	Wave period (s)	Wave length (cm)	Filter / No filter	Beach slope	Water temperature (deg C)
24/6/81	h=27.8	m=10	b=5	b/h=0.18	S=2.0	T=1.37	λ_w=203.67	NF	1:10	23.4

Gauge positions(x) (m)				Max/min surface elevation (cm)				Wave reflection results from Gauges 1 & 2					Wave reflection results from Gauges 3 & 4				
1	2	3	4	1	2	3	4	a_I (cm)	a_R (cm)	H_I (cm)	H_I/λ_w	K	a_I (cm)	a_R (cm)	H_I (cm)	H_I/λ_w	K
-10.25	-9.75	-9.50	-9.00	4.52 -3.596	1.488 -1.252	2.185 -2.352	3.795 -3.155	2.49	1.56	4.97	0.02443	0.627	2.44	1.53	4.88	0.02397	0.627
-9.25	-8.75	-8.50	-8.00	4.35 -3.664	1.473 -1.171	2.379 -2.299	3.608 -3.204	2.42	1.59	4.84	0.02378	0.655	2.41	1.53	4.82	0.02367	0.634
-8.25	-7.75	-7.50	-7.00	4.36 -3.513	1.515 -1.612	2.063 -2.104	3.838 -3.418	2.42	1.56	4.84	0.02379	0.645	2.43	1.56	4.86	0.02388	0.642
-7.25	-6.75	-6.50	-6.00	4.23 -3.532	1.672 -1.539	1.943 -1.906	4.149 -3.270	2.41	1.59	4.83	0.02373	0.658	2.39	1.58	4.78	0.02346	0.662
-6.25	-5.75	-5.50	-5.00	4.15 -3.419	1.754 -1.846	1.816 -1.740	4.012 -3.513	2.35	1.57	4.70	0.02309	0.669	2.36	1.57	4.72	0.02318	0.664
-5.25	-4.75	-4.50	-4.00	4.05 -3.250	1.900 -1.914	1.490 -1.646	4.248 -3.329	2.36	1.58	4.72	0.02320	0.668	2.32	1.59	4.64	0.02280	0.684
-4.25	-3.75	-3.50	-3.00	3.76 -3.299	2.018 -1.933	1.507 -1.477	4.200 -3.425	2.28	1.56	4.55	0.02237	0.687	2.29	1.60	4.59	0.02253	0.698
-3.25	-2.75	-2.50	-2.00	3.54 -3.034	2.025 -2.256	1.133 -1.330	4.263 -3.600	2.25	1.56	4.49	0.02207	0.693	2.28	1.63	4.56	0.02241	0.715
-2.25	-1.75	-1.50	-1.00	3.34 -3.105	2.356 -2.160	1.143 -1.135	4.433 -3.492	2.22	1.61	4.44	0.02183	0.723	2.25	1.70	4.50	0.02210	0.757
-1.25	-0.75	-0.50	0.	3.28 -3.084	2.043 -2.425	0.570 -0.608	4.284 -3.674	2.18	1.64	4.36	0.02142	0.752	2.25	1.69	4.49	0.02208	0.755
-0.25	0.25	0.50	1.00	3.29 -2.909	2.306 -2.388	1.079 -1.042	4.065 -3.140	2.17	1.60	4.34	0.02134	0.737	2.04	1.53	4.09	0.02800	0.747
0.75	1.25	1.50	2.00	3.10 -2.620	2.028 -2.364	1.114 -0.705	3.442 -3.050	2.01	1.46	4.03	0.01982	0.725	1.92	1.32	3.83	0.01879	0.691
1.75	2.25	2.50	3.00	2.77 -2.277	2.095 -2.164	0.952 -0.792	3.340 -2.574	1.92	1.26	3.83	0.01882	0.659	1.78	1.13	3.57	0.01308	0.632
2.75	3.25	3.50	4.00	2.29 -2.227	2.061 -1.809	1.114 -0.673	2.847 -2.042	1.75	1.07	3.49	0.01713	0.613	1.64	0.96	3.27	0.01605	0.586
3.75	4.25	4.50	5.00	2.08 -1.654	1.781 -1.878	0.852 -0.720	2.401 -2.199	1.58	0.86	3.17	0.01556	0.542	1.51	0.74	3.02	0.01481	0.492
4.75	5.25	5.50	6.00	1.59 -1.690	1.753 -1.402	1.073 -0.653	2.136 -1.760	1.45	0.67	2.90	0.01423	0.465	1.36	0.58	2.71	0.01330	0.425
5.75	6.25	6.50	7.00	1.63 -1.432	1.603 -1.495	0.995 -0.789	1.750 -1.774	1.36	0.53	2.71	0.01331	0.393	1.30	0.43	2.60	0.01275	0.330
6.75	7.25	7.50	8.00	1.06 -1.252	1.359 -1.030	1.059 -0.718	1.485 -1.193	1.08	0.32	2.15	0.01058	0.294	1.02	0.24	2.03	0.01000	0.234
7.75	8.25	8.50	9.00	1.00 -0.866	1.049 -0.955	0.826 -0.775	1.017 -1.004	0.92	0.19	1.85	0.00907	0.203	0.90	0.12	1.79	0.00878	0.132
8.75	9.25	9.50	10.00	1.19 -0.958	1.113 -1.138	1.030 -1.038	1.142 -1.046	1.06	0.11	2.11	0.01038	0.107	1.03	0.04	2.06	0.01013	0.035
9.75	10.25	10.50	11.00	1.00 -1.001	1.175 -1.048	1.219 -0.946	1.199 -0.900	1.06	0.04	2.11	0.01038	0.038	1.06	0.02	2.12	0.01043	0.022
10.75	11.25	11.50	12.00	1.19 -0.909	1.197 -0.986	1.107 -0.975	1.071 -1.007	1.03	0.03	2.06	0.01011	0.025	1.04	0.01	2.08	0.01022	0.013
11.75	12.25	12.50	13.00	1.44 -1.296	1.461 -1.362	1.442 -1.292	1.591 -1.272	1.39	0.03	2.77	0.01359	0.022	1.37	0.04	2.74	0.01347	0.030
12.75	13.25	13.50	14.00	1.56 -1.240	1.635 -1.202	1.463 -1.134	1.469 -1.358	1.36	0.07	2.72	0.01335	0.049	1.33	0.09	2.66	0.01308	0.068
13.75	14.25	14.50	15.00	1.42 -1.185	1.403 -1.405	1.258 -1.252	1.461 -1.329	1.33	0.09	2.66	0.01306	0.064	1.29	0.12	2.58	0.01266	0.093
14.75	15.25	15.50	16.00	1.22 -1.203	1.541 -1.295	1.478 -1.096	1.509 -1.184	1.28	0.10	2.57	0.01263	0.079	1.28	0.10	2.57	0.01261	0.074
15.75	16.25	16.50	17.00	1.36 -1.056	1.469 -1.329	1.288 -1.269	1.281 -1.349	1.27	0.10	2.53	0.01245	0.077	1.28	0.09	2.56	0.01258	0.073
16.75	17.25	17.50	18.00	1.20 -1.205	1.376 -1.297	1.334 -1.133	1.345 -0.933	1.26	0.07	2.52	0.01240	0.059	1.16	0.05	2.32	0.01140	0.044

TABLE 4i

Monochromatic wave reflection results. CERC 150x3x3 ft Wave Tank.

Date(s)	Depth (cm)	No.of ripples	Ripple amplitude (cm)	Amplitude / Depth ratio	Stroke (cm)	Wave period (s)	Wave length (cm)	Filter / No filter	Beach slope	Water temperature (deg C)
24/6/81-25/6/81	h=25.0	m=10	b=5	b/h=0.20	S=2.0	T=1.42	λ_w=203.80	NF	1:10	24.1

Gauge positions(x) (m)				Max/min surface elevation (cm)						Wave reflection results from Gauges 1 & 2					Wave reflection results from Gauges 3 & 4				
1	2	3	4	1		2		3		4		a_I (cm)	a_R (cm)	H_I (cm)	H_I/λ_w	K	a_I (cm)	a_R (cm)	H_I (cm)	H_I/λ_w	K
-10.25	-9.75	-9.50	-9.00	4.30	-3.448	1.234	-1.187	1.898	-2.494	3.587	-2.934	2.34	1.51	4.67	0.02293	0.645	2.29	1.50	4.58	0.02250	0.653
-9.25	-8.75	-8.50	-8.00	4.10	-3.371	1.676	-1.268	2.066	-2.033	3.650	-3.131	2.26	1.54	4.53	0.02222	0.681	2.22	1.53	4.44	0.02177	0.690
-8.25	-7.75	-7.50	-7.00	4.44	-3.187	1.492	-1.638	2.151	-1.831	3.779	-3.222	2.24	1.58	4.47	0.02193	0.708	2.30	1.56	4.60	0.02258	0.677
-7.25	-6.75	-6.50	-6.00	4.24	-3.329	1.483	-1.607	1.486	-2.146	4.119	-3.144	2.31	1.56	4.61	0.02265	0.675	2.28	1.57	4.55	0.02235	0.692
-6.25	-5.75	-5.50	-5.00	3.60	-3.114	1.639	-1.437	1.512	-1.671	3.648	-3.047	2.06	1.47	4.11	0.02015	0.716	2.01	1.49	4.02	0.01974	0.739
-5.25	-4.75	-4.50	-4.00	3.68	-2.823	1.380	-1.754	1.549	-1.280	3.501	-3.064	1.98	1.47	3.96	0.01943	0.741	2.00	1.42	4.01	0.01970	0.710
-4.25	-3.75	-3.50	-3.00	3.36	-2.892	1.505	-1.743	0.958	-1.480	3.806	-2.924	1.99	1.41	3.98	0.01955	0.709	1.97	1.45	3.94	0.01934	0.736
-3.25	-2.75	-2.50	-2.00	3.05	-2.808	1.942	-1.817	1.099	-1.208	3.861	-3.011	1.91	1.43	3.82	0.01876	0.748	1.91	1.52	3.81	0.01870	0.796
-2.25	-1.75	-1.50	-1.00	3.12	-2.589	1.651	-2.067	1.111	-0.858	3.784	-3.153	1.86	1.48	3.73	0.01829	0.794	1.94	1.52	3.89	0.01911	0.784
-1.25	-0.75	-0.50	0.	2.89	-2.674	1.956	-2.128	0.754	-0.994	4.019	-3.042	1.89	1.48	3.78	0.01857	0.782	1.92	1.55	3.85	0.01888	0.805
-0.25	0.25	0.50	1.00	2.68	-2.635	2.180	-2.039	0.374	-0.658	3.652	-2.656	1.83	1.47	3.65	0.01794	0.805	1.69	1.42	3.38	0.01160	0.838
0.75	1.25	1.50	2.00	2.73	-2.174	1.690	-2.197	0.891	-0.416	2.830	-2.805	1.67	1.34	3.33	0.01635	0.806	1.58	1.20	3.16	0.01550	0.757
1.75	2.25	2.50	3.00	2.39	-1.915	1.914	-1.945	0.529	-0.558	2.684	-2.278	1.60	1.16	3.20	0.01572	0.726	1.45	1.01	2.91	0.01429	0.691
2.75	3.25	3.50	4.00	1.60	-1.990	2.038	-1.569	0.989	-0.523	2.576	-1.871	1.42	0.97	2.84	0.01395	0.683	1.28	0.87	2.57	0.01260	0.680
3.75	4.25	4.50	5.00	1.90	-1.479	1.648	-1.703	0.845	-0.529	2.004	-2.063	1.28	0.82	2.56	0.01258	0.637	1.22	0.71	2.44	0.01199	0.584
4.75	5.25	5.50	6.00	1.59	-1.273	1.472	-1.455	0.720	-0.613	1.744	-1.635	1.25	0.66	2.49	0.01221	0.529	1.15	0.54	2.30	0.01129	0.470
5.75	6.25	6.50	7.00	1.08	-1.508	1.717	-1.169	1.058	-0.508	1.826	-1.334	1.14	0.52	2.28	0.01119	0.456	1.05	0.43	2.09	0.01027	0.408
6.75	7.25	7.50	8.00	1.41	-1.065	1.506	-1.183	0.926	-0.783	1.383	-1.484	1.06	0.39	2.13	0.01045	0.370	1.03	0.31	2.05	0.01007	0.298
7.75	8.25	8.50	9.00	1.13	-1.070	1.098	-1.203	0.950	-0.954	1.303	-1.141	1.06	0.26	2.13	0.01044	0.248	1.00	0.17	2.01	0.00987	0.174
8.75	9.25	9.50	10.00	0.90	-1.186	1.504	-1.040	1.300	-0.778	1.376	-0.898	1.01	0.16	2.02	0.00994	0.162	0.96	0.08	1.92	0.00942	0.080
9.75	10.25	10.50	11.00	1.13	-0.685	1.436	-0.963	1.033	-1.138	0.997	-1.160	0.98	0.11	1.96	0.00961	0.117	1.01	0.09	2.02	0.00992	0.091
10.75	11.25	11.50	12.00	1.00	-1.098	0.949	-1.166	1.010	-1.176	1.273	-0.924	1.01	0.08	2.02	0.00992	0.078	0.99	0.08	1.99	0.00977	0.078
11.75	12.25	12.50	13.00	0.94	-1.019	1.379	-0.990	1.259	-0.742	1.391	-0.790	0.98	0.06	1.95	0.00956	0.059	0.95	0.06	1.91	0.00936	0.064
12.75	13.25	13.50	14.00	1.22	-0.692	1.191	-0.940	0.940	-1.075	0.941	-1.090	0.95	0.07	1.89	0.00926	0.077	0.95	0.10	1.89	0.00928	0.109
13.75	14.25	14.50	15.00	0.97	-0.980	0.939	-1.177	0.798	-1.090	1.158	-1.012	0.95	0.08	1.90	0.00932	0.089	0.92	0.12	1.85	0.00907	0.131
14.75	15.25	15.50	16.00	0.86	-0.901	1.269	-1.001	1.178	-0.652	1.351	-0.672	0.92	0.11	1.84	0.00905	0.118	0.91	0.10	1.82	0.00892	0.115
15.75	16.25	16.50	17.00	1.15	-0.628	1.165	-1.003	1.058	-0.996	0.880	-1.046	0.90	0.11	1.80	0.00883	0.121	0.92	0.11	1.84	0.00903	0.124
16.75	17.25	17.50	18.00	0.95	-0.890	0.914	-1.173	0.798	-1.014	0.969	-0.882	0.91	0.09	1.83	0.00898	0.099	0.83	0.06	1.66	0.00816	0.075

TABLE 5

Estimates of the differences in phase between the observed and predicted envelopes of wave elevation on the up-wave side of the ripple patch, for m = 10, 4 and 2 ripples. The estimates were obtained from the data shown in Figs 18(a) - 18(g). It should be noted that the observed and predicted wave envelopes are in phase over the ripple patch. The phase differences tabulated below are estimated cumulative lags of the observed wave envelopes on the predicted wave envelopes in the negative x-direction (ie towards the wave generator).

m	h (cm)	Phase difference (° per wave)
10	62.5	3.25
	50.0	3.30
	41.7	0.98
	35.7	2.64
	31.3	- (gave constant phase shift of about 12°)
4	15.6	4.69
2	15.6	6.94

TABLE 6

Variation of the reflection coefficient $|K_R|$ of the ripple patch with the stroke of the wave generator S, for m = 10 ripples and for different values of (b/h). (Note that the wave steepness has been defined as H_I/λ_w. Elsewhere the definition $a_I k = \pi H_I/\lambda_w$ has been adopted.)

m = 10, h = 62.5 (cm), b/h = 0.08

S (cm)	$\|K_R\|$	H_I (cm)	H_I/λ_w
1.0	.161	1.95	.00954
2.0	.169	3.86	.01888
3.0	.168	5.63	.02754
4.0	.165	7.21	.03527
5.0	.162	8.58	.04142
6.0	.170	9.77	.04777
7.0	---	---	-----
8.0	---	---	-----

m = 10, h = 50.0 (cm), b/h = 0.10

S (cm)	$\|K_R\|$	H_I (cm)	H_I/λ_w
1.0	.303	2.05	.00999
2.0	.308	4.12	.02010
3.0	.297	5.68	.02773
4.0	.307	7.03	.03434
5.0	.309	8.07	.03944
6.0	.317	9.04	.04416
7.0	.321	9.92	.04846
8.0	.304	10.92	.05336

m = 10, h = 41.7 (cm), b/h = 0.12

S (cm)	$\|K_R\|$	H_I (cm)	H_I/λ_w
1.0	.428	1.62	.00797
2.0	.435	3.19	.01574
3.0	.427	4.55	.02245
4.0	.433	5.86	.02888
5.0	.432	6.97	.03438
6.0	.421	8.00	.03943
7.0	.411	9.00	.04438
8.0	.396	9.92	.04891

m = 10, h = 35.7 (cm), b/h = 0.14

S (cm)	$\|K_R\|$	H_I (cm)	H_I/λ_w
1.0	.532	2.40	.01175
2.0	.537	4.80	.02349
3.0	.541	7.09	.03471
4.0	.541	9.09	.04446
5.0	.534	10.56	.05169
6.0	.520	11.49	.05624
7.0	.536	12.07	.05906
8.0	.482	12.43	.06083

m = 10, h = 31.3 (cm), b/h = 0.16

S (cm)	$\|K_R\|$	H_I (cm)	H_I/λ_w
1.0	.625	1.08	.00535
2.0	.617	2.14	.01066
3.0	.611	3.22	.01600
4.0	.610	4.24	.02109
5.0	.606	5.24	.02602
6.0	.601	6.32	.03138
7.0	.584	7.61	.03783
8.0	.538	9.14	.04542

m = 10, h = 27.8 (cm), b/h = 0.18

S (cm)	$\|K_R\|$	H_I (cm)	H_I/λ_w
1.0	.666	2.38	.01168
2.0	.663	4.69	.02305
3.0	.663	6.29	.03091
4.0	.659	7.73	.03799
5.0	.657	8.84	.04342
6.0	.648	9.95	.04887
7.0	.642	9.02	.04430
8.0	---	---	-----

m = 10, h = 25.0 (cm), b/h = 0.20

S (cm)	$\|K_R\|$	H_I (cm)	H_I/λ_w
1.0	.729	2.44	.01197
2.0	.739	4.26	.02090
3.0	.750	5.24	.02575
4.0	.754	5.99	.02942
5.0	.781	6.61	.03243
6.0	.649	6.78	.03326
7.0	.600	7.55	.03704
8.0	---	---	-----

APPENDIX A

The method of Goda and Suzuki for the determination of the wave reflection coefficient

In this Appendix, the method of Goda and Suzuki (1977) for the determination of the wave reflection coefficient, K, is described. In addition, some comments are made about the phase angles of the incident and reflected waves, and a simple result which is used in the main body of the report (§4.1) is discussed. Finally, some detailed discussion is included about the method adopted for analysing the wave gauge data from the laboratory experiments.

The method of Goda and Suzuki

Consider a system of incident and reflected sinusoidal waves of small amplitude travelling in water of constant depth h, with frequency σ and wave-number k related by the dispersion equation (16). If the incident (I) and reflected (R) waves travel in the +x and -x directions, their surface elevations may be expressed by

$$\left.\begin{aligned} \eta_I &= a_I \cos(kx - \sigma t + \varepsilon_I) \\ \text{and} \\ \eta_R &= a_R \cos(kx + \sigma t + \varepsilon_R) \end{aligned}\right\} \qquad (A.1)$$

respectively, where t is the time, and where the amplitude and phase angle of the incident wave are a_I and ε_I, and of the reflected wave are a_R and ε_R. It follows that, if measurements of surface elevation are made at positions $x = x_1$ and $x = x_2 = x_1 + \Delta x$, for example with a gauge pair, the observed wave forms may be expressed by

$$\left.\begin{aligned} \eta_1 &= \{\eta_I + \eta_R\}_{x=x_1} = A_1 \cos(\sigma t) + B_1 \sin(\sigma t) \\ \text{and} \\ \eta_2 &= \{\eta_I + \eta_R\}_{x=x_2} = A_2 \cos(\sigma t) + B_2 \sin(\sigma t) \end{aligned}\right\} \qquad (A.2)$$

where, from (A.1) and (A.2),

$$\left.\begin{aligned} A_1 &= a_I \cos(\delta_I) + a_R \cos(\delta_R) \,, \\ B_1 &= a_I \sin(\delta_I) - a_R \sin(\delta_R) \,, \\ A_2 &= a_I \cos(\delta_I + k\Delta x) + a_R \cos(\delta_R + k\Delta x) \,, \\ \text{and} \quad B_2 &= a_I \sin(\delta_I + k\Delta x) - a_R \sin(\delta_R + k\Delta x) \,, \end{aligned}\right\} \tag{A.3}$$

in which

$$\left.\begin{aligned} \delta_I &= kx_1 + \varepsilon_I \\ \text{and} \quad \delta_R &= kx_1 + \varepsilon_R \,. \end{aligned}\right\} \tag{A.4}$$

From Equation (A.3), the amplitudes of the incident and reflected waves are then given by

$$\left.\begin{aligned} a_I &= \frac{1}{2|\sin(k\Delta x)|} \sqrt{\left\{(A_2 - A_1\cos(k\Delta x) - B_1\sin(k\Delta x))^2 + (B_2 - B_1\cos(k\Delta x) + A_1\sin(k\Delta x))^2\right\}} \\ \text{and} \quad a_R &= \frac{1}{2|\sin(k\Delta x)|} \sqrt{\left\{(A_2 - A_1\cos(k\Delta x) + B_1\sin(k\Delta x))^2 + (B_2 - B_1\cos(k\Delta x) - A_1\sin(k\Delta x))^2\right\}} \end{aligned}\right\} \tag{A.5}$$

respectively, and the reflection coefficient K may be defined simply by

$$K = \frac{a_R}{a_I} \cdot \qquad (A.6)$$

(Note here that the reflection coefficient is defined positive, as distinct from K_R in Eqs (65) and (66).)

In general, when reflection coefficients K are obtained on the basis of observations of surface elevation made above a flat bed, it is assumed that there is a fixed partitioning of the total wave energy into kinetic and potential energies. For waves of small amplitude, these two component parts are equal, and results obtained for K are therefore expected to be independent of horizontal position (x), at least if the wave measurements are made sufficiently far from the region of bed disturbance, or from the structure, being considered. If, however, measurements of elevation are made above a region of undulating bed, and values of K are obtained by the method of Goda and Suzuki, such values need to be interpreted carefully. The reason for this is that, in general, the partitioning of the total wave energy will depend upon horizontal position, from which it follows that K will depend upon position also. Since this dependence may be rather complicated, a proper interpretation of K in such situations calls for a reliable theory for surface elevation as a function of position. In the present laboratory study, in which wave measurements were made over a ripple patch (see §4.3), the calculated values of K have been interpreted on the basis of the theory described in §2.

Goda and Suzuki's (1977) method requires certain optimum gauge spacings (Δx). In particular, they have shown that, for adequate resolution of the amplitudes a_I and a_R, the gauge spacing should be such that

$$0.05 < \frac{\Delta x}{\lambda_w} < 0.45 \cdot$$

For the work described in this report a more stringent condition was applied, namely

$$0.15 < \frac{\Delta x}{\lambda_w} < 0.35 \cdot$$

In particular, in the determination of the variation of K with the quotient of the

free surface and ripple wavelengths (Fig 14), the gauge spacing was varied as follows:

Water wavelength (λ_w) (m)	Gauge spacing (Δx) (m)
0.75 -1.5	0.25
1.5 -3.0	0.5
3.0 -6.0	1.0

Close to resonance ($\lambda_w \simeq 2$m), the gauge spacing of $\Delta x = 0.5$ m gave values of $x/\lambda_w \simeq 0.25$, at the centre of the above range. Goda and Suzuki have argued further that, under normal operating conditions, gauges should be positioned well away from the reflecting structure, and have suggested that this distance should be at least one surface wavelength. However, they have shown that, under certain circumstances, it is acceptable to place the nearest gauge pair as close as $0.1\lambda_w$ from the structure. In this study, wave gauges were positioned throughout the wave tank, as mentioned earlier; in particular, gauges were placed both over, and on either side of, the patch of undulating bed, with results which are discussed in §4.3.

The phases of the incident and reflected waves

The phase angles of the incident and reflected waves, ε_I and ε_R, may be determined from Eq (A.4) in which x_1 and k are known for any experimental run, and in which δ_I and δ_R may be determined from

$$\left.\begin{aligned} \tan(\delta_I) &= -\frac{A_2 - A_1\cos(k\Delta x) - B_1\sin(k\Delta x)}{B_2 - B_1\cos(k\Delta x) + A_1\sin(k\Delta x)} \\ \text{and} \\ \tan(\delta_R) &= \frac{A_2 - A_1\cos(k\Delta x) + B_1\sin(k\Delta x)}{B_2 - B_1\cos(k\Delta x) - A_1\sin(k\Delta x)}. \end{aligned}\right\} \quad (A.7)$$

It will be recalled from §2.7.1 that the elevation of the reflected wave obtained from Eq (64) undergoes sign changes as (2k/l) is varied. In particular, sign

changes occur in both the elevation, and in K_R given by Eq (65), when $\sin 2kL/\{(2k/l)^2 - 1\}$ changes sign. Such sign changes will be apparent in the phase angles ε_I and ε_R. This may be demonstrated most clearly by introducing a new timescale t' defined by

$$\sigma t' = \sigma t - \varepsilon_I$$

such that, from Eq (A.1),

$$\eta_I = a_I \cos(kx - \sigma t')$$

and

$$\eta_R = a_R \cos(kx + \sigma t' + \varepsilon_I + \varepsilon_R) .$$

Evidently, sign changes in η_R are associated with π-phase shifts in the sum $(\varepsilon_I + \varepsilon_R)$. In practice, however, the determination of such phase shifts is complicated by the fact that the method described earlier involves the calculation of, firstly, δ_I and δ_R from Eq (A.7) and, secondly, ε_I and ε_R from Eq (A.4) in which, for a given ripple wavelength, k varies as (2k/l) varies. Despite this difficulty, in §4.1 the behaviour of $(\varepsilon_I + \varepsilon_R)$ is displayed in one special case in which a π-phase shift of the kind described above is clearly apparent.

The analysis of the wave gauge data

For a given bed geometry, and for waves of single frequency σ, there will be a single reflection coefficient K. However, in general cases in which there is a spectrum of incident waves, there will be a reflection coefficient associated with each constituent present. For the experiments described in §4, the intention in any run was to generate waves of a single frequency and, thereby, to obtain just one value of K. In practice, however, spectral analysis of measured surface elevations generally revealed both a spreading of wave energy into frequencies adjacent to the fundamental, and also the presence of a small amount of energy in the first, and higher, harmonics (see §5.2). The former effect is, to a large extent, the result of the spectral analysis method; in particular, it is due to the presence of a non-integral number of waves in the records analysed. The latter effect is probably the result of the non-linear transfer of a small amount of the total wave energy from the fundamental frequency into higher harmonics, over the

undulating bed. (It could also be due, in principle, to the wave steepness being rather too large in certain runs, or to slight imperfections in the ability of the wave generator to produce a pure fundamental.)

In order to obtain a single overall value for the reflection coefficient, it is necessary to adopt an approach which makes a proper allowance for the distribution of wave energy in the various constituent frequencies. The approach adopted in the CERC programme "REFLECT" was to obtain simultaneous records from a pair of wave gauges at a known separation (Δx), to digitize these records at a frequency of 16 Hz for a period of 64 secs (1024 points per record), and to Fourier analyze each record using a Fast Fourier Transform (FFT) routine. Due to the limited data storage capacity of the Data Acquisition System (DAS) it was not possible to retain all of the 1024 Fourier coefficients for each record. Instead, only the eight pairs of coefficients adjacent to the fundamental frequency 1/T, where T is the wave period, and to each of the harmonics 2/T, 3/T and 4/T, were retained. Previous work at CERC (Seelig, personal communication) had shown that for supposedly monochromatic waves, very little energy exists at other frequencies. Thus the only spectral coefficients retained for each gauge pair were

$$A_{1j}\ ,\ B_{1j}\ ,\ A_{2j} \text{ and } B_{2j}\ ,\ j = 1 \text{ to } 32\ ,$$

(cf Eq (A.2)), corresponding to four groups of eight coefficients centred on the fundamental and the first three harmonics. For each of the thirty two frequencies, the surface wavenumber k_j was obtained from Eq (16). The incident and reflected wave amplitudes corresponding to the j^{th} spectral estimate were obtained by setting $A_1 = A_{1j}$, $A_{2j} = A_{2j}$, $B_1 = B_{1j}$, $B_2 = B_{2j}$ and $k = k_j$ in Eq (A.5), for $j = 1$ to 32. The reflection coefficient K_j, for each value of j, was then obtained from Eq (A.6). Finally the overall reflection coefficient was obtained from the quotient of the total reflected ($\overline{a}_R$) and incident ($\overline{a}_I$) wave amplitudes; that is, K was defined by

$$K = \frac{\overline{a}_R}{\overline{a}_I}\ ,$$

where

$$\overline{a}_R = \left(\sum_{j=1}^{32} a_{Rj}^2 \right)^{1/2}$$

and

$$\overline{a}_I = \left(\sum_{j=1}^{32} a_{Ij}^2 \right)^{1/2} .$$

In a typical experimental run (see §3.3), a reflection coefficient was obtained on this basis both from a pair of wave gauges on the up-wave side of the ripple patch, and also from a pair on the down-wave side, the latter calculation being made to give an indication of the reflection coefficient of the wave-absorbing beach. In certain extended runs, pairs of wave gauges were traversed across the entire ripple patch to examine the variation of the reflection coefficient with horizontal position (x). As pointed out earlier, particular care is needed in interpreting such results.

In order to estimate the phase angles ε_I and ε_R, and hence $(\varepsilon_I + \varepsilon_R)$, for the purpose of detecting changes of sign in the reflected wave elevation η_R, a different approach was adopted involving a re-analysis of the gauge data (by a computer programme written at IOS Taunton). Initially, the gauge records were truncated in such a way that each record contained, as nearly as possible, an integral number of waves. The purpose of this was to obtain unambiguous estimates of δ_I and δ_R from Eq (A.7), by concentrating as much of the available wave energy as possible into a single (fundamental) frequency. The procedure followed in the programme was to calculate cos δ_I, sin δ_I, cos δ_R and sin δ_R for the fundamental frequency (which, typically, contained more than 95% of the total energy). Slightly more detailed information about the phase angles than suggested by Eq (A.7) was obtained therefore, and this enabled δ_I and δ_R to be assigned their correct values in the range $(-\pi, \pi)$. Each of these calculated values was arbitrary to $\pm 2\pi$, $\pm 4\pi$ ....., and, therefore, each of the values of ε_I and ε_R, subsequently calculated from Eq (A.4), was also arbitrary to $\pm 2\pi$, $\pm 4\pi$ ..... . Hence, the calculated values of $(\varepsilon_I + \varepsilon_R)$ were also arbitrary to $\pm 2\pi$, $\pm 4\pi$, ... Since such phase shifts of 2π were irrelevant in the context of the present experiment, but shifts of π were significant, the procedure followed was to identify any sudden shifts of $\pm 2\pi$ in the sum $(\varepsilon_I + \varepsilon_R)$ as (2k/l) was varied, and to correct

for such shifts by the addition of $\mp 2\pi$ to all the results following a shift. This became a cumulative process if more than one shift of $\pm 2\pi$ occurred over the range of values of (2k/1) considered. What remained following this process of correction was a new set of values of $(\varepsilon_I + \varepsilon_R)$, within which phase shifts of $\pm\pi$ took on the significance mentioned earlier, but in which no shifts of $\pm 2\pi$ occurred. No allowance for the (very small amount of) energy in the first, and higher, harmonics was made at any stage in the argument. An example of the results obtained is discussed in §4.1 (see Figure 14c).

Other quantities calculated by both the CERC and IOS computer programmes included the incident wave height $H_I = 2a_I$ and the wave steepness H_I/λ_w, where $\lambda_w = 2\pi/k$ is the surface wavelength calculated from Eq (16). (Note that, elsewhere in this report, the definition $a_I k = \pi H_I/\lambda_w$ has been adopted for the wave steepness.)

APPENDIX B

Wave filter design and characteristics

As a separate aspect of this study, tests were carried out to determine the wave transmission and reflection characteristics of some simple rubberised fibre, or 'hogshair', wave filters. In many cases in which it is required to determine the wave reflection coefficient of a structure (eg a breakwater), by a method other than that of Goda and Suzuki (1977), it is necessary to eliminate or minimise the possibility of re-reflection of wave energy from the wave generator. This is usually done by inserting a wave filter between the wave generator and the test structure. While incident waves have to pass through the filter only once, re-reflected waves have to pass through the filter twice and they are, therefore, more strongly attenuated than the incident wave.

To investigate the wave transmission characteristics of such units a series of wave filters was designed and built and placed in the tank mid-way between the ripples and the generator. The filters were constructed of 5 cm thick sheets of rubberised fibre (hogshair) mounted vertically on edge, in wire cages, transverse to the direction of wave propagation. Each cage was 91 cm in width (equal to the width of the wave tank), 91 cm in height and 30 cm in length. Three such units were constructed from 2.5 cm wire mesh to give a total filter length of 90 cm. The filter units and their supports are shown schematically in Figure B.1.

Filter tests were carried out with the arrangements shown schematically in Figure B.2, with the filter units mid-way between the wave generator and the patch of bottom ripples. The wave reflection and transmission characteristics of the filters were determined using standard wave gauge techniques; in particular, wave reflection coefficients were determined using the method of Goda and Suzuki (1977) (Appendix A). A pair of wave gauges was situated 2 m from the filter unit(s) on their up-wave side, while another pair of gauges was situated 2 m on their down-wave side (Figure B.2). All tests were carried out with a water depth of 50 cm, and for different combinations of surface water wavelength, wave steepness and filter length. The wave gauge spacing was determined in accordance with the criteria given in Appendix A. The results of these tests are tabulated in Tables B.1a-B.1f, and are plotted in Figures B.3 and B.4.

Figure B.3 shows the variation of wave attenuation, expressed by $(1 - H_T/H_I)$, as a function of the quotient of the filter length L_f and the water wavelength λ_w, for various wave steepnesses H_I/λ_w $(= 1/\pi \cdot a_I k)$. Here H_T is the transmitted

wave height measured down-wave of the filters, and H_I is the incident wave height. Figure B.3 shows the experimental trends of $(1 - H_T/H_I)$ for the steepest waves $(H_I/\lambda_w > .05)$, and also for the lowest waves $(0 < H_I/\lambda_w < 0.01)$. Intermediate trend curves are shown for the remaining wave steepness groups. The results show that waves may be attenuated by up to 50% in amplitude in only 0.125-0.20 of their own length, dependent upon the wave steepness, and also that, for constant L_f/λ_w, steep waves generally experience more attenuation than low waves. This is consistent with the effects of viscous dissipation within the filters and, as shown in Figure B.4, is not due to the wave reflection characteristics of the filters. In Figure B.4, the variation of the reflection coefficient of the filters is shown as a function of the wave steepness (H_I/λ_w). It may be seen that the filters had a comparatively low, and fairly constant, reflection coefficient of the order of 0.2 or less (a minimum of about 0.12 at $H_I/\lambda_w \approx 0.045$). The experimental procedure adopted was that the filter length L_f was held constant while the wave period, and hence the surface wavelength, was varied over a range of values of L_f/λ_w. Although the tests were not specifically designed to determine wave transmission characteristics at constant wave steepness, the measurements were subsequently grouped into the wave steepness ranges given in Tables B.1 a-f. The variation of the wave steepness within each range is expressed by the standard deviation of H_I/λ_w, which is both quoted in the tables, and indicated by the error bars in Figure B.4.

The method of Goda and Suzuki (1977) permits wave reflection coefficients to be determined in situations in which re-reflection of wave energy may take place (see §4.1). Thus the introduction of filters between the wave generator and the ripple test section would not be expected to influence, for example, measurements of the reflection coefficient $|K_R|$ of the ripple patch . Furthermore, any non-linearities in the generated wave, which are transmitted by the filters, would not be expected to influence the reflection coefficient, on account of the way in which the energy contributions at various frequencies are summed in the calculation of K (see Appendix A). In order to confirm this, measurements of K were made both with and without filters. It may be seen in Figures B.5 and B.6 that there was little systematic difference in the results for the various cases examined.

Although it was not necessary to use wave filters in the present study, the tests have shown that rubberized filter units of simple construction may be used to absorb wave energy and, in particular, to absorb secondary reflections where these are likely to have an adverse effect on the results.

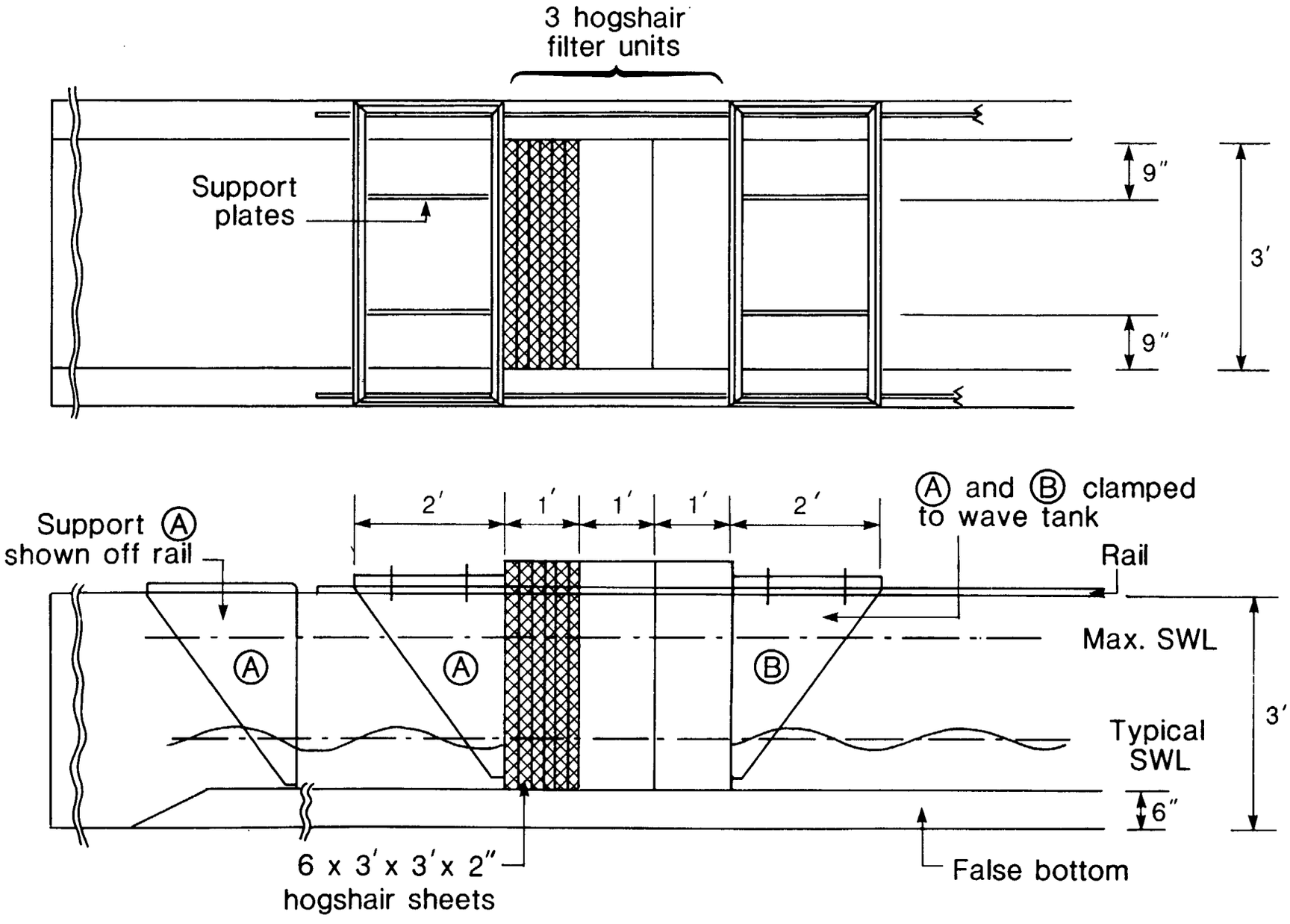

Figure B 1 Schematic diagram of the filter units and their supports.

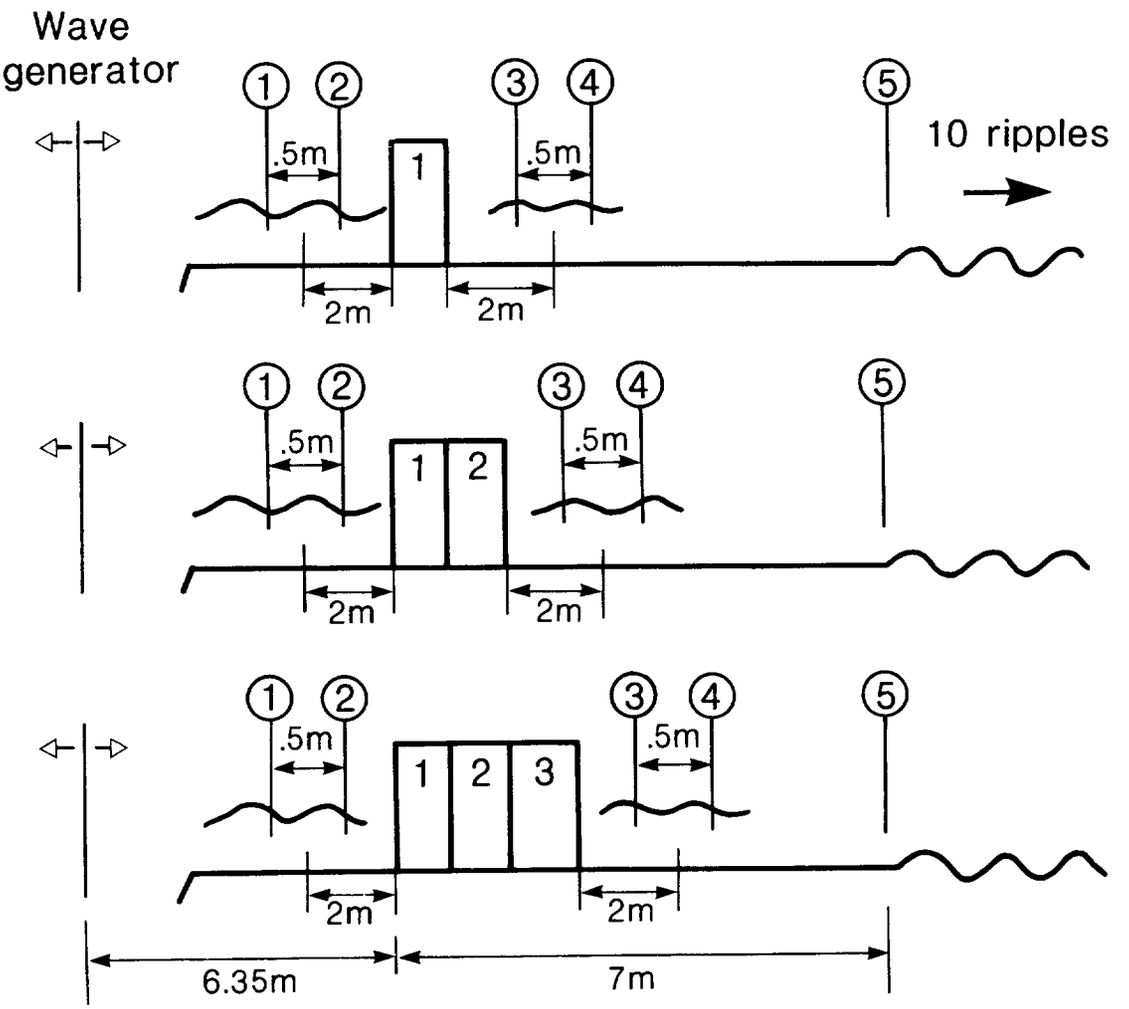

Figure B 2 Schematic diagram of the filter units in the wave tank.

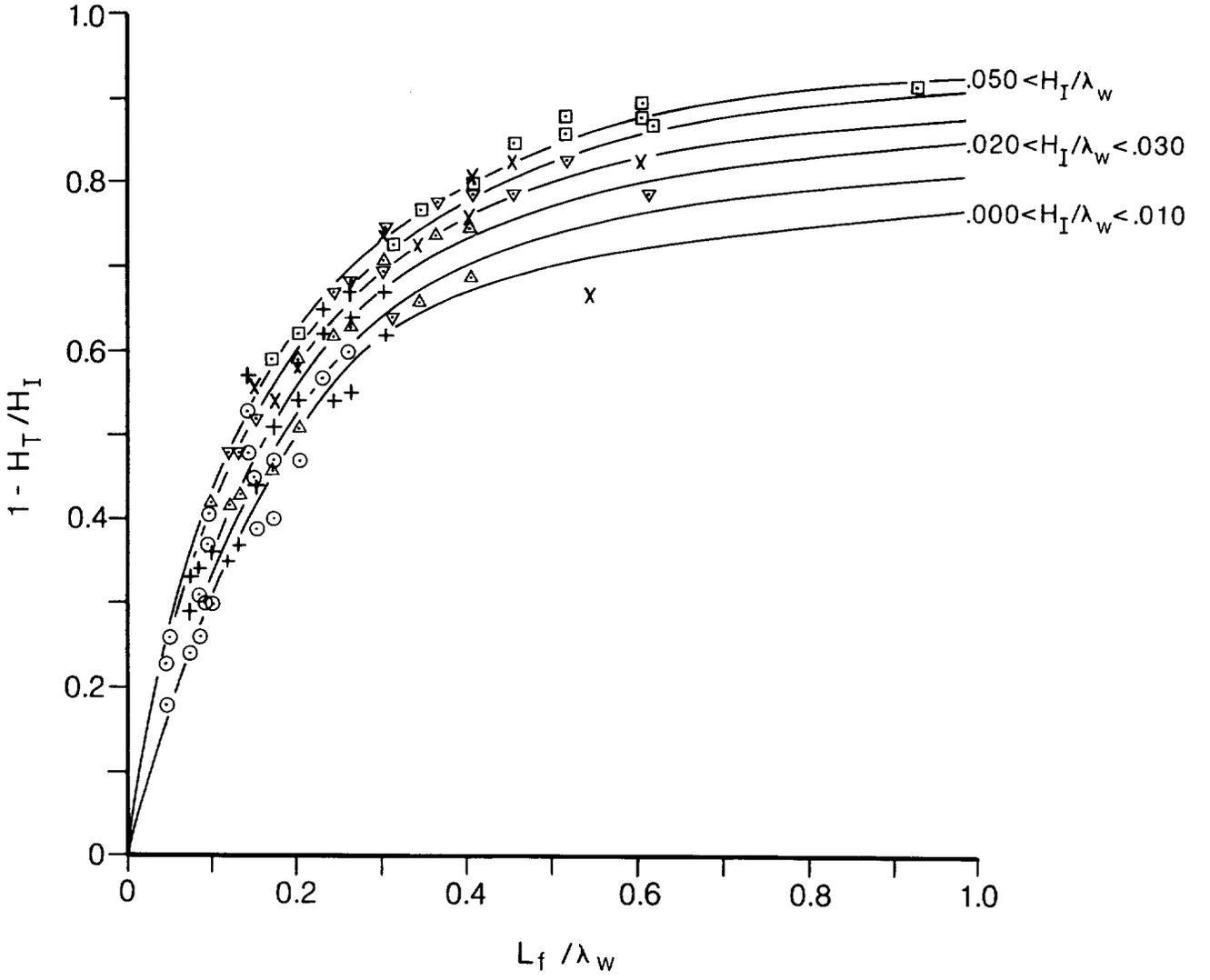

Figure B 3 Measurements of the wave attenuation factor ($1 - H_T/H_I$) as a function of the quotient L_f/λ_w, where H_T and H_I are the transmitted and incident wave heights respectively, where L_f is the filter length and where λ_w is the surface water wavelength. The observations have been grouped into wave steepness ranges as follows:

⊙	$0.000 < H_I/\lambda_w \leqq 0.010$
+	$0.010 < H_I/\lambda_w \leqq 0.020$
△	$0.020 < H_I/\lambda_w \leqq 0.030$
▽	$0.030 < H_I/\lambda_w \leqq 0.040$
×	$0.040 < H_I/\lambda_w \leqq 0.050$
⊡	$0.050 < H_I/\lambda_w$

Trend curves have been drawn for the steepest and lowest groups of waves; intermediate values have been interpolated between these limits. Further details of these measurements are given in Table B 1. (Note that, for convenience, the wave steepness has been defined as H_I/λ_w. Elsewhere the definition $ak = \pi H_I/\lambda_w$ has been adopted.)

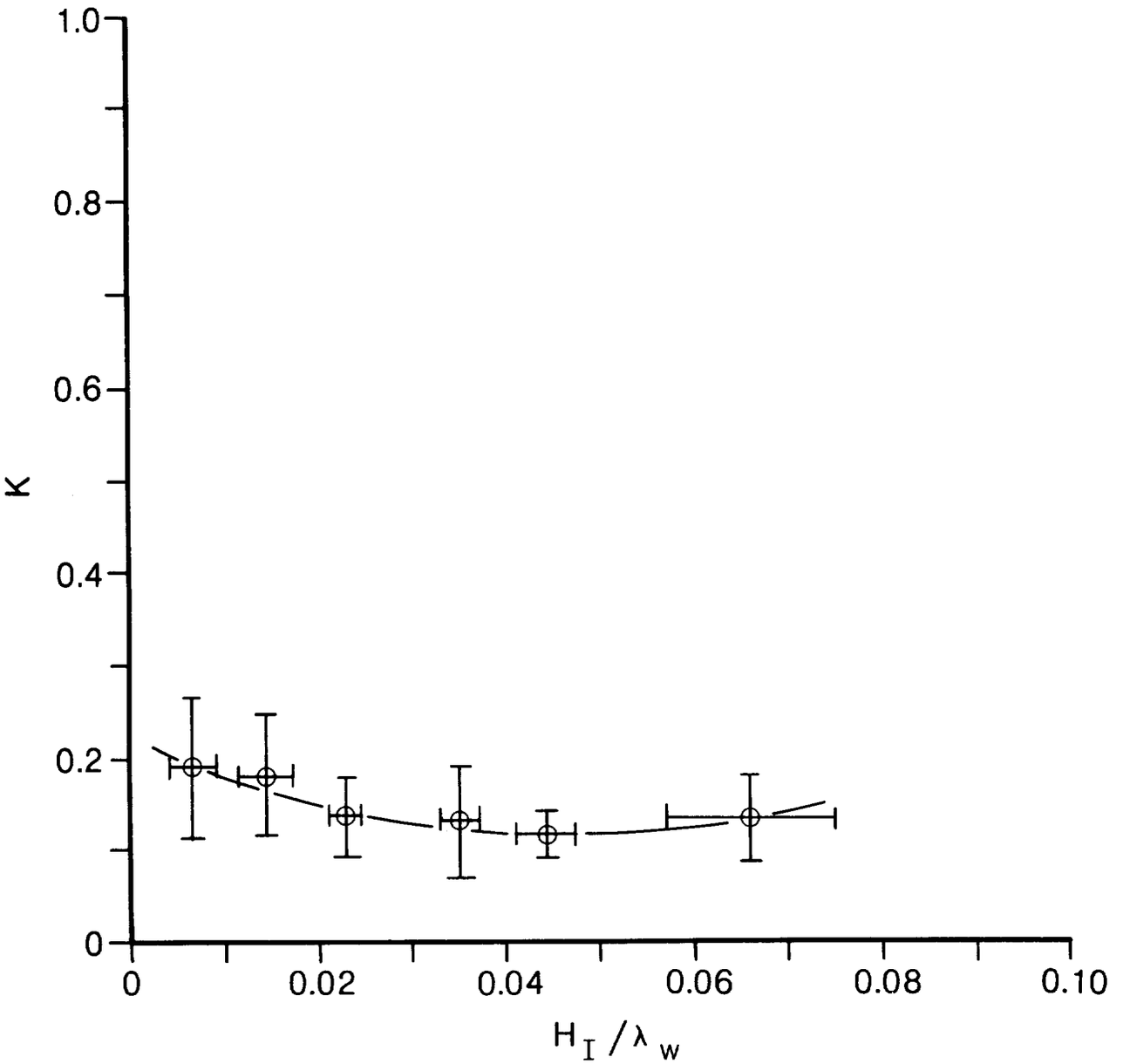

Figure B4 Measurements of the reflection coefficient K of the rubberised fibre wave filters, for all the wave steepness groups, as a function of the steepness H_I/λ_W. Mean values and standard deviations of K and H_I/λ_W in each wave steepness group are given in Table B1. (Note that, for convenience, the wave steepness has been defined as H_I/λ_W. Elsewhere the definition $ak = \pi H_I/\lambda_W$ has been adopted.)

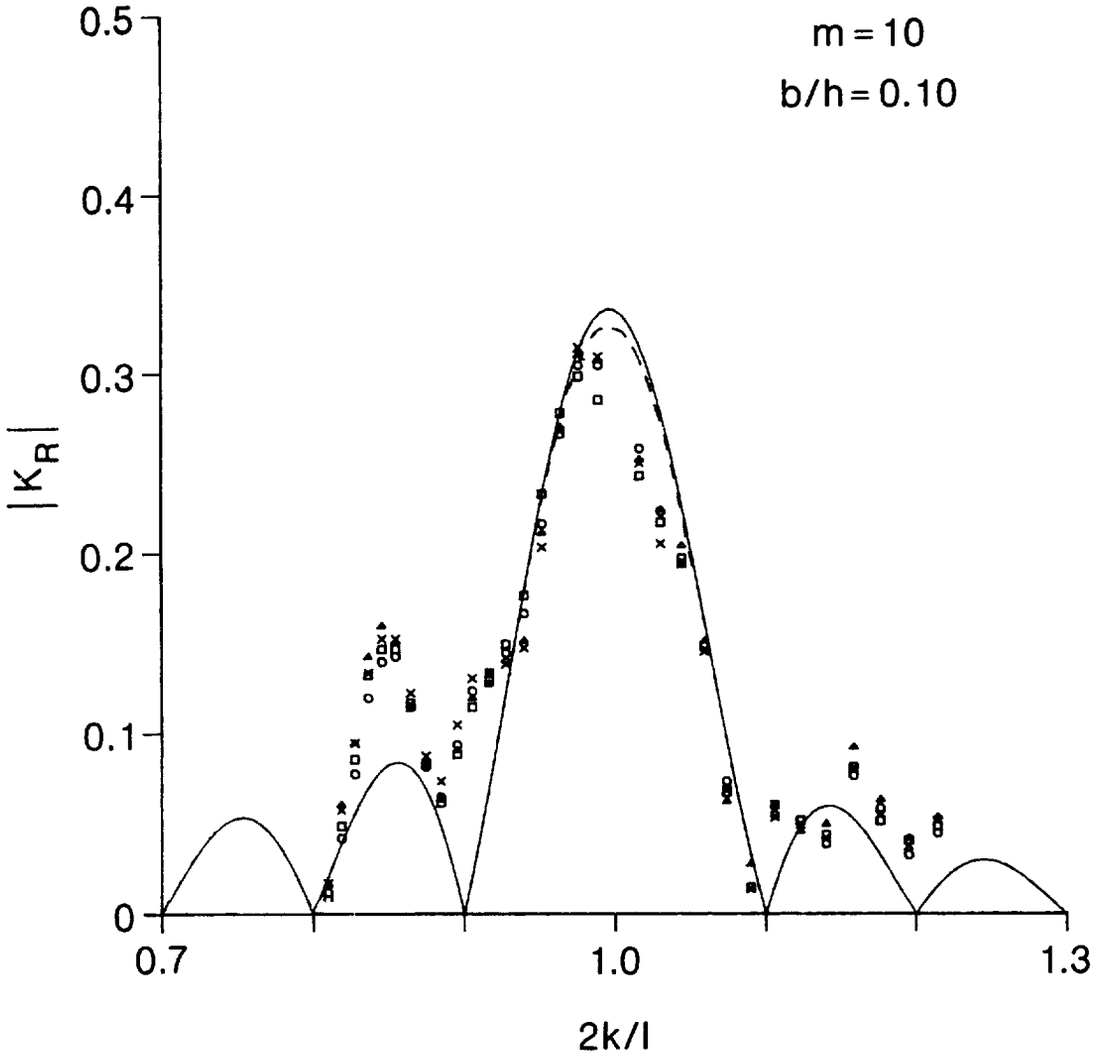

Figure B5 Results of measurements of the reflection coefficient of the ripple patch $|K_R|$ as a function of 2k/1, with and without the filters:

× no filter
△ L_f = 60 cm
⊙ L_f = 30 cm
⊡ L_f = 90 cm

For these tests, m = 10 ripples and b/h = 0.10.

Figure B6 Variation of the wave reflection coefficient K throughout the tank with (⊡) and without (⊙) filters. The filter length was approximately 90 cm. Results are shown for m = 10 ripples only, and the solid and broken curves represent uncorrected and corrected theoretical predictions, respectively. No theoretical curves are shown in Fig 22b since, in this case, the uncorrected theory predicts over-reflection.

Figure B6a m = 10, b/h = 0.16, T = 1.31 s, $L_f/\lambda_W \cong 0.45$

Figure B6b m = 10, b/h = 0.20, T = 1.42 s, $L_f/\lambda_W \cong 0.44$

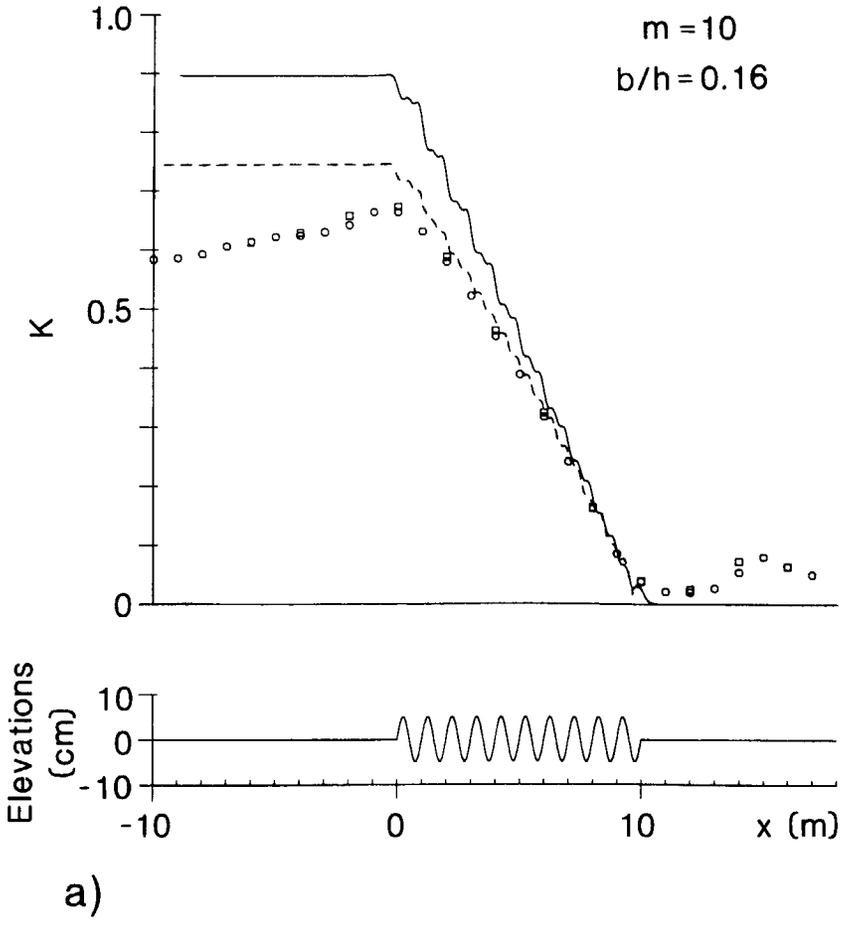
1.0
0.5
0
K
m = 10
b/h = 0.16
Elevations (cm)
10
0
-10
-10
0
10
x (m)

a)

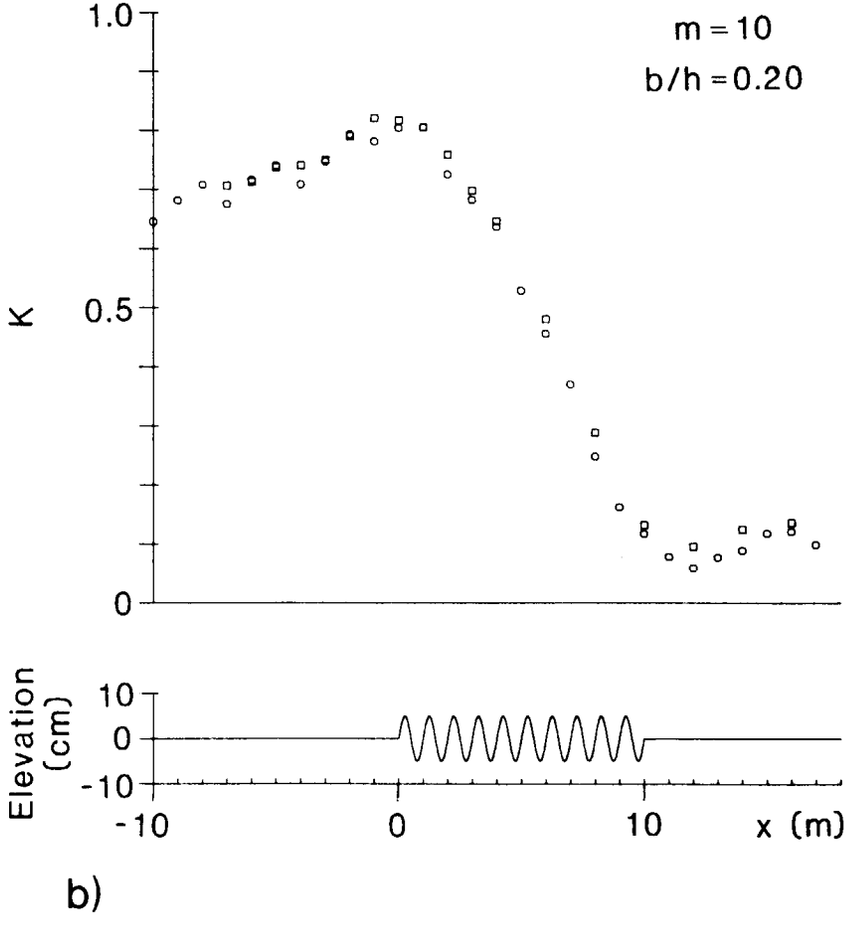
1.0
0.5
0
K
m = 10
b/h = 0.20
Elevation (cm)
10
0
-10
-10
0
10
x (m)

b)

TABLE B.1

Wave filter transmission and reflection characteristics. The observations have been grouped into wave steepness ranges as follows:

Table B.1a	Wave steepness:	$.000 \leqq H_I/\lambda_w < .010$
Table B.1b	Wave steepness:	$.010 \leqq H_I/\lambda_w < .020$
Table B.1c	Wave steepness:	$.020 \leqq H_I/\lambda_w < .030$
Table B.1d	Wave steepness:	$.030 \leqq H_I/\lambda_w < .040$
Table B.1e	Wave steepness:	$.040 \leqq H_I/\lambda_w < .050$
Table B.1f	Wave steepness:	$.050 \leqq H_I/\lambda_w$

Wave attenuation is denoted by the factor $1 - H_T/H_I$, and K is the reflection coefficient of the filters. L_f/λ_w denotes the quotient of filter length and surface wavelength, and the figures at the bottom of each table are the means and standard deviations (SD) of H_I/λ_w and K, in each wave steepness group. These results are also summarized in Figure B 3.

TABLE B.1a

$.000 \leq H_I/\lambda_w < .010$

H_I/λ_w	L_f/λ_w	$1 - H_T/H_I$	H_I/H_T	K
.00219	.048	.18	1.22	.164
.00502	.075	.24	1.32	.123
.00510	.085	.26	1.35	.080
.00794	.099	.30	1.43	.085
.00457	.048	.23	1.29	.189
.00992	.085	.31	1.44	.120
.00716	.048	.26	1.35	.223
.00236	.095	.30	1.42	.218
.00499	.15	.39	1.64	.164
.00486	.17	.40	1.66	.141
.00801	.20	.47	1.88	.138
.00502	.095	.37	1.58	.271
.00980	.15	.45	1.82	.200
.00964	.17	.47	1.88	.169
.00792	.095	.41	1.70	.305
.00518	.14	.48	1.91	.299
.00958	.23	.57	2.35	.206
.00982	.26	.60	2.47	.177
.00819	.14	.53	2.13	.336
mean .0066984				.1898947
S D .0025206				.0725694

TABLE B.1b

$.010 \leq H_I/\lambda_w < .020$

H_I/λ_w	L_f/λ_w	$1 - H_T/H_I$	H_I/H_T	K
.01081	.12	.35	1.54	.092
.01137	.13	.37	1.57	.137
.01780	.15	.44	1.78	.152
.01009	.075	.29	1.41	.154
.01627	.099	.36	1.57	.129
.01539	.075	.33	1.50	.185
.01462	.085	.34	1.52	.153
.01145	.24	.54	2.16	.136
.01124	.26	.55	2.20	.139
.01693	.30	.62	2.63	.086
.01625	.20	.54	2.17	.178
.01475	.15	.50	1.98	.238
.01426	.17	.51	2.04	.204
.01613	.30	.67	2.99	.186
.01445	.23	.62	2.63	.237
.01448	.26	.64	2.75	.205
.01119	.14	.57	2.32	.362
.01923	.23	.65	2.87	.261
.01892	.26	.67	3.00	.226
mean .0145068				.1821053
S D .002811				.065163

TABLE B.1c

$.020 \leqq H_I/\lambda_w < .030$

H_I/λ_w	L_f/λ_w	$1 - H_T/H_I$	H_I/H_T	K
.02018	.17	.46	1.86	.064
.02309	.20	.51	2.05	.100
.02242	.12	.42	1.71	.124
.02253	.13	.43	1.76	.140
.02509	.099	.42	1.71	.164
.02035	.34	.66	2.92	.093
.02237	.40	.69	3.19	.119
.02394	.24	.62	2.61	.167
.02243	.26	.63	2.73	.138
.02487	.20	.59	2.44	.203
.02478	.36	.74	3.86	.158
.02299	.40	.75	3.99	.098
.02472	.30	.71	3.47	.214
mean .0230585				.1370769
S D .0016097				.043792

TABLE B.1d

$.030 \leq H_I/\lambda_w < .040$

H_I/λ_w	L_f/λ_w	$1 - H_T/H_I$	H_I/H_T	K
.03549	.31	.64	2.80	.062
.03469	.15	.52	2.07	.127
.03544	.12	.48	1.91	.153
.03347	.13	.48	1.90	.164
.03590	.61	.79	4.76	.013
.03796	1.09	.80	5.07	——
.03316	.30	.70	3.31	.085
.03734	.24	.67	3.03	.198
.03336	.26	.68	3.10	.166
.03192	.45	.79	4.87	.076
.03945	.51	.83	6.05	.151
.03872	.36	.78	4.63	.187
.03401	.40	.79	4.73	.120
.03321	.30	.75	3.93	.233
mean .0352943				.1334615
S D .002322				.0613129

TABLE B.1e

$.040 \leqq H_I/\lambda_w < .050$

H_I/λ_w	L_f/λ_w	$1 - H_T/H_I$	H_I/H_T	K
.04575	.54	.67	3.06	.116
.04007	.17	.54	2.17	.104
.04329	.20	.58	2.37	.120
.04941	.15	.56	2.27	.129
.04028	.34	.73	3.70	.140
.04240	.40	.76	4.11	.147
.04790	.30	.74	3.83	.086
.04207	.60	.83	6.84	.108
.04703	.45	.83	5.87	.077
.04433	.40	.81	5.31	.151
mean .0443569				.1178
S D .0031839				.0248185

TABLE B.1f

$.050 \leqq H_I/\lambda_w$

H_I/λ_w	L_f/λ_w	$1 - H_T/H_I$	H_I/H_T	K
.07461	.31	.73	3.66	.081
.05764	.17	.59	2.41	.138
.06123	.20	.62	2.66	.128
.07670	.61	.87	7.71	——
.05866	.34	.77	4.30	.182
.06092	.40	.80	4.87	.151
.07500	.92	.92	12.86	.141
.05579	.51	.86	7.20	.162
.06066	.60	.88	8.57	.115
.05998	.45	.85	6.67	.086
.07015	.51	.88	8.06	.232
.08284	.60	.90	10.26	.074
mean .06618				.1352727
S D .0091033				.0469363

APPENDIX C

Wave energy dissipation in the tank

1. A progressive wave system

Consider, for simplicity, the situation in which waves travel down a flat-bottomed tank and are absorbed by a beach. Energy conservation requires that

Rate of doing work by the wavemaker	=	Rate of energy absorbtion by the beach	+	Rate of energy dissipation at the bed and the side walls.

The rate of doing work (per second) by the wavemaker may be expressed by

$$\overline{W} = \tfrac{1}{2}\rho g a^2 \sigma \left\{ \frac{2kh + \sinh(2kh)}{2k \sinh(2kh)} \right\} W_T \quad , \qquad (C.1)$$

where ρ is the fluid density, g is gravity, a is the wave amplitude, σ is the wave frequency, k is the wavenumber, h is the depth and W_T is the width of the tank.

To calculate the wave energy dissipated at the bed and the side walls, we may use Jonsson's (1967) expression for the mean specific energy loss (per second) for laminar boundary layer flow. (The assumption of laminar flow is justified, since the wave Reynolds number in the present experiments was always very small; typically, Reynolds number = RE = $U^2/\sigma\nu_w \approx 10^3$, where U and ν_w are as defined below.) Jonsson's expression is as follows:

$$\text{Rate of dissipation} = \tfrac{1}{2}\rho U^2 \sqrt{\frac{\sigma\nu_w}{2}} \quad , \text{ per unit area.} \qquad (C.2)$$

Here ν_w is the kinematic viscosity, and U is the local velocity amplitude in the potential flow region outside the thin wave boundary layer.

If we assume that the waves are sufficiently long that the water particle motions close to all points on both the walls and the bed are simply rectilinear oscillations, we may use Jonsson's result in the following way. On the two side walls, where from Eq 15 (§2) we have

$$U = \frac{gak}{\sigma} \cdot \frac{\cosh\{k(y+h)\}}{\cosh(kh)} \quad ,$$

the energy dissipation rate is expressed by

$$\rho\sqrt{\frac{\sigma\nu_w}{2}}\cdot\int_{-h}^{0}U^2\,dy \qquad \text{per unit distance along the tank,}$$

where y is the vertical coordinate (y = 0 is the free surface, y = -h is the bed). If the distance along the tank is L_T, the energy dissipation rate at the side walls is equal to

$$\frac{1}{2}\rho L_T\sqrt{\frac{\sigma\nu_w}{2}}\cdot\left(\frac{gak}{\sigma\cosh(kh)}\right)^2\cdot\left\{\frac{2kh+\sinh(2kh)}{2k}\right\}. \qquad (C.3)$$

By an equivalent argument, the energy dissipation rate at the bed is expressed by

$$\frac{1}{2}\rho L_T W_T\left(\frac{gak}{\sigma\cosh(kh)}\right)^2\sqrt{\frac{\sigma\nu_w}{2}}\,. \qquad (C.4)$$

The total energy dissipation rate $\overline{D}$ is given by the sum of (C.3) and (C.4), as follows

$$\overline{D}=\frac{1}{2}\rho L_T\sqrt{\frac{\sigma\nu_w}{2}}\left(\frac{gak}{\sigma\cosh(kh)}\right)^2\left\{h+\frac{\sinh(2kh)}{2k}+W_T\right\}. \qquad (C.5)$$

Since the velocity amplitude U has been assumed to be unattenuated along the tank, the value given by this equation is an overestimate (though probably only a slight overestimate in most cases) of the energy dissipation rate.

We may express $\overline{D}$ as a proportion of the energy generated by the wavemaker by dividing (C.5) by (C.1), such that

$$\frac{\overline{D}}{\overline{W}}=\sqrt{2\sigma\nu_w}\cdot\frac{gk^2}{\sigma^3}\cdot\frac{L_T}{W_T}\tanh(kh)\left\{1+\frac{2kW_T}{2kh+\sinh(2kh)}\right\}. \qquad (C.6)$$

This quantity is tabulated in Table C.1 for representative ranges of values of h

and k, and for the fixed values L_T = 4 x 10^3 cm, W_T = 91 cm, g = 981 cm/sec^2 and $\nu_W = 10^{-2}$ cm^2/sec. (Note that σ is related to h and k by the dispersion relation (16).) The proportion of the total wave energy which is dissipated is greatest for waves of short wavelength in shallow water, and is least for waves of long wavelength in deep water. In the table, the extreme values of the proportion are 0.64 for h = 12.5 cm and λ_w = 80 cm, and 0.08 for h = 62.5 cm and λ_w = 400 cm, respectively. Although the former value of 0.64 is substantial, it should be emphasized that it represents energy dissipation over the entire length of the tank. (In terms of wave amplitude it represents a decrease of 40%.) Moreover, it is probably an overestimate, for the reason stated earlier.

2. An incident, reflected and transmitted, wave system

The situation is rather more complicated if, as in the experiments discussed in this report, there is an incident, reflected and transmitted, wave system. In arriving at Eq (C.6), we assumed that the velocity field was independent of position in the tank. If there is a patch of ripples in the middle of the tank, which causes some proportion of the incident wave energy to be back-reflected, this will not be the case. For simplicity, let us assume that the wave field consists of two parts. Between the wavemaker and the mid-point of the ripple patch, over a horizontal distance $L_T/2$ say, suppose that there is a partially standing wave structure in which the velocity field may be expressed by

$$U \sin(kx - \sigma t) + U \cdot |K_R| \cdot \sin(kx + \sigma t + \delta_1) , \qquad (C.7)$$

where $|K_R|$ is the reflection coefficient and δ_1 is an arbitrary phase angle. Between the mid-point of the ripple patch and the beach, also over a horizontal distance of $L_T/2$, suppose that there is a purely progressive wave which, from energy conservation, is expressed by

$$U\sqrt{1 - |K_R|^2} \cdot \sin(kx - \sigma t + \delta_2) , \qquad (C.8)$$

where δ_2 is an arbitrary phase angle. For the wave field expressed by (C.7), the energy dissipation rate is greater than that given by (C.5). In particular, it is simply shown that the (spatially averaged) energy dissipation rate in this half of the tank is equal to $\frac{1}{2}(1 + |K_R|^2)\overline{D}$. Conversely, for the wave field expressed by (C.8), the energy dissipation rate is equal to $\frac{1}{2}(1 - |K_R|^2)\overline{D}$. Although

the sum of these two parts is equal to $\overline{D}$, which indicates that the overall dissipation rate in the tank is the same as for a purely progressive wave system, the energy dissipation rate is rather larger up-wave of the ripple patch, than on its down-wave side. The effect of dissipation will be to reduce gradually the incident wave height between the wave maker and the ripple patch, and to reduce also the reflected wave height between the ripple patch and the wavemaker. This will lead to underestimates of the reflection coefficient $|K_R|$ for wave gauges positioned mid-way between the wavemaker and the ripple patch (Figs 14, 16 and 17), and to general decreases in the reflection coefficient with distance from the ripple patch on the up-wave side (Figs 19 and 20).

TABLE C.1

Estimates of the proportion of the generated wave energy which is dissipated at the side walls, and at the bed of the wave tank, for different water depths (h) and surface wavenumbers (k)

WAVENUMBER k (cm^{-1})	0.079	0.052	0.039	0.031	0.026	0.022	0.020	0.017	0.016
WAVELENGTH λ_W (cm)	80.0	120.0	160.0	200.0	240.0	280.0	320.0	360.0	400.0
DEPTH h (cm)									
12.5	0.64	0.58	0.52	0.47	0.44	0.40	0.38	0.36	0.34
17.5	0.40	0.39	0.36	0.33	0.31	0.29	0.27	0.25	0.24
22.5	0.28	0.29	0.27	0.25	0.24	0.22	0.21	0.20	0.19
27.5	0.22	0.23	0.22	0.21	0.19	0.18	0.17	0.17	0.16
32.5	0.19	0.19	0.18	0.18	0.17	0.16	0.15	0.14	0.14
37.5	0.18	0.16	0.16	0.15	0.15	0.14	0.13	0.13	0.12
42.5	0.17	0.15	0.14	0.14	0.13	0.12	0.12	0.11	0.11
47.5	0.17	0.14	0.13	0.12	0.12	0.11	0.11	0.10	0.10
52.5	0.17	0.13	0.12	0.11	0.11	0.10	0.10	0.10	0.09
57.5	0.17	0.13	0.11	0.11	0.10	0.10	0.09	0.09	0.09
62.5	0.17	0.12	0.11	0.10	0.10	0.09	0.09	0.08	0.08